

# **Investigating metabotropic glutamate receptor 5 (mGlu<sub>5</sub>) as a novel therapeutic target in motor neuron disease (MND)**

Heledd Brown-Wright BSc (Hons), MSc



Thesis submitted for the degree of Doctor of Philosophy,

The University of Sheffield

August 2018

## Abstract

The only therapy approved for the treatment of motor neuron disease, a devastating neurodegenerative condition which leads to death of motor neurons and consequent motor system degeneration and death, is riluzole, thought to exert its effect by reducing glutamate excitotoxicity. Despite this our understanding of how glutamate contributes to motor neuron degeneration in MND is still limited.

One candidate pathway involves the metabotropic glutamate type 5 (mGlu<sub>5</sub>) receptor for which there is genetic and pharmacological evidence supporting its role in motor neuron degeneration. This thesis investigates the effects of HTL0014242, a novel mGlu<sub>5</sub> negative allosteric modulator (NAM) developed by Heptares Therapeutics in the *SOD1<sup>G93A</sup>* mouse model of MND.

The overall approach was to first validate mGlu<sub>5</sub> as a target in the context of the *SOD1<sup>G93A</sup>* model, then define the pharmacology of HTL0014242 in this model to ensure target engagement and define an appropriate dosing regimen before moving on to investigate efficacy.

Surprisingly we were unable to confirm others' data indicating expression of mGlu<sub>5</sub> in astrocytes in this model, whereas mGlu<sub>5</sub> was expressed in ventral horn motor neurons. HTL0014242 showed excellent pharmacokinetics with significant brain penetration and target engagement, as measured using receptor occupancy. A dose of 30mg/kg was able to substantially occupy mGlu<sub>5</sub> receptors in brain for up to 24h post dose. At these levels, HTL0014242 showed a profound effect on glial activation and a significant slowing of late stage disease progression. The point of intervention was crucial however, these effects on late stage progression were only seen when HTL001424 was dosed from an intermediate stage of disease, whereas dosing from an early stage of disease, prior to any motor function decline, had no effect on progression but still limited glial activation. Riluzole was not able to limit glial activation in the same way suggesting a distinct mechanism of action.

These results have important implications for our understanding of the role of glutamate in driving neurodegeneration and indicate that HTL0014242 has potential as a novel disease modifying therapy in the treatment of MND.

## Acknowledgements

I would like to take this opportunity to acknowledge the excellent supervision I have received throughout my PhD from my three supervisors, Dr Richard Mead, Dr Kirstie Bennett and Professor Dame Pamela Shaw. Thanks to you, I am lucky enough to have experienced an enjoyable and fulfilling (not to mention challenging) PhD project.

I would like to express my sincere gratitude to Richard for his unwavering encouragement and patience over the years. I have been very fortunate to have had such a kind and supportive supervisor – his ability to empathise and motivate students is inspiring and has made being a member of the Mead Group a pleasure. I am extremely grateful to Kirstie for her continuous support, encouragement and passionate enthusiasm for the project. Thank you for being a great mentor and taking on the role of tutor during my two placements at Heptares. Her ability to explain and simplify complex theories enabled me to get the most out of my placements; and thanks to her I have been introduced to a new and exciting area of research. I am very appreciative of the guidance and instruction from Pam that has supported me throughout my PhD studies, thank you for all the time you have invested in me.

Thank you to The University of Sheffield and Heptares Therapeutics for funding my PhD and to Dr Fiona Marshall, Dr Matt Barnes and Dr Alastair Brown for providing this opportunity and for making our collaboration a successful one. Further, I would like to extend my thanks to the Pharmacology Team at Heptares for their lab assistance and making my placements so enjoyable. A heartfelt thanks to the Mead Group, past and present, for being such a supportive team and making my PhD experience a fun one! I would also like to thank the wider SITraN community who have made working here a real pleasure.

Furthermore, I would like to thank my wonderful parents, family and friends, for their continuous support, words of encouragement and for inspiring me throughout my endeavours to always strive to do my best. To my Rich, a special thank you – this chapter has been so much better with you by my side.

Last but not least, I would like to dedicate this thesis to the memory of Harry Levinson, a close family friend, who we sadly lost to MND in 2011. This is for you Harry.

# Contents

<b>List of Figures</b> .....	8
<b>List of Tables</b> .....	11
<b>Abbreviations</b> .....	12
<b>1 Introduction</b> .....	16
<b>1.1 Motor Neuron Disease (MND)</b> .....	16
1.1.1 Epidemiology .....	16
1.1.2 Clinical Features .....	17
1.1.3 Pathology.....	17
1.1.4 Prognosis.....	18
1.1.5 Therapy and Management.....	18
1.1.6 Aetiology.....	19
1.1.7 Pathogenic Mechanisms.....	19
1.1.8 Histopathological Features of MND.....	22
1.1.9 MND Causative Genes .....	23
1.1.10 <i>SOD1</i> MND.....	25
1.1.11 The <i>SOD1</i> Mouse Model of MND.....	25
1.1.12 Our <i>SOD1</i> Mouse Model of MND.....	26
1.1.13 MND Mouse Models .....	28
<b>1.2 G-Protein Coupled Receptors</b> .....	30
1.2.1 GPCRs as a Therapeutic Target in MND .....	32
<b>1.3 Glutamate Receptors</b> .....	33
1.3.1 Metabotropic Glutamate Receptors.....	36
1.3.2 Metabotropic Glutamate Receptor 5 .....	36
1.3.3 Metabotropic Glutamate Receptor 5 (mGlu <sub>5</sub> ) involvement in Human Diseases.....	37
<b>1.4 Glutamate-Mediated Excitotoxicity</b> .....	38
1.4.1 Glutamate-Mediated Excitotoxicity in MND .....	39
<b>1.5 Role of Glial Cells in MND</b> .....	40
<b>1.6 Metabotropic Glutamate Receptor 5 (mGlu<sub>5</sub>) as a therapeutic target for MND</b> .....	42
<b>1.7 Summary</b> .....	46
<b>1.8 Hypothesis</b> .....	46
<b>1.9 Aims and Objectives</b> .....	48

<b>2</b>	<b>Materials and Methods</b> .....	49
<b>2.1</b>	<b>Materials</b> .....	49
2.1.1	List of Reagents.....	49
2.1.2	Solutions and Buffers.....	50
2.1.3	Antibodies.....	51
2.1.4	Formulas.....	52
<b>2.2</b>	<b>Methods</b> .....	53
2.2.1	C57BL/6 <i>SOD1</i> <sup>G93A</sup> Transgenic Mouse Model of MND.....	53
2.2.2	Ethical Statement.....	53
2.2.3	Housing .....	53
2.2.4	Genotyping .....	54
2.2.5	<i>In vivo</i> Pharmacology Mouse Studies .....	55
2.2.6	Mouse Behavioural Readouts .....	59
2.2.7	Immunohistochemistry in Non-Transgenic and <i>SOD1</i> <sup>G93A</sup> Mouse Lumbar Spinal Cord Tissue .....	62
2.2.8	ChAT Staining and Motor Neuron Counting .....	64
2.2.9	Immunocytochemistry in iAstrocytes .....	66
2.2.10	Image Analysis .....	68
2.2.11	[ <sup>3</sup> H] M-MPEP Radioligand Binding Assays .....	70
2.2.12	[ <sup>3</sup> H] M-MPEP Binding Assay for <i>Ex Vivo</i> Receptor Occupancy .....	73
2.2.13	Statistical Analysis .....	76
<b>3</b>	<b>Characterisation of mGlu<sub>5</sub> as a novel therapeutic target</b> .....	77
<b>3.1</b>	<b>Introduction</b> .....	77
<b>3.2</b>	<b>Results</b> .....	78
3.2.1	Characterisation of mGlu <sub>5</sub> in the <i>SOD1</i> <sup>G93A</sup> mouse model of MND .....	78
3.2.2	Characterisation of mGlu <sub>5</sub> in human derived iAstrocytes from <i>SOD1</i> patients.....	89
3.2.3	Characterisation of brain mGlu <sub>5</sub> receptor number in the <i>SOD1</i> <sup>G93A</sup> mouse model of MND.....	92
<b>3.3</b>	<b>Discussion</b> .....	98
3.3.1	Characterisation of mGlu <sub>5</sub> in the <i>SOD1</i> <sup>G93A</sup> mouse model of MND .....	98
3.3.2	Characterisation of mGlu <sub>5</sub> in human derived iAstrocytes from <i>SOD1</i> patients.....	100
3.3.3	Characterisation of brain mGlu <sub>5</sub> receptor number in the <i>SOD1</i> <sup>G93A</sup> mouse model of MND.....	101
<b>4</b>	<b>Characterisation of HTL0014242 in <i>SOD1</i><sup>G93A</sup> model of MND</b> .....	105

<b>4.1 Introduction</b> .....	105
<b>4.2 Results</b> .....	107
4.2.1 HTL0014242 competition binding in non-transgenic and <i>SOD1<sup>G93A</sup></i> mouse brain membranes.....	107
4.2.2 <i>In vivo</i> pharmacokinetics of HTL0014242 in the <i>SOD1<sup>G93A</sup></i> mouse model of MND .....	111
4.2.3 Optimisation of [ <sup>3</sup> H] M-MPEP binding assay to measure receptor occupancy (RO) of mGlu <sub>5</sub> receptors by HTL0014242 in mouse brain collected from <i>in vivo</i> dosing studies.....	117
<b>4.3 Discussion</b> .....	125
4.3.1 HTL0014242 competition binding in non-transgenic and <i>SOD1<sup>G93A</sup></i> mouse brain membranes.....	125
4.3.2 <i>In vivo</i> pharmacokinetics of HTL0014242 in the <i>SOD1<sup>G93A</sup></i> mouse model of MND .....	126
4.3.3 Optimisation of [ <sup>3</sup> H] M-MPEP binding assay to measure RO of mGlu <sub>5</sub> receptors by HTL0014242 in mouse brain collected from <i>in vivo</i> dosing studies .....	128
<b>5 90D dose-response study of HTL0014242 in the <i>SOD1<sup>G93A</sup></i> mouse model</b> .....	131
<b>5.1 Introduction</b> .....	131
<b>5.2 Results</b> .....	134
5.2.1 90D dose-response study of HTL0014242 in the <i>SOD1<sup>G93A</sup></i> mouse model of MND .....	134
5.2.2 Glial staining in ventral horns of lumbar spinal cord sections collected from dose-response study at 90 days .....	143
5.2.3 [ <sup>3</sup> H] M-MPEP binding assay to measure RO of mGlu <sub>5</sub> receptors by HTL0014242 in mouse brain collected from dose-response study at 90 days.....	148
5.2.4 90D study in the <i>SOD1<sup>G93A</sup></i> mice to compare the difference in ventral horn glial staining of mice dosed with HTL0014242 and riluzole versus riluzole alone .....	152
<b>5.3 Discussion</b> .....	158
5.3.1 90D dose-response study of HTL0014242 in the <i>SOD1<sup>G93A</sup></i> mouse model of MND .....	158
5.3.2 Glial staining in ventral horns of lumbar spinal cord sections collected from dose-response study at 90 days .....	162

5.3.3 [3H] M-MPEP binding assay to measure RO of mGlu <sub>5</sub> receptors by HTL0014242 in mouse brain collected from dose-response study at 90 days	164
5.3.4 90D study in the <i>SOD1<sup>G93A</sup></i> mice to compare the difference in ventral horn glial staining of mice dosed with HTL0014242 and riluzole versus riluzole alone	165
<b>6 Early vs late dosing of HTL0014242 through to end-stage disease in the <i>SOD1<sup>G93A</sup></i> mouse model of MND</b>	168
<b>6.1 Introduction</b>	168
<b>6.2 Results</b>	171
6.2.1 Pre-onset vs post-onset dosing of HTL0014242 up to end-stage in the <i>SOD1<sup>G93A</sup></i> mouse model of MND	171
6.2.2 Glial staining in ventral horns of lumbar spinal cord sections collected at 90D and end-stage from the survival study	185
6.2.3 Motor neuron counts in ventral horns of lumbar spinal cord sections collected at 90D and end-stage from survival study	194
6.2.4 Immunofluorescent staining with mGlu <sub>5</sub> and ChAT in ventral horns of lumbar spinal cord sections collected at 90D from survival study	196
6.2.5 [3H] M-MPEP binding assay to measure RO of mGlu <sub>5</sub> receptors by HTL0014242 in mouse brain collected from survival study at end-stage	199
<b>6.3 Discussion</b>	203
6.3.1 Early vs late dosing of HTL0014242 up to end-stage in the <i>SOD1<sup>G93A</sup></i> mouse model of MND	203
6.3.2 Glial staining in ventral horns of lumbar spinal cord sections collected from dose-response study at 90 days	210
6.3.3 Motor neuron counts in ventral horns of lumbar spinal cord sections collected at 90D and end-stage from the survival study	213
6.3.4 Immunofluorescent staining with mGlu <sub>5</sub> and ChAT in ventral horns of lumbar spinal cord sections collected at 90D from survival study	215
6.3.5 [3H] M-MPEP binding assay to measure RO of mGlu <sub>5</sub> receptors by HTL0014242 in mouse brain collected from survival study at end-stage	216
<b>7 Discussion</b>	220
<b>7.1 mGlu<sub>5</sub> as a novel therapeutic target in the <i>SOD1<sup>G93A</sup></i> mouse model of MND</b>	220
<b>7.2 Updated Hypothesis</b>	225
<b>7.3 Potential mechanisms by which HTL0014242 exerts its therapeutic effect</b>	226

7.4 Potential mechanism to explain the improved efficacy of pre-synaptic mGlu <sub>5</sub> signalling in <i>SOD1<sup>G93A</sup></i> mice .....	233
7.5 Future Directions.....	236
7.6 Concluding remarks.....	239
8 References .....	240

# List of Figures

<b>Figure 1.1.</b>	Proposed pathogenic mechanisms involved in MND .....	22
<b>Figure 1.2.</b>	The disease course of our <i>SOD1</i> mouse model .....	26
<b>Figure 1.3.</b>	Interaction between GPCR and G-Protein.....	31
<b>Figure 1.4.</b>	The structure of the mGlu <sub>5</sub> receptor and its binding sites.....	37
<b>Figure 1.5.</b>	Structure for MPEP .....	47
<b>Figure 2.1.</b>	An overview of the procedures carried out for immunohistochemistry .....	62
<b>Figure 2.2.</b>	An overview of the procedures carried out for immunocytochemistry .....	66
<b>Figure 3.1.</b>	mGlu <sub>5</sub> is predominantly expressed in the dorsal horn of mouse lumbar spinal cord sections. ....	81
<b>Figure 3.2.</b>	mGlu <sub>5</sub> is not expressed by astrocytes in mouse lumbar spinal cord..	83
<b>Figure 3.3.</b>	mGlu <sub>5</sub> is not expressed on microglia in mouse lumbar spinal cord...	85
<b>Figure 3.4.</b>	mGlu <sub>5</sub> is expressed on motor neurons in mouse lumbar spinal cord. .....	87
<b>Figure 3.5.</b>	mGlu <sub>5</sub> is expressed in both control and <i>SOD1</i> human iAstrocytes..	90
<b>Figure 3.6.</b>	Specific binding with 4nM [ <sup>3</sup> H] M-MPEP is linear with increasing protein concentrations of mouse brain membranes.....	94
<b>Figure 3.7.</b>	<i>SOD1</i> <sup>G93A</sup> disease progression does not change brain mGlu <sub>5</sub> receptor number .....	96
<b>Figure 4.1.</b>	Competition binding shows that the inhibitory constant for HTL0014242 is not altered between non-transgenic and <i>SOD1</i> <sup>G93A</sup> mouse brain membranes .....	109
<b>Figure 4.2.</b>	HTL0014242 demonstrates an excellent pharmacokinetic profile in <i>SOD1</i> <sup>G93A</sup> mouse spinal cord and blood. ....	114
<b>Figure 4.3.</b>	Estimated receptor occupancy (%RO) of mGlu <sub>5</sub> in mouse spinal cord demonstrates that 3,10 and 30mg/kg of HTL0014242 represent a good dosing range. ....	116
<b>Figure 4.4.</b>	10x K <sub>d</sub> concentration of [ <sup>3</sup> H] M-MPEP increases rate of binding in mouse non-transgenic brain membrane.....	120
<b>Figure 4.5.</b>	Specific binding with 20nM [ <sup>3</sup> H] M-MPEP increases proportionally in mouse brain membranes. ....	121

<b>Figure 4.6.</b>	The % of mGlu <sub>5</sub> receptors occupied with HTL0014242 in brain is highest at peak exposure of HTL0014242.....	122
<b>Figure 4.7.</b>	Validation of a 10-minute incubation time in order to accurately determine the % of mGlu <sub>5</sub> receptors occupied with HTL0014242 in brain .....	123
<b>Figure 4.8.</b>	Predicted receptor occupancy is not predictive of measured receptor occupancy.....	124
<b>Figure 5.1.</b>	Timeline for 90D dose-response study in <i>SOD1<sup>G93A</sup></i> mouse model of MND .....	133
<b>Figure 5.2.</b>	No significant difference between vehicle and HTL0014242-dosed groups for age of onset. ....	137
<b>Figure 5.3.</b>	No difference in the fastrac running wheel performance of HTL0014242-dosed mice.....	138
<b>Figure 5.4.</b>	No difference in the rotarod performance of HTL0014242 dosed mice .....	139
<b>Figure 5.5.</b>	HTL0014242 dosed mice weigh less than vehicle dosed mice .....	141
<b>Figure 5.6.</b>	Catwalk gait analysis across several parameters was inconclusive .....	142
<b>Figure 5.7.</b>	Reduced astrocyte staining in ventral horns of HTL0014242 dosed mice at 90 days of age.....	144
<b>Figure 5.8.</b>	Reduced microglial staining in ventral horns of HTL0014242 dosed mice at 90 days of age.....	146
<b>Figure 5.9.</b>	A good range of mGlu <sub>5</sub> receptor occupancy by HTL0014242 was achieved across all of the doses .....	149
<b>Figure 5.10.</b>	Predicted receptor occupancy broadly correlated with measured RO but was not predictive of measured receptor occupancy.....	150
<b>Figure 5.11.</b>	Riluzole does not reduce astrocyte activation in 90-day old <i>SOD1<sup>G93A</sup></i> mice.....	154
<b>Figure 5.12.</b>	Riluzole reduces microglial staining index but not staining area in 90 day old <i>SOD1<sup>G93A</sup></i> mice.....	156
<b>Figure 6.1.</b>	Onset was significantly delayed for 75D cohort. ....	176
<b>Figure 6.2.</b>	The 75D cohort perform significantly better on rotarod than the vehicle group and 25D cohort at early and late stages of the disease .....	177
<b>Figure 6.3.</b>	No difference in time taken to reach 20% decline in rotarod performance .....	178
<b>Figure 6.4.</b>	75D cohort retain motor function for longer .....	179

<b>Figure 6.5.</b>	HTL0014242 dosed from 25D is associated with weight loss.....	181
<b>Figure 6.6.</b>	Catwalk gait analysis across several parameters was inconclusive .....	182
<b>Figure 6.7.</b>	Dosing with HTL0014242 has no effect on survival .....	183
<b>Figure 6.8.</b>	Reduced astrocyte staining in ventral horns of HTL0014242 dosed mice at 90 days of age.....	188
<b>Figure 6.9.</b>	Reduced microglial staining in ventral horns of HTL0014242 dosed mice at 90 days of age .....	190
<b>Figure 6.10.</b>	Increased area of astrocyte staining in ventral horns of 75D cohort at end-stage of disease.....	192
<b>Figure 6.11.</b>	Increased microglial staining in ventral horns of 75D cohort at end- stage of disease.....	193
<b>Figure 6.12.</b>	Increased number of motor neuron counts in ventral horns of 75D cohort at 90 days of age.....	195
<b>Figure 6.13.</b>	Increased mGlu <sub>5</sub> staining in ventral horns of 75D cohort at 90 days of age .....	197
<b>Figure 6.14.</b>	Increased ChAT staining area in ventral horns of 75D cohort at 90 days of age. ....	198
<b>Figure 6.15.</b>	Dosing with 30mg/kg HTL0014242 from 75 days compared with 25 days does not change mGlu <sub>5</sub> receptor occupancy at peak and trough exposure.....	200
<b>Figure 6.16.</b>	Predicted RO in brain overpredicts measured RO in brain .....	201
<b>Figure 7.1.</b>	Potential mechanism by which HTL0014242 exerts its therapeutic effect.....	229
<b>Figure 7.2.</b>	Potential mechanism to explain how improved efficacy of pre- synaptic mGlu <sub>5</sub> signalling in <i>SOD1<sup>G93A</sup></i> mice causes astrocyte activation.....	235

## List of Tables

<b>Table 1.1.</b>	Clinical classification of MND .....	16
<b>Table 1.2.</b>	Focal sites of onset in MND .....	17
<b>Table 1.3.</b>	MND causative genes.....	24
<b>Table 1.4.</b>	Comparison between our <i>SOD1</i> mouse model and the original G1H <i>SOD1</i> mouse model.....	28
<b>Table 1.5.</b>	Other mouse models of MND.....	29
<b>Table 1.6.</b>	Glutamate receptors.....	34
<b>Table 2.1.</b>	Primary antibodies for immunofluorescence .....	51
<b>Table 2.2.</b>	Secondary antibodies for immunofluorescence.....	51
<b>Table 2.3.</b>	PCR program for genotyping .....	54
<b>Table 2.4.</b>	Summary of the clinical details for each patient sample .....	67
<b>Table 4.1.</b>	Exposure of HTL0014242 in spinal cord and blood following a single dose of HTL0014242 at 10mg/kg and calculated receptor occupancy .....	112
<b>Table 4.2.</b>	Exposure of HTL0014242 following sub-chronic HTL0014242 dosing at 10mg/kg for 7 consecutive days .....	113
<b>Table 5.1.</b>	90 day dose-response study data for HTL0014242 dosed at 3, 10 and 30mg/kg .....	151
<b>Table 5.2.</b>	Summary of the key 90D dose-response study readouts .....	167
<b>Table 6.1.</b>	Exposure data for HTL0014242 dosed at 30mg/kg from 25 days of age (25D cohort) and from 75 days of age (75D cohort).....	202
<b>Table 6.2.</b>	Summary of the key survival study readouts.....	219

# Abbreviations

25D	25 day cohort
3,5-DHPG	3,5-dihydroxyphenylglycine
75D	75 day cohort
7TM	7 transmembrane domain
90D	90 day
A1	Classically activated astrocyte
A2	Alternatively activated astrocyte
AC	Adenylyl cyclase
AD	Autosomal dominant
AIDA	1-aminoindan-1,5-dicarboxylic acid
ALS	Amyotrophic lateral sclerosis
ALSTDI	ALS therapy development institute
AMPA	$\alpha$ -amino-3-hydroxy-5-methyl-4-isoxazolepropionic acid
ANOVA	Analysis of variance
AR	Autosomal recessive
ARRIVE	Animal Research: Reporting of In Vivo Experiments
BAC	Bacterial artificial chromosome
BCA	Bicinchoninic acid
B <sub>max</sub>	Total receptor density
BSA	Bovine serum albumin
C9ORF72	Chromosome 9 open reading frame 72
CBP	Calcium binding protein
ChAT	Choline acetyl-transferase
CMAP	Compound muscle action potential
CNS	Central nervous system
cpm	Counts per minute
CSF	Cerebrospinal fluid

Cy3	Carbocyanine 3
DAG	Diacylglycerol
DAPI	4',6-diamidino-2-phenylindole
DMEM	Dulbecco's modified eagle medium
DMSO	Dimethyl sulfoxide
DNA	Deoxyribonucleic acid
DPM	Disintegration per minute
EAAT2	Excitatory amino acid transporter 2
EDTA	Ethylenediaminetetraacetic acid
EGF	Epidermal growth factor
EGFP	Enhanced green fluorescent protein
FACS	Fluorescent-activated cell sorting
FDA	U.S Food and Drug Administration
FGF2	Basic fibroblast growth factor
FITC	Fluorescein isothiocyanate
FMR <sub>1</sub>	Fragile X mental retardation 1
FMRP	Fragile X mental retardation protein
FTD	Fronto-temporal dementia
FUS	Fused in sarcoma
FXS	Fragile X syndrome
GABA	Gamma-aminobutyric acid
GDP	Guanosine diphosphate
GFAP	Glial fibrillary acidic protein
GluR2	glutamate receptor 2
GPCR	G-protein coupled receptor
GTP	Guanosine triphosphate
HCS	High content screening
HEPES	4-(2-hydroxyethyl)-1-piperazineethanesulfonic acid
Iba1	Ionized calcium binding adaptor molecule 1
IC <sub>50</sub>	Half maximal inhibitory concentration
ICC	Immunocytochemistry

IHC	Immunohistochemistry
iNPC	Induced neural progenitor cell
IP <sub>3</sub>	Inositol-1,4,5-triphosphate
iPSC	Induced pluripotent stem cell
K <sub>d</sub>	Dissociation constant
K <sub>i</sub>	Inhibitory constant
KLF4	Kruppel-like factor 4
K <sub>obs</sub>	Observed rate constant
K <sub>off</sub>	Dissociation rate constant
K <sub>on</sub>	Association rate constant
M1	Classically activated microglia
M2	Alternatively activated microglia
mGlu	Metabotropic glutamate receptor
MND	Motor neuron disease
MPEP	2-Methyl-6-(phenylethynyl)pyridine
mRNA	messenger RNA
NAM	Negative allosteric modulator
NMDA	N-methyl-D-aspartate
NPC	Neural progenitor cell
NSB	Non-specific binding
O/N	Overnight
OCT4	Octamer-binding transcription factor 4
PAM	Positive allosteric modulator
PBS	Phosphate-buffered saline
PCR	Polymerase chain reaction
PD	Parkinson's disease
PD-LID	Parkinson's disease and L-DOPA-induced dyskinesia
PEI	Polyethylenimine
PET	Positron emission tomography
PFA	Paraformaldehyde
PIP <sub>2</sub>	Phosphatidylinositol-4,5-bisphosphate

PK	Pharmacokinetic
PKC	Protein kinase C
PLC	Phospholipase C
RNA	Ribonucleic acid
RO	Receptor occupancy
RT	Room temperature
SA	Specific activity
SBDD	Structure based drug discovery
SC	Spinal cord
SD	Standard deviation
SDS	Sodium dodecyl sulphate
SGPC	Spheroid GFAP-positive cells
SOD1	Superoxide dismutase 1
Sox2	SRY-Box 2
SPF	Specified pathogen free
SRY	Sex-determining region Y
$t_{1/2}$	Half life
TAE	Tris-acetate-EDTA
TDP-43	TAR DNA binding protein 43
TMD	Transmembrane domain
TRIS	Tris(hydroxymethyl)aminomethane
uHPLC-TOF	Ultra-high performance liquid chromatography/time-of-flight
VFT	Venus fly trap domain

# 1 Introduction

## 1.1 Motor Neuron Disease (MND)

Motor neuron disease (MND) is an umbrella term used to describe a group of adult onset neurodegenerative disorders targeting the motor neurons in the motor cortex, brainstem, and spinal cord (Cooper-Knock et al. 2013). Of the four clinical subtypes comprising MND, amyotrophic lateral sclerosis (ALS) is the most common variant, accounting for approximately 80% of all cases (Table 1.1).

**Table 1.1. Clinical classification of MND**

Subtype	Motor neuron involvement at onset
Amyotrophic lateral sclerosis (ALS)	Both upper and lower motor neuron involvement
Progressive muscular atrophy (PMA)	Lower motor neuron involvement predominates
Primary lateral sclerosis (PLS)	Upper motor neuron involvement predominates
Progressive bulbar palsy (PBP)	Bulbar muscle involvement predominates

Source: Cooper-Knock et al, 2013.

Of note, ALS and MND are often used interchangeably in the literature to describe the selective degeneration of both upper and lower motor neurons. Therefore, for this thesis both terms are considered to be synonymous.

### 1.1.1 Epidemiology

MND is the third most common neurodegenerative disorder with a global incidence of 2-3 per 100,000. However, as the occurrence of MND increases with age, the incidence is reduced in countries with lower life expectancies (Cooper-Knock et al. 2013). The majority of MND cases are sporadic (~ 95%), usually presenting in the sixth and seventh decades of life (McDermott & Shaw 2008). The mean age of onset is between 55-60 years, with males being affected more commonly than women. A younger disease onset is more often associated with familial MND, which accounts for the remaining 5% of cases (Byrne et al, 2011).

### 1.1.2 Clinical Features

Familial and sporadic MND are clinically indistinguishable. Patients present with a combination of both upper and lower motor neuron features and their symptoms tend to reflect the pattern of disease onset. Disease onset usually starts focally, in the limb, bulbar or respiratory muscles, before spreading to anatomically contiguous motor neuron groups (McDermott & Shaw 2008) (Table 1.2).

**Table 1.2. Focal sites of onset in MND**

Site of Onset	Prevalence
Upper or Lower Limb	74%
Bulbar	25%
Respiratory	1%

Source: Cooper-Knock et al, 2013.

Onset of disease within the respiratory musculature is uncommon. However, as disease progresses, respiratory function declines. Consequently, the presence of respiratory muscle weakness is a negative prognostic factor in MND (Cooper-Knock et al. 2013).

Although it is the motor neurons which are predominantly affected in MND, occasionally patients report sensory pathway and extra-motor involvement. For instance, 51% of MND patients develop features of cognitive impairment on detailed neuropsychological testing (Goodall et al. 2012). Further, it is widely accepted that MND and fronto-temporal dementia (FTD) are part of the same neurodegenerative disease spectrum, (overlapping both clinically and pathologically) with approximately 5% of MND patients developing FTD (Cooper-Knock et al. 2013).

### 1.1.3 Pathology

Accumulation of abnormal aggregates of ubiquitinated proteins in the cytoplasm of affected neurons is the hallmark of most neurodegenerative diseases, including MND (Mackenzie et al. 2010). The formation of these aggregates in surviving motor neurons indicates that proteasome recycling of abnormal proteins is impaired (Sreedharan et al. 2008). In MND one of the major components of these intracellular inclusions is the aberrant TAR DNA binding protein 43 (TDP-43). Of note, TDP-43 is the pathological protein most often found in the frontal and temporal lobes of FTD patients. Fused in sarcoma (FUS) is another disease related protein linked to both

MND and FTD (Mackenzie et al. 2010). This shared pathology accounts for why some MND patients also have features of FTD (MND-FTD) and vice versa.

#### **1.1.4 Prognosis**

MND is a fatal disorder. Eventual paralysis follows progressive muscle weakness due to the loss of connection between the brain and voluntary muscles (Goodall et al. 2012). The disease trajectory is usually rapidly progressive, without intervals of remission and invariably culminates in death, often as a result of type II respiratory failure. Although variable, disease survival is typically 2-3 years from symptom onset with only ~ 20% of patients surviving longer than 5 years (Cooper-Knock et al. 2013). The reason for this heterogeneity in disease duration is unclear and remains an important topic of research, with the ultimate aim being to elucidate potential avenues for therapeutic intervention(s).

#### **1.1.5 Therapy and Management**

There is no cure for MND. Over one hundred therapeutic drugs have been trialled for the disease, yet most have been unsuccessful. Currently, there is a single neuroprotective drug on the market in Europe, riluzole (Gordon 2011). However, its effect is somewhat modest, extending patient survival by approximately 3 months (Miller et al, 2011). Present guidelines recommend that a multidisciplinary team of healthcare professionals collaborate, to optimise the overall care of the patient (NICE, 2016).

The U.S Food and Drug Administration (FDA) approved edaravone for the treatment of MND patients in 2017. Edaravone is a free-radical scavenger that has been shown to attenuate motor symptoms and slow motor neuron degeneration in the *SOD1<sup>G93A</sup>* mouse model of MND (Ito et al. 2008). In addition, a six-month Japanese clinical trial demonstrated that at 24 weeks participants receiving edaravone declined less on the revised ALS functional rating scale (ALSFRS-R) than participants receiving placebo (Yoshino & Kimura 2006). However, there are limitations with this clinical trial that could make it difficult to prescribe edaravone to a large proportion of MND patients. For example, due to the stringent inclusion criteria of this trial it has been estimated that less than 7% of the MND patient population in Ireland and the Netherlands would be eligible for this drug (Hardiman & van den Berg 2017b). Furthermore, the duration of the trial was relatively short (6 months) by European standards, with guidelines suggesting trial duration should be at least 12-18 months (Hardiman & van den Berg 2017b). Consequently, the long-term effects of dosing edaravone from its potentially beneficial effects to its possible adverse effects are currently unknown. For these

reasons, additional clinical trials demonstrating efficacy over an extended period of time and with a larger number of participants are needed before edaravone is likely to be approved for the treatment of MND patients in the UK.

### **1.1.6 Aetiology**

The aetiology of sporadic MND is complex and remains poorly understood. It is currently considered to be triggered by the interaction of multiple genetic and environmental disease modifiers (Cooper-Knock et al. 2013). Identifying similarities in clinical and pathological features between both sporadic and familial forms of the disease, has led to the theory that investigating familial MND, will reveal disease mechanisms that are also applicable to sporadic MND.

### **1.1.7 Pathogenic Mechanisms**

MND pathogenesis is multifactorial comprising many mutually compatible processes (Ferraiuolo et al. 2011b). To date, the causative mechanisms underlying MND have not been fully determined. The urgent need for effective disease modifying therapies is the 'driving force' behind the extensive research into this area. Figure 1.1 summarises the key pathogenic mechanisms implicated in MND.

There are multiple cellular processes that contribute to the pathobiology of *SOD1* MND including oxidative stress, mitochondrial dysfunction, excitotoxicity, protein aggregation and neuroinflammation. A brief overview of several of the key mechanisms implicated in *SOD1* MND are discussed below.

#### **Oxidative Stress**

Mutations in the *SOD1* gene which encodes a major free radical scavenging enzyme have been shown to be associated with MND (Rosen et al. 1993). For this reason, the role of oxidative stress in MND is of particular interest. Oxidative stress occurs when the production of reactive oxygen species (ROS) cannot be counteracted by their removal which ultimately culminates in ROS-induced cellular damage. Oxidative damage has been extensively researched using mutant *SOD1* mouse models. It has previously been shown that mutant *SOD1*-expressing microglia cause an increase in the production of reactive oxygen species via a NADPH oxidase (NOX) -mediated mechanism which increases superoxide synthesis (Harrasz et al. 2008). In addition, it has been demonstrated that survival of *SOD1*<sup>G93A</sup> mice can be extended by knockout of *Nox1* or *Nox2* (Wu et al. 2006; Marden et al. 2007). Oxidative stress is also thought to be involved in mediating other pathogenic mechanisms of MND such as

mitochondrial dysfunction, excitotoxicity and protein aggregation (Rao & Weiss 2004; Duffy et al. 2011; Wood et al. 2003).

### **Mitochondrial Dysfunction**

Mitochondria play a key role in the generation of intracellular ATP, calcium homeostasis and regulating apoptotic cell death. Mitochondrial dysfunction is thought to contribute to motor neuron injury in MND. For example, it has been shown previously that in patients with MND the morphology of mitochondria are altered within skeletal muscles and spinal motor neurons (Menzies et al. 2002). Furthermore, calcium levels are increased within motor neuron terminals of patients with sporadic MND suggesting a dysregulation of calcium buffering (Siklós et al. 1996). Mitochondrial dysfunction has been widely investigated using mutant *SOD1* transgenic mice and it has been reported that oxidative stress within mitochondria results in reduced ATP production which is detectable at disease onset (Mattiuzzi et al. 2002). It has also been shown that creatine (a compound that modulates mitochondrial function) improves motor function and extends survival of *SOD1*<sup>G93A</sup> mice in a dose-dependent manner (Klivenyi et al. 1999).

### **Excitotoxicity**

Glutamate is the major excitatory neurotransmitter in the CNS. Glutamate-mediated excitotoxicity is caused by excess glutamate levels in the synapse which results in the overstimulation of glutamate receptors (Van Damme et al. 2005). Excitotoxicity is well recognised to cause both astrocyte and neuronal injury in MND (Shaw 2005). Furthermore, in some patients with MND the reuptake of glutamate from the synapse by glutamate reuptake transporters is impaired. For example, expression and function of the glial excitatory amino acid transporter 2 (EAAT2) has been shown to be reduced in MND patients (Howland et al. 2002). It has also been shown in mutant *SOD1* mouse models of MND that electrophysiological properties of motor neurons are impaired early on in the disease course and that this renders these cells more vulnerable to excessive glutamate levels (Meehan et al. 2010). Finally, one of the most convincing pieces of evidence for the role of glutamate-mediated toxicity in MND stems from the fact that riluzole (which is an anti-glutamatergic compound) has a modest effect on survival in human cases of MND (Lacomblez et al. 1996). Glutamate-mediated excitotoxicity in MND is discussed further in Section 1.4.1.

## **Protein Aggregation**

As mentioned previously in section 1.1.3, protein aggregation is a key feature of both sporadic and familial MND. Exactly how these protein aggregates contribute to disease pathogenesis is not fully understood. It is not clear whether ubiquitinated inclusions in MND are themselves pathogenic or rather a cytoprotective response (Shaw 2005). For example, these inclusions could sequester aberrant proteins that would otherwise be toxic to the cell or alternatively they may sequester proteins that are required for normal cellular processes. Despite this, it is clear that proteasome recycling which is essential for the turnover of abnormal proteins is impaired. The identification of mutations in the *TARDBP* gene which encodes the protein TDP-43, the major protein constituent of these pathological aggregates, has served to consolidate the role of protein aggregation in MND (Neumann et al. 2006).

## **Neuroinflammation**

There is accumulating evidence to suggest an involvement of non-neuronal cells such as activated microglia and astrocytes in MND disease pathogenesis. Proliferation of activated glial cells is a common histological feature observed within the ventral horns of lumbar SC of mutant *SOD1* transgenic mice and in human cases of both familial and sporadic MND (Alexianu et al. 2001a; Kawamata et al. 1992). These observations in mouse SC tissue often occur before the onset of clinical signs of disease and before significant motor neuron loss (Mead et al. 2011). There is a body of evidence to suggest that glial activation is a driver of disease progression in MND (Boillée et al. 2006b; Yamanaka, Boillée, et al. 2008). The role of glial cells in MND is discussed further in section 1.5.

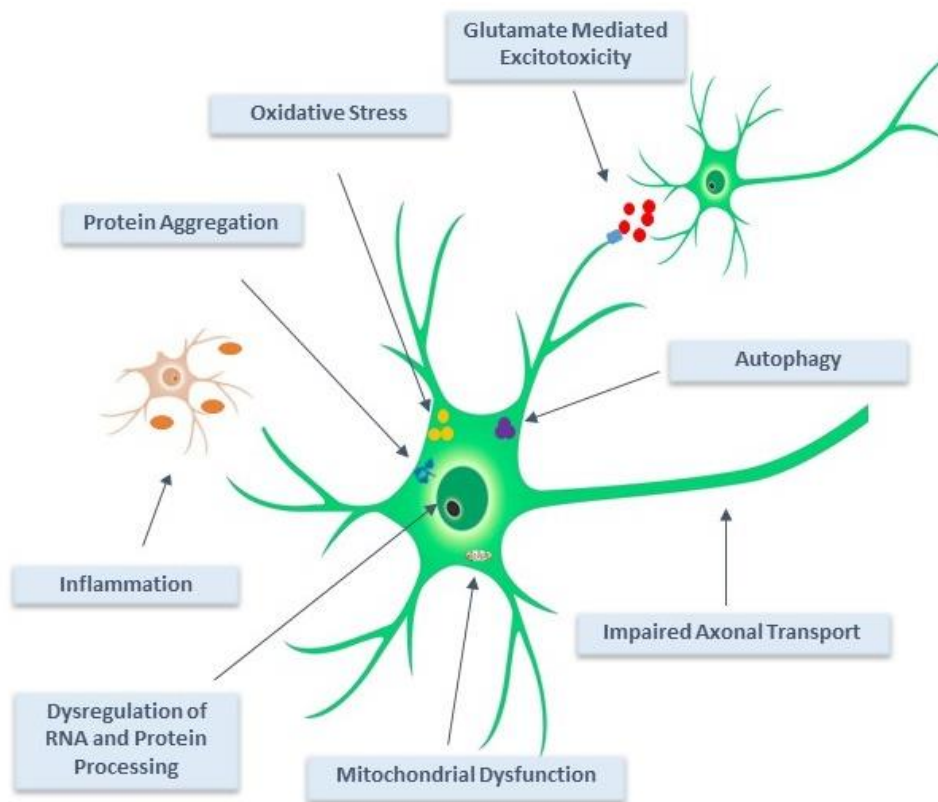


**Figure 1.1. Proposed pathogenic mechanisms involved in MND**

*Source: Adapted from Ferraiuolo et al, 2011b*

### 1.1.8 Histopathological Features of MND

The most prominent pathological hallmark of MND is the accumulation of aberrant protein aggregates. TDP-43, FUS or SOD1 proteins are often found in these aggregates, with both wild-type and mutant forms of the protein making up these insoluble inclusions (Matus et al. 2013). It has been proposed that misfolded aggregates self-propagate within neurons and in addition spread to neighbouring cells (Münch & Bertolotti 2011). Of note, cell-to-cell propagation of mutant SOD1 aggregates has been shown to trigger the aggregation of wild-type SOD1 protein (Lee & Kim 2015). Interestingly, this cell to cell propagation of misfolded aggregates correlates with the clinical observation that onset of disease starts in a focal region, before the disease spreads in an orderly manner to anatomically contiguous areas. Whilst the propagation of misfolded aggregates in MND is a similar parallel to that

observed in prion disease, unlike prion proteins, misfolded protein aggregates found in MND are not considered to be infectious. Consequently, cell-to-cell propagation of misfolded protein aggregates observed in MND is said to occur via a prion-like mechanism (Lee & Kim 2015).

#### **1.1.9 MND Causative Genes**

Table 1.3 summarises the main MND causative genes identified to date. For the most part, the genes associated with familial MND are inherited in an autosomal dominant manner. Occasionally, these genetic mutations are observed in apparently sporadic MND cases. This suggests that there is some degree of genetic overlap (Goodall et al. 2012). The four most common genetic variants of MND are caused by mutations in *SOD1*, *FUS*, *TARDBP* and *C9ORF72*. Together, these genes account for approximately 70% of familial cases. Of all the genes identified to date, the hexanucleotide repeat expansion in intron 1 of chromosome 9 open reading frame 72 (*C9ORF72*) is the most common genetic cause of MND (Goodall et al. 2012).

**Table 1.3. MND causative genes**

Known ALS Loci and Causative Genes				
Genetic subtype	Chromosomal Locus	Gene	Inheritance	Onset
ALS1	21q22	<b>SOD1</b>	AD and AR	Adult
ALS2	2q33	ALS2	AR	Juvenile
ALS3	18q21	Unknown	AD	Adult
ALS4	9q34	SETX	AD	Juvenile
ALS5	15q15-q21	SPG11	AR	Juvenile
ALS6	16p11.2	<b>FUS</b>	AD and AR	Adult
ALS7	20p13	Unknown	AD	Adult
ALS8	20q13.33	VAPB	AD	Adult
ALS9	14q11.2	ANG	AD	Adult
ALS10	1p36.2	<b>TARDBP</b>	AD	Adult
ALS11	6q21	FIG4	AD	Adult
ALS12	10p13	OPTN	AD and AR	Adult
ALS13	12q23-q24.1	ATXN2	AD	Adult
ALS14	9p13	VCP	AD	Adult
ALS15	Xp11.21	UBQLN2	X-linked	Adult
ALS16	9p13	SIGMAR1	AD and AR	Adult and Juvenile
ALS17	3p12.1	CHMP2B	AD	Adult
ALS18	17p13.3	PFN1	AD	Adult
ALS19	2q33.3-q34	ERBB4	AD	Adult
ALS20	12q13.1	hnRNPA1	AD	Adult
ALS21	5q31.2	MATR3	AD	Adult
ALS22	2q35	TUBA4A	AD	Adult
Known ALS Loci and Causative Genes				
Genetic Subtype	Chromosomal Locus	Gene	Inheritance	Onset
ALS + FTD1	9p21.2	<b>C9ORF72</b>	AD	Adult
ALS + FTD2	22q11.23	CHCHD10	AD	Adult
ALS + FTD3	5q35	SQSTM1	AD	Adult
ALS + FTD4	12q14	TBK1	Unknown	Adult

Source: (Hardiman et al. 2017a)

*(AD=Autosomal Dominant. AR = Autosomal Recessive)*

### 1.1.10 *SOD1* MND

Mutations in the superoxide dismutase 1 (*SOD1*) gene were the first genetic cause of MND to be identified (Rosen et al. 1993). *SOD1* mutations account for around 20% of familial cases and are the most common genetic cause of MND after the *C9ORF72* repeat expansion. Currently, in excess of 150 missense mutations in the *SOD1* gene have been noted and they are predominantly inherited in an autosomal dominant manner (Lill et al. 2011).

The *SOD1* protein functions as a free radical scavenging enzyme and is ubiquitously expressed throughout the central nervous system (CNS). Initially it was thought that *SOD1* MND resulted from a loss of function mechanism, as reviewed by Barber & Shaw (2010). However, it has been shown that *SOD1* knockout mice do not develop MND (Reaume et al. 1996). Furthermore, overexpression of the mutant human *SOD1* gene in transgenic mice produces a phenotype similar to human MND, supporting a gain of function mechanism of disease (Barber & Shaw 2010). Whilst misfolding and aggregation are the key events in which mutant *SOD1* causes disease, there is evidence that all of the mechanisms highlighted in Figure 1.1 contribute to motor neuron injury.

Unlike the majority of MND cases, cytoplasmic TDP-43 and/or FUS proteins are not present in *SOD1* MND, suggesting that its pathology is unique (Goodall et al. 2012). Finally, a dominant lower motor neuron involvement with rapid progression is typical of *SOD1* MND, whilst dementia is rare (Renton et al. 2014).

### 1.1.11 The *SOD1* Mouse Model of MND

Genetic models of MND facilitate both the identification of disease-related pathogenic mechanisms and also the development of novel therapeutic candidates. The most widely used animal models for testing drugs in MND are transgenic mice expressing high copy numbers of a human mutant form of the *SOD1* gene, with a pathogenic glycine to alanine mutation at amino acid position 93 (*SOD1<sup>G93A</sup>*). The *SOD1<sup>G93A</sup>* mouse model is the most robust and well characterised mouse model to study MND, demonstrating both pathological and clinical similarities to human *SOD1* MND (Gurney et al. 1994). These mice recapitulate the selective vulnerability of motor neurons observed in human cases of MND (Fischer et al., 2004). Also, similarly to patients with the human disease, *SOD1<sup>G93A</sup>* mice develop progressive muscle weakness throughout the disease course and increasing paralysis due to the loss of motor neurons (Fischer et al., 2004). Further, it has been shown that riluzole (the only disease modifying therapy approved for MND patients in the UK), modestly extends

survival in *SOD1<sup>G93A</sup>* mice, reinforcing the authenticity of this model (Gurney et al. 1996).

Unfortunately, there is a discordance between the positive findings of therapeutic drugs in the *SOD1<sup>G93A</sup>* mouse model and human MND patients (Benatar 2007), with suggestions that the *SOD1<sup>G93A</sup>* mouse model of MND is a poor predictor of drug effectiveness in humans (Perrin 2014). However, the ALS therapy development institute (ALSTDI), a non-profit drug discovery centre created to test potential therapeutic compounds in the *SOD1<sup>G93A</sup>* mouse model of MND, have called into question the quality of a large proportion of preclinical *in vivo* studies (Scott et al. 2008). For example, it is thought that many of the preclinical mouse studies demonstrating therapeutic effectiveness in the *SOD1<sup>G93A</sup>* mouse model were not rigorously designed resulting in a multitude of false positive findings (Scott et al. 2008). To combat this problem, the ALSTDI have provided recommendations for subsequent preclinical *in vivo* studies using the *SOD1<sup>G93A</sup>* mouse model of MND. These recommendations have been incorporated into a set of preclinical guidelines introduced to standardise the procedures of preclinical animal research in MND (Ludolph et al. 2010). Adopting these guidelines should reduce the number of false positive preclinical studies and ultimately prevent unfounded human clinical trials from taking place (Perrin 2014).

### 1.1.12 Our *SOD1* Mouse Model of MND

The *SOD1<sup>G93A</sup>* mouse line used throughout this project was the inbred C57BL/6 mouse line (characterised by Mead et al. 2011) which originates from the original G1 mixed background SJLxC57BL/6 transgenic line (Gurney et al. 1994). The mice on the inbred C57BL/6 background show a remarkably consistent disease course (Figure 1.2).

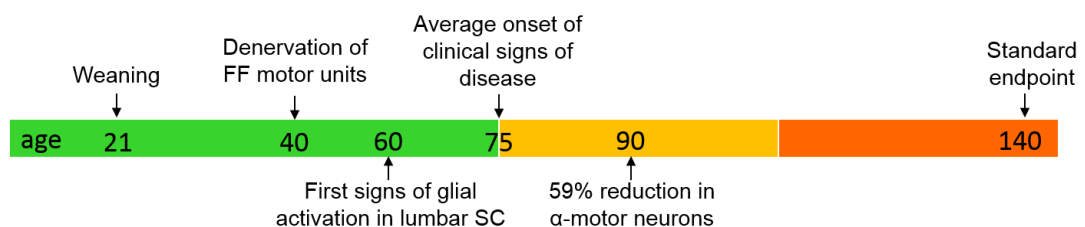


**Figure 1.2. The disease course of our *SOD1* mouse model**

At ~40 days of age the mice demonstrate a large decline in motor performance compared with non-transgenic mice which is thought to correspond to the denervation of fast fatigable motor units (Mead et al. 2011). The decline in motor performance observed for the transgenic mice compared to the non-transgenic mice at ~40 days of age provides an early readout on rotarod for testing therapeutics early on in the disease course.

At 60 days of age the ventral horns of lumbar spinal cord sections show an increase in glial activation compared to non-transgenic mice. By 90 days of age there is ~5-fold increase in astrocyte activation in the ventral horns of the transgenic (unpublished data). In addition, at 90 days of age there is ~60% reduction in alpha motor neurons within the ventral horns of lumbar spinal cord (Kirby et al. 2018). The average onset of clinical signs of disease is ~75D of age and this is defined by the presence of a hind-limb tremor in combination with a hind-limb splay defect (Mead et al. 2011). Finally, the standard end-point in our mouse model is 140 days of age. The following table compares the key differences in phenotype between our *SOD1* mouse model and the G1H (H for high copy number), the progeny of the original G1 Gurney *SOD1* transgenic mouse line (Table 1.4).

**Table 1.4. Comparison between our *SOD1* mouse model and the original G1H *SOD1* mouse model**

Phenotype	G1H mixed SJLxC57BL/6 <i>SOD1</i> <sup>G93A</sup> mouse model (Tu et al. 1996)	Inbred C57BL/6 <i>SOD1</i> <sup>G93A</sup> mouse model (Mead et al. 2011)
<i>SOD1</i> <sup>G93A</sup> transgene copy number	~25 copies	~23 copies
Onset of clinical signs of disease	~90 days of age	~75 days of age
Astrocyte activation in ventral horn of lumbar SC	Observed at ~82 days of age and beyond	Observed between 60-90 days of age
Motor neuron loss in ventral horn of lumbar SC	~50% reduction by end-stage	~60% reduction in α-motor neurons at 3 months of age
Standard end-point	~145 days of age (gender variation due to background)	~140 days of age (no significant gender variation)

### 1.1.13 MND Mouse Models

Transgenic mice overexpressing the human *SOD1* mutation were the first models of MND to be developed after mutations in the *SOD1* gene were found to be associated with MND (Gurney et al. 1994). Mice with multiple copies of the mutant *SOD1* transgene develop adult onset neurodegeneration of spinal motor neurons and progressive motor deficits that ultimately leads to paralysis (Gurney et al. 1994). Copy number expression of the transgene and genetic background have been shown to significantly affect the severity and onset of the disease (Heiman-Patterson et al. 2011; Mancuso et al. 2012). Mice that express high copy numbers (~25 copies) of the transgene (G1H) have a much more aggressive disease course than the original G1 transgenic line which express ~18 copies of the transgene (Chiu et al. 1995).

Whilst the *SOD1*<sup>G93A</sup> mouse model is the most widely used *in vivo* model of MND, alternative *SOD1* mouse lines and mouse lines modelling other MND causative genes have also been generated. The table below gives an overview of some of the other mouse models of MND (Table 1.5).

**Table 1.5. Other mouse models of MND**

MND Mouse model	Phenotype	Pathology	Reference
Human <i>SOD1</i> <sup>G37R</sup> transgenic	+++	+++	Wong et al. 1995
Human <i>SOD1</i> <sup>WT</sup> transgenic	+	none	Lino et al. 2002
Mouse <i>SOD1</i> <sup>D83G</sup> mutation	++	++	Joyce et al. 2015
Mouse <i>SOD1</i> <sup>G85R</sup> mutation	+++	+++	Bruijn et al. 1997
Human <i>TDP-43</i> <sup>A315T</sup> transgenic	++	+++	Wegorzewska et al. 2009
Human <i>TDP-43</i> <sup>M337V</sup> transgenic	+++	+++	Arnold et al. 2013
Human <i>TDP-43</i> <sup>Q331K</sup> transgenic	++	++	Arnold et al. 2013
Conditional human <i>TDP-43</i> ΔNLS knockout	+++	+++	Walker et al. 2015
Human (G <sub>4</sub> C <sub>2</sub> ) <sub>500</sub> repeat expansion transgenic	none	++	Peters et al. 2015
Human (G <sub>4</sub> C <sub>2</sub> ) <sub>100-1000</sub> repeat expansion transgenic	none	++	O'Rourke et al. 2015
Endogenous (G <sub>4</sub> C <sub>2</sub> ) <sub>66</sub> repeat expansion	++	+++	Chew et al. 2015
Human (G <sub>4</sub> C <sub>2</sub> ) <sub>450</sub> repeat expansion transgenic	++	++	Jiang et al. 2016
Human (G <sub>4</sub> C <sub>2</sub> ) <sub>37-500</sub> repeat expansion transgenic	+++	+++	Lieu et al. 2016

+ a few features of MND, ++ several features of MND, +++ most features of MND

## 1.2 G-Protein Coupled Receptors

G-Protein-Coupled Receptors (GPCRs) are the largest family of cell surface receptors in eukaryotes (Lagerström & Schiöth 2008). They are expressed in every cell type of the human body and are implicated in a variety of physiological processes (Lin 2013). Consequently, they are thought to play an important role in a broad spectrum of diseases.

These membrane receptors are crucial for cell-to-cell communication. Instead of activating ion channels directly, GPCRs stimulate G-proteins which results in the production of second messenger signalling proteins (Rang et al. 2007). A diverse range of extracellular stimuli bind to GPCRs including neurotransmitters, hormones, photons, peptides and proteins (Venkatakrisnan et al. 2013). Interaction with a ligand induces a conformational change in the receptor, stimulating an associated G-protein (or similar membrane bound protein), which in-turn activates intracellular signalling pathways. Of note, G-proteins are the predominant trigger for these intracellular mechanisms.

GPCRs are characterised by an extracellular N-terminus, a seven transmembrane (7TM) domain of  $\alpha$ -helices and an intracellular C-terminus (Lin 2013). The 7TM structure comprises three extracellular loops and three intracellular loops. The third intracellular loop is slightly larger than the other two and forms the site at which the G-protein binds to the GPCR (Rang et al. 2007). G-proteins are heterotrimeric, consisting of an alpha subunit, a beta subunit and a gamma subunit (Figure 1.2).

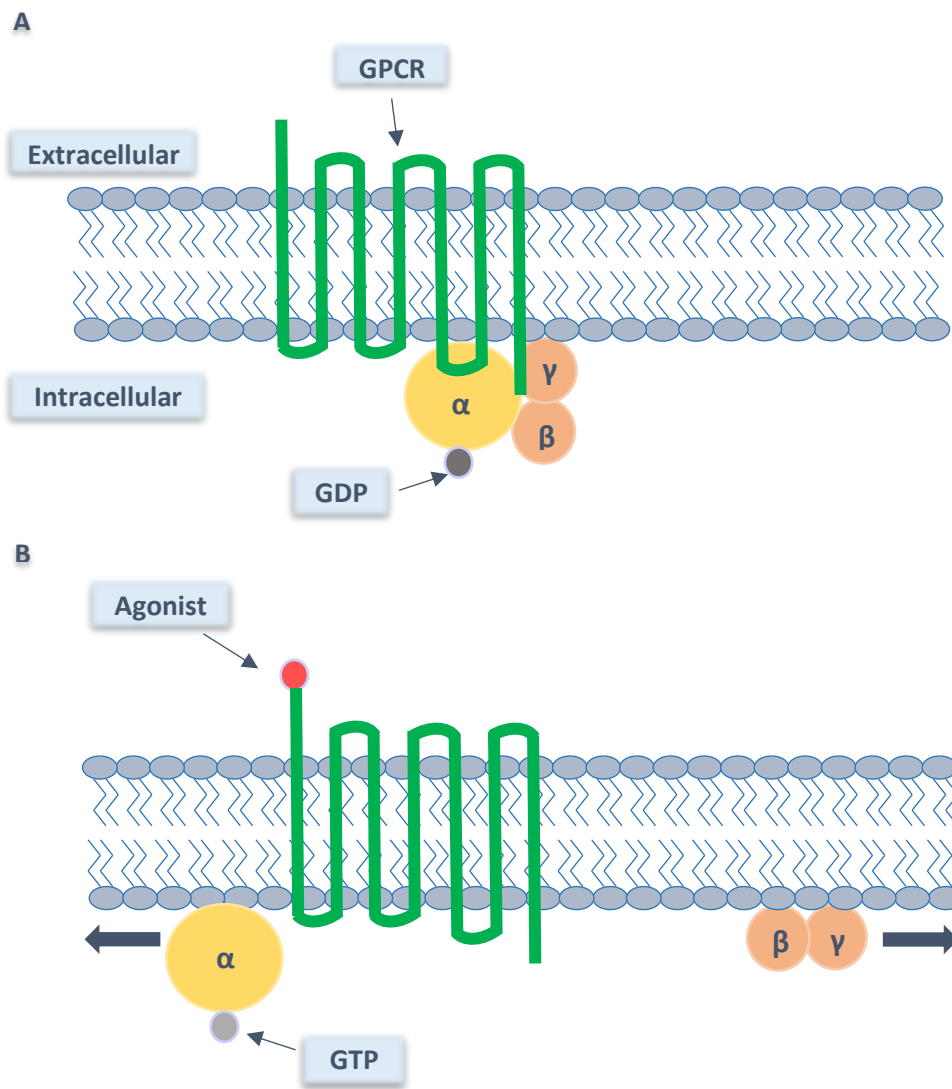


**Figure 1.3. Interaction between GPCR and G-Protein**

*Source: Adapted from Rang et al, 2007*

At rest, the G-protein associates with a GPCR and guanosine diphosphate (GDP) is bound to the alpha subunit (A). When an agonist binds to the GPCR, the G-protein becomes activated and guanosine triphosphate (GTP) replaces GDP on the alpha subunit. The G-protein dissociates from the GPCR and splits into a GTP bound alpha subunit and a beta/gamma dimer. These two parts of the G-protein diffuse laterally in the plane of the membrane to activate other membrane bound proteins (B). Finally,

hydrolysis of the GTP back to GDP terminates their activity and the G-protein subunits re-associate to form a heterotrimer, attached to a now inactive GPCR.

There are three major GPCR subfamilies:

- class I (family A or rhodopsin-like receptors)
- class II (family B or secretin receptors)
- class III (family C or metabotropic glutamate receptors)

The 7TM  $\alpha$ -helical structure along with the mechanism of signal transduction are common features of all GPCRs. However, there is a lack of sequence homology between classes (Rang et al. 2007). For example, the length of the extracellular N-terminus and the location of the agonist binding site both differ. The class I receptors are the largest GPCR subfamily and are characterised by a short extracellular N terminus. This receptor has ligand binding domains within both the 7TM structure and the extracellular loops. Ligands that bind to this receptor type include amine neurotransmitters, purines, prostaglandins and peptides. In contrast, the class II receptors have a longer glycosylated N-terminal which contains a ligand binding domain. This subgroup is activated by large peptide hormones such as secretin and glucagon. Class III is the smallest GPCR subfamily. These receptors are characterised by a very long extracellular N terminal, which also incorporates a ligand binding domain. This group includes the metabotropic glutamate receptors, GABA<sub>B</sub> receptors and Ca<sup>2+</sup> sensing receptors.

### **1.2.1 GPCRs as a Therapeutic Target in MND**

GPCRs have been associated with many diseases and at present, approximately 30% of available drugs target this receptor family (Zalewska et al. 2014). Clearly, GPCRs are a major druggable class of receptors. Previously, the instability of this receptor class when removed from the cell membrane limited the progress of GPCR structure based drug discovery (SBDD) (Andrews et al. 2014). However, the innovative StaR® (stabilised receptor) technology pioneered by Heptares Therapeutics enables purification of GPCRs in detergent allowing the receptor to be crystallised to determine the structure via X ray crystallography. The protein can also be used in biophysical methods such as surface plasmon resonance. This provides a platform from which the SBDD technique can be applied to biologically relevant GPCRs. This approach enables the design of small molecule therapeutics directed at previously undruggable GPCRs. Applied to the field of neurodegeneration, this

technology facilitates the use of high quality pharmacological tools in order to dissect the role of specific GPCRs in the disease process of MND.

### **1.3 Glutamate Receptors**

Glutamate is the most widely expressed amino acid in the human body and the main excitatory neurotransmitter in the CNS, involved in most physiological brain functions (Alexander 2009). Its main purpose is to produce post-synaptic excitation of neural cells and it mediates this action through binding to and activating glutamate receptors. There are two main classes of glutamate receptors (Table 1.4), ionotropic glutamate receptors and metabotropic glutamate receptors (Nakanishi 1992). The main differences between these two classes of receptor is that whilst ionotropic receptors are ligand-gated ion channels that are activated directly when glutamate binds, metabotropic receptors (GPCRs) mediate their response to glutamate binding by indirectly activating ion channels through downstream intracellular signalling pathways. Consequently, ionotropic receptors tend to produce fast excitatory neurotransmission whereas metabotropic receptors have a slower modulatory effect on excitatory neurotransmission and are typically associated with a more prolonged response (Nakanishi 1992).

**Table 1.6. Glutamate receptors**

Ionotropic Receptors	Transduction	Signalling	Expression	Function
<b>AMPA Receptors</b>	Single channel receptors that rapidly desensitise in the presence of glutamate. Affinity for glutamate is relatively low compared with NMDA receptors	High permeability to Na <sup>2+</sup> ions. Permeability to Ca <sup>2+</sup> controlled by GluR2 subunit. Channels containing GluR2 are impermeable to Ca <sup>2+</sup> , those lacking GluR2 are Ca <sup>2+</sup> permeable	Widely expressed in CNS in all neuronal types and glia	Mediate majority of fast excitatory synaptic transmission in the CNS
<b>Kainate Receptors</b>	Single channel receptors. Activated by glutamate and have a similar conductance to AMPA receptors. However, postsynaptic potentials generated are slightly slower than that of AMPA receptors.	Similar to AMPA receptors these ion channels have high permeability for Na <sup>2+</sup> ions and lower permeability for Ca <sup>2+</sup> ions	Widely expressed throughout the brain.	Mediate fast excitatory synaptic transmission. Presynaptically modulate excitatory and inhibitory transmission. Postsynaptically regulate neuronal excitability. Produce small but prolonged effects.
<b>NMDA Receptors</b>	Single channel receptors. Requires two agonists for activation (glutamate and either glycine or D-Serine)	Ligand gated ion channel- opening depends on a change in voltage across the membrane dislodging Mg <sup>2+</sup> or Zn <sup>2+</sup> from blocking the channel. This allows Na <sup>2+</sup> and a small amount of Ca <sup>2+</sup> to flow in whilst K <sup>+</sup> flows out of the cell	Expressed throughout the brain and SC on neurons and glia	Mediate slow excitatory response. Usually glutamate transmission starts with a fast response generated by AMPA receptors which depolarise membranes enabling activation of NMDA receptors

Metabotropic Receptors		Transduction	Signalling	Expression	Function
Group 1	mGlu <sub>1</sub>	Seven transmembrane domains that span the cell membrane. Contain an orthosteric binding site where the endogenous ligand (glutamate) binds. Also contain allosteric binding sites where effector molecules bind	Couple to G <sub>q/11</sub> which activates phospholipase C (PLC), increasing the turnover of phosphoinositide causing the release of intracellular calcium stores	Abundantly expressed throughout the brain and SC. Predominantly postsynaptic although mGlu <sub>5</sub> autoreceptors are presynaptically expressed and facilitate glutamate release	These receptors modulate rather than mediate excitatory neurotransmission. Role is to potentiate fast excitatory synaptic transmission
	mGlu <sub>5</sub>				
Group 2	mGlu <sub>2</sub>		Couple to G <sub>i</sub> /G <sub>o</sub> and inhibit adenylyl cyclase (AC) which results in activation of K <sup>+</sup> channels and inhibition of Ca <sup>2+</sup> channels	Abundantly expressed throughout the brain and SC. Postsynaptic and presynaptic	Broadly responsible for decreasing cell excitability by inhibiting glutamate release from pre-synaptic terminals
	mGlu <sub>3</sub>				
Group 3	mGlu <sub>4</sub>		Couple to G <sub>i</sub> /G <sub>o</sub> and inhibit adenylyl cyclase (AC) which results in activation of K <sup>+</sup> channels and inhibition of Ca <sup>2+</sup> channels )	Abundantly expressed throughout the brain and SC. Predominantly presynaptic	Broadly responsible for decreasing cell excitability by inhibiting glutamate release from pre-synaptic terminals
	mGlu <sub>6</sub>				
	mGlu <sub>7</sub>				
	mGlu <sub>8</sub>				

Sources: Conn & Pin., 1997; Rang et al., 2007 ; Gereau & Swanson., 2008

### 1.3.1 Metabotropic Glutamate Receptors

The metabotropic glutamate receptors are members of subclass C within the GPCR family. There are eight different types of metabotropic glutamate receptors (mGlu<sub>1-8</sub>) and they are subdivided into three groups, based on sequence homology, signal transduction and pharmacology (Pin et al. 2003). Group I (mGlu<sub>1</sub> and mGlu<sub>5</sub>) are coupled to phospholipase C (PLC) and intracellular calcium signalling, whilst group II (mGlu<sub>2</sub> and mGlu<sub>3</sub>) and group III (mGlu<sub>4</sub> and mGlu<sub>6-8</sub>) are negatively coupled to adenylyl cyclase activity (Conn & Pin 1997). Unlike class II and III GPCRs, metabotropic glutamate receptors have a unique extracellular structure consisting of a 'venus fly trap' (VFT) domain; this is the site at which glutamate binds (Conn & Pin 1997).

### 1.3.2 Metabotropic Glutamate Receptor 5

Metabotropic glutamate receptor 5 (mGlu<sub>5</sub>) is a member of the group I metabotropic glutamate receptor subclass and demonstrates preferential coupling to the G<sub>q/11</sub> family of G-proteins (Conn & Pin 1997). Binding of glutamate to mGlu<sub>5</sub> activates the phospholipase C (PLC) cascade whereby phosphatidylinositol-4,5-bisphosphate (PIP<sub>2</sub>) is hydrolysed into diacylglycerol (DAG) and inositol-1,4,5-triphosphate (IP<sub>3</sub>). Increases in DAG activate protein kinase C (PKC) enzymes whilst IP<sub>3</sub> is responsible for mobilising intracellular stores of Ca<sup>2+</sup> ions (Abe et al. 1992; Pin et al. 1992; Joly et al. 1995; Watabe et al. 2002).

The mGlu<sub>5</sub> receptor has an orthosteric binding site on the VFT domain (where the endogenous ligand glutamate binds) and two distinct allosteric binding sites. The allosteric sites are non-competitive ligand binding sites in the transmembrane domain (TMD) of the receptor (Doré et al. 2014). A characteristic of mGlu<sub>5</sub> receptors is that they exist as dimers through an interaction between the VFT domain and the TMD (Figure 1.3) (Morikawa et al. 2000).

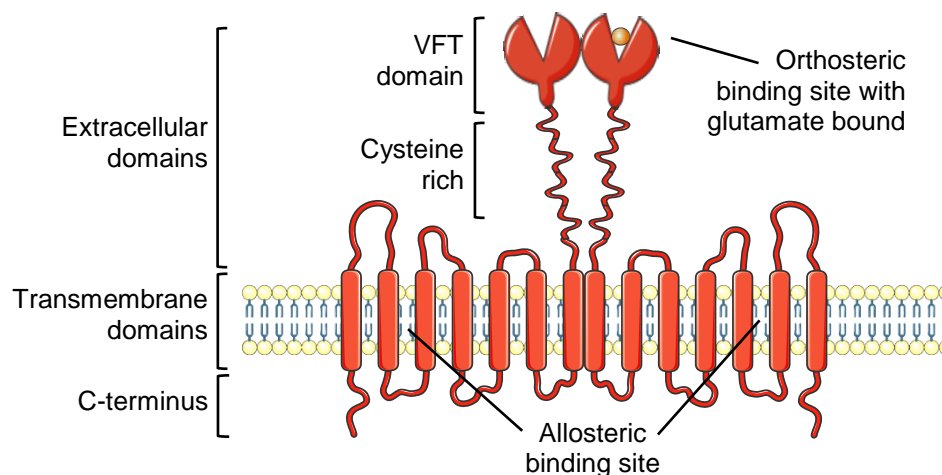


**Figure 1.4. The structure of the mGlu<sub>5</sub> receptor and its binding sites**

These receptors are expressed both pre and post-synaptically (Musante et al. 2008), and are abundantly expressed throughout the CNS, especially in adult hippocampus, corpus striatum and cerebral cortex (Romano et al. 1996). In addition to neurons, mGlu<sub>5</sub> receptors are also found on astrocytes, microglia and oligodendrocytes. Interestingly, astrocytic expression of mGlu<sub>5</sub> is highly variable and is modified in response to alterations in cell activation state and under pathological conditions (Miller et al. 1996; Balázs et al. 1997; Aronica et al. 2000; Geurts et al. 2003).

### **1.3.3 Metabotropic Glutamate Receptor 5 (mGlu<sub>5</sub>) involvement in Human Diseases**

There is considerable evidence linking mGlu<sub>5</sub> to several different human diseases with varying beneficial effects demonstrated by modulating the activity of this receptor. Previous drug discovery screening focused on the orthosteric binding site of mGlu<sub>5</sub> have demonstrated that compounds targeting this binding site are often associated with poor pharmacological profiles (Bennett et al. 2015). However, efforts targeting allosteric binding sites (Emmitte 2011; Emmitte 2013), located within the TMD, have had more success.

Until recently, mGlu<sub>5</sub> negative allosteric modulators (NAMs) were being tested for therapeutic use in Fragile X syndrome (FXS). This disorder is the major inherited cause of intellectual disability and autism (Garber et al. 2008). FXS is caused by the silencing of the fragile X mental retardation 1 (FMR<sub>1</sub>) gene which results in a lack of expression of the fragile X mental retardation protein (FMRP) (Verkerk et al. 1991).

The 'mGlu<sub>5</sub> theory' in FXS hypothesises that the absence of FMRP results in elevated glutamatergic activity mediated by mGlu<sub>5</sub> (Bear et al. 2004). Preclinical studies aimed at reducing mGlu<sub>5</sub> mediated glutamate signalling by using mGlu<sub>5</sub> NAMs such as mavoglurant, dipraglurant and fenobam were encouraging (Cole 2012). However, interestingly Novartis and Roche have now discontinued their FXS drug development programs which used mGlu<sub>5</sub> antagonists (Mullard 2015).

Excessive glutamate activity in the basal-ganglia is one of the pathophysiological mechanisms implicated in Parkinson's disease (PD) and L-DOPA-induced dyskinesia (PD-LID). The high expression of metabotropic glutamate receptor 5 (mGlu<sub>5</sub>) in the basal-ganglia make this receptor an attractive therapeutic target for modulating increased glutamatergic neurotransmission in PD. Of note, mGlu<sub>5</sub> NAMs have shown good efficacy in pre-clinical models of both PD and PD-LID (Berg et al. 2011; Tison et al. 2016). Currently, the mGlu<sub>5</sub> negative allosteric modulator, dipraglurant, is in clinical development for the treatment of PD-LID.

Furthermore, whilst there is compelling evidence to suggest that mGlu<sub>5</sub> NAMs may hold promise in the treatment of chronic pain, drug addiction and anxiety; mGlu<sub>5</sub> positive allosteric modulators (PAMs) could provide a novel approach for the treatment of schizophrenia (Nicoletti et al. 2011).

#### **1.4 Glutamate-Mediated Excitotoxicity**

The term excitotoxicity was first introduced in 1969 by John Olney when he demonstrated that glutamate induced neuronal necrosis in immature mouse brains (Olney 1969). Following on from this, *in vivo* studies have demonstrated that inhibiting glutamate receptor activity in cases of ischaemic brain damage has a neuroprotective effect (Schwarcz et al. 1983; Ozyurt et al. 1988). It is now widely accepted that glutamate-mediated-excitotoxicity contributes to neuronal cell death in both acute CNS injury and chronic neurodegenerative diseases, including MND (Meldrum & Garthwaite 1990).

The major excitatory neurotransmitter in the mammalian CNS is glutamate which exerts its effect through binding to both ionotropic and metabotropic glutamate receptors (Arundine & Tymianski 2003). Glutamate-mediated excitotoxicity is a pathological process whereby excess levels of extracellular glutamate activate excitatory glutamate receptors, resulting in cell death. Most glutamate receptors have been shown to play a role in mediating this neurotoxicity, predominantly through calcium-dependent mechanisms (Choi 1985; Choi 1987; Choi 1995). However, the

ionotropic glutamate receptor, NMDA and group I metabotropic glutamate receptors (mGlu<sub>1</sub> and mGlu<sub>5</sub>) are considered to be the main contributors to glutamate-mediated cell death (Orlando et al. 2001) .

Whilst activation of ionotropic glutamate receptors results in increased permeability to sodium, potassium and calcium ions, activation of metabotropic glutamate receptors stimulate associated G-proteins and the production of secondary messenger signals which mobilise the release of calcium ions from internal stores (Arundine & Tymianski 2003). Therefore, the influx of extracellular calcium ions and release of calcium ions from intracellular stores both contribute to increases in cytosolic calcium ion concentrations (Dennis W. Choi 1988a). Overstimulation of glutamate receptors results in an excessive influx of calcium ions. This disrupts the cell's capacity to maintain calcium homeostasis and subsequently culminates in glutamate-mediated cell death (D W Choi 1988b; Tymianski & Tator 1996; Sattler & Tymianski 2000). Whilst inhibiting ionotropic glutamate receptors has been shown to have adverse clinical side effects, it is thought that compounds targeting metabotropic glutamate receptors may have more success in the clinic as they are responsible for modulating glutamate transmission, having only a modest effect on fast excitatory neurotransmission, (Bruno et al. 2001). This may be an advantage for diseases such as MND, where therapeutic treatment is likely to be long term.

#### **1.4.1 Glutamate-Mediated Excitotoxicity in MND**

One of the pathogenic mechanisms underlying MND is glutamate-mediated excitotoxicity (Heath & Shaw 2002; Van Den Bosch et al. 2006). Despite MND being a heterogeneous disease, glutamate-mediated excitotoxicity is thought to play an important role in all cases of MND, however the evidence for this is indirect. For example, the only drug that has been shown to modestly prolong survival in MND is riluzole and it is considered to exert its therapeutic effect through the indirect antagonism of glutamate transmission (Lacomblez et al. 1996b; Kretschmer et al. 1998; Bellingham 2011).

In the context of MND, excitotoxicity is thought to result from a combination of glutamate receptor overstimulation and a failure to rapidly remove glutamate from the synapse. Of note, glutamate levels are elevated in the CSF of a subset of MND patients (Shaw et al. 1994; Shaw et al. 1995; Spreux-Varoquaux et al. 2002; Rothstein et al. 1991). Synaptic glutamate levels are regulated by glial and neuronal glutamate re-uptake transporters when levels reach and exceed a threshold. The major glutamate reuptake transporter in the mammalian brain is the excitatory amino

acid transporter 2 (EAAT2/GLT-1) protein. This astroglial protein is responsible for the rapid removal of synaptic glutamate and clears at least 90% of glutamate from the synapse. Interestingly, it has been demonstrated in both familial and sporadic patients with MND and rodent models of MND that expression and function of the EAAT2 transporter is impaired (Rothstein et al. 1995; Fray et al. 1998; Bendotti et al. 2001).

Furthermore, changes to ionotropic AMPA receptors could, in part, account for the degeneration of motor neurons in MND. These receptors are responsible for mediating a large proportion of the fast-excitatory glutamatergic neurotransmission in the CNS. The permeability of AMPA receptors to calcium is determined by the presence of the GluR2 subunit (Hollmann et al. 1991). Whilst expression of the GluR2 subunit ensures that AMPA receptors remain impermeable to calcium, a lack of GluR2 renders these receptors permeable to calcium. Consequently, motor neurons that express calcium permeable AMPA receptors are more vulnerable to glutamate-mediated excitotoxicity. Under physiological conditions astrocytes have been shown to positively regulate GluR2 subunit expression of AMPA receptors on motor neurons, controlling the receptors' permeability to calcium ions (Van Damme et al. 2007). Interestingly, astrocytes expressing mutant *SOD1* were found to lose their ability to maintain calcium homeostasis within motor neurons. For example, motor neurons in the vicinity of astrocytes expressing mutant *SOD1* displayed a higher level of AMPA receptors lacking the GluR2 subunit. The absence of this subunit increased the motor neurons' permeability to calcium ions and as a result increased their vulnerability to glutamate toxicity (Van Damme et al. 2007). This shows that non-neuronal cells also play an important role in MND disease pathogenesis demonstrating that MND is clearly a non-cell autonomous disease.

### **1.5 Role of Glial Cells in MND**

Glial cells such as astrocytes and microglia are neural cells responsible for maintaining CNS homeostasis (Heneka et al. 2010). Whilst astrocytes provide trophic support to surrounding neurons, microglia are largely considered the brain's resident immune cell (Lasiene & Yamanaka 2011). However, it is now widely recognised that glia cells are involved in a great deal more than just regulating structural and metabolic processes. For example, astrocytes are considered to play an important role in the processing, transfer and storage of information in the CNS (Perea et al. 2009). The term 'tripartite synapse' was established in 1999 to conceptualise the notion that astrocytes communicate with neurons in a bidirectional manner (Araque

et al. 1999). Astrocytes express receptors for neurotransmitters found in their surrounding area (Verkhatsky et al. 1998). This enables astrocytes to respond to neural activity and in turn release gliotransmitters which can activate neuronal receptors to bring about a response (Rossi & Volterra 2009a). Consequently, in pathological conditions such as MND it is perhaps not surprising that astrocytes too become vulnerable to excessive glutamate concentrations and also undergo glutamate-mediated cell death (Rossi & Volterra 2009a).

Despite MND being considered primarily as a motor neuron disorder, there is convincing evidence to suggest that non-neuronal cells within the microenvironment of motor neurons are involved in the pathogenesis and/or propagation of the disease (Gonzalez-Scarano & Baltuch 1999; L H Barbeito et al. 2004). For example, both astrogliosis and microgliosis are pathological hallmarks of MND, with glial activation correlating with regions of motor neuron cell death, both in human MND and mouse models (Hall et al. 1998; Alexianu et al. 2001b; Turner et al. 2004; Alshikho et al. 2018). The precise mechanisms by which glial cells contribute to motor neuron degeneration have not been fully determined. However, it is thought that glial cells could cause damage to motor neurons both directly, by releasing factors selectively toxic to motor neurons and indirectly through the loss of their physiological functions (Nagai et al. 2007; Di Giorgio et al. 2008; Van Damme et al. 2007; Xiao et al. 2007; Ferraiuolo et al. 2011a). Whilst this evidence has been largely generated from *SOD1* mouse models of MND, it has also been shown that post-mortem derived SC astrocytes from patients with both familial and sporadic MND are toxic towards motor neurons (Haidet-Phillips et al. 2011). Furthermore, it has been found that fibroblast derived astrocytes from patients with both familial and sporadic MND demonstrate toxicity towards motor neurons (Meyer et al. 2014). The finding that both post-mortem and fibroblast derived astrocytes from sporadic MND patients are equally as toxic to motor neurons as derived astrocytes from familial patients would suggest that the mechanism of non-neuronal toxicity towards motor neurons is a common theme across the spectrum of MND (Haidet-Phillips et al., 2011; Meyer et al., 2014).

Studies in genetic and chimeric mice have provided additional evidence in support of a role for non-neuronal cells in the propagation of disease in MND. Whilst Gurney et al. (1994), demonstrated that ubiquitous expression of high levels of the mutated human *SOD1* gene causes MND in transgenic mice, it has been shown that expression of mutant human *SOD1* in motor neurons alone is not adequate to cause motor neuron degeneration (Pramatarova et al. 2001; Lino et al. 2002). Interestingly, wild-type motor neurons in chimeric mice with both wild-type and mutant *SOD1*

expressing cells were shown to develop aspects of MND pathology when surrounded by non-neuronal cells expressing mutant *SOD1*. In addition, wild-type non-neuronal cells were found to delay degeneration and extend survival of mutant *SOD1* expressing motor neurons (Clement et al. 2003). This clearly demonstrates that mutant *SOD1* toxicity within non-neuronal cells is an important contributor to MND pathogenesis.

The differential contribution of mutant *SOD1* damage within motor neurons and non-neuronal cells in initiating disease onset and progression of disease has also been investigated using experiments on mice carrying a Cre-lox deletable mutant *SOD1* gene (Boillée et al. 2006a; Ilieva et al. 2009). Deletion of mutant *SOD1* from mouse motor neurons was found to delay disease onset but had no effect on disease progression after onset (Boillee et al. 2006a). Conversely, deletion of mutant *SOD1* from mouse microglial cells delayed later phases of the disease yet had no effect on disease onset (Boillee et al. 2006a). Of note, deletion of mutant *SOD1* from mouse astrocytes delayed disease progression and doubled the length of disease duration after onset (Yamanaka et al., 2008). However, there was conflicting evidence regarding its involvement in initiating disease onset. Whilst Yamanaka et al. (2008) demonstrated that a lack of mutant *SOD1*<sup>G37R</sup> expression in astrocytes did not affect disease onset, Wang et al. (2011), showed that restriction of a different mutant *SOD1* variant (*SOD1*<sup>G85R</sup>), delayed both MND disease onset and progression (Wang et al., 2011; Yamanaka et al., 2008). Interestingly, selective reduction of mutant *SOD1*<sup>G37R</sup> in astrocytes was found to delay microglial activation. This finding suggests that there must be some cross-talk between mutant glial cells (Yamanaka et al., 2008). To summarise, mutant *SOD1* expression in non-neuronal cells such as astrocytes and microglia must clearly play an important role in driving disease progression after disease onset.

## **1.6 Metabotropic Glutamate Receptor 5 (mGlu<sub>5</sub>) as a therapeutic target for MND**

There is accumulating evidence to suggest that mGlu<sub>5</sub> plays a role in the pathophysiology of MND and consequently this receptor may represent a novel therapeutic target for MND. mGlu<sub>5</sub> is a glutamate receptor and as mentioned previously glutamate-mediated excitotoxicity is a recognised mechanism of both neuronal and astrocyte injury in MND. It is well documented that mGlu<sub>5</sub> receptors modulate the activity of fast excitatory receptors like NMDA and AMPA receptors and consequently it is possible that therapeutic blockade of mGlu<sub>5</sub> could demonstrate a

more prolonged effect for counteracting glutamate-mediated excitotoxicity (Bruno et al. 2017).

Evidence suggests that MND is a non-cell autonomous disease characterised by a pathological interplay between motor neurons and their surrounding glial cells (Boillee et al., 2006b; Yamanaka et al., 2008). Astroglial activation is a pathological hallmark of MND, with astrocyte activation being shown to localise to regions of motor neuron cell death, both in animal and human cases of MND. (Boillee et al. 2006a; Yamanaka et al. 2008). In human MND patients, both group I and II mGlu receptors were found to be upregulated on reactive astrocytes of post-mortem SC sections compared to that of healthy controls; mGlu<sub>5</sub> was most upregulated, followed by mGlu<sub>1</sub> and then mGlu<sub>3</sub> (Aronica et al. 2001; Anneser 2004). Furthermore, mGlu<sub>5</sub> expression was found to parallel the degree of astroglial activation in MND patient SC sections perhaps indicating a link between elevated mGlu<sub>5</sub> expression and astrocyte activation.

Of note, when CSF from MND patients was added to chick astroglial cultures *in vitro* this increased their proliferation rate compared to CSF added from controls. Interestingly, the group I metabotropic glutamate receptor antagonist, AIDA, demonstrated a significant reduction in the number of proliferating cells. This suggests that mGlu<sub>5</sub> activation is implicated in astrocyte proliferation in MND (Anneser 2004).

The expression of mGlu<sub>5</sub> on activated astrocytes has also been shown to be upregulated in a rodent model of MND. For example, SC astrocytes from end-stage *SOD1<sup>G93A</sup>* rats demonstrated much higher levels of mGlu<sub>5</sub> than controls (Vermeiren et al. 2006). The functional significance of increased mGlu<sub>5</sub> levels on reactive astrocytes was investigated by D'Antoni et al. (2011), using an *in vitro* assay. Rat spinal cord motor neurons were co-cultured with rat spinal cord astrocytes displaying a reactive phenotype, in order to measure the protective effect of the mGlu<sub>5</sub> antagonist, MPEP, against excitotoxic damage towards motor neurons. The findings from this study demonstrated that therapeutic blockade of mGlu<sub>5</sub> *in vitro* reduced AMPA-mediated glutamate toxicity and protected spinal cord motor neurons against excitotoxic degeneration (D'Antoni et al. 2011). Interestingly, it was found that the protective effect of MPEP was absent in cultures with fewer numbers of astrocytes. This suggests that the toxicity exhibited by the activated astrocytes towards the motor neurons is mediated by astrocytic mGlu<sub>5</sub> activity (D'Antoni et al. 2011).

Of note, there is conflicting evidence in the literature regarding mGlu<sub>5</sub> receptor level changes throughout the disease course of the *SOD1<sup>G93A</sup>* transgenic mouse model of

MND. Whilst Martorana et al. (2012), found that mGlu<sub>5</sub> mRNA levels were elevated at 30 days compared to 100 days in lumbar SC tissue, Brownell et al. (2015), observed by *in vivo* PET imaging that mGlu<sub>5</sub> levels increased throughout the disease trajectory in SC and across several brain areas (hippocampus, striatum, cortex and whole brain). Indeed, the discrepancy between these findings in SC may reflect the different techniques used to detect mGlu<sub>5</sub> expression changes. For example, the mGlu<sub>5</sub> mRNA levels measured in SC do not directly inform on the levels of expressed mGlu<sub>5</sub> in SC and consequently may account in part for the inconsistency in these two findings.

Furthermore, it has been suggested that mGlu<sub>5</sub> expression is developmentally regulated in human and murine astrocytes. Whilst astrocytic mGlu<sub>5</sub> is expressed during early development (up to post-natal week 3), its expression is undetectable in adult murine cortical and hippocampal astrocytes or in human cortical astrocytes (Wei Sun et al. 2013). Although this finding has been disputed by others, it is possible that the increased mGlu<sub>5</sub> expression observed on activated SC astrocytes during adulthood in both human and rodent cases of MND is a disease-specific feature.

Additional work investigating the effects of increasing the concentration of the mGlu<sub>1</sub> and mGlu<sub>5</sub> receptor agonist, 3,5 -DHPG, on glutamate release was carried out in synaptosomes of *SOD1*<sup>G93A</sup> mice lumbar SC and compared to that of control mice (Giribaldi et al. 2013). It was found that glutamate was detectable in *SOD1*<sup>G93A</sup> mice at much lower concentrations of 3,5 -DHPG than in control mice. Whilst the abnormal glutamate release observed in the synaptosomes of *SOD1*<sup>G93A</sup> mice was shown to be mediated by both mGlu<sub>1</sub> and mGlu<sub>5</sub> receptors at higher concentrations of 3,5 -DHPG, at the lower concentrations it was mostly mediated by mGlu<sub>5</sub>. For example, at the lower concentrations of 3,5 -DHPG abnormal glutamate release could be mostly prevented using mGlu<sub>5</sub> antagonists. However, mGlu<sub>1</sub> antagonists did not produce the same effect (Giribaldi et al. 2013). This suggests that the abnormal release of glutamate in *SOD1*<sup>G93A</sup> mice is mediated predominantly by mGlu<sub>5</sub> receptors.

It has also been demonstrated *in vitro* that cultured astrocytes expressing mutant h*SOD1*<sup>G93A</sup> and h*SOD1*<sup>G85R</sup> are much more vulnerable to glutamate than wild-type astrocytes (Rossi et al. 2008). For example, mutant *SOD1* expressing astrocytes were found to degenerate in response to moderate increases in glutamate levels which in contrast were not detrimental to wild-type astrocytes. Interestingly, the glutamate-mediated degeneration of mutant *SOD1* expressing astrocytes was shown to be mediated by mGlu<sub>5</sub> (Rossi et al. 2008). Following on from this an *in vivo* study

demonstrated that inhibiting mGlu<sub>5</sub> with MPEP delayed motor decline and extended survival in the *SOD1<sup>G93A</sup>* mouse model of MND (Rossi et al. 2008). Of note, it was reported that MPEP exerted its therapeutic effect through blocking mGlu<sub>5</sub> activity, reducing glutamate-mediated toxicity which in turn slowed down astrocyte degeneration (Rossi et al. 2008). Whilst this study provides convincing evidence in support of mGlu<sub>5</sub> as a novel therapeutic target for MND, there are limitations associated with MPEP such as its non-specific actions. For example, not only is MPEP a negative allosteric modulator of mGlu<sub>5</sub> but it is also a weak NMDA antagonist and a positive allosteric modulator of the mGlu<sub>4</sub> receptor at high concentrations (Lea et al. 2009; Mathiesen et al. 2003).

More recently it has been shown that heterozygous knockdown of the mGlu<sub>5</sub> receptors in *SOD1<sup>G93A</sup>* mice delayed clinical onset of disease, reduced motor neuron death, reduced microglia and astrocyte activation and prolonged survival (Bonifacino et al. 2017). Interestingly, this study demonstrated an improvement in motor function only within male *SOD1<sup>G93A</sup>Grm5<sup>+/-</sup>* mice. This gender difference was thought to be related to the B6SJL mixed genetic background that the *SOD1<sup>G93A</sup>* mice used in this study were bred on. For example, it has previously been shown that female *SOD1<sup>G93A</sup>* mice on the B6SJL mixed genetic background demonstrate improved disease onset and survival versus male *SOD1<sup>G93A</sup>* mice on the same mixed background (Pfohl et al. 2015). Bonifacino et al. (2017) noted that heterozygous knockdown of mGlu<sub>5</sub> may also have contributed to the gender difference observed for motor function.

There is evidence to support a role for the mGlu<sub>1</sub> receptor in MND too. As mentioned earlier, mGlu<sub>1</sub> was also found to be upregulated on activated astrocytes in spinal cord tissue of MND patients collected at post-mortem. In addition, Giribaldi et al. (2013) noted that glutamate release was abnormal in spinal cord synaptosomes of *SOD1<sup>G93A</sup>* mice and that this was mediated by both mGlu<sub>1</sub> and mGlu<sub>5</sub> receptors at higher concentrations of the group I agonist, 3,5 -DHPG. Finally, an *in vivo* study using *SOD1<sup>G93A</sup>* mice expressing half the levels of mGlu<sub>1</sub> (*SOD1<sup>G93A</sup>/Grm1<sup>crv4/+</sup>*), demonstrated that heterozygous knockdown of mGlu<sub>1</sub> delayed onset of disease pathology, slowed disease progression and prolonged survival (Milanese et al. 2014). This finding suggests that blocking mGlu<sub>1</sub> could also have a therapeutic benefit in MND. However, it was interesting to note that knocking down mGlu<sub>1</sub> also reduced mGlu<sub>5</sub>, consequently it is difficult to know whether the beneficial effects were solely mGlu<sub>1</sub> mediated.

## 1.7 Summary

MND is a fatal disease for which there is an urgent need for more effective disease modifying therapies. In light of the evidence presented in the previous section, it is conceivable that mGlu<sub>5</sub> may offer a novel therapeutic target for MND. Despite motor neurons being particularly susceptible to degeneration in MND, it is clear that the pathogenesis of this disease is the result of a deleterious 'cross-talk' between neuronal and non-neuronal cells. Consequently, it is highly likely that an effective intervention for MND will comprise both neuronal and non-neuronal cell directed therapies. In the context of MND, glutamate-mediated excitotoxicity and non-neuronal cell toxicity are both pathogenic mechanisms that could potentially be modulated by inhibiting mGlu<sub>5</sub> activity. For example, it has been shown in both human and mouse cases of MND that mGlu<sub>5</sub> expression is elevated on reactive astrocytes which is thought to be indicative of a functional link between increased mGlu<sub>5</sub> activity and astrogliosis (Anneser et al. 2004). Furthermore, it was demonstrated *in vitro* that mutant *SOD1* expressing astrocytes are more sensitive to extracellular glutamate levels and undergo cell death (Rossi et al. 2008). The revelation that therapeutic blockade of mGlu<sub>5</sub> with MPEP abolished glutamate toxicity warranted further investigation of the mGlu<sub>5</sub> target *in vivo*. Consequently, the most compelling evidence to support a role for mGlu<sub>5</sub> in MND stemmed from an *in vivo* study demonstrating that the mGlu<sub>5</sub> antagonist, MPEP, delayed onset of disease and extended survival in the *SOD1*<sup>G93A</sup> mouse model of MND (Rossi et al. 2008). More recently the beneficial effects of mGlu<sub>5</sub> genetic ablation in the *SOD1*<sup>G93A</sup> mouse model of MND has provided additional support for probing mGlu<sub>5</sub> as a novel therapeutic target in MND (Bonifacino et al. 2017).

## 1.8 Hypothesis

It is widely established that impaired glutamate homeostasis plays an important role in MND pathogenesis, with consistent reports of elevated levels of extracellular glutamate in both familial and sporadic MND patients (Shaw et al. 1994; Shaw et al. 1995; Spreux-Varoquaux et al. 2002; Perry et al. 1990; Rothstein et al. 1991). However, perhaps the strongest evidence supporting glutamate-mediated excitotoxicity as a mechanism of pathogenesis in MND, is the modest efficacy of the indirect glutamate antagonist, riluzole (Lacomblez et al. 1996b; Bellingham 2011).

A growing body of evidence supports a role for the GPCR, metabotropic glutamate receptor type 5 (mGlu<sub>5</sub>), in MND (Rossi et al. 2008; Anneser et al. 2006; Anneser et

al. 2004; D'Antoni et al. 2011; Martorana et al. 2012; Giribaldi et al. 2013; Aronica et al. 2001). As mentioned previously, the interplay between motor neurons and neighbouring astrocytes is crucial for MND disease progression. For example, astrogliosis has been shown to localise with areas of motor neuron pathology and interestingly, elevated levels of mGlu<sub>5</sub> have been observed on these reactive astrocytes (Boillee et al. 2006b; Yamanaka et al. 2008; Martorana et al. 2012; Vermeiren et al. 2006). In addition, astrocytes expressing mutant *hSOD1<sup>G93A</sup>* are more vulnerable to increased glutamate levels and undergo cell death mediated by mGlu<sub>5</sub> (Rossi et al. 2008). The mGlu<sub>5</sub> antagonist, MPEP, delays onset of motor symptoms and extends survival in the *SOD1<sup>G93A</sup>* mouse model of MND (Rossi et al. 2008). Traditional mGlu<sub>5</sub> negative allosteric modulators such as MPEP are limited by the presence of an acetylene group (Figure 1.4).

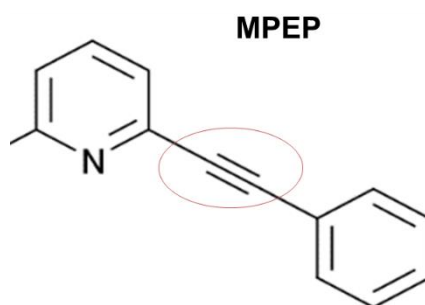


**Figure 1.5. Structure for MPEP (acetylene group circled)**

This acetylene group is highly reactive and is often associated with liver toxicity and poor pharmacokinetics (Shimada et al. 2007; Gasparini et al. 1999). For example, in order to achieve therapeutic levels using a short half-life drug such as MPEP, high doses are needed. This can result in  $C_{max}$  driven CNS side effects (Smith et al. 2017). Using their StaR<sup>®</sup> technology, Heptares Therapeutics have designed a novel mGlu<sub>5</sub> negative allosteric modulator (NAM), HTL0014242, which lacks the acetylene group (Christopher et al. 2015). Consequently, this compound has optimised properties for *in-vivo* testing.

It is hypothesised that astrocytic mGlu<sub>5</sub> plays a role in disease progression in the *SOD1<sup>G93A</sup>* mouse model of MND and that blocking astrocytic mGlu<sub>5</sub> activity with HTL0014242 will slow disease progression and extend survival of *SOD1<sup>G93A</sup>* transgenic mice.

## 1.9 Aims and Objectives

### Aim:

The overall aim of this project is to investigate mGlu<sub>5</sub> as a novel therapeutic target in the *SOD1<sup>G93A</sup>* mouse model of MND with a view to validating mGlu<sub>5</sub> as potential therapeutic target for MND.

### Objectives:

- To characterise the expression profile of mGlu<sub>5</sub> in *in vivo* and *in vitro* models of *SOD1* MND.
- To characterise the mGlu<sub>5</sub> negative allosteric modulator, HTL0014242, in the *SOD1<sup>G93A</sup>* mouse model of MND.
- To investigate the efficacy of HTL0014242 in an intermediate stage of disease (up to 90 days of age) in the *SOD1<sup>G93A</sup>* mouse model of MND and from this ascertain whether efficacy of HTL0014242 should be probed at a later more severe stage of disease, to investigate its effects on survival.

## 2 Materials and Methods

### 2.1 Materials

All reagents and laboratory consumables, unless otherwise stated, were purchased from Sigma, UK.

#### 2.1.1 List of Reagents

Access Revelation pH 6.5 (MP-607—x500), A. Menarini Diagnostics, UK

Acetic Acid, Thermo Fisher Scientific

Bovine serum albumin (BSA), Thermo Fisher Scientific

Cresyl Violet, Merck, Millipore, UK

Dimethyl sulfoxide (DMSO) (100%)

Ethylenediaminetetraacetic acid (EDTA)

[<sup>3</sup>H] M-MPEP, custom synthesis Tritec, UK

HEPES (1M), Melford, UK

HTL0014242, Heptares Therapeutics, UK

Hydrogen Chloride (HCl)

Mavoglurant custom synthesis Heptares Therapeutics, UK

Methyl cellulose

Methanol, (100%) Thermo Fisher Scientific

M-MPEP, Tocris, UK

OCT embedding matrix, CellPath, UK

Pentobarbitone (JML)

Photosensitive syntalin

Potassium chloride (KCl)

Potassium hydrogen phosphate (KH<sub>2</sub>PO<sub>4</sub>)

Riluzole, Apollo Scientific, UK

Sodium Chloride (NaCl)

Sodium hydrogen phosphate (Na<sub>2</sub>HPO<sub>4</sub>)

Sodium hydroxide (NaOH)

Sucrose

Triton X- 100

Vectashield hardset aqueous mountant with 4',6-diamidino-2-phenylindole (DAPI),  
Vector Laboratories, UK

### **2.1.2 Solutions and Buffers**

All solutions and buffers were made up to volume with dH<sub>2</sub>O water unless otherwise stated

#### **Harvesting Buffer**

10mM HEPES, 0.9% (w/v) NaCl, 0.2% (w/v) EDTA, pH 7.4

#### **Homogenisation Buffer**

10mM HEPES, 10mM EDTA, pH 7.4

#### **Resuspension Buffer**

10mM HEPES, 0.1mM EDTA, pH 7.4

#### **Binding Buffer**

50mM HEPES, 150mM NaCl, pH 7.5

#### **Paraformaldehyde (PFA)**

4% (w/v) PFA, PBS, pH 7.4

#### **TAE Buffer**

40mM TRIS, 1mM EDTA, 0.11% glacial acetic acid, pH 8.0

#### **TAE Agarose**

TAE buffer, 2% agarose

#### **Polyethylenimine (PEI)**

0.1% (w/v) PEI

## Phosphate Buffered Saline (PBS)

137mM NaCl, 2.7mM KCl, 10mM Na<sub>2</sub>HPO<sub>4</sub>, 1.8mM KH<sub>2</sub>PO<sub>4</sub>, pH 7.4

### 2.1.3 Antibodies

**Table 2.1. Primary antibodies for immunofluorescence**

Antibody/Peptide	Host Species	Concentration	Dilution	Source,
mGlu <sub>5</sub>	Rabbit monoclonal	0.13mg/ml	1:250	Abcam, ab76316,
GFAP	Rabbit polyclonal	2.9mg/ml	1:500	Dako
GFAP	Chicken polyclonal	3.3mg/ml	1:500	Abcam, ab4674
Iba1	Rabbit polyclonal	0.5mg/ml	1:500	Alpha Laboratories
Iba1	Goat polyclonal	0.5mg/ml	1:500	Abcam, ab5076
ChAT	Goat polyclonal	1mg/ml	1:200	Merck Millipore, UK
Isotype control	Rabbit IgG monoclonal	1.622mg/ml	1:250	Abcam, ab172730,
mGlu <sub>5</sub> peptide	Synthetic peptide	0.2mg/ml	Variable	Abcam, ab76316

**Table 2.2. Secondary antibodies for immunofluorescence**

Antibodies	Host Species	Concentration	Dilution	Source, Reference
Alexa Fluor 488 (green) anti-rabbit	Donkey	2mg/ml	1:1000	Life Technologies, A21206
Alexa Fluor 555 (red) anti-rabbit	Donkey	2mg/ml	1:1000	Life Technologies, A31572
Alexa Fluor 488 (green) anti-chicken	Goat	2mg/ml	1:1000	Life Technologies, A11039
Alexa Fluor 555 (red) anti-goat	Donkey	2mg/ml	1:400	Life Technologies, A31570

## 2.1.4 Formulas

### Equation 2.1. Cheung-Prusoff Equation

$$K_i = \frac{IC_{50}}{1 + \frac{[ligand]}{K_D}}$$

[ligand] = concentration of [<sup>3</sup>H] M-MPEP in nM

K<sub>D</sub> = affinity (K<sub>D</sub>) in nM of [<sup>3</sup>H] M-MPEP for mGlu<sub>5</sub> determined in mouse brain membranes

### Equation 2.2. Predicted % RO

$$\text{Formula: RO \%} = \left( \frac{\text{nM}}{\text{nM} + K_i} \right) \times 100\%$$

nM = HTL0014242 concentration

K<sub>i</sub> = Affinity (K<sub>i</sub>) in nM of HTL0014242 for mGlu<sub>5</sub>

### Equation 2.3. [<sup>3</sup>H] Radioligand Concentration

$$\text{Concentration} = \frac{\text{Average DPM count}}{\text{Vol.} \times \text{SA} \times 2220}$$

Vol. = Volume of radioligand added to sample (ml)

SA = Specific activity of the radioligand

2220 = the conversion factor between DPM and Curies

#### Equation 2.4. % Measured [<sup>3</sup>H] M-MPEP

$$\% \text{ [}^3\text{H] M-MPEP} = \left( \frac{\text{Specific [}^3\text{H] M-MPEP binding in HTL14242 dose group (cpm)}}{\text{Specific [}^3\text{H] M-MPEP binding in vehicle dose group (cpm)}} \right) \times 100$$

#### Equation 2.5. % Measured RO

$$\% \text{ Measured RO} = 100 - \% \text{ [}^3\text{H] M-MPEP}$$

## 2.2 Methods

### 2.2.1 C57BL/6 *SOD1<sup>G93A</sup>* Transgenic Mouse Model of MND

Mice used throughout this project were originally obtained from the Jackson Laboratory, B6SJL-Tg (*SOD1<sup>G93A</sup>*) 1Gur/J (stock number 002726). The mice were subsequently backcrossed onto the C57BL/6 background (Harlan UK, C57BL/6 J OlaHsd) for > 20 generations to create a line on an inbred genetic background with reduced variability. The *SOD1<sup>G93A</sup>* transgene is maintained as a hemizygous trait by breeding hemizygous males with wildtype females (C57BL/6J, OlaHsd, Harlan UK) (as described in (Mead et al. 2011)).

### 2.2.2 Ethical Statement

All mouse experiments were carried out in compliance with the Animals (Scientific Procedures) Act 1986 and under a UK Home Office Project Licence. Mice were housed and cared for according to the Home Office Code of Practice for the Housing and Care of Animals Used in Scientific Procedures. The ARRIVE guidelines have been followed for all *in vivo* mouse studies reported in this thesis (Kilkenny et al. 2010).

### 2.2.3 Housing

Whilst mice were initially bred in a Specified Pathogen Free (SPF) unit, all subsequent *in vivo* mouse studies were carried out in a conventional facility with a 12h light/dark cycle and the room temperature maintained at 21°C. The mouse cages were lined with fine sawdust (eco-pure flakes 6, Datesand, UK) containing a plastic house and paper wool (Datesand, UK). Mice were fed with the 2018 rodent diet (Harlan, UK) and

water *ad libitum*. Cages and bedding were changed every two weeks and water bottles were changed every four weeks. The mice were housed in same-sex littermate pairs or quadruplets however occasionally males were separated due to fighting.

#### 2.2.4 Genotyping

Mice were identified by ear clipping and the ear clip was retained for DNA extraction. DNA was extracted by incubating the ear clips at 65°C for 20 minutes in a 30µl volume of QuickExtract DNA Extraction Solution (Epicentre, Cambridge, UK) followed by a 2-minute incubation at 98°C. 0.5µl of DNA was then combined with 2µl of Firepol (Solis Biodyne, Estonia), 5µl of dH<sub>2</sub>O, 150nM each of human *SOD1<sup>G93A</sup>* primers (forward 5'-CCAAGGAGCAGATCATAGGGC-3', reverse 5'-AGAGCATTGGAGAAGGCAGG-3') and control interleukin-2 receptor (IL-2R) primers (forward 5'-CTAGGCCACAGAATTGAAAGATCT-3', reverse 5'-GTAGGTGGAAATTCTAGCATCATC -3'). Subsequently the polymerase chain reaction (PCR) mix was run on a PCR machine (G-Storm, UK) set to the following program (see Table 2.3).

**Table 2.3. PCR program for genotyping**

Step	Temperature	Time	Cycles
Initiation	94°C	5 minutes	
Melting,	94 °C	1 minute	30 cycles
Annealing	60 °C	45 seconds	
Extension	72 °C	30 seconds	
Final Extension	72 °C	10 minutes	
Cooling	15 °C	Hold	

The PCR product was then separated using gel electrophoresis on a 2% w/v agarose in TAE gel (containing 1% ethidium bromide) run at 120 V for 40 mins. Non-transgenic PCR products were identified by the presence of a single DNA band at 234 bp for IL-2R, whilst transgenic products were visualised by the presence of an additional DNA band at 236 bp for the h*SOD1<sup>G93A</sup>* transgene. Female mice that were positive for the h*SOD1<sup>G93A</sup>* transgene were subsequently recruited for *in vivo* pharmacological studies. Of note, no difference between male and female *SOD1<sup>G93A</sup>* mice has been

observed for onset or time taken to reach end-stage of disease within our model (Mead et al. 2011). For logistical reasons male mice were needed for breeding and consequently female mice were used for *in vivo* pharmacology studies.

## **2.2.5 *In vivo* Pharmacology Mouse Studies**

### **2.2.5.1 HTL0014242 Pharmacokinetic Study Design**

Female C57BL/6 *SOD1<sup>G93A</sup>* mice ~60 days of age were recruited to this study. Three mice were allocated to each time-point. The time-points for the oral PK profile were at 0, 0.08, 0.25, 0.5, 1, 2, 4, 8 and 24 hours after dosing. Two additional time-points were at peak (2h post-dose) and trough (24h post-dose) following 7 days of repeated dosing, to investigate sub-chronic dosing of HTL0014242. The mice were dosed by oral gavage at 10mg/kg. Oral formulation of HTL0014242 was as a suspension in 0.5% methyl cellulose (10ml/kg of 1mg/ml solution).

At each time-point the mice were terminally anaesthetised with pentobarbitone (JML), at 2.5ml/kg. When the pedal reflex was absent, whole blood was collected by cardiac puncture, EDTA added to 10mM, mixed 1:2 with dH<sub>2</sub>O and immediately snap frozen in liquid nitrogen. In addition, plasma, spinal cord, brain, ear clip and liver tissue were collected and snap frozen in liquid nitrogen immediately. Tissue was sent for determination of HTL0014242 compound levels by uHPLC - TOF mass spectrometry using electrospray ionisation (Pharmidex, UK). Free fraction in spinal cord was determined by equilibrium dialysis experiments *in vitro* (Pharmidex, UK).

### **2.2.5.2 HTL0014242 90D Dose Response Study Design**

Female C57BL/6 *SOD1<sup>G93A</sup>* mice were recruited to this study. Mice were orally dosed each day with either vehicle (0.5% methyl cellulose) at 10ml/kg or HTL0014242 at 3, 10, 30mg/kg from 25 days of age through to 90 days of age. Oral formulation of HTL0014242 was as a suspension in 0.5% methyl cellulose (10ml/kg of 1mg/ml solution).

To determine group size, statistical power analysis using G\*Power 3.1.9.2 (Faul et al. 2007) was carried out based on detection of a 6 day extension in time taken to reach a 20% decline in distance ran (the least variable measure on fastrac running wheel (Bennett et al. 2014)). For control mice this is 43.85±3.93 days (mean ± SD). A power of 80% was used with a two-tailed t-test and adjusted threshold p-value of 0.0167 following a Bonferroni correction, assuming three t-tests (each dose versus the control). Power analysis suggested that a group size of 11 mice per group would

detect a difference in time taken to reach a 20% decline in fastrac running wheel performance. It was not always possible to maintain the recommended group size number due to mice dropping out of the study as a result of incorrect genotyping or reasons unrelated to development of motor dysfunction.

Mice in this study were individually housed in cages (L36 x W21 x H18.5cm) containing an in-cage fastrac running wheel (LBS Biotech, UK) which recorded their daily voluntary running behaviour. Female mice were used for this study as it had previously been shown that females display a higher frequency of running behaviour compared to male mice (De Bono et al. 2006). In addition, rotarod tests were conducted once a week from 5 weeks of age to monitor forced motor function. Catwalk gait analysis was carried out at 84 days of age to measure several gait parameters of the mice following onset of visible signs of disease (~75 days of age). Mice were also weighed on a daily basis before dosing and from 60 days of age mice underwent neurological scoring twice a week to determine classical signs of disease onset.

At ~90 days of age 6 mice from each dose group were terminally anaesthetised with pentobarbitone (JML), at 2.5ml/kg at either peak (2h post-dose) or trough (24h post-dose) exposure of HTL0014242 (3 at peak and 3 at trough). When the pedal reflex was absent, whole blood (1:2 with dH<sub>2</sub>O) was collected by cardiac puncture. In addition, spinal cord, brain and ear clip tissue were collected and snap frozen in liquid nitrogen immediately. Half brain and half SC tissue was sent for determination of unbound HTL0014242 compound levels by uHPLC - TOF mass spectrometry using electrospray ionisation (Pharmidex, UK). The other half brain tissue was used to determine the proportion of mGlu<sub>5</sub> receptors occupied by HTL0014242 using a [<sup>3</sup>H] M-MPEP radioligand binding assay (Heptares Therapeutics). Three half brains were analysed at peak exposure and three half brains were analysed at trough exposure for each of the HTL0014242 dose groups. The remaining mice (5 per dose group) were perfused under terminal anaesthesia (pentobarbitone at 2.5ml/kg) with PBS followed by 4% PFA and subsequently SC tissue was collected to determine the effect of HTL0014242 on pathologic markers of disease progression, such as glial activation.

### **2.2.5.3 HTL0014242 Survival Study Design**

Female C57BL/6 *SOD1*<sup>G93A</sup> mice were recruited to this study. Mice were orally dosed each day with either vehicle (0.5% methyl cellulose) at 10ml/kg or HTL0014242 at 30mg/kg from 25 days of age through to end-stage of disease. In addition, a third

group of mice were dosed with 30mg/kg HTL0014242 from 75 days of age through to end-stage of disease. Oral formulation of HTL0014242 was as a suspension in 0.5% methyl cellulose (10ml/kg of 1mg/ml solution).

To determine group size statistical power analysis using G\*Power 3.1.9.2 was carried out based on detection of a 10-day extension in time taken to reach a 20% decline in rotarod performance. A power of 80% (two-tailed Student's T test,  $\alpha=0.05$ ,  $\beta=0.8$ ) suggested that a group size of 14 mice per group would detect a difference in time taken to reach a 20% decline in rotarod performance. An additional 6 mice per group were recruited in order to collect tissue at 90 days of age to compare markers of disease pathology (GFAP and Iba1), in the ventral horns of lumbar spinal cord sections. Consequently, a total group size of 20 mice per dose group was required for this survival study.

Mice in this study were block randomised and housed in same-sex pairs or quadruplets. Female mice were recruited at 21 days of age for this study as it had previously been shown that females demonstrate substantially reduced variability in time taken to reach a 20% decline in rotarod performance (Mead et al. 2011). Rotarod tests were conducted twice a week from 5 weeks of age or 75 days of age to monitor forced motor function. Catwalk gait analysis was carried out at 70, 84, 98 and 112 days of age to measure changes in gait parameters of the mice throughout the *SOD1<sup>G93A</sup>* disease trajectory. Mice were also weighed daily before dosing and from 60 days of age mice underwent neurological scoring three times a week to determine classical signs of disease onset. From ~125 days of age onwards, mice were closely monitored and scored for signs of distress to determine whether they had reached the humane end-point: inability to right within 10s of being on their sides or  $\geq 30\%$  weight loss for 72h.

At 89-91 days of age 6 mice per dose group were perfused under terminal anaesthesia (pentobarbitone at 2.5ml/kg) with PBS followed by 4% PFA and subsequently SC tissue was collected to determine the effect of HTL0014242 on pathologic markers of disease progression, such as glial activation. In addition, the ventral horns were ChAT stained throughout the lumbar region of the SC to quantify the number of remaining motor neurons at 90 days of age for each of the dose groups. Staining for mGlu<sub>5</sub> and the motor neuronal marker, ChAT, also took place on lumbar SC ventral horns collected at 90 days of age.

At the end of the study (humane end-point reached), 8 mice in each of the dose groups were terminally anaesthetised with pentobarbitone (JML), at 2.5ml/kg at either peak (2h post-dose) or trough (24h post-dose) exposure of HTL0014242 (4 at peak and 4 at trough). When the pedal reflex was absent, whole blood was collected by cardiac puncture, EDTA added to 10mM, mixed 1:2 with dH<sub>2</sub>O and immediately snap frozen in liquid nitrogen. In addition, spinal cord, brain and ear clip tissue were collected and snap frozen in liquid nitrogen immediately. Half brain and half SC tissue were sent for determination of the unbound HTL0014242 compound levels by uHPLC - TOF mass spectrometry using electrospray ionisation (Pharmidex, UK). The other half brain tissue was used to determine the proportion of mGlu<sub>5</sub> receptors occupied by HTL0014242 using a [<sup>3</sup>H] M-MPEP radioligand binding assay. Four half brains were analysed at peak exposure and four half brains were analysed at trough exposure for each of the HTL0014242 dose groups.

The remaining mice (6 per dose group) at end-stage were perfused under terminal anaesthesia (pentobarbitone at 2.5ml/kg) with PBS followed by 4% PFA and subsequently SC tissue was collected and prepared for histology. Lumbar SC ventral horns were immuno-stained with markers of glial activation such as GFAP and Iba1. Furthermore, end-stage ventral horns were ChAT stained throughout the lumbar region of the SC to quantify the number of the remaining motor neurons.

#### **2.2.5.4 Riluzole Plus HTL0014242 Study Design**

Female C57BL/6 *SOD1<sup>G93A</sup>* mice were recruited to this study. Six mice were allocated to three dose groups which included a vehicle group (0.1% DMSO in drinking water), a HTL0014242 dose group (30mg/kg orally dosed each day) and a HTL0014242 in combination with riluzole dose group (30mg/kg HTL0014242 orally dosed and ~70mg/kg of riluzole (240µg/ml in 0.1% DMSO) in drinking water). Oral formulation of HTL0014242 was as a suspension in 0.5% methyl cellulose (10ml/kg of 1mg/ml solution). It has previously been shown that the average half-life of riluzole after repeated dosing is relatively short in humans at 12h (Bryson et al. 1996). Mice have a much faster metabolism than humans and therefore riluzole clearance is much faster in mice. Consequently, riluzole was administered in drinking water to ensure the plasma levels of riluzole in mouse remained constant. A dose of 240µg/ml riluzole (~70mg/kg) was selected as previous in-house studies have demonstrated that this dose significantly reduced the decline in motor function in *SOD1<sup>G93A</sup>* mice, without demonstrating any sedative effects and lead to blood exposures within the range seen in MND patients treated with riluzole.

Dosing was commenced at 25 days of age and was continued through to 90 days of age when SC tissue was collected from all three dose groups for histological analysis of markers of glial activation (GFAP and Iba1).

## **2.2.6 Mouse Behavioural Readouts**

### **2.2.6.1 Neurological Scoring and Distress Scoring**

Mice were scored either twice or three times a week from 60 days of age to determine visible signs of disease onset. Onset was defined as the point at which defects in hind-limb splay were observed in combination with hindlimb tremor (a score of at least 1 in each category). Mice were considered to have disease onset at the time of the first score of two consecutive onset recordings. Tremor scores were recorded independently for forelimbs and hindlimbs after suspending the mouse by the tail. The scoring scale consisted of 0-normal, 1- mild tremor, 2-moderate tremor, 3- strong tremor. Hind-limb splay defects were scored at the same time and the splay score was recorded separately for left and right hind-limbs on a scale of 0–4 with 0 representing normal, 1 representing mild defect, 2 moderate, 3 strong and 4 paralysis of hind limb.

From 125 days of age onwards mice were put on a severe protocol which meant they were monitored on a daily basis and scored for signs of distress. The distress scoring scale used a standardised scoring system based on appearance, provoked behaviour, weight loss and an overall neurological score. Provoked behaviour is the initial behaviour observed when the mice are first disturbed when opening the cage. The scoring scale was as follows; 0 - normal, bright and inquisitive mice, 1 - mild impairment or exaggeration in provoked response, 2 - a moderate reduction in provoked response or disinterested mice, 3 - a strong reduction in provoked response and 4 - a moribund animal. The neurological score was used to give an overall score of the disease state of the mice for the purpose of monitoring distress levels and was scored as follows; 0 - normal, 0.5 - tremor and hind limb splay defect (onset), 1 - abnormal gait, 2 - partial hind-limb paralysis (first signs of dragging), 3 - hindlimb paralysis plus forelimb weakness, 4 - significant forelimb and hindlimb paralysis. Distress scoring commenced from 125 days of age and continued until the humane end-point. The humane end-point for mice on a severe protocol (125 days onwards) was defined as an inability to right within 10 seconds of being placed on their back or weight loss of **≥30% for 72 hours**. Once the criteria for the humane-end point were met the mice were euthanised with an overdose of anaesthetic (intraperitoneal injection of approximately 20 ml/kg pentobarbitone) and tissue was collected.

Of note, both neurological scoring and distress scoring was carried out blinded to the dose group and where possible by the same investigator. This was a measure put in place as an attempt to avoid bias and variability in scoring between different investigators.

From 125 days of age, when *SOD1<sup>G93A</sup>* mice were put on a severe protocol and mice typically show first signs of hind-limb paralysis, the bedding material was optimised to consist of short strands to prevent the mice from getting stuck and the cages were lined with blue paper roll instead of sawdust to improve their locomotion. The mice were also provided with wetted mash in their cages.

#### **2.2.6.2 Fastrac Running Wheels**

The fastrac running wheel system consisted of an in-cage fastrac running wheel (LBS Biotech, UK) with a 37.8cm circumference. The wheel was mounted on a fixed post at a height of 4cm at an angle of 25° below horizontal and this was located 5-10mm from the side of the cage. Fitted on the underside of the wheel was a 5 x 10mm neodymium magnet (First4magnets.com) which activated a reed switch attached to the outside of the cage and this was connected to a bike computer (Cateye Velo, Japan). The bike computer measured the daily total time spent running, total distance ran, and average speed ran of each mouse and this was recorded every morning. The distance ran in km was subsequently adjusted for the circumference of the running wheel. For example, the total number of wheel revolutions was multiplied by the circumference of the wheel (37.8cm).

#### **2.2.6.3 Rotarod**

A Ugo Basile 7650 accelerating rotarod was used to monitor the motor function of mice. The mice were placed on a rotating bar which was set to accelerate from 4-40rpm over 300 seconds and the time taken for the mice to fall from this bar was recorded in seconds. Mice were trained on the rotarod over the course of three consecutive days, usually around ~32 days of age and their first test day was on the fourth day at ~ 35 days of age. Subsequent rotarod testing was conducted either once or twice a week thereafter. Rotarod was carried out at the same time of day (afternoons) and on each occasion the mice were tested twice with a rest between trials and the best performance recorded for analysis.

#### **2.2.6.4 Catwalk Gait Analysis**

The catwalk gait analysis system version 7.1 (Noldus Information Technology B.V., Netherlands) was used to monitor several aspects of gait following video capture and manual segmentation of step pattern. Eight mice from each dose group underwent catwalk gait analysis which started from ~10 weeks of age and continued weekly through to ~16 weeks of age. Mice were placed at one end of the glass catwalk corridor in complete darkness and the run/walk to the opposite end was recorded using catwalk software 7.1 in a separate room. Six catwalk runs were recorded for each mouse and the best three (straight and continuous runs) were selected for analysis. Analysis of the gait parameters was performed using dedicated catwalk software whereby the pawprint of each limb was allocated manually before automated calculation of gait parameters took place.

### 2.2.7 Immunohistochemistry in Non-Transgenic and *SOD1<sup>G93A</sup>* Mouse Lumbar Spinal Cord Tissue

The following experimental procedures were carried out to characterise the expression profile of mGlu<sub>5</sub> in both *SOD1<sup>G93A</sup>* transgenic mice and non-transgenic mice spinal cord tissue at 90 days of age. (Figure 2.1).

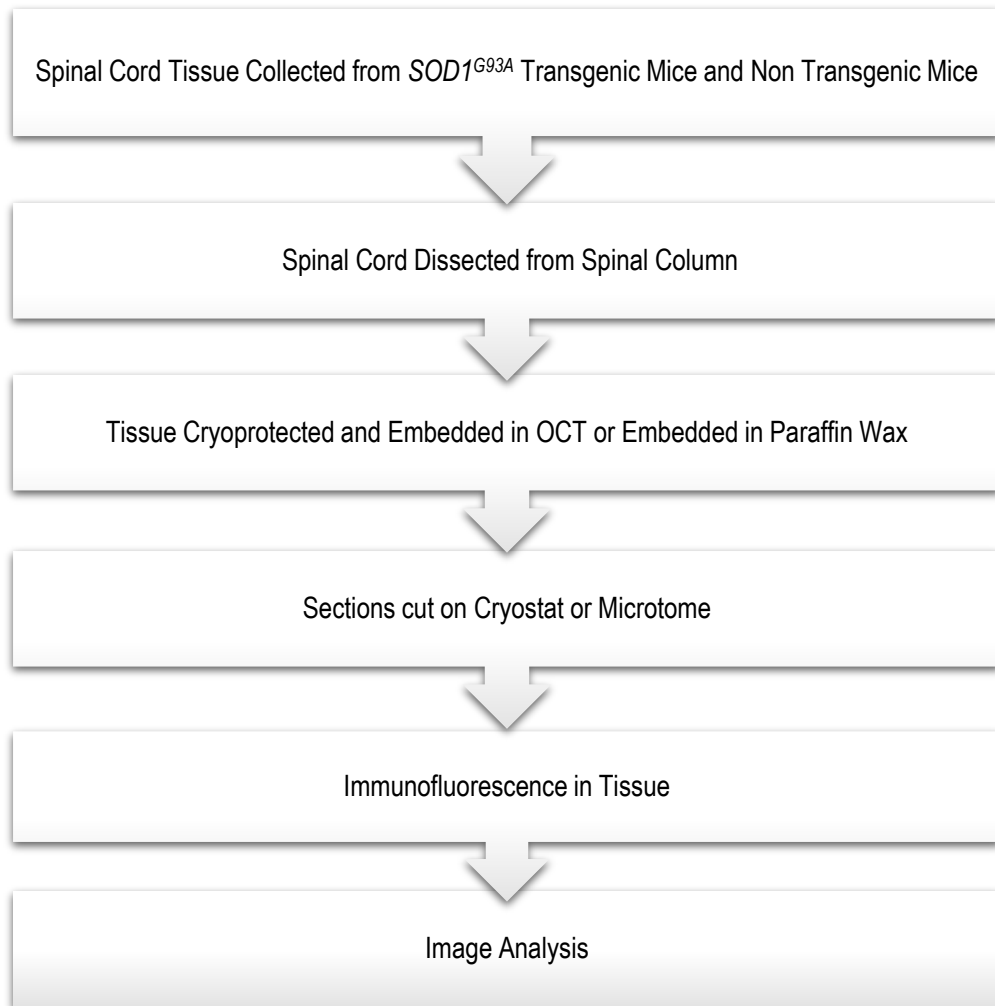


**Figure 2.1. An overview of the procedures carried out for immunohistochemistry**

### **2.2.7.1 Collecting Spinal Cord Tissue**

Mice were injected intraperitoneally and anaesthetised with 2.5ml/kg of pentobarbitone (JML). A trans-cardiac perfusion was then carried out with 6-10ml of PBS followed by 6-10ml of 4% paraformaldehyde (PFA, Sigma), in PBS at pH 7.2. Brain and spinal column were removed and post-fixed in the same fixative overnight (O/N).

### **2.2.7.2 Dissecting Spinal Cord from Spinal Column and Cryoprotection**

The spinal cord was removed from the spinal column by dissecting the column, one vertebra at a time. Following this, frozen cut tissue was cryoprotected prior to embedding in OCT. Tissue was cryoprotected in 5%, 10% and 15% sucrose (Melford) in PBS baths for 5 minutes at room temperature (RT). This was followed by cryoprotection in 20% sucrose (Melford) in PBS O/N at 4°C. Tissue for paraffin embedding did not need cryoprotecting.

### **2.2.7.3 Spinal Cord Embedding in OCT and Cryostat Cutting**

The spinal cords from drug naïve non-transgenic and *SOD1<sup>G963A</sup>* mice collected at 90 days of age were cut into cervical, thoracic, lumbar and sacral segments. The lumbar spinal cord segment (12mm) was then placed into a mould containing OCT (CellPath) and plunged into dry ice soaked with 100% methanol (Thermo Fisher Scientific). This was then stored at -80°C until ready to cut on the cryostat.

Lumbar spinal cord sections were serially cut at 10µm on a cryostat and collected on slides for immunofluorescent staining. The chamber temperature was set at -20°C and the objective temperature was set at -20°C. Each slide was dried for at least 30 minutes at RT before being stored at -20°C until ready to stain.

### **2.2.7.4 Spinal Cord Embedding in Paraffin Wax and Microtome Cutting**

The spinal cords from pharmacological *in vivo* mouse studies were cut into cervical, thoracic, lumbar and sacral segments. The lumbar spinal cord segment (12mm) was halved into two 6mm segments which were then paraffin embedded in the same wax block. The wax block was sectioned serially across 5 slides at 10µm. Following this, 5 sections were discarded (50µm), and a new row of serial sections were cut on the same 5 slides. A total of 4 rows were cut in this way, resulting in a total of 8 sections per slide. A further 9 sets of 5x slides were prepared in this manner meaning that

sections were cut across a total of 50 slides. These slides were then used for immunofluorescence staining.

#### **2.2.7.5 Immunofluorescence in Spinal Cord Tissue**

Frozen lumbar SC sections were initially dried by warming at 37°C for 30 minutes, this step improved tissue adhesion to the slides. Following this the sections were washed in PBS with gentle agitation (3x 5-minute washes) at RT. Next the sections were permeabilised in 5% BSA, 0.5% Triton X-100 in PBS, overnight at RT.

For paraffin embedded lumbar SC sections, one slide (at the same level of the cord) was selected for immunofluorescence staining for each mouse. Consequently, a total of 8 sections per mouse were stained. First paraffin embedded lumbar SC sections were dewaxed in xylene (2x 5 minutes) and rehydrated for 5 minutes in baths of graded alcohols (100% x2, 95% x1 and 70% x1) before being washed in water. The sections were then washed in PBS with gentle agitation (3x 5-minute washes) at RT.

Following the steps above, heat mediated antigen retrieval was carried out using a pressure cooker and the antigen retrieval buffer 'Access Revelation' pH 6.5 (MenaPath), for a 30-minute cycle at 125°C and 20 psi. The sections were then washed in PBS (3x 5-minute washes) with gentle agitation at RT. Next, the slides were blocked in 5% BSA, 0.25% Triton X-100 in PBS, for 10 minutes at RT. Primary antibodies (see Table 2.1) diluted in 1% BSA and 0.25% Triton X-100 in PBS were applied to the sections and incubated at 4°C O/N. Control sections were incubated in 1% BSA and 0.25% Triton X-100 in PBS. Following incubation with the primary antibody, six quick washes with PBS and 3x 5-minute washes in PBS with gentle agitation were carried out at RT. The sections were then blocked with 5% BSA for 10 minutes at RT. Secondary antibodies (see Table 2.2) were then applied to the sections diluted in 1% BSA in PBS and incubated for 1hr30min at RT. This was followed by two quick washes, 3x 5-minute washes in PBS and 1x 5-minute wash in filtered water, with gentle agitation at RT. The slides were then dried with tissue, mounted in Vectashield hard set aqueous mountant with DAPI (Vector Laboratories, Peterborough, UK) and a cover slip was applied before leaving the slides to dry O/N. Images of the tissue sections were then captured on the In Cell Analyzer 2000.

#### **2.2.8 ChAT Staining and Motor Neuron Counting**

For each mouse, 1 slide (at the same level of the cord) out of a total of 50 was ChAT stained with at least 100µm between sections to prevent double counting. This ensured a representative distribution of sections throughout the L2 and L3 region of

the lumbar SC were ChAT stained for motor neuron counting. In total, eight lumbar SC sections per mouse were stained and motor neurons counted.

ChAT staining consisted of initially dewaxing the paraffin sections in xylene (2x 5 minutes) followed by rehydration through graded alcohols (2x 100%, 1x 95%, 1x 70%) and then washing in water. Following the steps above, heat mediated antigen retrieval was carried out using a pressure cooker and the antigen retrieval buffer 'Access Revelation' pH 6.5 (MenaPath), for a 30-minute cycle at 125°C and 20 psi. The sections were then washed in PBS (3x 5-minute washes) with gentle agitation at RT. Next, the slides were blocked in 5% BSA, 0.25% Triton X-100 in PBS, for 10 minutes at RT. Slides were then ChAT stained (see Table 2.1) and incubated at 4°C for 72 hours. Control sections were incubated in 1% BSA and 0.25% Triton X-100 in PBS. Following incubation with the ChAT antibody, six quick washes with PBS and 3x 5-minute washes in PBS with gentle agitation were carried out at RT. The sections were then blocked with 5% BSA for 10 minutes at RT. Secondary antibodies (see Table 2.2) were then applied to the sections diluted in 1% BSA in PBS and incubated for 1hr30min at RT. This was followed by two quick washes, 3x 5-minute washes in PBS and 1x 5-minute wash in filtered water, with gentle agitation at RT. The slides were then dried with tissue, mounted in Vectashield hard set aqueous mountant with DAPI (Vector Laboratories, Peterborough, UK) and a cover slip was applied before leaving the slides to dry O/N. Images of the tissue sections were then captured on the In Cell Analyzer 2000.

Subsequently motor neurons within the left and right ventral horn of each section were counted using ImageJ. This was carried out blinded to the dose group and by the same investigator to avoid bias and variability in the motor neuron counting method. Of note, only alpha motor neurons containing a nucleolus were counted. Alpha motor neurons were identified by their large size (diameter of ~20µm). Once motor neuron counts per section had been counted, the average number of motor neuron counts per section was calculated for each mouse and this was recorded on an excel spreadsheet. The data for each mouse were sorted into the corresponding dose group and these data were then analysed in GraphPad Prism 7 by one-way ANOVA and Tukey's post-test.

## 2.2.9 Immunocytochemistry in iAstrocytes

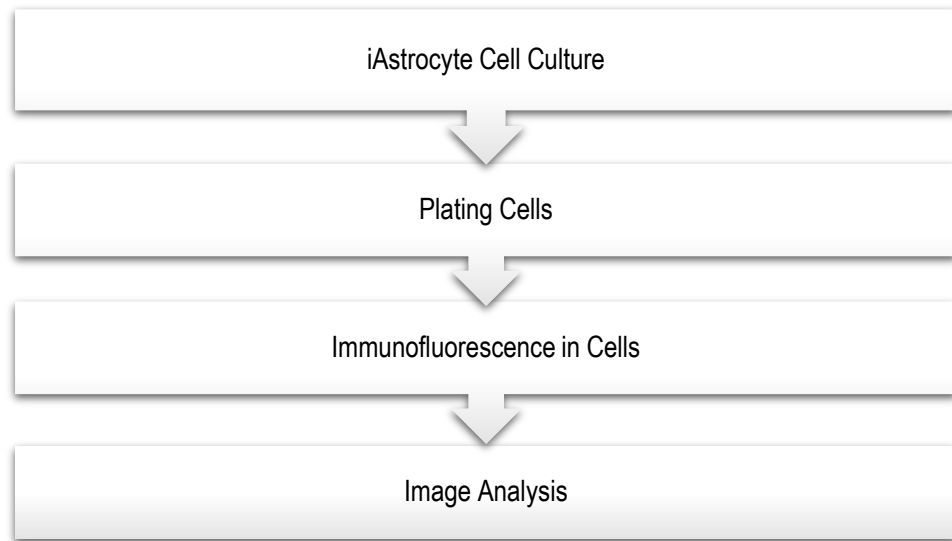


**Figure 2.2. An overview of the procedures carried out for immunocytochemistry**

### 2.2.9.1 Patient Samples

iAstrocytes were obtained by taking a small skin biopsy of fibroblast cells from three *SOD1* MND patients and three age matched healthy controls (see Table 2.4). The average age at the time of biopsy for the *SOD1* MND patients was 53 years (range 42-60) compared to 55 years (range 40-69) for the healthy controls. Skin biopsies were obtained from the forearm of each subject following approval from Yorkshire and the Humber Research Ethics Committee. These fibroblasts were then reprogrammed into iAstrocytes by the Ferraiuolo Group.

**Table 2.4. Summary of the clinical details for each patient sample**

Sample Group	Sample Number	Gender	Age at Biopsy
Control	155	Male	40
Control	209	Female	69
Control	154	Female	55
SOD1 (I33T)	91	Male	60
SOD1 (D90A)	295	Male	56
SOD1 (D76Y)	210	Male	42

#### **2.2.9.2 Methodology for Fibroblast Differentiation into iAstrocytes**

1x10<sup>6</sup> fibroblasts were seeded in a well of a six-well-plate and treated with retro viral vectors for OCT4, Sox2, KLF4 and C-MYC for 12 hours. 48 hours after transduction, the fibroblast media was changed to NPC conversion medium which consisted of DMEM/F12, 1% N2, 1% B27, 20 ng/ml FGF2, 20 ng/ml EGF, and heparin (5 µg/ml; Sigma-Aldrich). Once the cells changed shape and formed sphere-like structures, they were collected with a pipette and expanded in an individual well of a six-well plate previously coated with human fibronectin. When the neural progenitor cell (NPC) culture became confluent, typically within 3 weeks, the medium was switched to NPC medium consisting of DMEM/F12, 1% N2, 1% B27, and FGF2 (40 ng/ml) only.

For astrocyte differentiation, the induced neural progenitor cells (iNPCs) were seeded in NPC medium at low density in a fibronectin-coated 10-cm dish. The next day, the medium was switched to DMEM containing 10% FBS and 0.3% N2. Astrocytes were then allowed to differentiate for a minimum of 7 days. The efficiency of this process is extremely high, with about 90-95% of cells positive for astrocyte markers, i.e. CD44 and S100β.

#### **2.2.9.3 Immunofluorescence in Cells**

The cells of interest were washed three times with 100µl of PBS for 5 minutes at RT. Cells were then permeabilised with 50µl of 5%BSA, 0.1% Triton X-100 and 0.05% sodium dodecyl sulphate (SDS) in PBS and incubated for 30 minutes at RT. The

blocking/permeabilisation solution was removed from each well and 50µl of primary antibody (see Table 2.1) in 1% BSA in PBS was added to the desired wells and incubated for 2 hours at RT. Control wells were incubated with 1% BSA in PBS.

Following incubation with the primary antibody, the cells were washed three times with 100µl of PBS for 5 minutes at RT. The PBS was removed from the wells and the cells were blocked with 5% BSA in PBS for 10 minutes at RT. After removing the blocking agent, the cells were incubated with 50µl of secondary antibody (see Table 2.2) in 1% BSA in PBS for 1 hour at RT. After the addition of the secondary antibody, the plate was covered with aluminium foil to avoid secondary antibody light exposure. Following this incubation step, the cells were washed three times with 100µl of PBS for 5 minutes. Next, 100µl of Hoechst in PBS (1:1000) was added to each well and incubated for 10 minutes at RT. Finally, the Hoechst was replaced with 100µl of PBS and the images were ready to be captured on the In Cell Analyzer 2000.

## **2.2.10 Image Analysis**

### **2.2.10.1 Images Captured using 'In Cell Analyzer 200'**

The 'InCell Analyzer 2000' (InCell, GE Healthcare) is used for fast, high-content screening (HCS) of both fixed and live cells. It has an automated microscope that can be used to capture images of both cells on a plate and whole tissue sections on microscope slides.

Hoechst/DAPI and the secondary antibodies used in the IHC and ICC experiments are tagged with specific fluorophores. On excitation by certain wavelengths of light, these fluorophores emit light of a specific wavelength which is then detected by the InCell. The 'InCell' microscope has several filters, corresponding to the different wavelengths of light. This enables the expression of more than one protein of interest to be captured, within the same cell/tissue section.

The protocol followed for capturing images of tissue sections was as follows: The template acquisition protocol for imaging slides was opened. The exposure for the different filters was set for GFAP and Iba1 staining (0.4 seconds for DAPI, 1.4 seconds for FITC and 1.4 seconds for Cy3) and for mGlu<sub>5</sub> and ChAT staining (0.5 seconds for DAPI, 2 seconds for FITC and 1 second for Cy3). The laser autofocus power level was set to 1% and the objective was set to 2x magnification. Once the tissue of interest had been selected, the objective was changed to either 60x magnification for ventral horn staining or 20x magnification for whole section staining. For whole section staining, software autofocus was turned on and a 20% overlap was

set between each of the fields to enable later image stitching. Finally, the fields were imaged with each of the corresponding filters in place.

The protocol followed for capturing images of the cells on a plate was as follows: The template acquisition protocol for a 96 well plate or 24 well plate was opened. The exposure for the different filters was set (0.04 seconds for DAPI, 2 seconds for FITC and 2 seconds for Cy3). The laser autofocus power level was set to 1% and the objective was set to 20 x magnification. For each well of interest on the plate, five randomly selected, non-overlapping fields were selected. These fields were then imaged with each of the corresponding filters in place.

#### **2.2.10.2 Generating Images on 'ImageJ'**

ImageJ was used to process the images captured by the InCell both at x20 and x60 magnification. The program enabled one image of the whole tissue section to be produced (composite), by stitching the individual fields at x20 magnification together. An image of the whole tissue section was generated for each filter and these composites were then merged. This enabled the expression of the proteins of interest to be characterised within the whole tissue section.

The program was also used to process images of the cells captured within the five, random fields of each well. Using ImageJ, it was possible to overlay the different channels of the same fields within each well, captured with different filters. The merged image allowed the expression profile of the proteins of interest to be defined, within a specific field of the cells.

#### **2.2.10.3 Analysis using Developer Toolbox**

Incell Developer Toolbox (GE Healthcare) was used to generate a protocol to analyse GFAP, Iba1, mGlu<sub>5</sub> and ChAT antibody staining in ventral horns of lumbar SC sections captured at x60 magnification. A cytoplasmic mask based on the antibody staining area was created and the pixel intensity and area of staining within the mask was measured. The values for staining area and pixel intensity were exported as an excel file. The data were then manually sorted into the different dose groups and the mean staining area and staining intensity for each group was entered into GraphPad Prism 7 for statistical analysis using one-way ANOVA and Tukey's post-test, unless otherwise stated.

Incell Developer Toolbox (GE Healthcare) was also used to automate image analysis of iAstrocytes. A nuclear mask was generated based on the DAPI staining. This was

then dilated to create a mask which covered the nucleus and part of the cytoplasm of each cell. This mask was then used to calculate the average pixel intensity for mGlu<sub>5</sub> staining for each cell which was exported as an excel spreadsheet. All cells within a field were averaged and individual fields within a well also averaged. Individual well averages were sorted into the corresponding groups and then analysed in GraphPad Prism 7 by Student's T Test.

## **2.2.11 [3H] M-MPEP Radioligand Binding Assays**

### **2.2.11.1 Membrane Preparation for Protein Linearity and Saturation Binding**

Whole brain was collected from *SOD1<sup>G93A</sup>* transgenic and non-transgenic mice at 30 and 120 days of age (3 mice per time-point). The brains in each of the 4 time-points were pooled and suspended in 10ml of harvesting buffer (0.9% (w/v) NaCl, 10mM HEPES, 0.2% (w/v) EDTA, pH 7.4) at 4°C and homogenized using a Polytron homogenizer (3x 30s bursts). The suspensions were centrifuged (5 mins, 200 xg, 4°C) using a Sorvall Legend bench top centrifuge before collecting the supernatants and re-homogenising once again (3x 30s bursts). The suspensions were balanced (30ml of harvesting buffer) and centrifuged (20 mins, 40,000 xg, 4°C) using an RC5 centrifuge with an SS34 rotor. The supernatants were then discarded, and the pellets were re-suspended in 30ml of ice cold homogenisation buffer (10mM HEPES, 10mM EDTA, pH 7.4) at 4°C. Next the pellets were re-homogenised (3x 30s bursts) before being centrifuged (5 mins, 200 xg, 4°C). Following this, the pellet was re-suspended in 30ml of re-suspension buffer (10mM HEPES, 0.1mM EDTA, pH 7.4) at 4°C, homogenised and then centrifuged (20 mins, 40,000 xg, 4°C). Finally, the pellet was re-suspended in 5ml of re-suspension buffer (10mM HEPES, 0.1mM EDTA, pH 7.4), homogenised and transferred onto ice. Finally, membranes were stored at -80°C.

### **2.2.11.2 BCA Protein Assay**

The BCA assay was used to determine the concentration of protein in tissue homogenates. BSA standards and membrane samples (neat, 1:5 dilution and 1:10 dilution) were added in triplicate to a 96 well microplate (25µl/well). Working reagent (BCA reagent A: B; 50:1) was added (200µl/well) and the plate was then incubated for 30 minutes at 37°C, before it was read on the PolarStaR (BCA protocol, absorbance at 492nm). The BSA standard curve (0-200µg/ml) was used to determine the protein concentration for each membrane sample. Protein concentrations were standardised to the membrane sample with the lowest concentration (1µg/µl for brain

membranes) using re-suspension buffer. Finally, brain membranes were stored at -80 °C in 1ml aliquots.

### **2.2.11.3 Protein Linearity**

Protein linearity experiments were carried out in triplicate at varying concentrations of brain membranes (0-30µg). After thawing, membranes were diluted to correct concentrations with mGlu<sub>5</sub> binding buffer (50mM HEPES, 150mM NaCl, pH 7.5) and re-homogenised to ensure even distribution of membrane protein in solution.

Non-specific binding (NSB) was determined by measuring [<sup>3</sup>H] M-MPEP radioligand binding in the presence of a high concentration (0.5mM) of an unlabelled compound, mavoglurant. The concentration of mavoglurant chosen was 500-fold the affinity of mavoglurant for the receptor to ensure that mavoglurant fully occupied all mGlu<sub>5</sub> binding sites. Consequently, any [<sup>3</sup>H] M-MPEP binding remaining is classed as non-specific binding.

The total reaction volume per well was 250µl. Non-specific binding (NSB) was determined by adding 2.5µl (1% of total reaction volume) mavoglurant (0.5mM) to each NSB well, whilst total radioligand binding at each concentration of membrane protein was measured by adding 2.5µl of DMSO to each total binding well. Radioligand ([<sup>3</sup>H] M-MPEP) was added to every well in the assay at a concentration of ~4nM. To calculate the radioligand concentration, the disintegration per minute (DPM) was measured in duplicate and averaged before being applied to Equation 1.3. Finally, brain membranes at specified protein concentrations were added (223µl) and incubated for 1.5 hours, with gentle agitation at RT.

Following incubation, assays were terminated by rapid filtration through 96-well GF/B glass microfiber filter plates, pre-soaked in 0.1% PEI buffer using a 96-well head harvester (TomTec, USA). Finally, membrane bound radioactivity was measured by liquid scintillation counting (25µl per well of Scintillant, Ultima Gold F, PerkinElmer, UK) on the MicroBeta (PerkinElmer, UK) using a standard tritium counting programme (1 min per well).

### **2.2.11.4 Saturation Binding in Brain**

[<sup>3</sup>H] M-MPEP saturation binding experiments were carried out in triplicate in mGlu<sub>5</sub> binding buffer (50mM HEPES, 150mM NaCl, pH 7.5), using 20µg of whole brain per well. The total reaction volume per well was 500µl. Total binding and NSB were measured for 8 increasing concentrations of [<sup>3</sup>H] M-MPEP radioligand, (0 - ~40nM).

NSB was determined by adding 5µl of 0.5mM mavoglurant (1% of total reaction volume) to each NSB well. Total binding for each radioligand concentration was measured by adding 5µl of DMSO per total binding well.

After thawing, membranes were diluted to correct concentrations (20µg/well) with mGlu<sub>5</sub> binding buffer (50mM HEPES, 150mM NaCl, pH 7.5), re-homogenised to ensure even distribution of membrane protein in solution and then added to each well on the assay plate (445µl). The plates were then incubated for 1.5 hours, with gentle agitation at RT.

Following incubation, assays were terminated by rapid filtration through 96-well GF/B glass microfiber filter plates, pre-soaked in 0.1% PEI buffer using a 96-well head harvester (TomTec, USA). Finally, membrane bound radioactivity was measured by liquid scintillation counting (50µl per well of Scintillant, Ultima Gold F, PerkinElmer, UK) on the MicroBeta (PerkinElmer, UK) using a standard tritium counting programme (1 min per well).

The amount of radioactivity bound (in counts per minute or cpm) was then converted to fmole of [<sup>3</sup>H] M-MPEP per mg of protein present. For example, cpm values were divided by cpm/fmole (57.02) to determine the number of fmoles and then this was divided by the number of mg (i.e. 0.02) to give fmole/mg. Non-specific binding was defined with 0.5mM mavoglurant and subtracted from total binding to determine specific binding in fmole/mg.

The data were globally fitted to a one site total and non-specific saturation binding isotherm and B<sub>max</sub> and K<sub>d</sub> values of [<sup>3</sup>H] M-MPEP in each of the brain membranes were calculated from non-linear regression analysis of the saturation curve data using the software package in Prism (GraphPad Prism, San Diego, USA).

#### **2.2.11.5 Competition Binding**

Competition binding was used to determine the ability of unlabelled HTL0014242 to compete with a fixed concentration of [<sup>3</sup>H] M-MPEP for binding to mGlu<sub>5</sub> receptors and in doing so establish the affinity of HTL0014242. The assay was carried out in duplicate in mGlu<sub>5</sub> binding buffer (50mM HEPES, 150mM NaCl, pH 7.5) using 20µg of whole brain per well. The total reaction volume per well was 500µl. The concentration of [<sup>3</sup>H] M-MPEP was fixed to 2nM (the K<sub>d</sub> concentration of [<sup>3</sup>H] M-MPEP previously determined by saturation binding) and *SOD1*<sup>G93A</sup> transgenic and non-transgenic mouse brain membranes were incubated with increasing half-log concentrations of unlabelled HTL0014242 (3.16pM – 0.1µM). NSB was determined

by adding 5µl of 0.74mM cold MPEP (1% of total reaction volume) to each NSB well whilst total binding was determined by adding 5µl of DMSO to each total binding well. The competition binding assay was incubated for 3 hours with gentle agitation at 4°C. Following incubation, the assay was terminated by rapid filtration through 96-well GF/B glass microfibre filter plates, pre-soaked in 0.1% PEI buffer using a 96-well head harvester (TomTec, USA). Membrane bound radioactivity was then measured by liquid scintillation counting (50µl per well of Scintillant, Ultima Gold F, PerkinElmer, UK) using a standard tritium counting programme (1 min per well) using a MicroBeta (PerkinElmer, UK).

Competition curves were generated by plotting the specific binding (total binding minus the NSB) as a percentage of the total binding for increasing half-log concentrations of unlabelled HTL0014242 (3.16pM -0.1µM). The competition curves were then fitted to a four-parameter logistic equation to determine the IC<sub>50</sub> value (the concentration of HTL0014242 that displaces the specific binding of [<sup>3</sup>H] M-MPEP by 50%) of HTL0014242 for each brain membrane. The Cheung-Prusoff equation (Equation 1.1) was then used to convert the IC<sub>50</sub> values to K<sub>i</sub> (inhibition constant) values, which is attributable to affinity. This equation uses the K<sub>d</sub> values previously determined by saturation binding and the [<sup>3</sup>H] M-MPEP concentration of 2nM.

## **2.2.12 [<sup>3</sup>H] M-MPEP Binding Assay for *Ex Vivo* Receptor Occupancy**

### **2.2.12.1 Optimisation of Assay Conditions**

A [<sup>3</sup>H] M-MPEP binding assay was set up to determine *ex vivo* mGlu<sub>5</sub> RO in half brain tissue collected from the *in vivo* pharmacological mouse studies. To ensure HTL0014242 did not dissociate from mGlu<sub>5</sub> receptors during the experimental procedure several parameters were optimised.

Prior to using the precious HTL0014242-dosed brain membranes prepared from the *in vivo* mouse studies, optimisation of the RO assay took place using drug naïve non-transgenic and *SOD1*<sup>G93A</sup> mouse brain membranes collected at 30 and 120 days of age.

### **2.2.12.2 Crude Preparation of Brain Membranes**

Unlike previous [<sup>3</sup>H] M-MPEP binding assays, brain membranes collected for receptor occupancy (RO) were crudely prepared to ensure limited HTL0014242 dissociation from mGlu<sub>5</sub> receptors. Half brains in 1.5ml Eppendorfs were placed on dry ice and individually weighed. The average weight of an empty Eppendorf (1.56g) was

subtracted from the total weight of the Eppendorf containing the half brain. The half brain was subsequently resuspended in the appropriate volume of binding buffer at 4°C to give a stock concentration of 20mg/ml. Following resuspension, the half brain was homogenized using a Polytron homogenizer (4x 10s bursts) and kept on ice before being added directly to the assay plate.

### **2.2.12.3 Protein Linearity**

Protein linearities were initially carried out on crude brain membranes prepared from drug naïve non-transgenic and *SOD1<sup>G93A</sup>* mice collected at 30 and 120 days of age to determine which protein concentration gave the optimal signal between total and non-specific binding (NSB). Half brains were crudely prepared (as above) and were diluted to either 100ug/well or 200ug/well with binding buffer and re-homogenised to ensure even distribution of membrane protein in solution.

Membranes were incubated with [<sup>3</sup>H] M-MPEP (4nM), in assay buffer, for 10 minutes at 4°C. The total reaction volume per well was 500µl. Non-specific binding (NSB) was determined by adding 5µl (1% of total reaction volume) of cold MPEP (0.74mM) to each NSB well, whilst total radioligand binding at each concentration of membrane protein was measured by adding 5µl of DMSO to each total binding well. Radioligand ([<sup>3</sup>H] M-MPEP) was added to every well in the assay at a concentration of ~4nM. Brain membranes at 100ug/well or 200ug/well were added to the designated wells on the assay plate (445µl) and incubated for 10 minutes, with gentle agitation at 4°C.

Following incubation, assays were terminated by rapid filtration through 96-well GF/B glass microfibre filter plates, pre-soaked in 0.1% PEI buffer using a 96-well head harvester (TomTec, USA). Finally, membrane bound radioactivity was measured by liquid scintillation counting (50µl per well of Scintillant, Ultima Gold F, PerkinElmer, UK) on the MicroBeta (PerkinElmer, UK) using the '[<sup>3</sup>H] binding assay' protocol.

Whilst total binding was defined by mGlu<sub>5</sub> receptors in the presence of 4nM [<sup>3</sup>H] M-MPEP, non-specific binding was determined by 0.74mM unlabelled MPEP to occupy all available mGlu<sub>5</sub> receptors in the presence of 4nM [<sup>3</sup>H] M-MPEP. Specific binding was calculated by subtracting non-specific binding from total binding. The lowest concentration of crude brain membrane that demonstrated a good range for detecting specific binding was chosen for subsequent RO experiments to conserve mouse tissue (100ug/well).

#### 2.2.12.4 [<sup>3</sup>H] M-MPEP Kinetics

To further improve the RO assay experimental design and ensure that HTL0014242 compound dissociation from mGlu<sub>5</sub> receptors was kept to a minimum, [<sup>3</sup>H] M-MPEP radioligand kinetics were performed to determine the optimal radioligand concentration. Experiments were carried out in brain membranes from drug naïve non-transgenic and *SOD1<sup>G93A</sup>* mouse brains collected at 30 and 120 days of age. [<sup>3</sup>H] M-MPEP binding experiments were carried out in duplicate in mGlu<sub>5</sub> binding buffer (see Solutions and Buffers), using 20µg of whole brain per well. The total reaction volume per well was 500µl. Total binding and NSB were measured at K<sub>d</sub> concentration (~2nM) and at 10x K<sub>d</sub> concentration (~20nM) of [<sup>3</sup>H] M-MPEP. NSB was determined by adding 5µl of 0.74mM cold MPEP (1% of total reaction volume) to each NSB well. Total binding for each radioligand concentration was measured by adding 5µl of DMSO per total binding well. 50µl of [<sup>3</sup>H] M-MPEP radioligand (either at ~2nM or 20nM) was added to the designated wells on the assay plate. Finally, 445µl of brain membranes (20ug/well) were added to the relevant wells and the assay plate was incubated for 10 minutes, with gentle agitation at 4°C.

Following incubation, assays were terminated by rapid filtration through 96-well GF/B glass microfibre filter plates, pre-soaked in 0.1% PEI buffer using a 96-well head harvester (TomTec, USA). Finally, membrane bound radioactivity was measured by liquid scintillation counting (50µl per well of Scintillant, Ultima Gold F, PerkinElmer, UK) on the MicroBeta (PerkinElmer, UK) using a standard tritium counting programme (1 min per well).

#### 2.2.12.5 Receptor Occupancy

Following optimisation of the RO assay, HTL0014242 RO of mGlu<sub>5</sub> receptors in mouse brain tissue collected from the *in vivo* pharmacological studies were measured. Brain membranes were crudely prepared from *SOD1<sup>G93A</sup>* half brains collected at peak and trough HTL0014242 exposures (3-4 mice per dose group).

The final concentration of brain membrane added to the RO assay plate was ~100µg/well. To limit HTL0014242 ligand dissociation from mGlu<sub>5</sub> receptors in the brain membranes prepared for RO, a BCA assay to determine the precise concentration of protein in the tissue homogenate was not performed. However, a previous BCA assay was conducted on four drug naïve non-transgenic half brains and this demonstrated that the average concentration of a half brain homogenate was 1.75mg/ml. Consequently, this average concentration was used to calculate the

volume of binding buffer added to the brain membrane homogenate to produce a final concentration of ~100µg/well.

Membranes at 100µg/well were incubated for 10 minutes at 4°C with 20nM [<sup>3</sup>H] M-MPEP (HEP0472) in binding buffer, this was followed by rapid filtration to terminate the reaction. The total reaction volume per well was 500µl. NSB was determined by adding 5µl of 0.74mM MPEP (1% of total reaction volume) to each NSB well (6 wells per sample). Total binding was measured by adding 5µl of DMSO per total binding well (6 wells per sample). Following this, 50µl of [<sup>3</sup>H] M-MPEP radioligand (~20nM) was added to each well on the assay plate. Finally, 445µl of brain membranes (100µg/well) were added to the relevant wells and the assay plate was incubated for 10 minutes, with gentle agitation at 4°C.

Following incubation, assays were terminated by rapid filtration through Whatman glass fibre filters (Brandel), pre-soaked in 0.1% PEI buffer using a Brandel harvester (Brandel Inc., Gaithersburg, MD). Finally, filter discs were deposited in vials containing scintillant, (Ultima Gold F, PerkinElmer, UK) and membrane bound radioactivity was measured using a Hidex 300L scintillation counter (LabLogic, UK). Finally, HTL0014242 % receptor occupancies were calculated from the average specific binding (cpm) of [<sup>3</sup>H] M-MPEP with the values from the vehicle mouse brain membranes taken as 100% RO (see Equation 1.4 and Equation 1.5).

### **2.2.13 Statistical Analysis**

GraphPad Prism 7 was used for all statistical analyses (GraphPad, San Diego, CA). The main statistical tests used were one-way ANOVA or two-way ANOVA followed by a Tukey's post-test as indicated in the figure legends. All data analysed presented as mean ± SD unless otherwise stated.

# 3 Characterisation of mGlu<sub>5</sub> as a novel therapeutic target

## 3.1 Introduction

Glutamate-mediated excitotoxicity plays a major role in several neurodegenerative diseases, including MND (Lewerenz & Maher 2015; Ferraiuolo et al. 2011b). Elevated levels of extracellular glutamate are known to result in cellular injury and often culminate in cell death (Shaw et al. 2001). Astrocytic glutamate re-uptake transporters such as EAAT2 are crucial for regulating glutamate levels when they reach or exceed a threshold (Zerangue & Kavanaugh 1996; Zhou & Danbolt 2013). It is widely reported that astrocytes and other glial cells are drivers of MND disease progression (Boillee et al. 2006a; Yamanaka et al. 2008). Whether this is through a lack of trophic support or a gain in toxic function has not been fully elucidated, but it is likely that both are contributing factors (Lobsiger & Cleveland 2007).

The metabotropic glutamate receptor, mGlu<sub>5</sub>, is expressed on both neuronal and glial cells such as astrocytes, microglia and oligodendrocytes (reviewed by Battaglia & Bruno 2018). Over recent years evidence has grown to support a role for mGlu<sub>5</sub> in MND disease pathophysiology and there is now a strong evidence-base to investigate this receptor's potential as a novel therapeutic target in *SOD1* MND (Giribaldi et al. 2013; D'Antoni et al. 2011; Rossi et al. 2008).

The initial aim was to assess the clinical relevance of mGlu<sub>5</sub> through a series of target validation experiments. One of the key questions was whether mGlu<sub>5</sub> receptors are localised in an anatomical area known to be associated with MND pathology. For example, in the *SOD1*<sup>G93A</sup> mouse model of MND, one of the earliest pathologies observed is the loss of motor neurons in the lumbar region of the spinal cord (Zang & Cheema 2002). Further, motor neurons and surrounding glia are the primary cell types affected in MND, therefore identifying which cells express mGlu<sub>5</sub> will be crucial for understanding its potential relevance to disease pathophysiology.

It has previously been shown that mGlu<sub>5</sub> expression on astrocytes is elevated in both mouse and human MND cases (Martorana et al. 2012; Aronica et al. 2001; Anneser et al. 2004). Further, it has been suggested that mGlu<sub>5</sub> receptors play a role in mediating the cell death of mutant *SOD1* expressing astrocytes (Rossi et al. 2008). Following characterisation of mGlu<sub>5</sub> expression, the next aim will be to delineate any

changes in astrocytic mGlu<sub>5</sub> levels in the *SOD1*<sup>G93A</sup> mouse model of MND and mGlu<sub>5</sub> expression changes in human fibroblast derived iAstrocytes from MND patients with *SOD1* mutations.

Receptor density can change in response to the concentration of the endogenous ligand (Maguire et al. 2012). In MND glutamate levels are known to be elevated in CSF (Rothstein et al. 1990; Shaw et al. 1994; Shaw et al. 1995; Spreux-varoquaux et al. 2002). When mGlu<sub>5</sub> receptors are exposed to increasing levels of endogenous glutamate (for example, in response to disease progression), the receptor may undergo a compensatory down-regulation. Therefore, in the case of mGlu<sub>5</sub> it might be expected that there are fewer receptors at later stages of the *SOD1*<sup>G93A</sup> disease course compared to early on. There is conflicting evidence regarding changes in mGlu<sub>5</sub> receptor number throughout the disease course of the *SOD1*<sup>G93A</sup> mouse model of MND. Whilst Martorana et al. (2012), found that mGlu<sub>5</sub> receptors were elevated at 30 days of age vs 100 days of age in lumbar spinal cord; Brownell et al. (2015), observed that mGlu<sub>5</sub> receptor levels increased throughout the disease trajectory in both spinal cord and across several brain areas (hippocampus, striatum, cortex and also in whole brain). In order to investigate this, changes in mGlu<sub>5</sub> receptor levels will be investigated at early and late stages of disease in the *SOD1*<sup>G93A</sup> mouse model used in this project.

## **3.2 Results**

### **3.2.1 Characterisation of mGlu<sub>5</sub> in the *SOD1*<sup>G93A</sup> mouse model of MND**

In order to characterise the expression profile of mGlu<sub>5</sub> in lumbar spinal cord tissue in non-transgenic and *SOD1*<sup>G93A</sup> transgenic mice, an immunofluorescent staining protocol for mGlu<sub>5</sub> was established. Tissue sections from non-transgenic and *SOD1*<sup>G93A</sup> transgenic mice at 90 days of age were stained with anti-mGlu<sub>5</sub>. This demonstrated that the most prominent mGlu<sub>5</sub> staining in the lumbar spinal cord was in the dorsal grey matter compared to the ventral grey matter, both in non-transgenic and *SOD1*<sup>G93A</sup> tissue (Figure 3.1b-c). The dorsal grey matter staining corresponded largely to the substantia gelatinosa; an area containing sensory afferents and neurons (Figure 3.1b-c dorsal horn panels). Despite the majority of mGlu<sub>5</sub> staining being observed in the substantia gelatinosa there was also some weaker staining in the neuropil of the ventral grey matter, an area populated by motor neurons (Figure 3.1b-c ventral horn panels). Of note, anti-mGlu<sub>5</sub> staining was absent in the secondary antibody only control (Figure 3.1d). To demonstrate specificity of staining for the anti-mGlu<sub>5</sub> antibody, a rabbit isotype control primary antibody was used at the same

concentration as the mGlu<sub>5</sub> antibody. Immunohistochemistry with this isotype control antibody revealed no specific staining throughout the lumbar spinal cord section (Figure 3.1e). Furthermore, antibody specificity was confirmed with a peptide competition experiment, by competing the binding of the anti-mGlu<sub>5</sub> antibody with an mGlu<sub>5</sub> peptide at 80x the molar concentration of the anti-mGlu<sub>5</sub> antibody. Following mGlu<sub>5</sub> peptide competition, no anti-mGlu<sub>5</sub> staining was observed across the lumbar spinal cord section (Figure 3.1f). Particularly convincing from both the isotype control and peptide competition experiments was the lack of staining in the dorsal grey matter, the region where mGlu<sub>5</sub> staining is predominant.

It has previously been reported that mGlu<sub>5</sub> is expressed on astrocytes across most brain regions (Biber et al., 1999), and on both neuronal and glial cells located in the lumbar spinal cord of both non-transgenic and *SOD1<sup>G93A</sup>* mice (Martorana et al. 2012). Dual labelling for anti-GFAP (an astrocytic marker) and anti-mGlu<sub>5</sub> was carried out in 90 day old non-transgenic and *SOD1<sup>G93A</sup>* mouse lumbar spinal cord, to first observe whether there was any co-localisation of mGlu<sub>5</sub> on astrocytes. Figure 3.2 (a and e) show typical anti-mGlu<sub>5</sub> staining in the substantia gelatinosa of mouse lumbar spinal cord. However, single channel staining of an enlarged area within the ventral horns indicates that anti-mGlu<sub>5</sub> does not co-localise with anti-GFAP staining in 90 day old non-transgenic or *SOD1<sup>G93A</sup>* mouse spinal cord (ventral horn panels, Figure 3.2b-d and f-h).

Interestingly, Rossi et al. (2008), reported the presence of a subpopulation of spheroid GFAP-positive cells (SGPCs) that exhibited an unusual morphology, unique to *SOD1<sup>G93A</sup>* mice. These SGPCs formed from ~75 days onwards in the ventral lumbar SC of *SOD1<sup>G93A</sup>* mice and increased in number by 21-fold at 100 days of age and by 57-fold at end-stage. The SGPCs were characterised by an enlarged rounded cell body and short, thick processes (Rossi et al. 2008). Despite the GFAP-positive staining observed in Figure 3.2f in *SOD1<sup>G93A</sup>* SC being somewhat more prominent in processes than the GFAP staining observed in non-transgenic SC (Figure 3.2b), it did not coincide with the description of the rounded-up spheroid shaped astrocytes described by Rossi et al. (2008). However, perhaps this can be explained, in part, by the fact that the GFAP staining in Figure 3.2 took place in SC sections at 90 days of age. Perhaps the formation of SGPCs is associated with a later stage of the disease in the *SOD1<sup>G93A</sup>* mouse model of MND used in this project. For example, the *SOD1<sup>G93A</sup>* mouse model used by Rossi et al. (2008), is on a different genetic background (mixed C57BL6/SJL genetic background) compared to the *SOD1<sup>G93A</sup>*

mouse model used throughout this project (inbred C57BL/6 genetic background) and consequently the disease trajectories are somewhat different.

Previous findings showing that mGlu<sub>5</sub> is expressed on astrocytes in mouse spinal cord could not be reproduced, therefore, the next cell type investigated was microglial cells. Anti-mGlu<sub>5</sub> was co-stained with anti-Iba1 (a microglial marker), in non-transgenic and *SOD1<sup>G93A</sup>* mouse lumbar spinal cord collected at 90 days of age. Figure 3.3 (a and e) shows the typical mGlu<sub>5</sub> expression observed in mouse spinal cord. Whilst typical microglial staining was observed within the ventral horns, it did not co-localise with anti-mGlu<sub>5</sub> staining (ventral horn panels, Figure 3.2b-d and f-h).

Finally, dual labelling for both mGlu<sub>5</sub> and choline acetyl-transferase (ChAT, a marker of cholinergic neurons) was carried out in non-transgenic and *SOD1<sup>G93A</sup>* mouse lumbar spinal cord at 90 days. Figure 3.4 (a and e) demonstrated that anti-mGlu<sub>5</sub> was expressed mostly in the dorsal horn, as shown previously. Motor neurons were identified by a combination of ChAT staining, their large size and their location (motor neurons are located in the ventral horns). Medium and large ChAT-positive cells were present in the ventral horns of both non-transgenic and *SOD1<sup>G93A</sup>* lumbar spinal cords (ventral horn panels, Figure 3.4b-d and f-h). Intriguingly, some but not all motor neurons expressed weak anti-mGlu<sub>5</sub> staining in their cell body, indicating that mGlu<sub>5</sub> is only found on some motor neurons. This finding was most apparent in the *SOD1<sup>G93A</sup>* tissue, whilst anti-mGlu<sub>5</sub> staining was also present on motor neurons in the non-transgenic tissue, the level of expression appeared to be much weaker.

Interestingly, there was also some mGlu<sub>5</sub> staining that did not co-localise with ChAT-positive cells in the ventral lumbar spinal cord sections of both non-transgenic and *SOD1<sup>G93A</sup>* mice (Figure 3.4c and 3.4g). The appearance of the mGlu<sub>5</sub> staining looked like fine axonal processes or possibly even brain capillaries. However, additional dual-staining experiments would need to be carried out to establish the precise nature of this mGlu<sub>5</sub> staining.

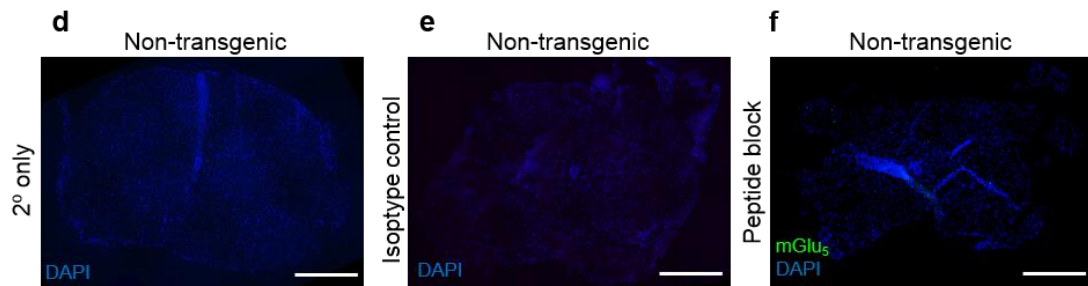
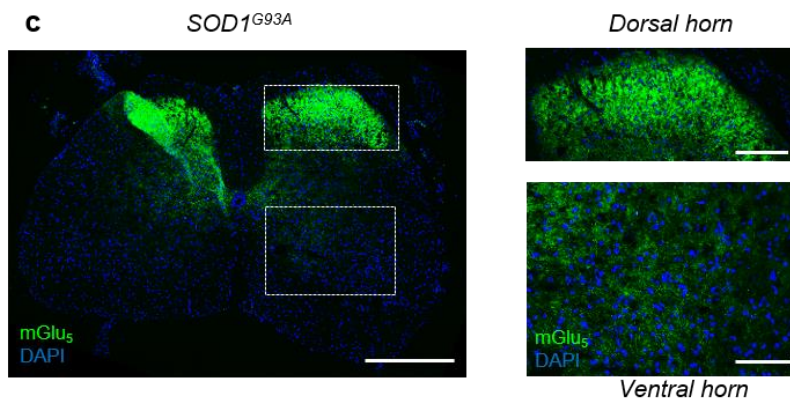
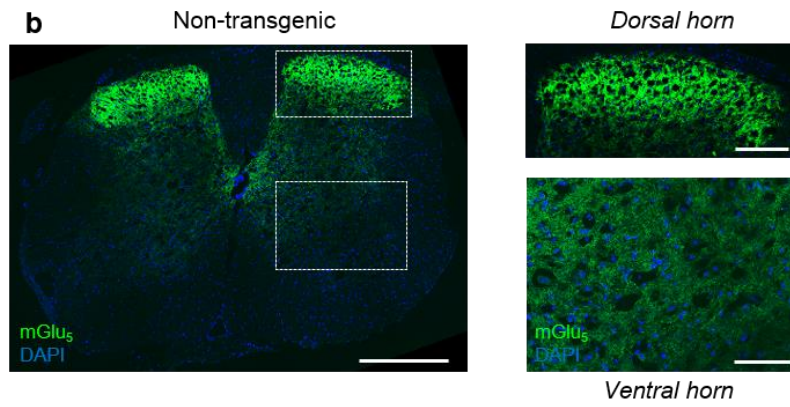
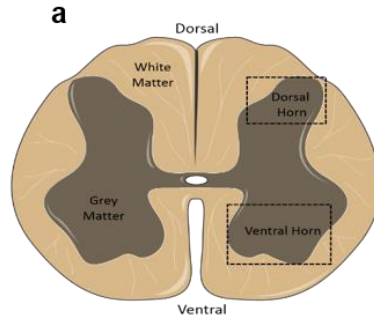


**Figure 3.1. mGlu<sub>5</sub> is predominantly expressed in the dorsal horn of mouse lumbar spinal cord sections.** a) Schematic of lumbar spinal cord section. Non-transgenic (b) and *SOD1<sup>G93A</sup>* (c) mouse lumbar spinal cord sections at 90 days of age were fixed, paraffin-embedded and immuno-stained with an anti-mGlu<sub>5</sub> antibody and DAPI. mGlu<sub>5</sub> staining is seen largely in dorsal grey matter, with some weaker staining observed in the neuropil of the ventral grey matter (b-c dotted white box insets). mGlu<sub>5</sub> staining was absent in the secondary only control (d), the isotype control (e) and the mGlu<sub>5</sub> peptide competition control (f). Scale bars, 500µm (main panels a-e). Dorsal and ventral horn insets, scale bar = 150 µm.

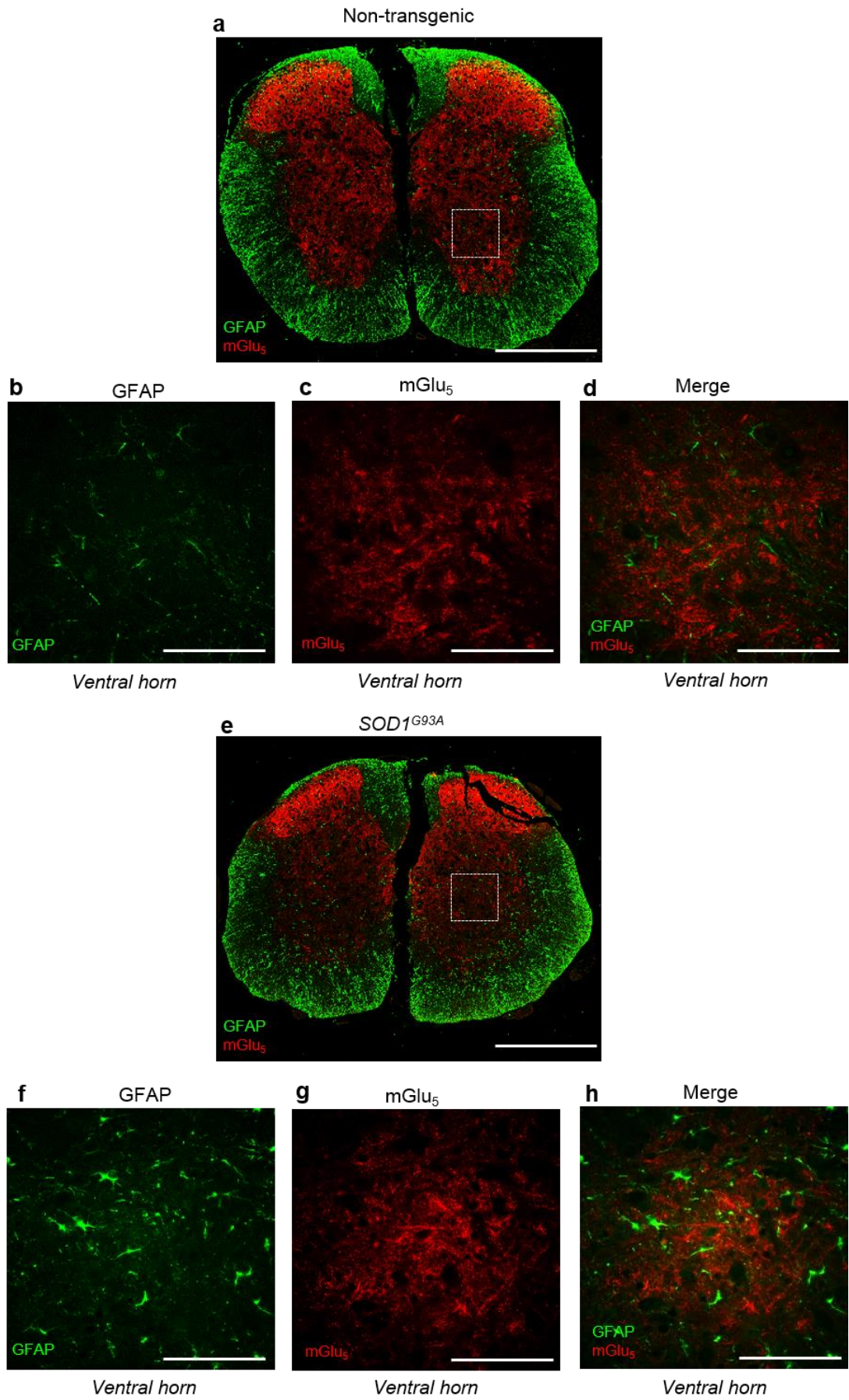
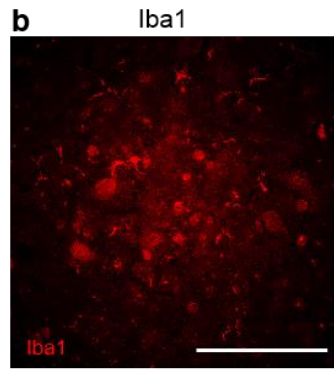
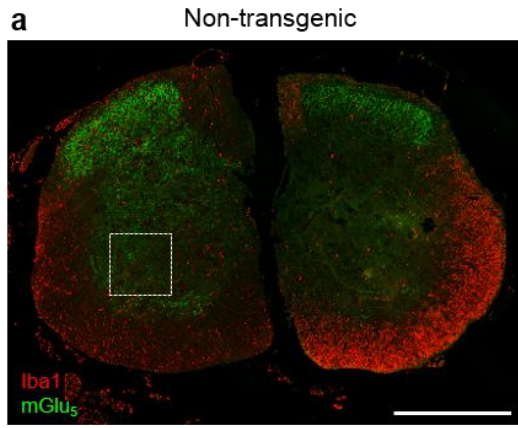
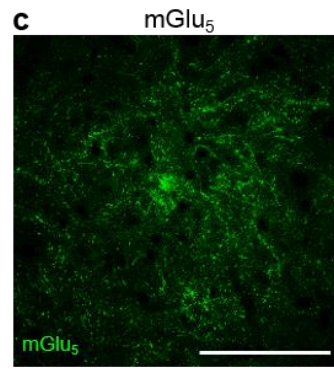


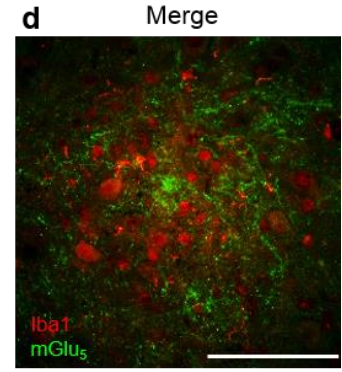
**Figure 3.2. mGlu<sub>5</sub> is not expressed by astrocytes in mouse lumbar spinal cord.** Non-transgenic (a) and *SOD1<sup>G93A</sup>* (e) mouse lumbar spinal cord sections at 90 days of age were fixed, paraffin-embedded and immuno-stained with anti-mGlu<sub>5</sub> and anti-GFAP antibodies. Insets of the dotted white boxes (b-d non-transgenic) and (f-h *SOD1<sup>G93A</sup>*). Scale bars, 500µm (main panels a-b). Ventral horn insets, scale bar = 100 µm.



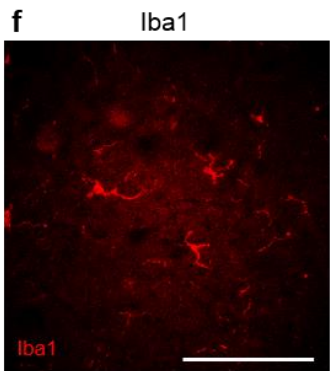
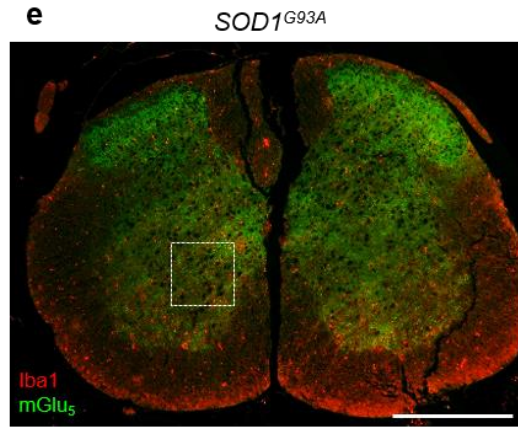
Ventral horn



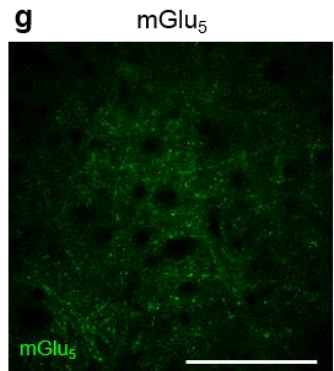
Ventral horn



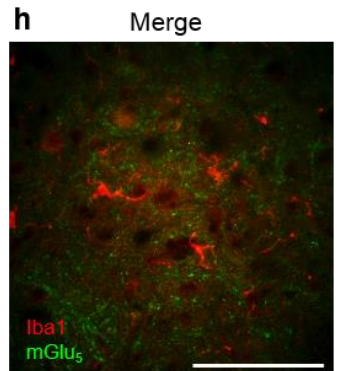
Ventral horn



Ventral horn



Ventral horn



Ventral horn

**Figure 3.3. mGlu<sub>5</sub> is not expressed on microglia in mouse lumbar spinal cord.** Non-transgenic (a) and *SOD1<sup>G93A</sup>* (e) mouse lumbar spinal cord sections at 90 days of age were fixed, paraffin-embedded and immuno-stained with anti-mGlu<sub>5</sub> and anti-Iba1 antibodies. Insets of the dotted white boxes (b-d non-transgenic) and (f-h *SOD1<sup>G93A</sup>*). Scale bars, 500µm (main panels a-b). Ventral horn insets, scale bar = 100 µm.

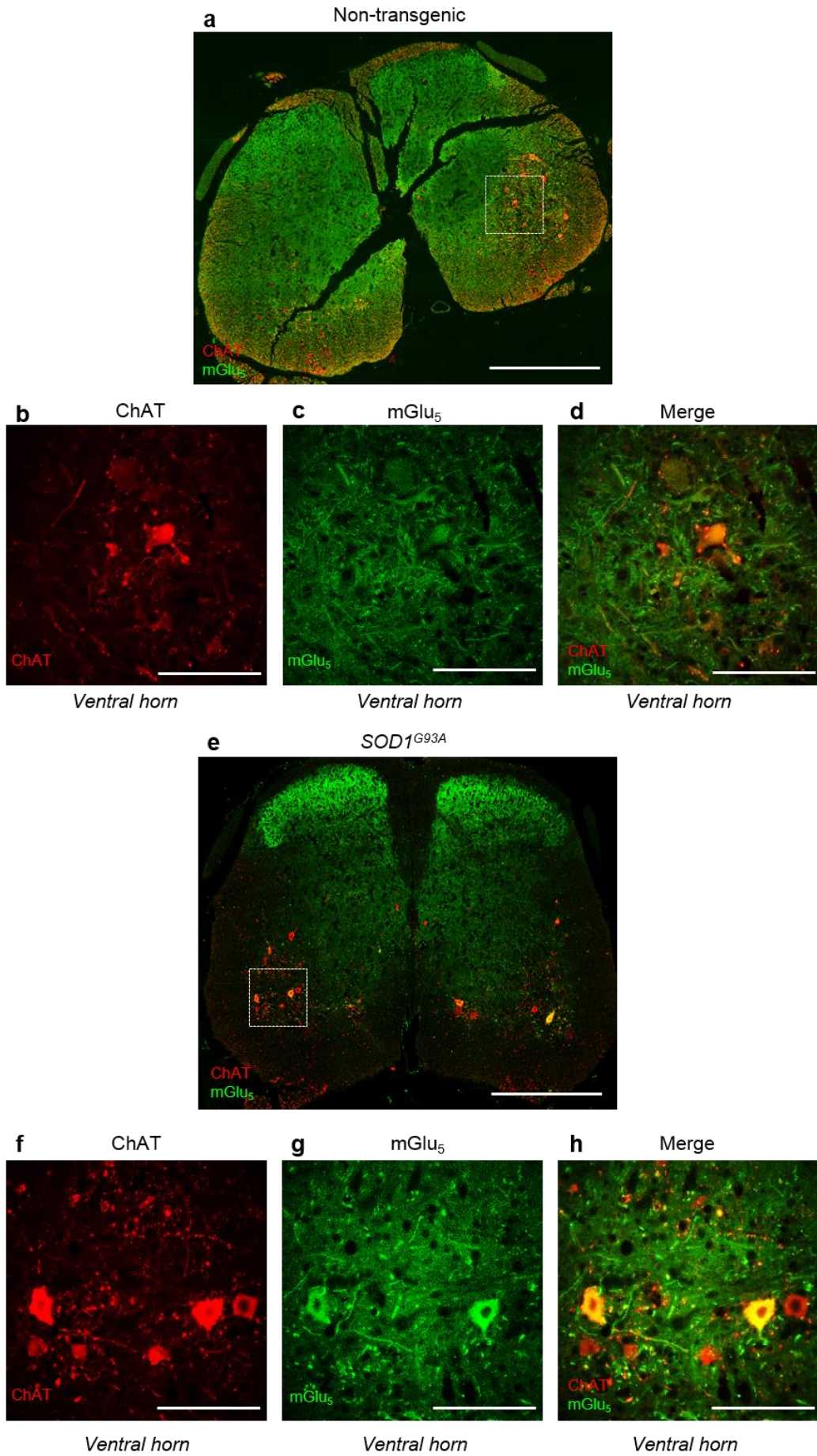


**Figure 3.4. mGlu<sub>5</sub> is expressed on motor neurons in mouse lumbar spinal cord.**

Non-transgenic (a) and *SOD1<sup>G93A</sup>* (e) mouse lumbar spinal cord sections at 90 days of age were fixed, paraffin-embedded and immuno-stained with anti-mGlu<sub>5</sub> and anti-ChAT antibodies. Insets of the dotted white boxes (b-d non-transgenic) and (f-h *SOD1<sup>G93A</sup>*). Scale bars, 500µm (main panels a-b). Ventral horn insets, scale bar = 100 µm.

### **3.2.2 Characterisation of mGlu<sub>5</sub> in human derived iAstrocytes from *SOD1* patients**

It has previously been shown that mGlu<sub>5</sub> is expressed on astrocytes in the ventral horn of lumbar spinal cords from MND patients and healthy controls (Anneser et al., 2004). In addition, it was found that mGlu<sub>5</sub> in the spinal cord of MND patients is upregulated compared to that of the controls (Anneser et al., 2004).

An immunocytochemistry (ICC) protocol was established for mGlu<sub>5</sub> on fibroblast derived iAstrocytes, obtained from MND patients with *SOD1* mutations and age matched healthy controls. The iAstrocytes were initially characterised with the astrocytic markers S100 $\beta$  and CD44 (Figure 3.5a-b, respectively). The cells were positive for both S100 $\beta$  and CD44 demonstrating that the cells expressed both astrocytic markers. Expression of mGlu<sub>5</sub> was defined in two *SOD1* and two control-matched iAstrocyte cell lines, Figure 3.5 (c-d). ICC revealed that mGlu<sub>5</sub> is expressed both in *SOD1* and control derived iAstrocytes. Quantification of mGlu<sub>5</sub> expression revealed there was no significant difference in mGlu<sub>5</sub> expression between the *SOD1* and control cell lines, as shown by Students' T test;  $p = 0.9183$  (Figure 3.5f).

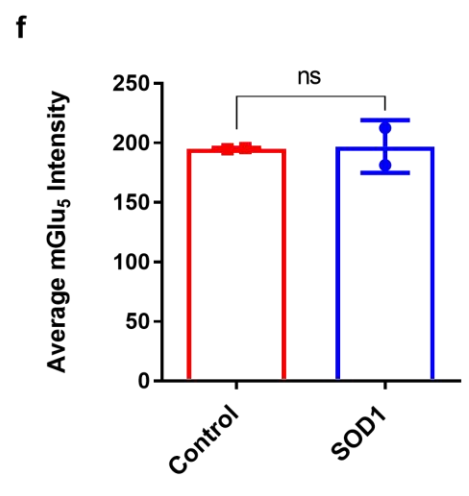
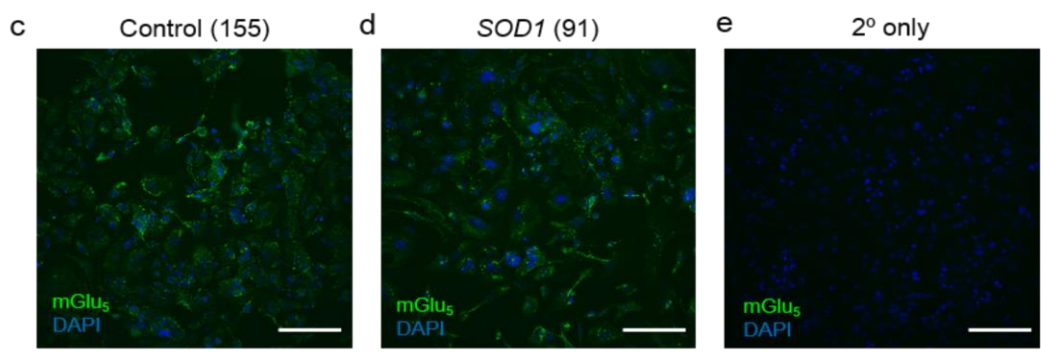
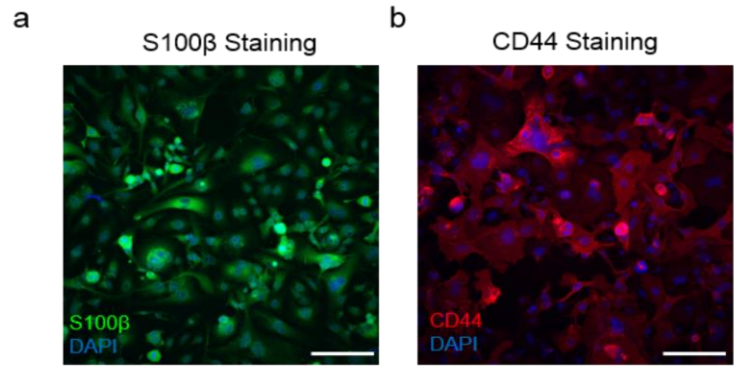


**Figure 3.5. mGlu<sub>5</sub> is expressed in both control and *SOD1* human iAstrocytes.** iAstrocyte cell lines were derived from patients with *SOD1* MND and age matched healthy controls by the Ferraiuolo lab group. Cells were fixed and immuno-stained with astrocytic markers anti-S100 $\beta$  and anti-CD44 antibodies, as shown in panels a and b respectively. Cells were also immunostained with an anti-mGlu<sub>5</sub> antibody and DAPI. Representative images for mGlu<sub>5</sub> staining in healthy control iAstrocytes and *SOD1* MND patient iAstrocytes shown in panels c and d respectively. Staining for mGlu<sub>5</sub> was absent in secondary only control (panel e). Scale bars, 50 $\mu$ m. Quantification of average mGlu<sub>5</sub> grey level intensities revealed there was no significant difference in expression between *SOD1* and control iAstrocytes (*SOD1*:  $196.9 \pm 21.9$ , Control;  $195.2 \pm 0.7$ ,  $p=0.9183$ ; Student's T Test). Data presented as mean  $\pm$  SD from two independent experiments; ns = non-significant (f).

### 3.2.3 Characterisation of brain mGlu<sub>5</sub> receptor number in the *SOD1<sup>G93A</sup>* mouse model of MND

Research suggests that mGlu<sub>5</sub> receptor levels change throughout the disease course in the *SOD1<sup>G93A</sup>* mouse model, however, data are conflicting on whether receptor levels increase or decrease in brain and spinal cord. The aim of this experiment was to characterise mGlu<sub>5</sub> expression changes in the *SOD1<sup>G93A</sup>* mouse model used in this project. Originally the aim was to prepare membranes from both non-transgenic and *SOD1<sup>G93A</sup>* whole brain and spinal cord tissue. Unfortunately, it was not possible to generate enough protein from a single spinal cord to perform saturation binding experiments. Consequently, mGlu<sub>5</sub> receptor density could only be analysed from whole brain tissue.

To determine the most suitable protein concentration for saturation binding experiments, different concentrations of membrane proteins (1, 2.5, 5, 10, 20, 30µg) prepared from both non-transgenic and *SOD1<sup>G93A</sup>* mouse brains at 30 and 120 days of age were incubated with around a  $K_d$  concentration (4nM) of [<sup>3</sup>H] M-MPEP. Total and non-specific radioligand binding were measured at each concentration of membrane protein (Figure 3.6a-d). Non-specific binding was defined by an excessive concentration of mavoglurant (0.5mM) to occupy all available mGlu<sub>5</sub> receptors. To determine the specific binding, non-specific binding was subtracted from total binding.

To avoid ligand depletion, the total binding of radioligand should be less than 10% of the total radioligand added to the assay (represented by the dotted line on the histograms). For all four membranes the total binding was less than 10% of the total radioligand added (Figure 3.6). As mouse tissue is being used, it was important to use the lowest concentration possible to conserve membrane stocks, therefore a protein concentration of 20µg/well was chosen as the optimum window for detecting specific binding (the difference between total and non-specific binding) and was used for all subsequent saturation binding experiments (Figure 3.6).

Saturation binding was carried out in triplicate for brain membranes prepared from non-transgenic and *SOD1<sup>G93A</sup>* mouse whole brains collected at 30 and 120 days of age (representative data shown in Figure 3.7a-d). 20µg/well of brain membranes were incubated with increasing concentrations of [<sup>3</sup>H] M-MPEP. The saturation curves plotted in Figure 3.7 (a-d), were generated by plotting total and non-specific binding versus the radioligand concentration. The  $K_d$  and  $B_{max}$  of [<sup>3</sup>H] M-MPEP for each membrane was calculated from non-linear regression analysis of the saturation curve data using the software package in Prism (GraphPad, San Diego, CA). Average  $K_d$

and  $B_{\max}$  shown in Figure 3.7e for each brain membrane were calculated from three independent experiments. Saturation binding showed a non-significant trend for higher receptor numbers at 30 days compared to 120 days, in both non-transgenic ( $B_{\max}$  (fmole/mg)  $1929 \pm 256$  and  $1799 \pm 235$ ; 30D and 120D respectively) and *SOD1<sup>G93A</sup>* ( $B_{\max}$  (fmole/mg) =  $1882 \pm 234$  and  $1462 \pm 206$ ; 30D and 120D respectively) membranes ( $p=0.1382$ ; 1-way ANOVA). Furthermore, there was no significant difference in  $K_d$  across all membranes ( $p = 0.8297$ , analysed by 1-way ANOVA), confirming that radioligand affinity for mGlu<sub>5</sub> is consistent within all brain membranes.

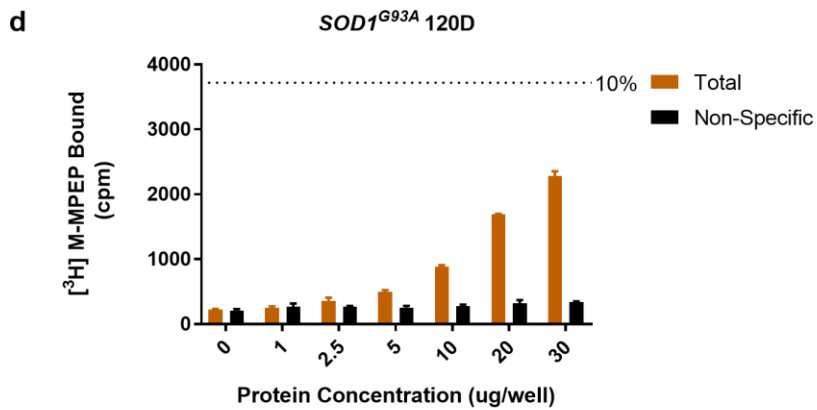
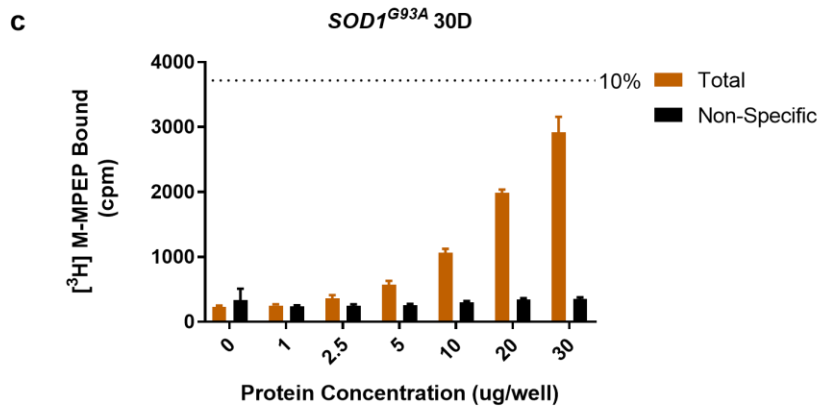
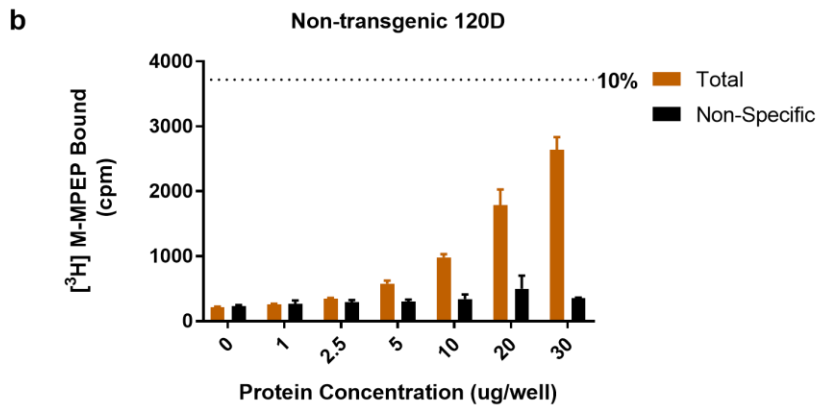
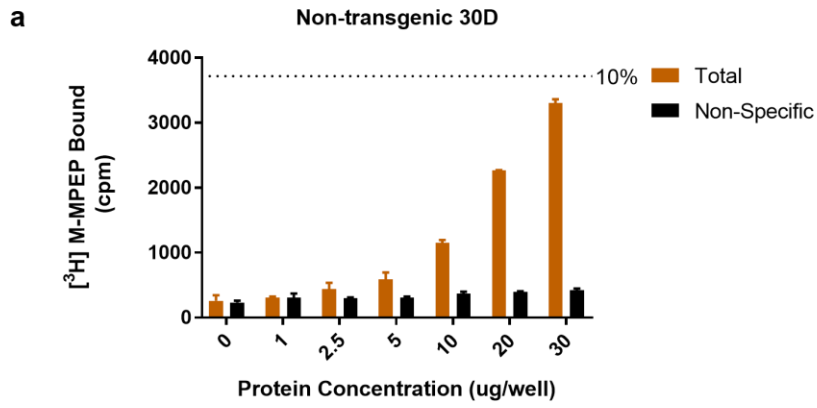
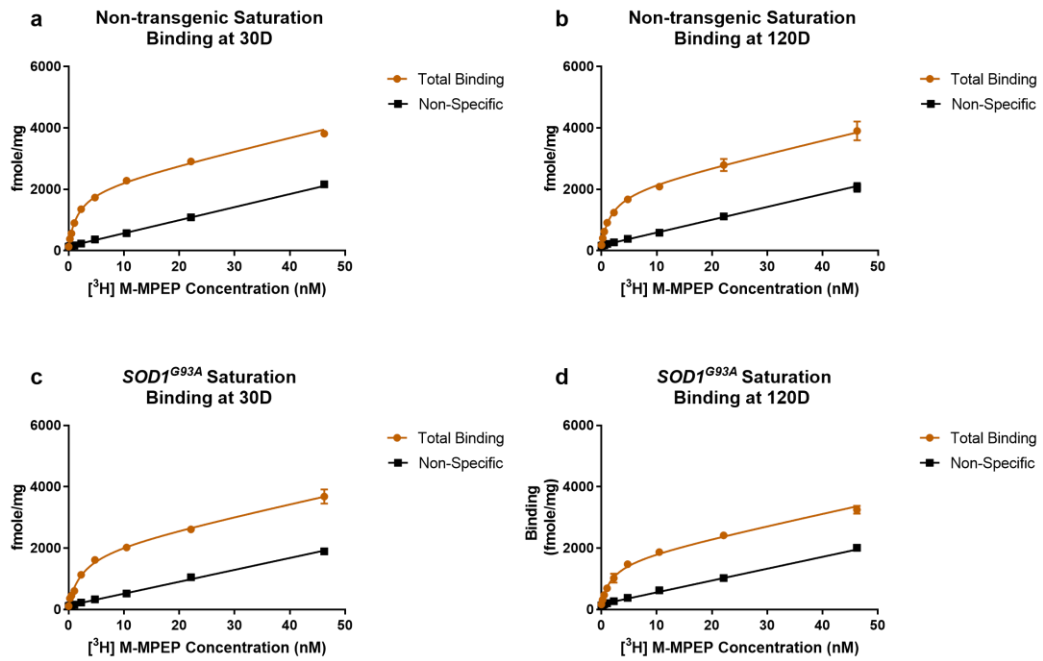


**Figure 3.6. Specific binding with 4nM [<sup>3</sup>H] M-MPEP is linear with increasing protein concentrations of mouse brain membranes.** Membranes were prepared from whole brains collected from non-transgenic and SOD1<sup>G93A</sup> mice at 30 and 120 days of age. Total and non-specific radioligand binding is shown at 6 protein concentrations for each brain membrane (a-d). The dotted line defines 10% of the total added radioligand ([<sup>3</sup>H] M-MPEP). To avoid ligand depletion the total binding of radioligand should be < 10% of the total radioligand added.



e

Tissue	$B_{max}$ (fmole/mg) Mean $\pm$ SD	$K_d$ (nM) Mean $\pm$ SD
Non-transgenic 30D	1929 $\pm$ 256	1.75 $\pm$ 0.13
Non-transgenic 120D	1799 $\pm$ 235	1.83 $\pm$ 0.33
<i>SOD1<sup>G93A</sup></i> 30D	1882 $\pm$ 234	2.12 $\pm$ 0.34
<i>SOD1<sup>G93A</sup></i> 120D	1462 $\pm$ 206	2.07 $\pm$ 0.45

**Figure 3.7. *SOD1<sup>G93A</sup>* disease progression does not change brain mGlu<sub>5</sub> receptor number.** Membranes (20  $\mu$ g/well) were prepared from whole brains collected from non-transgenic and *SOD1<sup>G93A</sup>* mice at 30 days (30D) and 120 days (120D) of age and incubated for 1.5 h at RT with increasing concentrations of radioligand [<sup>3</sup>H] M-MPEP in assay buffer. The assay was terminated by rapid filtration and the amount of radioactivity bound to membrane was measured by liquid scintillation counting. The amount of radioactivity bound (in counts per minute or cpm) was then converted to fmole of ([<sup>3</sup>H] M-MPEP per mg of protein present. For example, cpm values were divided by cpm/fmole (57.02) to determine the number of fmoles and then this was divided by the number of mg (i.e. 0.02) to give fmole/mg. Non-specific binding was defined with 0.5mM mavoglurant and subtracted from total binding to determine specific binding. Representative data for each of the brain membranes are shown (a-d) from three independent saturations. For each

experiment 8 increasing concentrations of radioligand were added in triplicate. Data presented as mean  $\pm$  S.E.M (a-d). e) Combined saturation binding data from three independent experiments showed no significant difference between the different brain membranes for  $B_{max}$  ( $p = 0.1382$ ; 1-way ANOVA) or [ $^3H$ ] M-MPEP affinity ( $p = 0.8297$ ; 1-way ANOVA).

### 3.3 Discussion

The purpose of this chapter was to identify the general staining pattern of mGlu<sub>5</sub> in non-transgenic and *SOD1<sup>G93A</sup>* mouse lumbar spinal cord sections. Following on from this, cell-specific expression of mGlu<sub>5</sub> in the *SOD1<sup>G93A</sup>* mouse model of MND was investigated. Previously, it has been shown that mGlu<sub>5</sub> is upregulated on glial cells in cases of both mouse and human MND (Martorana et al. 2012; Aronica et al. 2001; Anneser 2004). Consequently, mGlu<sub>5</sub> immunoreactivity was characterised and levels quantified in human derived iAstrocytes from MND patients with *SOD1* mutations and healthy controls. Finally, literature reports on whether mGlu<sub>5</sub> receptor levels increase or decrease throughout the disease trajectory of the *SOD1<sup>G93A</sup>* mouse model of MND are inconsistent (Martorana et al. 2012; Brownell et al. 2015). Consequently, a radioligand binding assay was set up to establish global mGlu<sub>5</sub> receptor densities in *SOD1<sup>G93A</sup>* brain tissue at both early and late stages of the disease. Global mGlu<sub>5</sub> receptor densities were also measured in non-transgenic mouse brains collected at the same time-points for comparison.

#### 3.3.1 Characterisation of mGlu<sub>5</sub> in the *SOD1<sup>G93A</sup>* mouse model of MND

An immunofluorescent staining method was established for mGlu<sub>5</sub> and specificity of staining confirmed by isotype control and mGlu<sub>5</sub> peptide competition experiments. Characterisation of mGlu<sub>5</sub> suggests that there is no obvious difference between mGlu<sub>5</sub> expression in non-transgenic and *SOD1<sup>G93A</sup>* mouse lumbar spinal cord tissue at 90 days of age (Figure 3.1b-c). In both sets of tissue mGlu<sub>5</sub> was expressed predominantly in laminae I and II of the dorsal horn, whilst some weaker staining was observed in the grey matter parenchyma in the ventral horn. Dual staining in spinal cord tissue was not suggestive of mGlu<sub>5</sub> co-expression on astrocytes or microglia (Figure 3.2 and Figure 3.3, respectively). However, weak mGlu<sub>5</sub> staining was observed in some ventral motor neurons (Figure 3.4).

Findings in mouse spinal cord are consistent with previous work looking at mGlu<sub>5</sub> expression in human post-mortem spinal cord tissue obtained from MND and healthy control patients (Aronica et al. 2001). It was previously reported that the staining pattern for mGlu<sub>5</sub> was comparable between control and MND spinal cords and predominantly that it was located in the dorsal horn (superficial laminae I and II). This finding is in keeping with reports that mGlu<sub>5</sub> may play a role in mediating sensory processing in the dorsal horn (Boxall et al. 1996).

Interestingly, mGlu<sub>5</sub> was not found to be expressed on GFAP-positive cells in the ventral horns of both non-transgenic and *SOD1<sup>G93A</sup>* mouse spinal cords (Figure 3.2). Martorana et al. (2012), demonstrated that mGlu<sub>5</sub> mRNA was present in astrocytes from spinal cords of both non-transgenic and *SOD1<sup>G93A</sup>* mice. Whilst this may be suggestive of mGlu<sub>5</sub> expression on astrocytes it is by no means confirmatory. Furthermore, in human post-mortem spinal cords of MND patients, Anneser et al. (2004), found that anti-GFAP and anti-mGlu<sub>5</sub> expression were highly positively correlated and that predominantly mGlu<sub>5</sub> was co-localised on astrocytes. However, they found that mGlu<sub>5</sub> staining was virtually absent in astrocytes of control spinal cords. Perhaps the inconsistency between human and mouse levels of astrocytic mGlu<sub>5</sub> detected in MND spinal cords, can be accounted for by the different stage of disease at which mGlu<sub>5</sub> staining took place. Characterisation of mGlu<sub>5</sub> levels in human post-mortem spinal cords was carried out at end-stage of disease, whereas in mouse spinal cords mGlu<sub>5</sub> expression was characterised at 90 days of age. Average age of onset in the *SOD1<sup>G93A</sup>* mouse model of MND is 75 days of age and end-stage ranges between approximately 130 to 170 days of age. Therefore, characterisation of mGlu<sub>5</sub> in mouse spinal cords took place at a much earlier stage of the disease compared to human spinal cords. Alternatively, expression of astrocytic mGlu<sub>5</sub> observed in the human post-mortem spinal cords of MND patients could be a pathological feature specific to the human disease.

Of note, Sun et al. (2013), have shown by immuno-electron microscopy that mouse astrocytic mGlu<sub>5</sub> is developmentally regulated and is undetectable after post-natal week 3. In contrast, mGlu<sub>3</sub> was found to be expressed on astrocytes at all developmental stages. Furthermore, microarray and quantitative PCR demonstrated that mGlu<sub>3</sub> was the predominant mGlu receptor expressed on human adult cortical astrocytes however, mGlu<sub>5</sub> was barely detectable (Wei Sun et al. 2013). If astrocytic mGlu<sub>5</sub> is developmentally regulated in mouse, this may account for the lack of co-localisation observed between mGlu<sub>5</sub> and GFAP-positive cells in both non-transgenic and *SOD1<sup>G93A</sup>* lumbar SC (Figure 3.2).

Whilst it has been shown previously that mGlu<sub>5</sub> is expressed in cultured microglia (Biber et al. 1999). Dual staining for anti-mGlu<sub>5</sub> and anti-Iba1 in mouse spinal cords demonstrated no co-localisation (Figure 3.3). This is consistent with work by Aronica et al. (2001), who also found that mGlu<sub>5</sub> was not expressed on microglia in human post-mortem spinal cords of MND patients or controls.

Consistent with the co-localisation of mGlu<sub>5</sub> on ChAT positive cells observed in ventral lumbar SC sections of non-transgenic and *SOD1*<sup>G93A</sup> mice (Figure 3.4), Aronica et al. (2001), also showed that mGlu<sub>5</sub> was expressed on neuronal cells throughout the spinal cord tissue. However, it is not clear why mGlu<sub>5</sub> was only expressed on some of the motor neurons detected by anti-ChAT in mouse lumbar spinal cords (Figure 3.4). Anti-ChAT detects choline acetyltransferase, a major neurotransmitter used by most motor neurons. This antibody is specific for all cholinergic neurons and therefore neurons that innervate motor neurons may also be detected (Barber et al. 1984). To account for this, size and location of the ChAT-positive cells were used to identify ventral motor neurons.

One explanation for why only some of the ChAT-positive cells expressed mGlu<sub>5</sub> could be accounted for by the selective vulnerability of certain motor neurons to degeneration. It is well documented that fast fatigable motor neurons are more susceptible to degeneration in MND due to their high metabolic demands and size (San Pun et al. 2006). In addition, the distribution of calcium binding proteins (CBP) expressed within motor neurons is also thought to be a determinant of their selective vulnerability to neurodegeneration. It has previously been documented that MND patients demonstrate a loss of calbindin-positive neuronal processes in their SC, brainstem and motor cortex compared with healthy controls (Ince et al. 1993). Furthermore, it has been shown in *SOD1*<sup>G86R</sup> mice, that calretinin-positive neurons are selectively vulnerable to degeneration, whereas calbindin-positive neurons are not (Morrison et al. 1996). Interestingly, mGlu<sub>5</sub> is predominantly expressed on calretinin containing motor neurons and consequently it has been suggested that mGlu<sub>5</sub> may contribute to their selective vulnerability (Aronica et al. 2001). It is conceivable that the ChAT-positive cells dual labelled for mGlu<sub>5</sub> (shown in Figure 3.4), are selectively vulnerable calretinin-positive motor neurons. However, further investigation with triple-labelling for mGlu<sub>5</sub>, ChAT and calretinin would need to be undertaken to validate this.

### **3.3.2 Characterisation of mGlu<sub>5</sub> in human derived iAstrocytes from *SOD1* patients**

The expression of mGlu<sub>5</sub> was also characterised in human iAstrocytes derived from MND patients with *SOD1* mutations. Both *SOD1* and control derived iAstrocytes showed low level expression of mGlu<sub>5</sub> *in vitro*. However, quantification of mGlu<sub>5</sub> expression on human derived iAstrocytes was not suggestive of increased mGlu<sub>5</sub> levels on *SOD1* astrocytes compared to controls (Figure 3.5). These data contradict

previous findings of increased mGlu<sub>5</sub> expression on reactive astrocytes in human post-mortem spinal cords from patients with both familial and sporadic MND (Aronica et al. 2001).

Perhaps the mGlu<sub>5</sub> profile observed for the *SOD1* iAstrocytes is not reflective of mGlu<sub>5</sub> receptor levels on reactive astrocytes. It is reported in the literature that mGlu<sub>5</sub> expression is relatively low on astrocytes cultured in conventional serum with media (Miller et al. 1995). When astrocytes are cultured in medium containing growth factors such as basic fibroblast growth factor, this triggers the activation of astrocytes, emulating reactive gliosis (Miller et al. 1995). It has previously been shown that mGlu<sub>5</sub> staining is elevated on reactive astrocytes in spinal cords of MND patients but not on non-activated astrocytes in spinal cords of controls (Anneser 2004). Perhaps co-culturing iAstrocytes with media containing growth factors would better recapitulate the mGlu<sub>5</sub> expression profile found on reactive astrocytes in human post-mortem spinal cords of patients with MND.

Whilst the iAstrocytes were derived from adult human fibroblasts (which are not themselves implicated in MND), being differentiated from induced neural progenitor cells (iNPCs) means that they retain phenotypic markers of MND (Meyer et al. 2014), unlike astrocytes differentiated from induced pluripotent stem cells (iPSCs) (Egawa et al. 2012). However, perhaps the native architecture found *in vivo* is necessary to recapitulate mGlu<sub>5</sub> expression levels found on reactive astrocytes in human cases of MND. For example, the relationship between different cell-types may influence mGlu<sub>5</sub> expression levels on astrocytes.

Alternatively, it is possible that elevated mGlu<sub>5</sub> levels on astrocytes is not a feature of *SOD1* MND. Reports of elevated mGlu<sub>5</sub> levels on astrocytes are from studies on human post-mortem spinal cords from patients with familial and sporadic MND (Aronica et al. 2001; Anneser 2004). It would be interesting to know how many of the spinal cords analysed were from patients with *SOD1* MND, if any, especially considering that mutations in the *SOD1* gene represent only approximately 2-3% of all MND cases (Chiò et al. 2008).

### **3.3.3 Characterisation of brain mGlu<sub>5</sub> receptor number in the *SOD1*<sup>G93A</sup> mouse model of MND**

Whilst Martorana et al. (2012), found that expression of mGlu<sub>5</sub> mRNA in lumbar SC was elevated at early stages in the *SOD1*<sup>G93A</sup> disease course, Brownell et al. (2015), used *in vivo* PET imaging to demonstrate that mGlu<sub>5</sub> receptor levels increased throughout the disease trajectory of *SOD1*<sup>G93A</sup> mice. This was shown not only in spinal

cord but across several brain areas, including hippocampus, striatum, cortex and whole brain.

As there is conflicting evidence regarding mGlu<sub>5</sub> expression changes throughout the *SOD1<sup>G93A</sup>* disease course, a [<sup>3</sup>H] M-MPEP saturation binding assay was set up to determine if there were any changes in mGlu<sub>5</sub> receptor number in the *SOD1<sup>G93A</sup>* mouse model of MND used in this project, compared to non-transgenic mice.

Martorana et al. (2012), had previously reported that mGlu<sub>5</sub> mRNA expression was elevated at 30 days compared to 100 days of age in both non-transgenic and *SOD1<sup>G93A</sup>* lumbar spinal cord. Whilst there was more mGlu<sub>5</sub> staining in the *SOD1<sup>G93A</sup>* spinal cord at 30 days of age compared to the non-transgenic spinal cord; mGlu<sub>5</sub> expression levels were similar in both non-transgenic and *SOD1<sup>G93A</sup>* spinal cords at 100 days. This finding suggests that mGlu<sub>5</sub> may play a role early on in MND disease progression. Furthermore, a reduction in mGlu<sub>5</sub> expression levels with disease progression ties in with reports that astrocytic mGlu<sub>5</sub> is developmentally regulated (Wei Sun et al. 2013). Interestingly, characterisation of mGlu<sub>5</sub> expression in non-transgenic and *SOD1<sup>G93A</sup>* mouse spinal cords shown earlier, was carried out at 90 days of age (Figure 3.1). This may provide some explanation for why the mGlu<sub>5</sub> expression levels in lumbar spinal cord remained relatively unchanged between non-transgenic and *SOD1<sup>G93A</sup>* mice.

The saturation binding experiments in whole brain revealed a general trend in both non-transgenic and *SOD1<sup>G93A</sup>* brain membranes for a higher mGlu<sub>5</sub> density ( $B_{max}$ ) at 30 days compared to 120 days, however this was not statistically significant as shown by 1-way ANOVA (Figure 3.7). Whilst the mGlu<sub>5</sub> density was slightly higher at 30 days compared to 120 days in the *SOD1<sup>G93A</sup>* brain membranes (in keeping with findings from Martorana et al. 2001), the same trend was also apparent for the non-transgenic brain membranes. This suggests that elevated mGlu<sub>5</sub> receptors at 30 days of age is not a disease specific feature of the *SOD1<sup>G93A</sup>* mouse model of MND.

Brownell et al. (2015) used *in vivo* PET imaging which may relate more closely to the localisation of mGlu<sub>5</sub> protein levels compared to quantitative PCR used by Martorana et al. (2012). Consequently, it was expected that the saturation binding results would produce similar findings to Brownell, et al. (2015). However, despite no significant difference in mGlu<sub>5</sub> receptor levels in whole brain membranes, this does not rule out significant changes in mGlu<sub>5</sub> receptor levels within spinal cord tissue or indeed within specific brain regions. For example, looking within distinct areas of the brain known to be involved in MND disease pathology would perhaps more accurately reveal

disease specific changes in mGlu<sub>5</sub> receptor number. Furthermore, it is important to note that the lack of a significant change in mGlu<sub>5</sub> receptor density, does not exclude the possibility that functionality of the mGlu<sub>5</sub> receptor is altered at various stages of the disease.

To summarise, immunofluorescence in both non-transgenic and *SOD1<sup>G93A</sup>* lumbar spinal cord showed that mGlu<sub>5</sub> is predominantly expressed within the dorsal horn in the substantia gelatinosa which is an area populated by sensory afferents. This is consistent with reports that mGlu<sub>5</sub> may be implicated in neuropathic pain (Nicoletti et al. 2011). Of note, mGlu<sub>5</sub> is also expressed within the ventral horns of lumbar SC and more specifically mGlu<sub>5</sub> is found on some ventral motor neurons. This demonstrates that not only is mGlu<sub>5</sub> expressed in a disease-relevant area but also, it is expressed on vulnerable cells in MND (motor neurons). Whilst the levels and distribution of mGlu<sub>5</sub> staining appears to be similar in both the non-transgenic and *SOD1<sup>G93A</sup>* lumbar SC tissue, the data generated thus far is qualitative. To assess whether there are any significant differences between the levels of mGlu<sub>5</sub> staining in non-transgenic versus *SOD1<sup>G93A</sup>* lumbar SC tissue, quantification of mGlu<sub>5</sub> staining in a larger cohort of tissue would need to be carried out.

Whilst dual staining in mouse spinal cord was not suggestive of mGlu<sub>5</sub> expression on astrocytes, low level expression was observed on human derived iAstrocytes from both MND patients with *SOD1* mutations and age matched healthy controls. These data contradict literature reports of increased mGlu<sub>5</sub> expression on reactive astrocytes in human post mortem spinal cords of MND patients. However, this inconsistency may be attributable to the absence of the native architecture found *in vivo*. Saturation binding demonstrated that whole brain mGlu<sub>5</sub> receptor densities are not significantly altered throughout the *SOD1<sup>G93A</sup>* disease trajectory. In addition, mGlu<sub>5</sub> receptor numbers were comparable in non-transgenic and *SOD1<sup>G93A</sup>* mouse whole brains both at early and later stages of *SOD1<sup>G93A</sup>* MND. The fact that mGlu<sub>5</sub> abundance does not appear to be significantly altered throughout the *SOD1<sup>G93A</sup>* disease course is desirable, as it means that the dosing regimen for blocking mGlu<sub>5</sub> and maintaining a consistent receptor occupancy will be more straightforward.

There is convincing evidence to support a role for mGlu<sub>5</sub> in the *SOD1<sup>G93A</sup>* mouse model of MND with both therapeutic blockade of mGlu<sub>5</sub> activity and genetic knockdown of mGlu<sub>5</sub> delaying disease onset and extending survival in *SOD1<sup>G93A</sup>* mice (Rossi et al. 2008; Bonifacino et al. 2017). Interestingly, the observed beneficial effect is thought to be mediated by inhibiting/reducing astrocytic mGlu<sub>5</sub> activity.

Consequently, it was initially hypothesised that astrocytic mGlu<sub>5</sub> plays a role in disease progression in the *SOD1<sup>G93A</sup>* mouse model of MND. However, the data generated thus far suggests that mGlu<sub>5</sub> is not expressed on astrocytes and is only expressed on some SC motor neurons in our *SOD1<sup>G93A</sup>* mouse model of MND at 90 days of age. Therefore, the updated hypothesis is that motor neuronal mGlu<sub>5</sub> activity plays a role in *SOD1<sup>G93A</sup>* disease progression and that blocking motor neuronal mGlu<sub>5</sub> activity with HTL0014242 will slow disease progression and extend survival in *SOD1<sup>G93A</sup>* mice.

The next chapter will characterise the mGlu<sub>5</sub> negative allosteric modulator, HTL0014242, for therapeutic use in the *SOD1<sup>G93A</sup>* mouse model of MND.

## 4 Characterisation of HTL0014242 in *SOD1<sup>G93A</sup>* model of MND

### 4.1 Introduction

Evidence from Chapter 3 demonstrates that mGlu<sub>5</sub> is expressed on some motor neurons within the ventral horns of both non-transgenic and *SOD1<sup>G93A</sup>* mouse lumbar SC. Consequently, it is hypothesised that motor neuronal mGlu<sub>5</sub> activity is the target of HTL0014242 blockade in order to slow disease progression and extend survival in the *SOD1<sup>G93A</sup>* mouse model of MND. This chapter will focus on the characterisation of HTL0014242, a novel mGlu<sub>5</sub> negative allosteric modulator (NAM), in the *SOD1<sup>G93A</sup>* mouse model of MND.

Pharmacological blockade of mGlu<sub>5</sub> receptors in the *SOD1<sup>G93A</sup>* mouse model has previously been investigated. A study by Rossi et al. (2008) found that the NAM, MPEP, delayed disease onset and extended survival of *SOD1<sup>G93A</sup>* mice. This suggests that mGlu<sub>5</sub> plays a role in disease progression of the *SOD1<sup>G93A</sup>* mouse model of MND and that modulating glutamate transmission through targeting mGlu<sub>5</sub> could provide an effective therapeutic target for the treatment of MND. Whilst this result is encouraging, the potential translation of MPEP from pre-clinical use in mouse to a novel therapeutic drug for the treatment of MND in humans, is somewhat unfavourable. MPEP was developed in the late 1990s by Novartis to investigate mGlu<sub>5</sub> activity in several CNS disorders including neurodegenerative diseases (Micheli 2000). However, it was subsequently demonstrated that MPEP demonstrates both significant non-specific interactions and off-target effects (Lea & Faden 2006). MPEP is now commonly used as a tool compound to investigate mGlu<sub>5</sub> activity in several neurological diseases.

Traditional mGlu<sub>5</sub> NAMs such as MPEP contain a central acetylene bond flanked by two aromatic groups (Christopher et al. 2015). Acetylene groups have the potential to be susceptible to metabolic activation such as extensive glutathione conjugation (Kalgutkar et al. 2005; Hughes et al. 2013; Sperry et al. 2012). Pfizer reported that the presence of the acetylene moiety in the compound, GRN-529, was associated with hepatotoxicity observed in both rat and non-human primate toxicology studies (L. Zhang et al. 2014a). An additional drawback of MPEP is its poor pharmacokinetic properties. For example, to achieve therapeutic levels with a short half-life drug such

as MPEP, higher doses of the compound are needed which often can result in  $C_{max}$  driven CNS side effects (Smith et al. 2017).

The undesirable pharmacokinetic properties associated with traditional mGlu<sub>5</sub> NAMs such as MPEP has led to the development of a novel class of compounds lacking the acetylene group (Emmitte 2011; Emmitte 2013). Using their StaR® technology, Heptares Therapeutics designed the non-acetylene, negative allosteric modulator of mGlu<sub>5</sub>, HTL0014242 (Christopher et al. 2015).

In house characterisation of this compound showed that HTL0014242 exhibits an excellent *in vitro* and *in vivo* profile. For example, HTL0014242 displays good oral bioavailability, high mGlu<sub>5</sub> affinity and potency and also seems to be well tolerated, demonstrating a clean repeat-dosing profile in a rat toxicology study. Further, out of all eight mGlu receptors, HTL0014242 is highly selective for the mGlu<sub>5</sub> receptor (Christopher et al. 2015). This is not the case for MPEP, not only is it a negative allosteric modulator of mGlu<sub>5</sub> but it is also a weak NMDA antagonist and a positive allosteric modulator of the mGlu<sub>4</sub> receptor (Lea et al. 2009; Mathiesen et al. 2003).

HTL0014242 has a much better pharmacological profile than MPEP both in terms of selectivity, potency and pharmacokinetics (Christopher et al. 2015). Consequently, this novel compound can be used to probe the role of mGlu<sub>5</sub> in the *SOD1<sup>G93A</sup>* mouse model of MND in a more comprehensive and precise manner. However, before commencing *in vivo* efficacy studies, further characterisation of the pharmacokinetics of HTL0014242 within the *SOD1<sup>G93A</sup>* mouse model of MND is needed to determine the extent of mGlu<sub>5</sub> receptor occupancy throughout the intended dosing cycle.

Confirmation of target engagement during pre-clinical experiments is fundamental to increase the probability of success when developing novel therapeutic compounds. Regardless of whether the compound of interest shows efficacy in the disease model, it is essential to demonstrate that the compound sufficiently occupies and activates the target receptor. For example, proof of target engagement serves to unequivocally establish the validity of the target for the intended clinical indication (Durham & Blanco 2015). Consequently, before embarking on an *in vivo* study probing HTL0014242 efficacy, it will be essential to first confirm sufficient mGlu<sub>5</sub> target engagement following oral dosing with HTL0014242 within the *SOD1<sup>G93A</sup>* mouse model of MND. Target occupancy using a [<sup>3</sup>H] M-MPEP binding assay was identified as the easiest method to assess this.

In this chapter the affinity of HTL0014242 for mGlu<sub>5</sub> in both non-transgenic and *SOD1<sup>G93A</sup>* mouse brains will be compared using a HTL0014242 competition binding

assay. This will identify whether the presence of the *SOD1*<sup>G93A</sup> mutation effects the interaction between HTL0014242 and the mGlu<sub>5</sub> receptor. Following on from this an initial *in vivo* pharmacokinetic (PK) study will be carried out to check that HTL0014242 crosses the blood brain barrier and accesses the relevant tissue at levels necessary to have an effect. Also, the HTL0014242 PK study will help guide a reasonable dosing strategy for future *in vivo* efficacy studies. Finally, ex-vivo receptor occupancy (RO) experiments will be performed on brain tissue collected from the PK study at peak and trough HTL0014242 exposures to verify the degree to which HTL0014242 occupies the target receptor, mGlu<sub>5</sub>. The information generated from these experiments will guide the design of an *in vivo* 90D dose response study to investigate the efficacy of HTL0014242, in the *SOD1*<sup>G93A</sup> mouse model of MND.

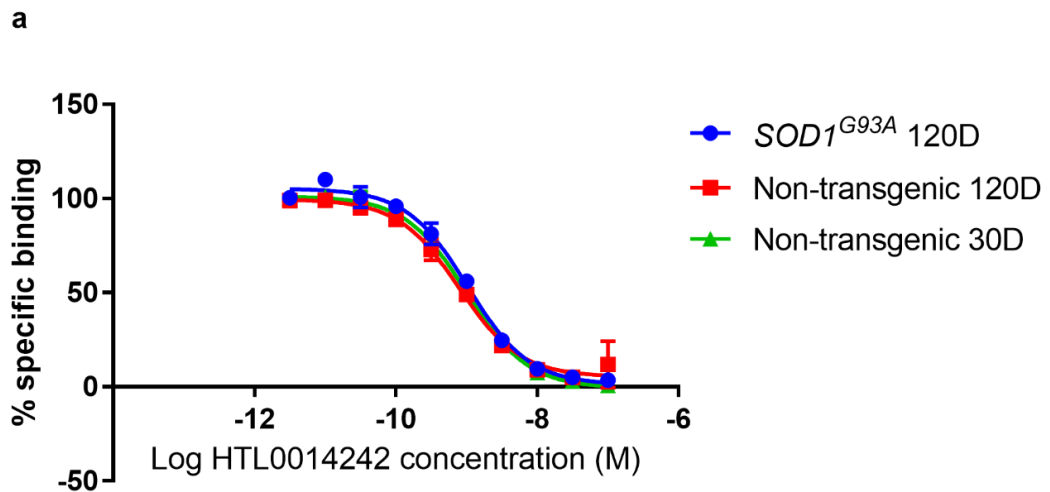
## 4.2 Results

### 4.2.1 HTL0014242 competition binding in non-transgenic and *SOD1*<sup>G93A</sup> mouse brain membranes

Previously, saturation binding assays were performed to determine the K<sub>d</sub> of [<sup>3</sup>H] M-MPEP for mGlu<sub>5</sub> receptors in membranes prepared from whole brain. This demonstrated that the K<sub>d</sub> of [<sup>3</sup>H] M-MPEP did not significantly change between different brain membranes (Figure 3.7). Saturation binding cannot be used to determine the affinity of an unlabelled ligand such as the mGlu<sub>5</sub> NAM, HTL0014242. In this instance, a competition binding assay was set up to establish the ability of HTL0014242 to compete with [<sup>3</sup>H] M-MPEP for binding to mGlu<sub>5</sub> receptors. These experiments enable the inhibition constant (K<sub>i</sub>) of HTL0014242 to be calculated which is attributable to affinity. The purpose of these competitive binding experiments was to determine whether the affinity of HTL0014242 for mGlu<sub>5</sub> receptors change between non-transgenic and *SOD1*<sup>G93A</sup> mouse whole brains. Whilst the *SOD1*<sup>G93A</sup> mutation should not directly affect HTL0014242 binding to mGlu<sub>5</sub>, these experiments would help identify whether the mutation indirectly affected binding through changing the levels of mGlu<sub>5</sub> accessory proteins or causing aberrant expression/folding of the mGlu<sub>5</sub> receptor.

Competition curves were generated by plotting the specific binding as a percentage of the total binding, (i.e. 2nM [<sup>3</sup>H] M-MPEP in the absence of a competitor) for increasing concentrations of unlabelled HTL0014242. Representative data are shown for membranes prepared from *SOD1*<sup>G93A</sup> whole brains collected at 120 days of age and non-transgenic whole brains collected at 30 and 120 days of age (Figure 4.1a).

The concentration of HTL0014242 that displaces the specific binding of [<sup>3</sup>H] M-MPEP by 50% (IC<sub>50</sub>) was determined from non-linear regression analysis of the competition curves, using the software package in Prism (GraphPad, San Diego, CA). To calculate the K<sub>i</sub> of HTL0014242, the IC<sub>50</sub> of HTL0014242 along with the dissociation constant (K<sub>d</sub>) of [<sup>3</sup>H] M-MPEP (defined in the saturation assays in Chapter 3, Figure 3.7) for each of the brain membranes were applied to the Cheung-Prusoff equation (Figure 4.1b). The HTL0014242 K<sub>i</sub> values for each of the brain membranes are displayed in Figure 4.1c. One-way ANOVA demonstrated that there was no significant difference in HTL0014242 K<sub>i</sub> between the different brain membranes (p = 0.3747). This shows that affinity of HTL0014242 for mGlu<sub>5</sub> is not altered between the non-transgenic and *SOD1*<sup>G93A</sup> brain tissue or by age of the brain tissue in the non-transgenic mice.



b

$$K_i = \frac{IC_{50}}{1 + \frac{[ligand]}{K_D}}$$

c

Tissue	$K_i$ (nM) Mean $\pm$ SD
Non-transgenic 30D	0.47
Non-transgenic 120D	0.43 $\pm$ 0.07
$SOD1^{G93A}$ 120D	0.63 $\pm$ 0.15

**Figure 4.1. Competition binding shows that the inhibitory constant for HTL0014242 is not altered between non-transgenic and  $SOD1^{G93A}$  mouse brain membranes.** Increasing concentrations of unlabelled HTL0014242 were added to 2nM [ $^3H$ ] M-MPEP to compete for binding to the mGlu<sub>5</sub> receptor. The concentration of HTL0014242 that inhibited the binding of [ $^3H$ ] M-MPEP by 50% ( $IC_{50}$ ) was determined by fitting a sigmoidal dose-response curve in Prism (GraphPad). Non-specific binding was defined with 0.74mM cold MPEP and subtracted from total binding to determine specific binding. The  $IC_{50}$  value of HTL0014242 was measured in non-transgenic mouse membranes (20  $\mu$ g/well) at 30 and 120 days of age and in  $SOD1^{G93A}$  mouse membrane (20  $\mu$ g/well) at 120 days of age (a). The inhibitory constant ( $K_i$ ) of HTL0014242 was calculated for each brain membrane using the Cheung-Prusoff equation (b). The  $K_d$  value of [ $^3H$ ] M-MPEP for each brain membrane

was determined and shown in Fig 3.7. Combined competition binding data (from two independent experiments for non-transgenic and *SOD1<sup>G93A</sup>* 120D membranes and from one experiment for non-transgenic 30D membrane), showed no significant difference between different brain membranes for HTL0014242  $K_i$ , as shown by 1-way ANOVA,  $p = 0.3747$  (c).

#### 4.2.2 *In vivo* pharmacokinetics of HTL0014242 in the *SOD1<sup>G93A</sup>* mouse model of MND

A pharmacokinetic (PK) study was carried out to define the blood and CNS concentration versus time-profile for HTL0014242 in the *SOD1<sup>G93A</sup>* mouse model of MND (Figure 4.2a). This was performed to support further therapeutic studies with HTL0014242 in this mouse model. The PK parameters are summarised in Figure 4.2b.

HTL0014242 dosed orally at 10mg/kg in 60 day old *SOD1<sup>G93A</sup>* mouse spinal cord shows that this compound has a long half-life (5.12h), low clearance (870ml/hr/kg) and good CNS exposure, with a CNS partition ratio of 5.42 (Figure 4.2b). An estimation of free fraction in spinal cord using equilibrium dialysis was calculated by Pharmidex and then used to plot the estimated free drug in spinal cord (Figure 4.2a). Despite this compound being highly protein bound in spinal cord (99.6%), the profile showing unbound HTL0014242 in spinal cord demonstrates that there is still enough free drug to achieve levels greater than the IC<sub>50</sub> for about 18 hours. This is a useful indication of the degree of inhibition of mGlu<sub>5</sub> following a single dose of HTL0014242.

Using the data obtained from the PK study, the percentage of mGlu<sub>5</sub> receptors in spinal cord that were occupied by HTL0014242 could be estimated. The affinity of HTL0014242 for mGlu<sub>5</sub> in *SOD1<sup>G93A</sup>* mouse whole brain collected at 120 days of age was previously defined by HTL0014242 competition binding (Figure 4.1c). Assuming the affinity of HTL0014242 for mGlu<sub>5</sub> in brain is comparable to that in SC, it was possible to predict receptor occupancy (RO) of mGlu<sub>5</sub> in spinal cord (Table 4.1). The % RO by HTL0014242 was estimated using the calculated free drug concentrations in SC after a single dose of 10mg/kg HTL0014242, assuming linearity of exposure for the 3 and 30mg/kg doses and applying the formula shown in Figure 4.3. The predicted mGlu<sub>5</sub> receptor occupancies in SC were plotted against the different post-dose time points, for each of the dose-groups. Figure 4.3 shows that 3, 10 and 30mg/kg of HTL0014242 provide a good range of mGlu<sub>5</sub> receptor occupancies over a 24 h period.

In addition, 6 mice were repeat- dosed with 10mg/kg HTL0014242 for 7 consecutive days. Considering that HTL0014242 will be chronically dosed in future *in vivo* efficacy studies, 7-day dosing enabled the effect of sub-chronic dosing on HTL0014242 exposure to be investigated. Previous dosing studies in mouse demonstrated that peak HTL0014242 exposure was ~2 h post oral dose. Therefore, at the end of this study the mice were collected at peak (2 h post-dose) and trough (24 h post-dose) HTL0014242 exposures, 3 mice per time-point. Concentrations of HTL0014242 at

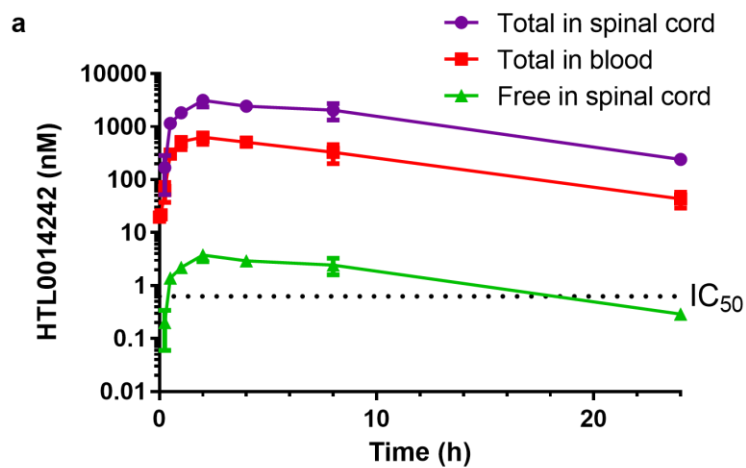
peak and trough time points are shown in Table 4.2. Peak concentrations of HTL0014242 in SC after sub-chronic dosing are comparable to the concentration of HTL0014242 in SC 2 h post-dose (peak exposure), following a single dose of HTL0014242 (Table 4.1). More variability was observed for trough HTL0014242 concentrations in SC following sub-chronic dosing. For example, one of the trough concentrations in SC was more than 10-times greater than the other trough HTL0014242 concentrations and approximately twice the concentration of peak HTL0014242 concentrations in SC (Table 4.2). Notably, the variability in HTL0014242 concentrations at trough in spinal cord correlated with blood exposure (Table 4.2).

**Table 4.1. Exposure of HTL0014242 in spinal cord and blood following a single dose of HTL0014242 at 10mg/kg and calculated receptor occupancy**

Time of tissue collection post-dose (h)	Total HTL0014242 in Blood (nM)	Total HTL0014242 in SC (nM)	Unbound HTL0014242 in SC (nM)	Predicted RO in SC (%)
0.08	15	< 39	< 0.02	< 2.4
0.25	63	170	0.068	9.7
0.50	302	1162	0.465	42.5
1.00	523	1838	0.735	53.8
2.00	634	3141	1.256	66.6
4.00	513	2440	0.976	60.8
8.00	331	2044	0.817	56.5
24.00	32	168	0.067	9.6

**Table 4.2. Exposure of HTL0014242 following sub-chronic HTL0014242 dosing at 10mg/kg for 7 consecutive days**

Time of tissue collection post-dose (h)	Total HTL0014242 in Blood (nM)	Total HTL0014242 in SC (nM)	Unbound HTL0014242 in SC (nM)	Predicted RO in SC (%)
Peak 1	< 39	1843	0.737	53.9
Peak 2	472	2913	1.165	64.9
Peak 3	409	2231	0.892	58.6
Trough 1	26	177	0.071	10.1
Trough 2	109	495	0.198	23.9
Trough 3	787	5069	2.028	76.3



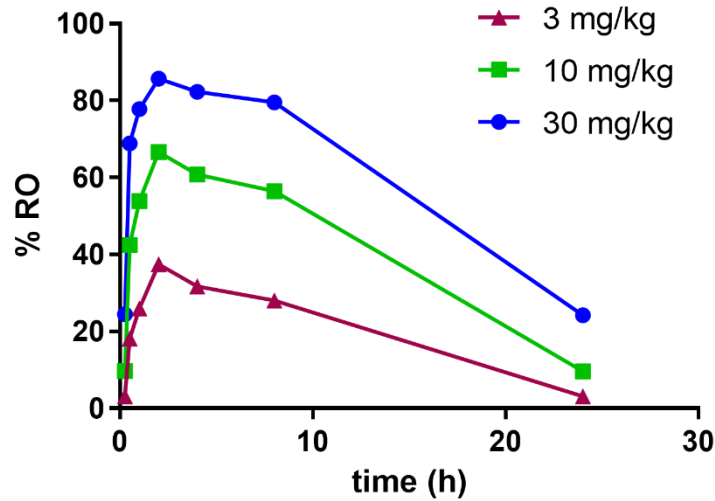
**b**

PK Parameters			
Parameter	Units	Blood	Spinal cord
$t_{1/2}$	hr	5.05	5.12
$T_{max}$	hr	2.0	2.0
$C_{max}$	ng/ml or g	197.0	976.4
$AUC_{last}$	hr*ng/ml or g	2043	11082
Clearance (predicted)	ml/hr/kg	4721	870
CNS partition ratio	$AUC_{cord}/AUC_{blood}$	5.42	

**c**

	mGlu <sub>5</sub> NAM	Mavoglurant	HTL0014242
mGlu <sub>5</sub> affinity (pK <sub>i</sub> )		8.0	9.3
mGlu <sub>5</sub> half maximal inhibitory concentration (pIC <sub>50</sub> )		8.0	9.2
Oral bioavailability ( $F_{po}$ ) from PK study in rat		32%	~100%
Half-life ( $t_{1/2}$ ) from PK study in rat		2.9h	4.0h

**Figure 4.2. HTL0014242 demonstrates an excellent pharmacokinetic profile in *SOD1<sup>G93A</sup>* mouse spinal cord and blood.** *SOD1<sup>G93A</sup>* mice were dosed at 10mg/kg orally and tissue collected at 8 time-points. a) Concentration-time profile for HTL0014242 in spinal cord and blood. *In vitro* experiments carried out by Pharmidex were used to calculate the % unbound drug in a spinal cord homogenate (calculated as 0.04% unbound) and used to plot the estimated free drug in spinal cord. The dotted line represents the  $IC_{50}$  for inhibition of mGlu<sub>5</sub> by HTL0014242. The  $IC_{50}$  for HTL0014242 in *SOD1<sup>G93A</sup>* mouse CNS is 0.63nM. This was determined from HTL0014242 competition binding in *SOD1<sup>G93A</sup>* mouse brain membranes collected from whole brain at 120 days of age (Figure 4.1a). a) Data presented as mean  $\pm$  SD. Data points represent individual animals (3 mice per time point). c) Comparison between the profile of a traditional mGlu<sub>5</sub> NAM, mavoglurant and the optimised mGlu<sub>5</sub> NAM, HTL0014242 demonstrates that the latter has better *in vitro* and pharmacokinetic characteristics.



$$\text{Formula: RO \%} = \left( \frac{\text{nM}}{\text{nM} + K_i} \right) \times 100\%$$

nM = HTL0014242 concentration in SC

$K_i$  =  $K_i$  in nM of HTL0014242 for mGlu<sub>5</sub>

**Figure 4.3. Estimated receptor occupancy (%RO) of mGlu<sub>5</sub> in mouse spinal cord demonstrates that 3,10 and 30mg/kg of HTL0014242 represent a good dosing range.** Using the pharmacokinetic data for 10mg/kg HTL0014242 exposure in SC (shown in Figure 4.2a) and assuming linearity of exposure at 30 and 3mg/kg HTL0014242, receptor occupancy was calculated using the RO formula shown above. The  $K_i$  of HTL0014242 for mGlu<sub>5</sub> was determined from HTL0014242 competition binding in *SOD1<sup>G93A</sup>* mouse brain membranes collected from whole brain at 120 days of age (shown in Figure 4.1c). The assumption is that HTL0014242  $K_i$  for mGlu<sub>5</sub> in brain is comparable to that in spinal cord.

#### 4.2.3 Optimisation of [<sup>3</sup>H] M-MPEP binding assay to measure receptor occupancy (RO) of mGlu<sub>5</sub> receptors by HTL0014242 in mouse brain collected from *in vivo* dosing studies

RO is a useful measure (post-study), to check that the compound of interest, HTL0014242, interacts as expected with the target receptor, mGlu<sub>5</sub>. A [<sup>3</sup>H] M-MPEP binding assay was set up to determine mGlu<sub>5</sub> RO in brain tissue collected from the PK study. Prior to using the HTL0014242-dosed brain membranes prepared from the PK study, optimisation of the RO assay took place over several months using drug naïve non-transgenic and *SOD1<sup>G93A</sup>* brain membranes.

One of the main issues with measuring RO in ex-vivo brain membranes is ensuring HTL0014242 does not dissociate from mGlu<sub>5</sub> receptors during the experimental procedure. Whilst saturation and competition binding experiments were carried out at steady state binding (after several hours of incubation) and at RT, RO experiments were carried out after a 10-minute incubation time and at 4°C. Shortening the incubation time and lowering the temperature at which the reaction was carried out, reduced the rate of HTL0014242 dissociation from mGlu<sub>5</sub> receptors in brain membranes.

Radioligand kinetics demonstrated that raising the concentration of [<sup>3</sup>H] M-MPEP from the K<sub>d</sub> concentration (~2nM) to 10x K<sub>d</sub> concentration (~20nM) increased the rate of specific binding (Figure 4.4). Experiments were carried out in brain membranes from non-transgenic and *SOD1<sup>G93A</sup>* mouse brains collected at 30 and 120 days of age, with representative data for non-transgenic membranes at 30 days of age shown in Figure 4.4. The observed rate constant (K<sub>obs</sub>) is a measure of how quickly the reaction reaches equilibrium. This parameter is dependent on the association rate constant (K<sub>on</sub>) and the dissociation rate constant (k<sub>off</sub>). K<sub>on</sub> is dependent on radioligand concentration and consequently increasing the concentration of the radioligand increases K<sub>on</sub> which results in the equilibrium being achieved faster. In subsequent RO experiments the objective is to occupy all available receptors quickly at the onset of equilibrium before HTL0014242 dissociation occurs (see dotted line on Figure 4.4). Figure 4.4 demonstrates that K<sub>on</sub> was faster at the higher radioligand concentration (~20nM). This is desirable as it reduces the time in which HTL0014242 can dissociate from mGlu<sub>5</sub> receptors.

Unlike before where membranes were prepared from mouse brains over several lengthy steps, RO assay membranes were crudely prepared from brain tissue. This involved suspending half-brains in assay buffer at 4°C and homogenising with a

Polytron homogeniser (4x10s bursts). These crude membrane preparations were added directly to the reaction mixture helping to minimise the time in which HTL0014242 could dissociate from the mGlu<sub>5</sub> receptors.

Protein linearities were performed on 30-day old non-transgenic crude brain membranes at different protein concentrations to establish the optimal signal between total and non-specific binding. Membranes were incubated with 4nM [<sup>3</sup>H] M-MPEP, in assay buffer, for 10 minutes at 4<sup>o</sup>C. Whilst total binding was defined by mGlu<sub>5</sub> receptors in the presence of 4nM [<sup>3</sup>H] M-MPEP, non-specific binding was determined by 0.74mM unlabelled MPEP to occupy all available mGlu<sub>5</sub> receptors in the presence of 4nM [<sup>3</sup>H] M-MPEP. Specific binding was calculated by subtracting non-specific binding from total binding.

Figure 4.5a shows total and non-specific binding for crude brain membranes at a concentration of 100µg/well and 200µg/well. Both protein concentrations show optimal signals between total and non-specific binding for detecting the specific binding (Figure 4.5a). Also, the total binding for both membrane concentrations is well below 10% of the total radioligand added (~0.2% for 100µg/well and ~0.4% for 200µg/well), indicating no risk of radioligand depletion. Despite the 200µg/well concentration of crude membrane having the largest range for detecting specific binding (Figure 4.5b), the signal between total and non-specific binding at 100µg/well was sufficient and this amount was chosen to conserve mouse tissue (allowing 6 replicates/point).

Following optimisation of the RO assay, HTL0014242 RO of mGlu<sub>5</sub> receptors in mouse brain tissue collected from the PK study were measured. Brain membranes were crudely prepared from *SOD1<sup>G93A</sup>* half brains collected at peak and trough HTL0014242 exposures after 7-day oral dosing with 10mg/kg of HTL0014242 (3 mice per group). The other half of the brain was sent for bioanalysis. Membranes at 100µg/well were incubated for 10 minutes at 4<sup>o</sup>C with 20nM [<sup>3</sup>H] M-MPEP in assay buffer, this was followed by rapid filtration to terminate the reaction. Receptor occupancies were calculated from the average specific binding with the values from control mouse brain membranes taken as 100% RO. Figure 4.6 shows the percentage of mGlu<sub>5</sub> receptors in brain occupied by HTL0014242 at peak and trough exposures. As expected, average HTL0014242 RO at peak exposure is higher than at trough exposure (76.3±2.8% at peak, 68.8±25.9% at trough). Whilst HTL0014242 RO values at peak were similar between the different mouse brains, at trough there was much more variability. Interestingly, this observation for trough HTL0014242 RO

values in brain is comparable to the variability seen for the HTL0014242 concentrations at trough exposure in spinal cord and blood (Table 4.2).

An additional RO assay was performed on crude brain membranes prepared from *SOD1<sup>G93A</sup>* half brains collected at 15 minutes, 30 minutes and 2 h post-dose from the HTL0014242 PK study. The aim was to compare HTL0014242 RO of mGlu<sub>5</sub> receptors in the different brain membranes after an assay incubation of 10 minutes versus 2 hours. For each of the brain membranes incubated for 2 hours, the % HTL0014242 RO is reduced compared to the brain membranes incubated for 10 minutes (Figure 4.7). Clearly, increasing the incubation time from 10 minutes to 2 hours results in HTL0014242 dissociation from mGlu<sub>5</sub> receptors in brain membranes. The findings from this experiment validate 10 minutes as the optimal incubation time for accurately determining the percentage of mGlu<sub>5</sub> receptors occupied by HTL0014242 in brain.

Measured mGlu<sub>5</sub> RO in brain was plotted versus predicted mGlu<sub>5</sub> RO in SC for peak and trough exposures of HTL0014242 following 10mg/kg repeat dosing for 7 days (using the formula in Figure 4.3). This was to establish the accuracy of predicted RO in spinal cord versus measured RO in brain. Figure 4.8 demonstrates that predicted RO in SC was consistently lower than measured RO in brain.

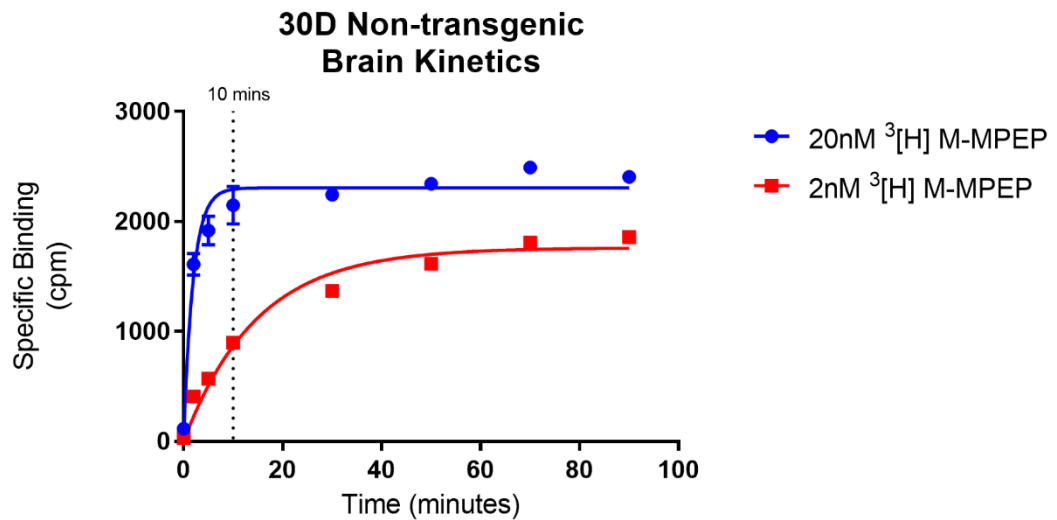


**Figure 4.4. 10x  $K_d$  concentration of  $[^3\text{H}]$  M-MPEP increases rate of binding in mouse non-transgenic brain membrane.** Time course of specific binding to mGlu<sub>5</sub> receptors in non-transgenic mouse brain membrane (20  $\mu\text{g}/\text{well}$ ) at both  $K_d$  concentration (2nM) and 10x  $K_d$  concentration (20nM) of  $[^3\text{H}]$  M-MPEP (a). Non-specific binding was defined with 0.74mM cold MPEP and subtracted from total binding to determine specific binding. Data shown as mean  $\pm$  SEM. Representative data for non-transgenic brain membrane at 30 days of age presented. Radioligand kinetics were determined for both non-transgenic and *SOD1<sup>G93A</sup>* brain membranes at 30 and 120 days of age. Dotted line indicates 10 minutes which is the time point chosen for future incubations as this was the earliest time-point with which HTL0014242 occupied all receptors.

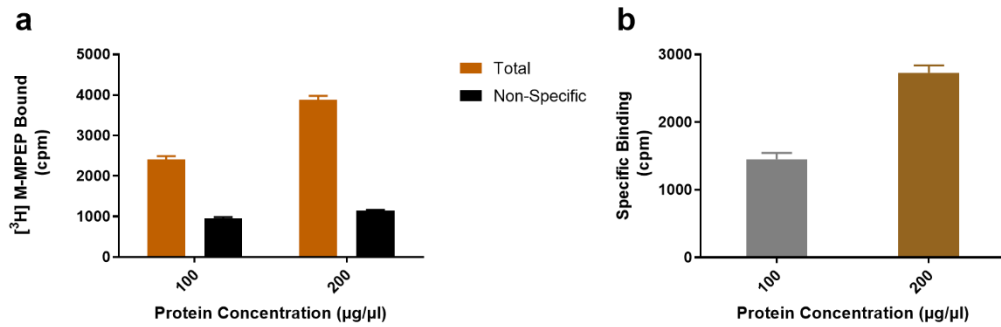


**Figure 4.5. Specific binding with 20nM  $[^3\text{H}]$  M-MPEP increases proportionally in mouse brain membranes.** Membranes were crudely prepared from whole brains collected from non-transgenic mice at 30 days of age. Total and non-specific radioligand binding is shown at both 100µg and 200µg of protein concentration (a). Non-specific binding was defined with 0.74mM cold MPEP and subtracted from total counts to determine specific binding (b). The specific binding for the 100µg brain membrane is 1453cpm compared to 2731 cpm for the 200µg brain membrane. The binding per unit protein (cpm/µg) is comparable at 100µg and 200µg of brain membrane concentration, cpm/µg = 14.5 and 13.7 respectively. Data shown as mean  $\pm$  SEM. The cpm value equal to 10% of the total added radioligand ( $[^3\text{H}]$  M-MPEP) was ~98982. To avoid ligand depletion the total binding of radioligand should be < 10% of the total radioligand added. Total binding of radioligand observed at both 100µg (~0.2%) and 200µg (~0.4%) were well below 10% of total added radioligand.

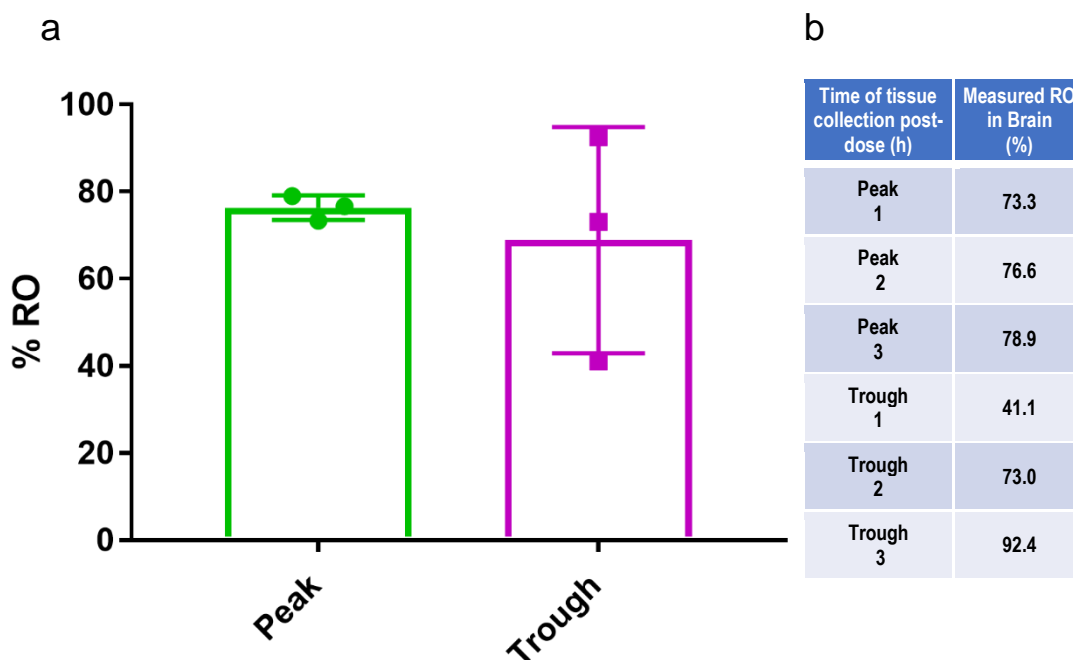


**Figure 4.6. The % of mGlu<sub>5</sub> receptors occupied with HTL0014242 in brain is highest at peak exposure of HTL0014242.** Membranes were crudely prepared from whole brains of *SOD1<sup>G93A</sup>* mice collected at peak (2 h post dose) and trough (24 h post dose) HTL0014242 exposures following 7-day repeat dosing of HTL0014242 at 10mg/kg in the pharmacokinetic *in vivo* study. Receptor occupancies at peak and trough were calculated using a <sup>3</sup>[H] M-MPEP radioligand binding assay a) Data presented as mean ± SD. Data points represent individual animals (3 mice per group). b) Average RO measured in brain at peak and trough HTL0014242 exposures.

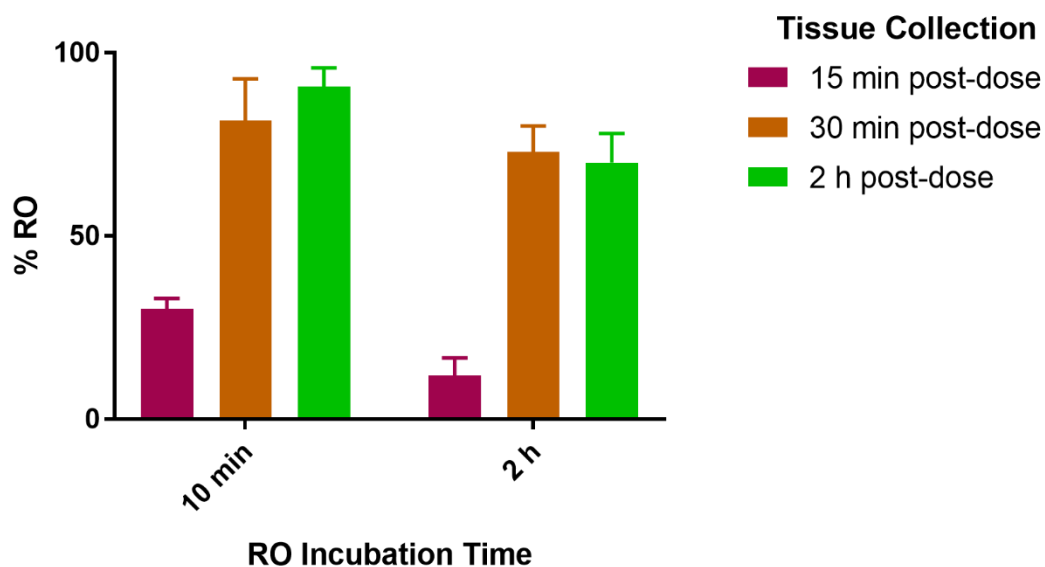


**Figure 4.7. Validation of a 10-minute incubation time in order to accurately determine the % of mGlu<sub>5</sub> receptors occupied with HTL0014242 in brain.** Membranes (100µg/well) were crudely prepared from whole brains of *SOD1<sup>G93A</sup>* mice collected 15 minutes, 30 minutes and 2 h post HTL0014242 (10mg/kg) dose. Receptor occupancies were calculated using a <sup>3</sup>[H] M-MPEP radioligand binding assay with either a 10-minute incubation or a 2 h incubation (a). Data presented as mean ± SEM from measurements performed in triplicate.

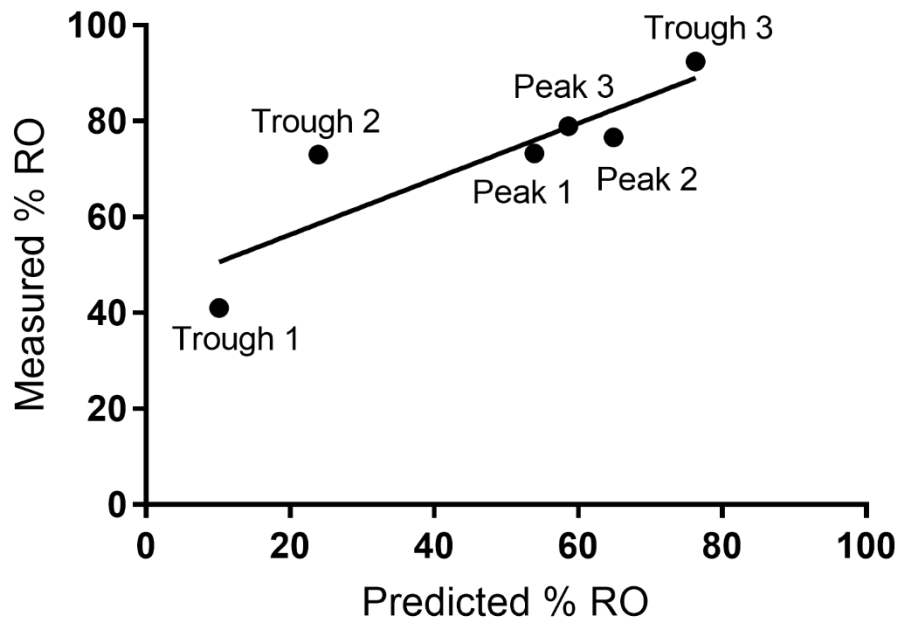


**Figure 4.8. Predicted receptor occupancy is not predictive of measured receptor occupancy.** The predicted mGlu<sub>5</sub> receptor occupancy was calculated using the equation (Predicted % RO = (HTL0014242 concentration / HTL0014242 concentration + K<sub>i</sub> of HTL0014242 for mGlu<sub>5</sub>) and plotted versus the measured mGlu<sub>5</sub> RO for mice repeat-dosed with 10mg/kg HTL0014242 for 7 days shown in Figure 4.6. Data points were plotted for individual animals, (3 mice at peak and trough).

### 4.3 Discussion

Acetylene-containing mGlu<sub>5</sub> NAMs like MPEP have been associated with poor pharmacological properties and off-target effects (Lea & Faden 2006). In contrast, the novel mGlu<sub>5</sub> NAM, HTL0014242, has previously been shown to have excellent *in vitro* and *in vivo* pharmacological characteristics (Christopher et al. 2015). The focus of this chapter was to further characterise the profile of HTL0014242 within the *SOD1*<sup>G93A</sup> mouse model of MND. The affinity of HTL0014242 for mGlu<sub>5</sub> was defined in both non-transgenic and *SOD1*<sup>G93A</sup> mouse brain membranes to identify whether the introduction of a human *SOD1*<sup>G93A</sup> mutant transgene indirectly influences HTL0014242 affinity for the mGlu<sub>5</sub> receptor. A PK study was then performed to check for adequate CNS exposure after dosing with 10mg/kg HTL0014242 in *SOD1*<sup>G93A</sup> mice. Predicted RO in SC was calculated at various time points following a single dose of 10mg/kg HTL0014242 and assuming linearity of exposure at 3 and 30mg/kg HTL0014242, it was also possible to predict mGlu<sub>5</sub> RO at these doses. This served as a guide for determining the optimal HTL0014242 doses for an *in vivo* 90D dose response study. A [<sup>3</sup>H] M-MPEP binding assay was optimised to establish mGlu<sub>5</sub> RO in *ex-vivo* crude brain membranes, at peak and trough HTL0014242 exposures following 7-days of HTL0014242 dosing. Sub-chronic dosing of HTL0014242 enabled the effect of dosing over a prolonged period of time on compound exposure to be investigated. Clearly, chronic dosing is a paradigm that will be used in future *in vivo* efficacy studies. Having established measured mGlu<sub>5</sub> receptor occupancies in brain, these values were then compared with predicted mGlu<sub>5</sub> RO in spinal cord, at peak and trough HTL0014242 exposures following 7-day repeated dosing.

#### 4.3.1 HTL0014242 competition binding in non-transgenic and *SOD1*<sup>G93A</sup> mouse brain membranes

Whilst HTL0014242 affinity for the mGlu<sub>5</sub> receptor was not expected to be altered by the presence of the human *SOD1*<sup>G93A</sup> mutant transgene directly, it was important to confirm that affinity was not indirectly affected. A HTL0014242-competition binding assay was used to determine the affinity of HTL0014242 for mGlu<sub>5</sub> receptors in non-transgenic and *SOD1*<sup>G93A</sup> brain membranes. No significant difference in HTL0014242 affinity was observed between non-transgenic and *SOD1*<sup>G93A</sup> membranes collected from brains at 120 days of age (0.43nM and 0.63nM, respectively). In addition, there was no significant difference between the 30-day and 120-day old non-transgenic brain membranes (0.47nM and 0.43nM, respectively), as shown by one-way ANOVA,  $p = 0.3747$  (Figure 4.1). From this it can be concluded that affinity of HTL0014242 for

mGlu<sub>5</sub> is not influenced by the *SOD1*<sup>G93A</sup> disease and further is not altered by the age of non-transgenic mouse brain. Membranes from *SOD1*<sup>G93A</sup> mouse brain at 30 days of age were not available for competition binding experiments and therefore the HTL0014242 affinity was not established at this time point. Considering HTL0014242 affinities in brain membranes of non-transgenic and *SOD1*<sup>G93A</sup> mice are comparable and the affinity in non-transgenic mice does not significantly change with age, it is highly likely that HTL0014242 pharmacology does not change in the *SOD1*<sup>G93A</sup> mouse model over time either.

#### **4.3.2 *In vivo* pharmacokinetics of HTL0014242 in the *SOD1*<sup>G93A</sup> mouse model of MND**

Current evidence supports mGlu<sub>5</sub> inhibition as a therapeutic intervention for *SOD1* MND (Rossi et al. 2008) . Using their innovative StaR ® technology, Heptares were able to design the optimised mGlu<sub>5</sub> NAM, HTL0014242. In-house studies have demonstrated that HTL0014242 has a favourable pharmacological profile for investigating the role of mGlu<sub>5</sub> in the *SOD1*<sup>G93A</sup> mouse model of MND (Christopher et al. 2015). However, further characterisation of HTL0014242 in the *SOD1*<sup>G93A</sup> mouse model was required to guide the design of an *in vivo* efficacy study.

The PK profile of HTL0014242 in the *SOD1*<sup>G93A</sup> mouse model of MND established that an oral dose of 10mg/kg results in an excellent PK profile, demonstrating a long-half-life, low clearance and good CNS exposure (Figure 4.2). Further, estimation of the free fraction in spinal cord showed that there was enough unbound drug to achieve levels greater than the IC<sub>50</sub> for about 18 hours (Figure 4.2a). This is important because it is the unbound drug that interacts with the receptor to produce a response. Consequently, HTL0014242 exposure in SC at 10mg/kg is sufficient to drive efficacy in the CNS. This provides a solid rationale for HTL0014242 at 10mg/kg to be used as one of the doses for a dose-response study probing the role of mGlu<sub>5</sub> in the *SOD1*<sup>G93A</sup> mouse model of MND.

The estimated % RO of mGlu<sub>5</sub> receptors in SC after a single dose of 10mg/kg HTL0014242 was calculated using the formula in Figure 4.3. Assuming linearity between the HTL0014242 concentrations from dosing at 10mg/kg and HTL0014242 dosed at 3 and 30mg/kg, it was also possible to determine the predicted % RO of mGlu<sub>5</sub> at these dose levels. Figure 4.3 demonstrates that HTL0014242 dosed at 3, 10 and 30mg/kg represents a good range of potential occupancies for a dose response study investigating whether HTL0014242 can reduce the rate of motor decline in the *SOD1*<sup>G93A</sup> mouse model of MND.

Interestingly, the HTL0014242 trough concentrations in SC and blood after repeat-dosing with 10mg/kg varied considerably between individual mice (Table 4.2). Some variability at trough exposure is expected due to the extended length of time between dosing and tissue collection. In addition, factors that influence drug metabolism like blood plasma albumin levels, renal function, food consumption and absorption will all differ between animals and could introduce variability in trough exposure.

It is not entirely clear why one mouse had a very high HTL0014242 trough concentration in both SC and blood (Table 4.2). The fact that the concentration of HTL0014242 was comparably high in SC and blood would suggest that it is indeed a real finding. An explanation for why this mouse had such a high concentration of HTL0014242 at trough exposure could be that its actual dose was much higher than its intended dose of 10mg/kg. Before oral dosing, HTL0014242 was suspended in 0.5% methyl cellulose to form a solution. Once in solution, care was taken to ensure that the compound remained in suspension. However, perhaps in this case HTL0014242 had fallen out of suspension and as consequence a much higher dose of HTL0014242 was administered to the mouse.

The study by Rossi et al. (2008), investigating the effect of MPEP in the *SOD1<sup>G93A</sup>* mouse model of MND does not mention a previous MPEP pharmacology study that guided their study design. For example, it is not clear what the rationale was for dosing MPEP at 30mg/kg. Does this dose result in CNS exposure sufficient to produce an effect and for how long? Also, it is not clear whether they checked to see if MPEP exposure changed following repeated dosing. These are important considerations that do not seem to be accounted for in their study. Furthermore, for studies investigating efficacy it is good practice to dose the compound at a range of doses. A drug dose-response study is integral for assessing efficacy as it helps delineate the minimum dose needed to demonstrate efficacy. Only dosing MPEP at 30mg/kg does not unequivocally validate that the efficacy observed was directly related to therapeutic blockade of mGlu<sub>5</sub> by MPEP, especially considering the non-selective actions of MPEP at higher doses. For example, it has previously been shown that MPEP dosed at 30mg/kg had robust analgesic effects in mGlu<sub>5</sub> knockout mice (Montana et al. 2009). This finding suggests that MPEP may exert its therapeutic effect in MND through additional mechanisms beyond that of blocking mGlu<sub>5</sub>.

### 4.3.3 Optimisation of [<sup>3</sup>H] M-MPEP binding assay to measure RO of mGlu<sub>5</sub> receptors by HTL0014242 in mouse brain collected from *in vivo* dosing studies

A [<sup>3</sup>H] M-MPEP binding assay was established to measure mGlu<sub>5</sub> RO in brain membranes collected from mice dosed with HTL0014242. The RO method established in this chapter is a robust and accurate measure of target occupancy. For example, the change in RO closely correlated with a change in exposure in the tissue (as measured by bioanalysis) and in addition the variability in measurements correlated with the variability in exposure. This demonstrates that it was not the assay itself that was intrinsically variable.

Following initial optimisation of the assay conditions, ex-vivo brain membranes at peak and trough exposures of HTL0014242 from the PK study were analysed. The proportion of mGlu<sub>5</sub> receptors occupied by HTL0014242 in each of the mouse brain membranes collected at peak exposure were similar, with mean RO at peak being 76.3±2.8% (Figure 4.6). In contrast, there was much more variability amongst the individual mouse brain membranes collected at trough exposure, the mean RO was 68.8±25.9% (Figure 4.6). The variability observed for measured % RO in brain membranes at trough exposure was comparable with the measured trough HTL0014242 concentrations in SC and blood (Table 4.2). As mentioned previously, increased variability at trough exposure compared with peak exposure is to be expected. However, like before where one mouse collected at trough exposure had very high HTL0014242 concentrations in SC and blood, the measured % RO in the brain membrane of this mouse was also increased at 92.4% (Figure 4.6). All the data collected for this mouse suggest that it had a much higher HTL0014242 exposure.

Measuring mGlu<sub>5</sub> RO in ex vivo brain membranes gives a useful indication of how HTL0014242 dosage correlates with mGlu<sub>5</sub> receptor interaction. The measured % RO in brain membranes at peak and trough HTL0014242 exposure, broadly positively correlated with peak and trough HTL0014242 concentrations in SC and blood (Table 4.2). For example, the mice with the highest HTL0014242 concentrations in SC and blood also had the highest mGlu<sub>5</sub> RO in brain membranes. This validates the [<sup>3</sup>H] M-MPEP binding assay as a useful measure of mGlu<sub>5</sub> target engagement. Whilst there are more precise ways of establishing RO, such as ex-vivo autoradiography, comparatively this technique is much more expensive. Consequently, the [<sup>3</sup>H] M-MPEP binding assay method is ideal for approximate indications of target interaction.

Interestingly, predicted RO was consistently lower than measured RO (Figure 4.8). Notably, the predicted RO was determined from calculating unbound HTL0014242 concentrations in SC whilst the measured RO was calculated in brain tissue. Consequently, it is quite possible that there are differences between SC and brain tissue that could influence receptor occupancy. For example, predicted RO in SC was determined by calculating the unbound HTL0014242 concentrations in SC from the SC free fraction. However, if HTL0014242 is more highly protein bound in SC compared to brain, this could explain why mGlu<sub>5</sub> RO in brain was higher. Furthermore, mGlu<sub>5</sub> receptor density may differ between tissue type and this could also account for the observed RO differences between SC and brain. In short, despite predicted % RO values being under estimates of the measured values, the rank order was the same as measured % RO. Lastly, the difference between the predicted and measured % RO highlights the necessity to measure RO in future *in vivo* mouse studies.

Furthermore, the equation used to calculate predicted RO only takes into consideration the unbound concentration of HTL0014242 in SC (as determined from measuring the free fraction (Fu) in SC) and the IC<sub>50</sub> of HTL0014242 in mouse brain. The measured Fu in SC was within the lower limit of detection (0.04%) and therefore may not have been very precise. Consequently, it is best to experimentally measure RO due to the simplicity of the predicted RO equation.

To summarise, competition binding experiments demonstrated that HTL0014242 affinity for mGlu<sub>5</sub> is not altered by the *SOD1*<sup>G93A</sup> disease or by age. This is reassuring as it indicates that HTL0014242 pharmacology is unlikely to change throughout a longitudinal repeat-dosing study. In addition, HTL0014242 dosed at 10mg/kg in *SOD1*<sup>G93A</sup> mouse spinal cord has an excellent PK profile. The compound demonstrated good CNS exposure, with enough free drug in SC to produce an effect for around 18 hours. Predicted receptor occupancy calculations from the PK data support a rationale for dosing at 3, 10 and 30mg/kg to investigate the efficacy of HTL0014242 in the *SOD1*<sup>G93A</sup> mouse model of MND. Finally, a [<sup>3</sup>H] M-MPEP binding assay for determining RO in ex-vivo crude brain membranes was developed. Using this method, it was possible to establish the proportion of mGlu<sub>5</sub> receptors in ex-vivo brain membranes that are occupied by HTL0014242, giving a robust indication of target engagement following *in vivo* dosing. Whilst estimations of RO in SC were not predictive of measured RO in brain there was a broad correlation between these values. The findings from this chapter validate HTL0014242 as a superior drug candidate for pharmacological blockade of mGlu<sub>5</sub>. Consequently, HTL0014242 has

been selected for future *in vivo* studies to investigate mGlu<sub>5</sub> as a novel therapeutic target in the *SOD1*<sup>G93A</sup> mouse model of MND.

# 5 90D dose-response study of HTL0014242 in the *SOD1*<sup>G93A</sup> mouse model

## 5.1 Introduction

Currently riluzole is the only therapeutic drug on the market for MND patients in Europe (Gordon 2011). However, its effects are modest, extending survival by approximately 2-4 months (Bensimon et al. 1994; Lacomblez et al. 1996b; Miller et al. 2003). For example, it is reported on the electronic Medicines Compendium (eMC) that there is a lack of evidence to suggest that RILUTEK (the brand name for riluzole) exerts a therapeutic effect on motor function, fasciculations, muscle strength or motor symptoms. Furthermore, it has not been shown to be effective in late stages of MND (eMC, 2014). Clearly, there is an urgent need for more effective disease modifying therapies in MND.

Whilst mGlu<sub>5</sub> was validated as a relevant therapeutic target in *SOD1* MND (Chapter 3), Chapter 4 confirmed HTL0014242 target engagement in brain when dosed orally at 10mg/kg in *SOD1*<sup>G93A</sup> mice. RO in brain at a dose of 10mg/kg was measured to be ~73-79% at peak HTL0014242 exposure. Further, HTL0014242 dosed at 10mg/kg was associated with an excellent pharmacokinetic profile, demonstrating a long half-life and good CNS exposure. Despite this compound being highly protein bound, there was enough unbound drug in SC to achieve levels greater than the IC<sub>50</sub> for around 18 hours.

Findings in Chapter 4 demonstrate that HTL0014242 has optimised pharmacological properties for *in vivo* testing compared with the previously investigated mGlu<sub>5</sub> NAM, MPEP. Not only is MPEP associated with poor pharmacokinetics, but also its lack of selectivity for the mGlu<sub>5</sub> receptor at high doses (Lea et al. 2009), makes it less than ideal for probing the role of mGlu<sub>5</sub> as a novel therapeutic target in MND.

The aim of this chapter was to robustly investigate whether inhibiting mGlu<sub>5</sub> with HTL0014242 has a therapeutic effect in the *SOD1*<sup>G93A</sup> mouse model of MND at early and intermediate stages of disease (up to 90 days of age) using a range of tests previously validated, including running wheel performance (Mead et al. 2011; Bennett et al. 2014). Previously, Rossi et al. (2008), tested the efficacy of MPEP at a single dose (30mg/kg) in *SOD1*<sup>G93A</sup> mice on a mixed genetic background. However, HTL0014242 was administered at several different doses, to *SOD1*<sup>G93A</sup> mice on an

inbred genetic background. Using mice on an inbred background reduces *SOD1*<sup>G93A</sup> disease variability, lowering the risk of producing false positive data (Mead et al. 2011).

Predicted mGlu<sub>5</sub> RO for HTL0014242 at 3, 10 and 30mg/kg was calculated using the 10mg/kg PK data and assuming linearity. This demonstrated that a good range of mGlu<sub>5</sub> occupancies could be achieved across these doses. Consequently, a dose-response study for HTL0014242 dosed at 3, 10 and 30mg/kg was designed in the *SOD1*<sup>G93A</sup> mouse model of MND to establish the effect of HTL014242 on early and intermediate stages of the disease, up to 90 days (90D) of age (see Figure 5.1).

In order to determine the effect of HTL0014242 on *SOD1*<sup>G93A</sup> disease progression, motor function was monitored daily using in-cage fastrac running wheels and rotarod tests conducted once per week from 5 weeks of age. Neurological scoring took place twice a week from 60 days of age to determine the age at onset of visible signs of disease. Following the onset of visible signs of disease (~75 days of age), catwalk gait analysis was carried out at 84 days of age to measure several gait parameters of the mice.

At 90 days of age the study was terminated, and tissue was collected at peak and trough HTL0014242 exposures. From this, total concentration in brain, estimated unbound concentration in brain and the proportion of mGlu<sub>5</sub> RO in brain was measured for each of the dose groups. This gave an indication of mGlu<sub>5</sub> target engagement across the different doses of HTL0014242. In addition, spinal cord tissue was collected at 90 days to determine the effect of HTL0014242 on pathologic markers of disease progression, such as glial activation. It has been shown that glial cells such as astrocytes and microglia are drivers of disease progression in MND (Boillee et al. 2006a; Yamanaka et al. 2008) . Consequently, the ventral horns of lumbar SC sections were immuno-stained for both GFAP and Iba1 (markers of astrocytes and microglia, respectively).

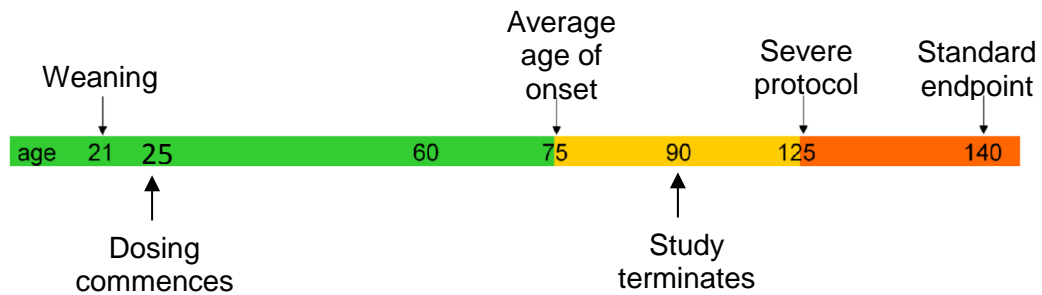


**Figure 5.1. Timeline for 90D dose-response study in *SOD1<sup>G93A</sup>* mouse model of MND**

Previously Rossi et al. (2008) found that the mGlu<sub>5</sub> NAM, MPEP, delayed onset and extended survival in the *SOD1<sup>G93A</sup>* mouse model of MND. Interestingly it was reported that MPEP exerted its therapeutic effect by inhibiting mGlu<sub>5</sub> activity, reducing glutamate toxicity and in turn slowing down the degeneration of astrocytes that directly surrounded the spinal motor neurons (Rossi et al. 2008). Whilst it has previously been reported that astrocytic mGlu<sub>5</sub> activity mediates glutamate toxicity in MND (Anneser et al. 2004; D'Antoni et al. 2011; Rossi et al. 2008), characterisation of mGlu<sub>5</sub> expression in our *SOD1<sup>G93A</sup>* mouse model of MND did not demonstrate any colocalisation of mGlu<sub>5</sub> on astrocytes in lumbar SC sections at 90 days of age. Despite the *in vivo* study carried out by Rossi et al. (2008), demonstrating that MPEP has a therapeutic effect in the *SOD1<sup>G93A</sup>* mouse model of MND by inhibiting mGlu<sub>5</sub> activity, this was not necessarily a result of blocking astrocytic mGlu<sub>5</sub> activity. Consequently, it is hypothesised that dosing with HTL0014242 will slow disease progression in the *SOD1<sup>G93A</sup>* mouse model of MND, by reducing mGlu<sub>5</sub> mediated glutamate toxicity.

Riluzole has become the gold standard for all new therapeutic compounds to treat MND. It is highly likely that any new therapeutic compound approved for use in MND patients, from an ethical standpoint, would have to be dosed concomitantly with riluzole. Riluzole is thought to exert its therapeutic effect through indirect modulation of glutamatergic toxicity (Debono et al. 1993). However the pharmacology of this compound is complex (Bellingham 2011). If HTL0014242 demonstrates efficacy in the *SOD1<sup>G93A</sup>* mouse model of MND by slowing down astrocyte degeneration as hypothesised by Rossi et al. (2008), considering that mGlu<sub>5</sub> is a glutamate receptor, it will be important to establish whether riluzole has the same effect on disease

progression as HTL0014242. For example, are any effects of HTL0014242 replicated with riluzole or not? Consequently, a 90D study in the *SOD1<sup>G93A</sup>* mouse model of MND will also be carried out to compare the effects of dosing riluzole with and without HTL0014242, on pathologic markers of disease progression, such as glial activation.

## 5.2 Results

### 5.2.1 90D dose-response study of HTL0014242 in the *SOD1<sup>G93A</sup>* mouse model of MND

The PK study for HTL0014242 dosed orally at 10mg/kg showed that this compound has an excellent pharmacokinetic profile in SC and demonstrates sufficient target engagement in brain. Consequently, a dose of 10mg/kg represented a good intermediate dosing level for a dose-response study in the *SOD1<sup>G93A</sup>* mouse model of MND. A 90-day study was designed to investigate the effects of this compound on early and intermediate stages of the disease following broadly the methods in Mead et al. (2011) and Bennett et al (2014). HTL0014242 was orally dosed at 3,10 and 30mg/kg every day from 25 days of age through to 90 days of age. In addition, a vehicle control group was orally dosed with 0.5% methylcellulose at 10ml/kg per day. Statistical power analysis demonstrated that a group size of 11 mice was needed to detect a difference in time taken to reach a 20% decline in fastrac running wheel performance. Neurological scoring took place twice a week from 60 days of age to determine classical signs of disease onset (hind-limb tremor in combination with hind-limb splay defect). The first of two consecutive onset scores was used to determine the age of onset for each mouse. Figure 5.2 shows that there was no significant difference in age at onset of visible signs of disease between the vehicle and HTL0014242 dosed groups, as shown by one-way ANOVA ( $p = 0.0587$ ). The average onset ranged from ~75 – 77 days of age.

Motor function was monitored using two motor readouts, in-cage fastrac running wheels and rotarod testing. Each mouse was singly housed in cages containing fastrac running wheels to measure their voluntary motor function from 25 days of age onwards. Female mice were used for this study as it had previously been shown that female mice display a higher frequency of running behaviour compared to male mice (De Bono et al. 2006). The parameters measured by the fastrac-running wheels were total time, total distance and average speed ran by the mouse over a 24 h period. Figure 5.3 shows that whilst there was an overall significant difference between groups for all three parameters (shown by two-way ANOVA,  $p = <0.0001$ ), the data was too variable to pick out any individual differences between groups at specific time

points for total time and total distance ran. Multiple comparisons (Tukey's post-test) between groups identified that the average speed ran for the 3mg/kg HTL0014242 dose-group was significantly faster than the 10mg/kg HTL0014242 dose group between 48-49 and 63-67 weeks ( $p = <0.05$ ). Although this study was originally powered based on the time taken to reach a 20% decline in running wheel performance, it was not possible to analyse this parameter due to the variability in individual mouse performance over time and the inability to define when a 20% decline was met.

Rotarod tests conducted once per week from 5 weeks of age measured forced motor activity. The mice were placed on a rotating bar which accelerates from 4-40rpm over the course of 5 minutes and the time taken for the mice to fall from the bar was measured. Figure 5.4a demonstrates an overall treatment effect for HTL0014242 dose groups on rotarod, as shown by two-way ANOVA ( $p = 0.0120$ ). Whilst all dose groups displayed a decline in motor performance with disease progression, the three HTL0014242 dose groups showed slightly reduced motor decline compared to the vehicle dosed mice. Despite observing an overall treatment effect on rotarod, there was no dose-response effect. Multiple comparison analysis demonstrated that there was no significant difference in motor performance between dose groups at any of the individual time points ( $p = >0.05$ ), perhaps reflective of the high variability observed for this measure. Previously it has been found that time taken to reach a 20% decline in rotarod performance is associated with much less variability within female *SOD1<sup>G93A</sup>* mice (Mead et al. 2011). Figure 5.4b demonstrates that whilst the time taken to reach a 20% decline in rotarod performance was earlier for the vehicle dose group compared to the HTL0014242 dose groups, one-way ANOVA demonstrated no significant difference between groups ( $p = 0.3615$ ). Notably, the data obtained for this measure were more variable (Figure 5.4c), with higher coefficients of variation than observed for historical data (Mead et al. 2011).

Each day, prior to being dosed, the mice were weighed and the data recorded. This was necessary due to the daily oral dose being determined from the weight of the mouse and it also served as an additional measure of general wellbeing. Interestingly, there was a significant difference between the weights of the mice in the vehicle and HTL0014242 dose groups (Figure 5.5), as shown by two-way ANOVA ( $p = 0.0113$ ). Multiple comparison analysis demonstrated that there was no initial significant difference between the weights of the mice in any of the dose groups, at 25 days of age when the mice were first recruited. However, between 27 and 75 days of age, the mean weight of the mice in one or more of the HTL0014242 dose groups was

significantly lower than the mean weight of the mice in the vehicle control group (p values ranged from 0.0500 – 0.0010). Despite some of the observed differences in weight being relatively small, overall the findings suggest that dosing with HTL0014242 could be associated with weight loss.

Catwalk gait analysis was carried out at 84 days of age to measure several gait parameters of the mice following onset of visible signs of disease (average onset is ~75 days of age). The mice were placed at the end of a glass platform in darkness and left to voluntarily traverse to the opposite side of the platform. The footprints of the mouse were video captured for analysis using the catwalk software which calculated statistics related to features of their gait and locomotion. The catwalk parameters shown in Figure 5.6 are amongst the most sensitive for detecting a difference between non-transgenic and *SOD1<sup>G93A</sup>* mice (Mead et al. 2011). Whilst non-transgenic mice typically spend more time supported by diagonal paws, *SOD1<sup>G93A</sup>* mice tend to progressively increase time spent on three paws with disease progression as it gives them more stability. Despite a small trend for vehicle dosed mice to spend more time on three paws (Figure 5.6a) and less time on diagonal paws (Figure 5.6b) compared to HTL0014242 dosed mice, one-way ANOVA demonstrated that there was no significant difference between the groups (p = 0.7164 and p = 0.5616, respectively).

Discrepancies in stride length have also been observed between healthy non-transgenic mice and *SOD1<sup>G93A</sup>* mice. Throughout the disease trajectory, *SOD1<sup>G93A</sup>* mice typically demonstrate a decrease in their stride length. Figure 5.6 (c-d) demonstrates an overall significant difference in both forelimb (c) and hindlimb (d) stride lengths at 84 days of age between dose groups (p = 0.0060 and p = 0.0079, respectively). Multiple comparison analysis showed that mice dosed with 10mg/kg HTL0014242 had significantly reduced forelimb (c) and hindlimb (d) stride lengths compared to mice dosed with 3mg/kg and 30mg/kg HTL0014242 (p = <0.0500). Despite this finding indicating that the 10mg/kg HTL0014242 dose group may fare worse than any of the other dose groups, it is worth noting that there was more variability observed for the data of the 10mg/kg HTL0014242 dose group compared to the other dose groups.

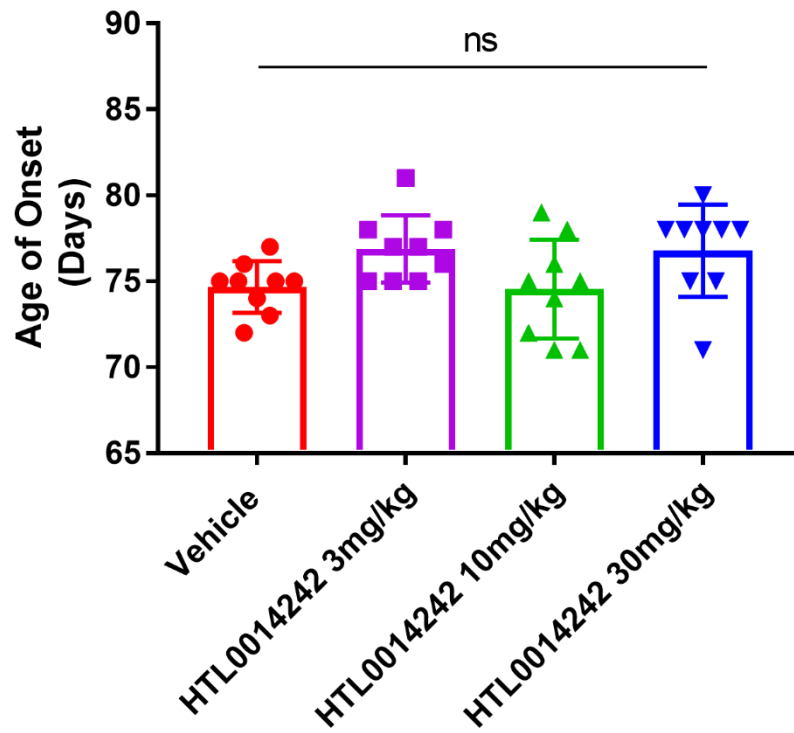


**Figure 5.2. No significant difference between vehicle and HTL0014242-dosed groups for age of onset.** *SOD1<sup>G93A</sup>* mice were orally dosed with 3, 10 and 30mg/kg of HTL0014242 and vehicle from 25 days of age. Neurological scoring took place twice a week from 60 days of age to determine classical signs of disease onset. Onset was defined by hind-limb tremor in combination with a hind-limb splay defect. Mice were considered to have disease onset at the time of the first score of two consecutive onset recordings. The mean age of onset ( $\pm$ SD) was plotted for each dose group (a). The mean age of onset for the vehicle, 3, 10 and 30mg/kg HTL0014242 dose groups were 74.7, 76.9, 74.6 and 76.8 days of age, respectively. Statistical analysis by one-way ANOVA and Tukey's post-test demonstrated no significant differences between groups for disease onset ( $p= 0.0587$ ). Data points represent individual animals (9 mice per group).

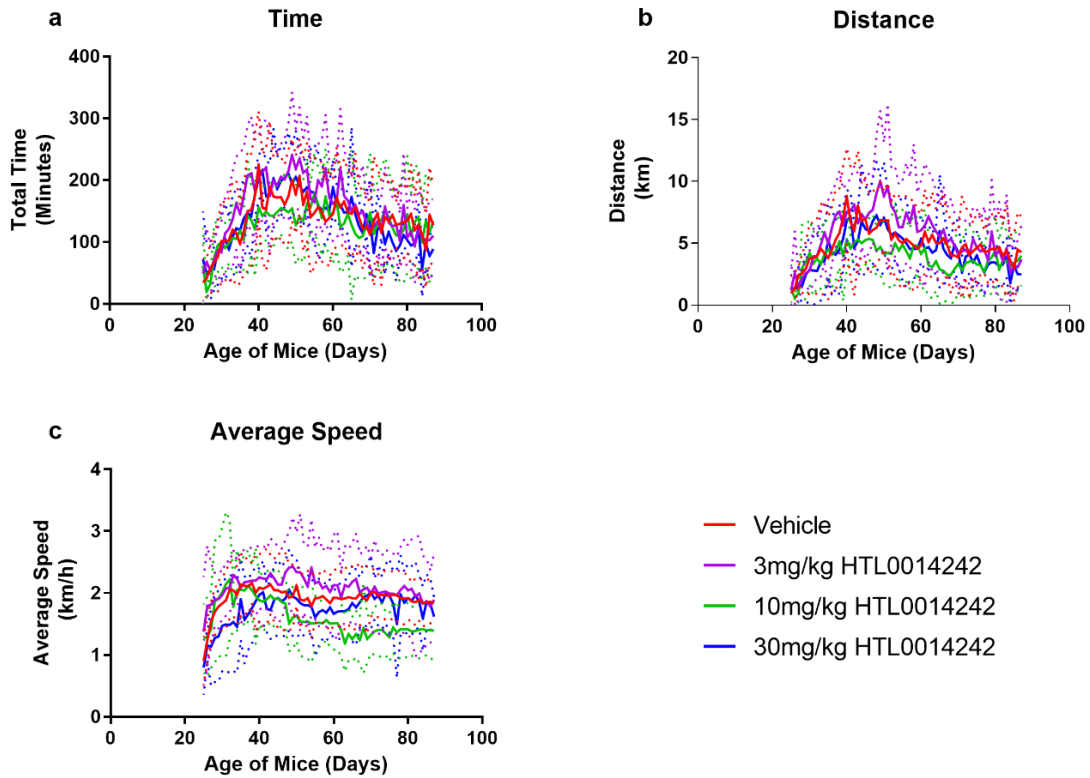


**Figure 5.3. No difference in the fastrac running wheel performance of HTL0014242-dosed mice.** *SOD1<sup>G93A</sup>* mice were orally dosed with 3, 10 and 30mg/kg of HTL0014242 and vehicle from 25 days of age. The mice were singly housed in cages containing fastrac running wheels to monitor their motor function. The fastrac system is a voluntary running wheel placed at an angle which allows the mouse to run at its own pace. The wheel has a small magnet attached to the rim and a reed switch connected to a bike computer measures the total time, total distance and average speed ran for each mouse per night (a-c). Statistical analysis by two-way ANOVA and Tukey's post-test demonstrated an overall significant difference between dose groups for total time, total distance and average speed ran ( $p = <0.0001$ ). Multiple comparisons between groups analysis showed there was no significant difference between any of the dose groups at any time point for total time or total distance ran ( $p = >0.0500$ ). The average speed ran for the 3mg/kg HTL0014242 dose group was significantly higher than that of the 10mg/kg HTL0014242 dose group between 48-49 weeks and 63-67 weeks ( $p = <0.0500$ ). Data presented as mean  $\pm$  SD (dotted lines). Data points represent mean score for each dose-group (11 mice per group).

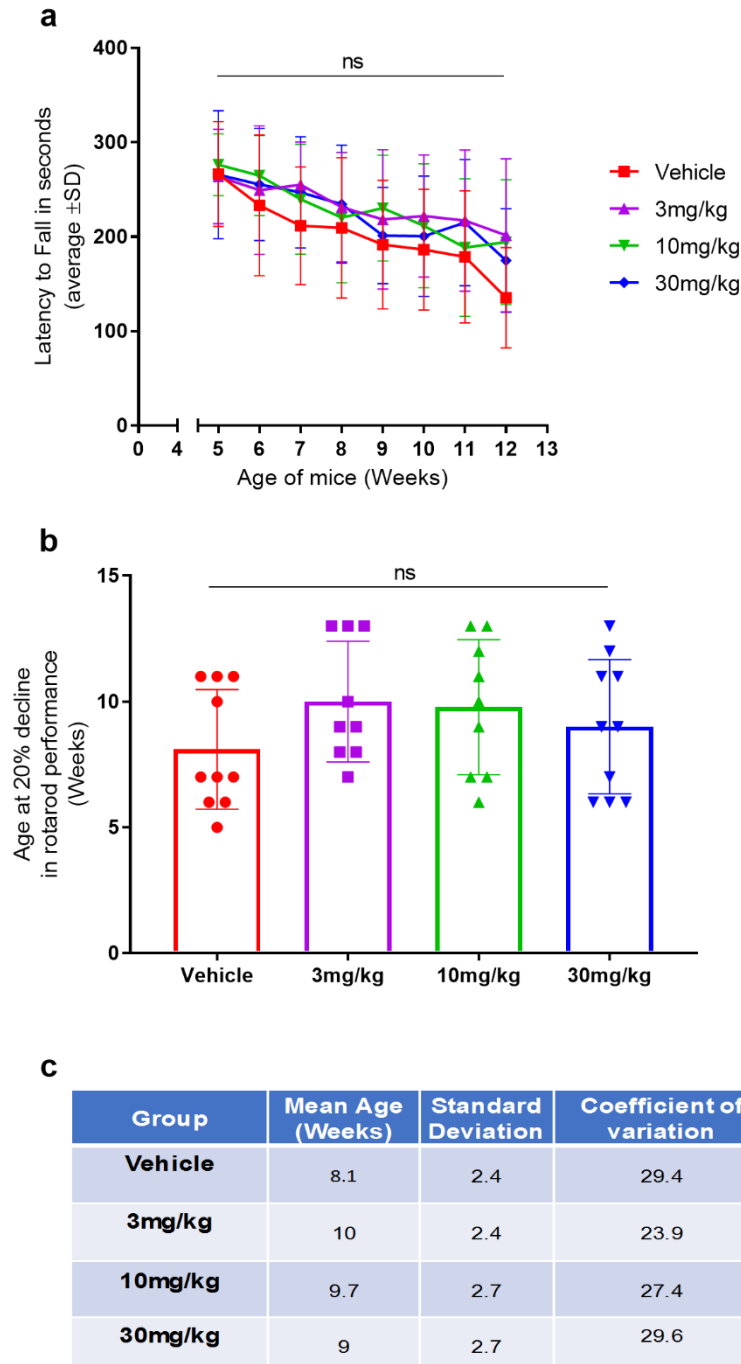


**Figure 5.4. No difference in the rotarod performance of HTL0014242 dosed mice.** *SOD1<sup>G93A</sup>* mice were orally dosed with 3, 10 and 30mg/kg of HTL0014242 and vehicle from 25 days of age. Rotarod tests were conducted once per week from 5 weeks of age. The rotarod test consists of a rotating rod that accelerates from 4-40 rpm over the course of 300 seconds and the time taken to fall recorded. All rotarod testing consisted of two attempts with the best score recorded for analysis. Mean

latency to fall ( $\pm$  SD) was plotted for each mouse (a). Statistical analysis by two-way ANOVA and Tukey's post-test demonstrated an overall significant difference between the dose groups ( $p= 0.0120$ ). Multiple comparisons analysis showed there was no significant difference between the groups at any of the individual time points ( $p = > 0.0500$ ). The mean age ( $\pm$ SD) for each mouse to reach a 20% decline in rotarod performance was also plotted (b). The mean age at which a 20% decline in rotarod performance was recorded for each dose group and presented in the table (c). Statistical analysis by one-way ANOVA and Tukey's post-test demonstrated no significant difference between groups ( $p= 0.3615$ ). Data points represent individual animals (9-10 mice per group).

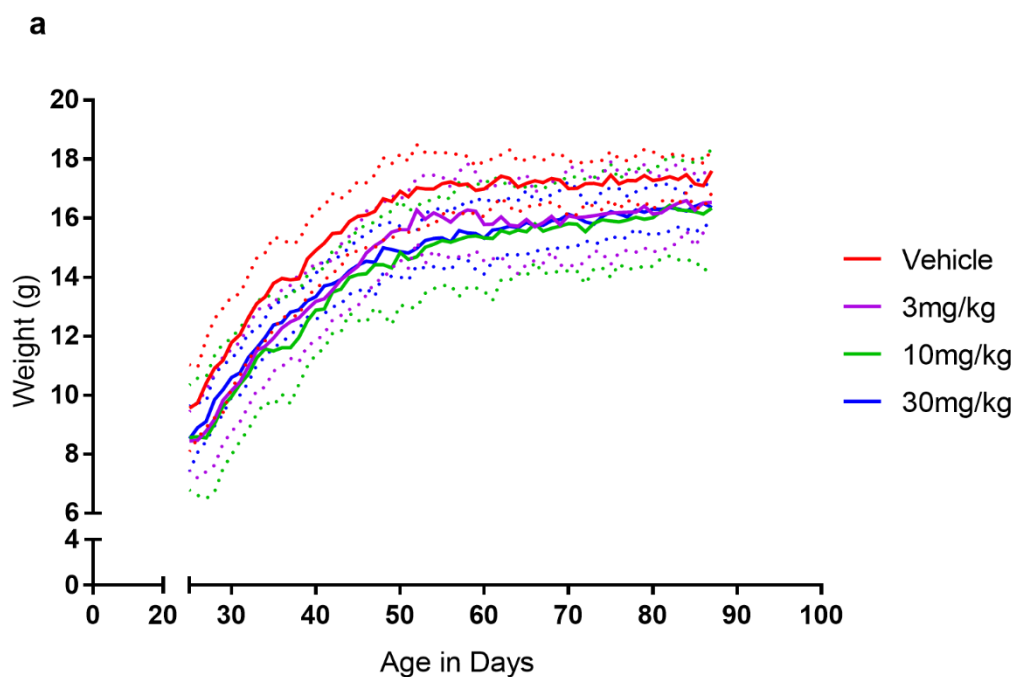


**Figure 5.5. HTL0014242 dosed mice weigh less than vehicle dosed mice.** *SOD1<sup>G93A</sup>* mice were orally dosed with 3, 10 and 30mg/kg of HTL0014242 and vehicle from 25 days of age through to 90 days of age. Mice were weighed daily prior to oral dosing as an additional measure of disease onset and drug tolerability. The weight for each mouse was plotted from 25 days onwards. Data presented as mean  $\pm$  SD (dotted lines), each data point represents the average weight of the mice in that dose-group (9-10 mice per group). Statistical analysis by two-way ANOVA with repeated measures and Tukey's post-test demonstrated a significant difference between dose groups ( $p = 0.0113$ ). Multiple comparisons analysis showed that the mean weight of the vehicle group was significantly higher than one or more of the HTL0014242 dosed groups between 27 and 75 days of age ( $p < 0.0500$ ).

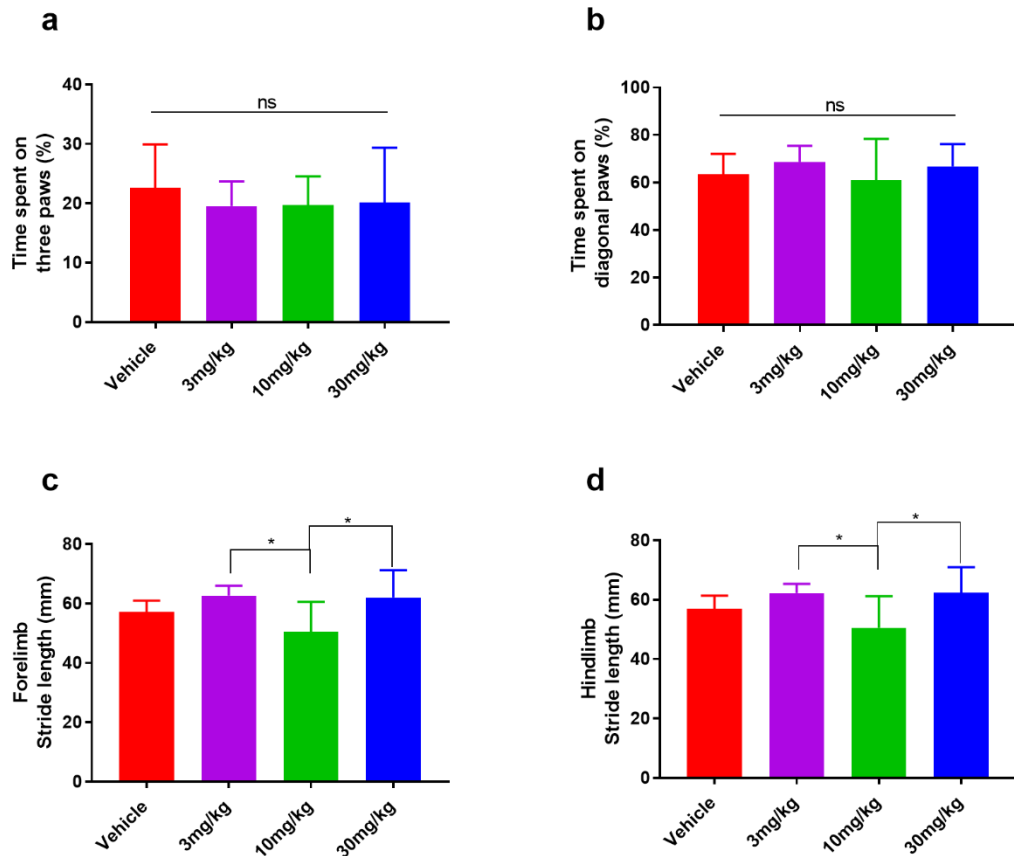


**Figure 5.6. Catwalk gait analysis across several parameters was inconclusive.**

*SOD1<sup>G93A</sup>* mice were orally dosed with 3, 10 and 30mg/kg of HTL0014242 and vehicle from 25 days of age through to 90 days of age. Catwalk gait analysis was performed at 84 days of age to monitor several aspects of their gait following video capture and manual segmentation of their step pattern. Percentage time spent on three paws and diagonal paws was plotted for each dose group (a and b, respectively). Statistical analysis by one-way ANOVA and Tukey's post-test demonstrated no significant difference between groups,  $p = 0.7164$  (a) and  $p = 0.5616$  (b). Forelimb and hindlimb stride length were also plotted for each dose group (c and d, respectively). Statistical analysis by one-way ANOVA and Tukey's post-test demonstrated an overall significant difference between groups,  $p = 0.0060$  (c) and  $p = 0.0079$  (d). Multiple comparisons analysis showed that the mean forelimb and mean hindlimb stride lengths were significantly reduced for the 10mg/kg HTL0014242 dose group compared to both the 3mg/kg and 30mg/kg HTL0014242 dose groups ( $p < 0.0500$ ). Data presented as mean  $\pm$  SD (7-10 mice per group).

### **5.2.2 Glial staining in ventral horns of lumbar spinal cord sections collected from dose-response study at 90 days**

Spinal cord tissue was collected from mice at 90 days of age and the ventral horns of lumbar SC sections were immuno-stained with the glial markers, anti-GFAP (Figure 5.7) and anti-Iba1 (Figure 5.8). Interestingly, a reduction in GFAP staining area was observed for all three HTL0014242 dose groups compared to the vehicle dose group, as shown by one-way ANOVA ( $p = 0.0039$ ). Multiple comparison analysis showed that the 10mg/kg and 30mg/kg HTL0014242 dose groups showed the biggest reduction in GFAP staining area compared to the vehicle group (71% and 88% reductions for the 10mg/kg and 30mg/kg HTL0014242 dose groups,  $p = 0.0042$  and  $p = 0.0018$ , respectively). The 3mg/kg HTL0014242 dose group showed a smaller 54% reduction in GFAP staining area compared to the vehicle dose group ( $p = 0.0309$ ). Whilst there was a trend for a dose-dependent reduction in GFAP staining area, there was no significant difference in GFAP staining area between the HTL0014242 dose groups. Perhaps due to the high variability observed for the GFAP staining data of the 10mg/kg HTL0014242 dose group (Figure 5.7b).

Furthermore, a reduction in Iba1 staining within the ventral horns of HTL0014242 dosed mice was also observed (Figure 5.8). Despite there being no overall significant difference in Iba1 staining area between the different dose groups, shown by one-way ANOVA ( $p = 0.0586$ ), there was a clear trend for less Iba1 in the HTL0014242 dose-groups compared with the vehicle dose group (Figure 5.8b). Whilst the reductions in Iba1 staining were not as profound as that observed for GFAP staining, multiple comparison analysis demonstrated a significant reduction (64%) in Iba1 staining for the 30mg/kg HTL0014242 dose group compared with the vehicle dose group,  $p = 0.0249$  (Figure 5.8b). Notably, the data observed for Iba1 staining were considerably more variable than that of GFAP staining.

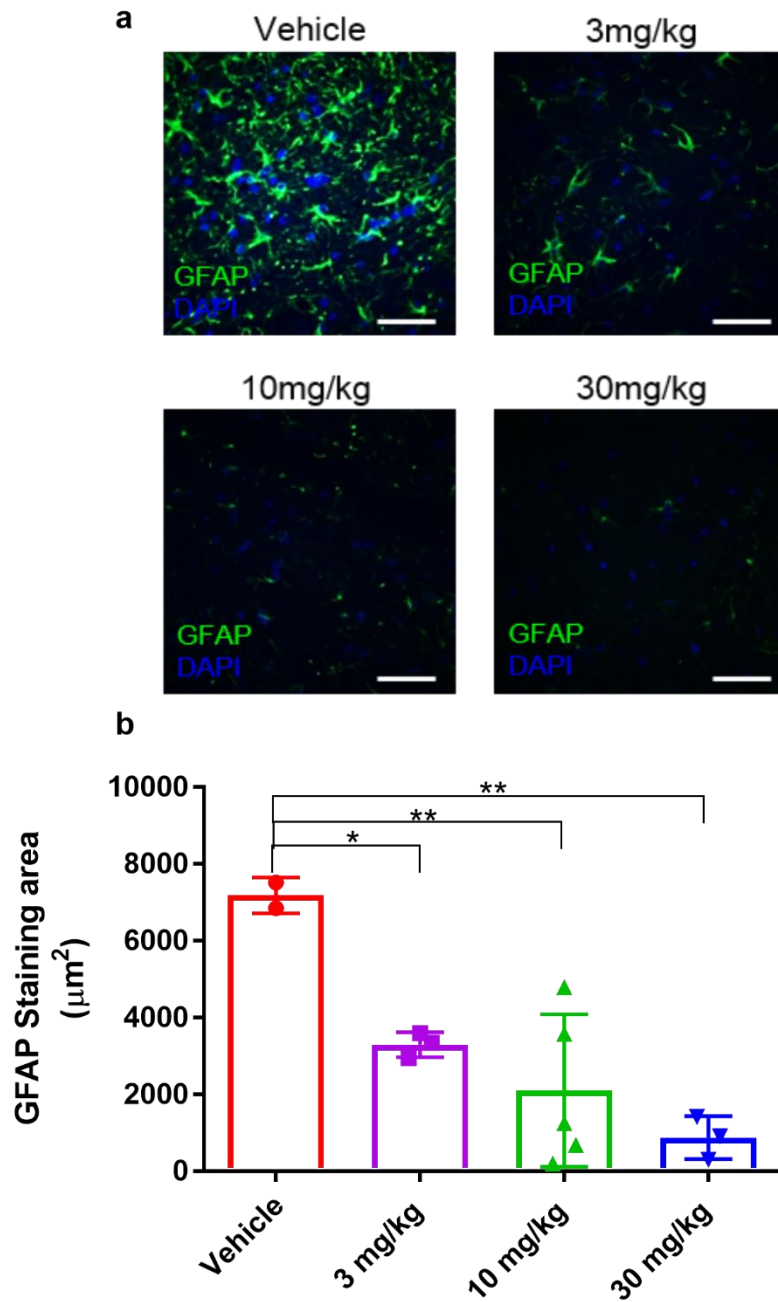


**Figure 5.7. Reduced astrocyte staining in ventral horns of HTL0014242 dosed mice at 90 days of age.** *SOD1<sup>G93A</sup>* mice were orally dosed with 3,10 and 30mg/kg of HTL0014242 and vehicle from 25 days of age through to 90 days of age. At 90 days of age lumbar spinal cord sections were fixed, paraffin-embedded and the ventral horns were immuno-stained with an anti-GFAP antibody and DAPI (a). Scale bars, 50µm. Quantification of the GFAP staining area showed that there was significantly less astrocyte activation in the HTL0014242 dose groups compared to the vehicle dose group (b), shown by one-way ANOVA and Dunnett's post-test ( $p = 0.0039$ ). Multiple comparisons analysis showed that the mean GFAP staining area for the

3mg/kg HTL0014242 dose group was significantly reduced compared to that of the vehicle dose group ( $p = 0.0309$ ), as was the case for the 10mg/kg HTL0014242 dose group and the 30mg/kg HTL0014242 dose group ( $p = 0.0042$  and  $p = 0.0018$ , respectively). Data presented as mean ( $\pm$  SD), data points represent individual animals (2-5 mice per group).

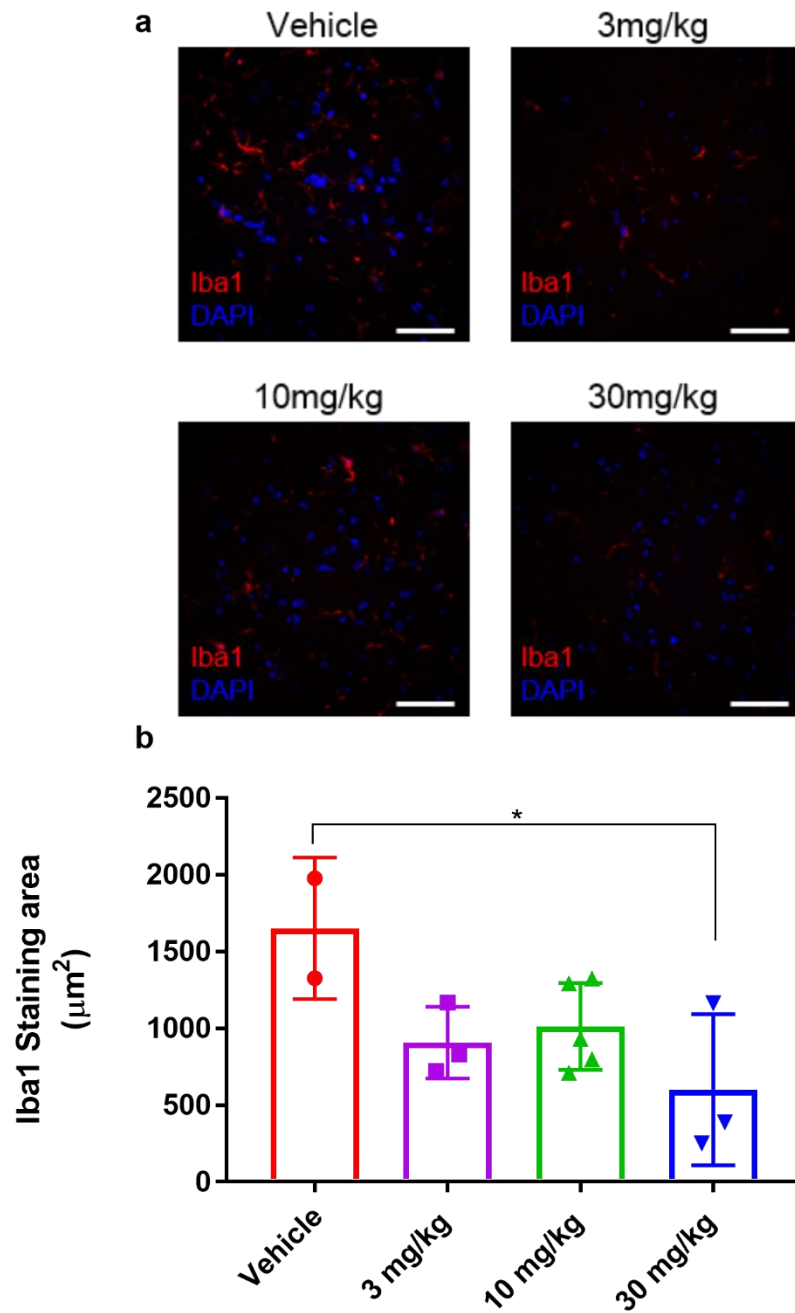


**Figure 5.8. Reduced microglial staining in ventral horns of HTL0014242 dosed mice at 90 days of age.** *SOD1<sup>G93A</sup>* mice were orally dosed with 3,10 and 30mg/kg of HTL0014242 and vehicle from 25 days of age through to 90 days of age. At 90 days of age lumbar spinal cord sections were fixed, paraffin-embedded and the ventral horns were immuno-stained with an anti-Iba1 antibody and DAPI (a). Scale bars, 50μm. Quantification of the Iba1 staining area showed that overall there was no significant difference in microglial staining between the HTL0014242 dose groups and the vehicle dose group (b), shown by one-way ANOVA and Dunnett's post-test ( $p =$

0.0586). Multiple comparisons analysis showed that the mean Iba1 staining area for the 30mg/kg HTL0014242 dose group was significantly reduced compared to that of the vehicle dose group ( $p = 0.0249$ ). Data presented as mean ( $\pm$  SD), data points represent individual animals (2-5 mice per group).

### **5.2.3 [<sup>3</sup>H] M-MPEP binding assay to measure RO of mGlu<sub>5</sub> receptors by HTL0014242 in mouse brain collected from dose-response study at 90 days**

Brain tissue was also collected from the dose-response study at 90 days for RO analysis. Brain membranes were processed to determine the proportion of mGlu<sub>5</sub> receptors occupied by HTL0014242 in the 3mg/kg, 10mg/kg and 30mg/kg HTL0014242 dose groups. This was established using the [<sup>3</sup>H] M-MPEP binding assay optimised in Chapter 4. Mean RO was established from the average specific binding at peak and trough HTL0014242 exposures for each of the HTL0014242 dose groups, with the values from the brain membranes of the vehicle dosed mice taken as 100% RO. Figure 5.9 demonstrates a good range of RO across all the HTL0014242 doses.

Predicted mGlu<sub>5</sub> RO in SC was calculated at peak and trough HTL0014242 exposures for the 3, 10 and 30mg/kg HTL0014242 dose groups (Table 5.1). Measured mGlu<sub>5</sub> RO in brain (Figure 5.9) was plotted versus the predicted mGlu<sub>5</sub> RO in SC at peak and trough HTL0014242 exposure for the 3, 10 and 30mg/kg HTL0014242 dose groups (Figure 5.10). From this it was possible to establish how accurate predicted RO in spinal cord was of measured RO in brain. As seen previously, despite a broad correlation between the two values, predicted RO in SC nearly always underestimated measured RO in brain (Figure 5.10). Unfortunately, it was not possible to determine HTL0014242 exposures in brain as the brain tissue was damaged in transit to Pharmidex for analysis.

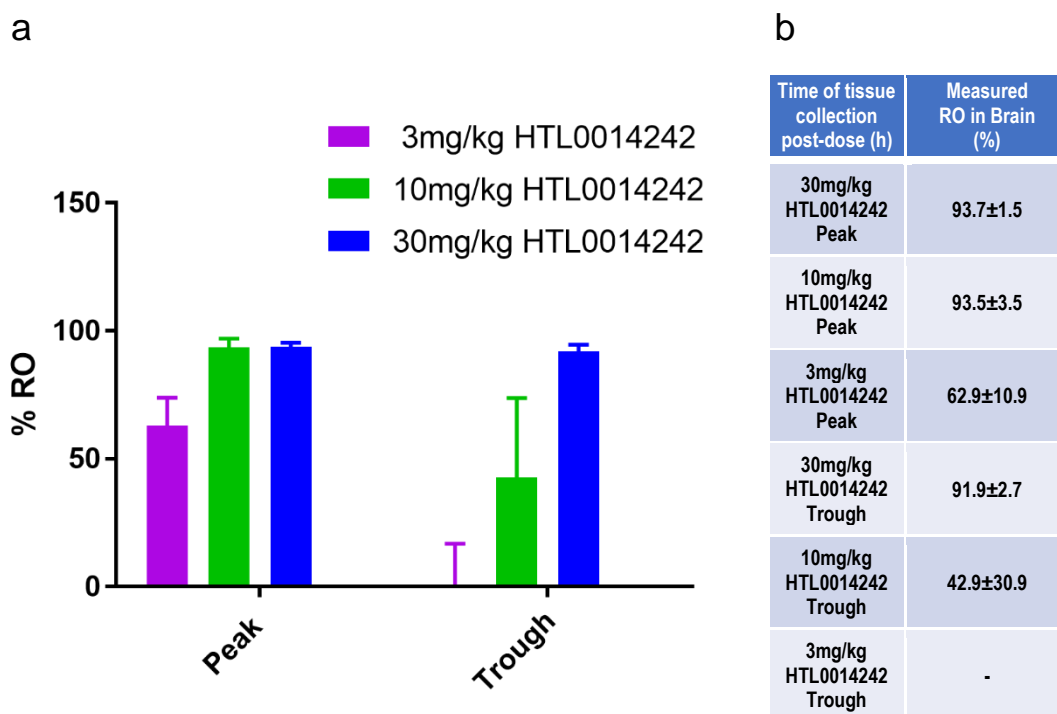


**Figure 5.9. A good range of mGlu<sub>5</sub> receptor occupancy by HTL0014242 was achieved across all of the doses.** Membranes were crudely prepared from 90-day old whole brains of *SOD1<sup>G93A</sup>* mice. The mice had either been dosed with 3,10, 30mg/kg of HTL0014242 or vehicle. Brain tissue was collected at peak (2 h post dose) and trough (24 h post dose) HTL0014242 exposures. The % receptor occupancy of mGlu<sub>5</sub> by HTL0014242 at peak and trough were calculated using a <sup>3</sup>[H] M-MPEP radioligand binding assay. a) Data presented as mean ± SEM (3 mice per group). b) Average RO measured in brain at peak and trough HTL0014242 exposures for each of the dose groups.

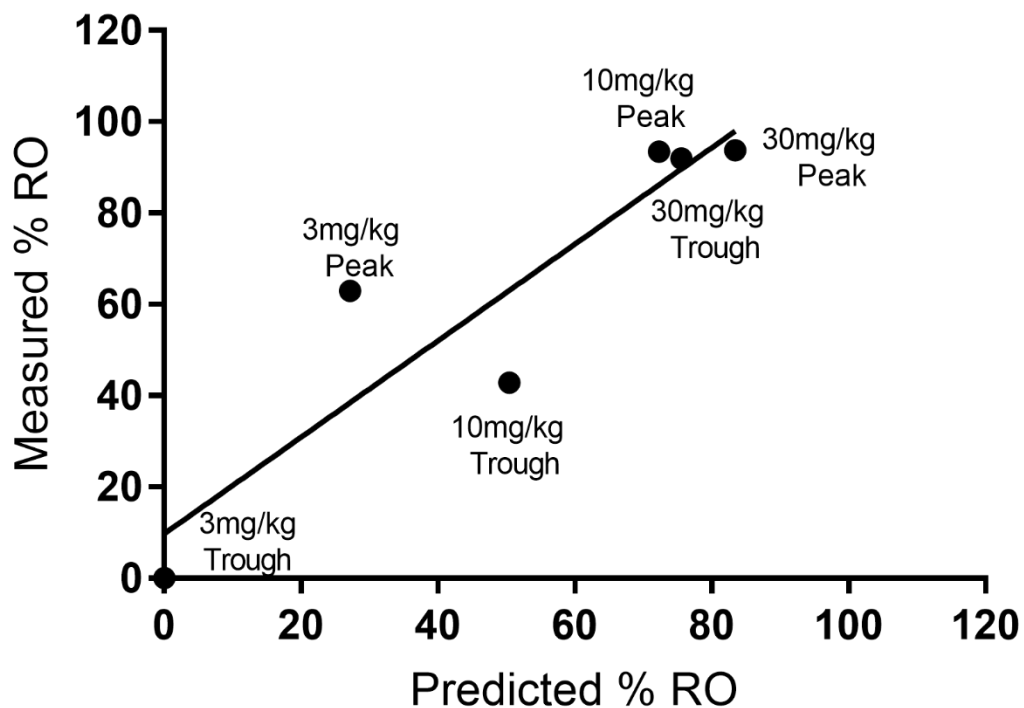


**Figure 5.10. Predicted receptor occupancy broadly correlated with measured RO but was not predictive of measured receptor occupancy.** The predicted mGlu<sub>5</sub> receptor occupancy was calculated using the equation (Predicted % RO = (HTL0014242 concentration / HTL0014242 concentration + K<sub>i</sub> of HTL0014242 for mGlu<sub>5</sub>) and plotted versus the measured mGlu<sub>5</sub> RO presented in Figure 5.9. The mean measured RO at peak and trough HTL0014242 exposure was plotted for each dose group (3 animals at peak and trough per group). The line of best fit through the data by linear regression demonstrates that there was a positive correlation between the predicted and measured RO values ( $r^2 = 0.83$ ,  $p = 0.01$ ).

**Table 5.1. 90 day dose-response study data for HTL0014242 dosed at 3, 10 and 30mg/kg** Total HTL0014242 concentration, unbound HTL0014242 concentration and predicted receptor occupancy for SC tissue collected at peak (2h) and trough (24h) HTL0014242 exposures.

Time of tissue collection post-dose (h)	Total HTL0014242 in SC (nM)	Unbound HTL0014242 in SC (nM)	Predicted RO in SC (%)
30mg/kg HTL0014242 Peak	7916	3.16	83.4
10mg/kg HTL0014242 Peak	4109	1.64	72.3
3mg/kg HTL0014242 Peak	588	0.23	27.2
30mg/kg HTL0014242 Trough	4868	1.95	75.6
10mg/kg HTL0014242 Trough	1603	0.64	50.4
3mg/kg HTL0014242 Trough	< 39	< 0.02	< 2.4

#### **5.2.4 90D study in the *SOD1<sup>G93A</sup>* mice to compare the difference in ventral horn glial staining of mice dosed with HTL0014242 and riluzole versus riluzole alone**

Findings from the 90D HTL0014242 dose-response study in *SOD1<sup>G93A</sup>* mice, demonstrated that inhibiting mGlu<sub>5</sub> receptors with HTL0014242 resulted in a reduction of glial activation (measured by GFAP and Iba1 staining area, Figure 5.7 and Figure 5.8, respectively).

Considering that riluzole is thought to exert its therapeutic effect through the indirect antagonism of glutamate and that HTL0014242 is a negative allosteric modulator of the glutamate receptor, mGlu<sub>5</sub>, it is important to establish whether riluzole has the same effect on glial activation as HTL0014242. Consequently, a 90D *in vivo* study was carried out to compare the effects of riluzole in combination with and without HTL0014242 on glial activation.

*SOD1<sup>G93A</sup>* mice were dosed with either vehicle (0.1% DMSO in drinking water), riluzole (~70mg/kg in drinking water) or riluzole (~70mg/kg in drinking water) plus HTL0014242 (30mg/kg orally dosed) from 25 days of age through to 90 days of age. At 90 days of age the study was terminated and SC tissue was collected. Lumbar ventral horns were immuno-stained with the glial markers, anti-GFAP (Figure 5.11) and anti-Iba1 (Figure 5.12).

Figure 5.11 (a-b) demonstrated that there was a significant difference in GFAP staining area and GFAP staining index between the different dose groups at 90 days of age (as shown by one-way ANOVA,  $p = < 0.0001$  and  $p = 0.0014$ , respectively). Multiple comparisons analysis showed that GFAP staining area was significantly reduced in the ventral horns of mice dosed with riluzole plus HTL0014242 compared to that of both vehicle dosed mice and riluzole only dosed mice,  $p = < 0.0001$  (Figure 5.11b). Further, GFAP staining index was also significantly reduced in ventral horns of the riluzole plus HTL0014242 dosed mice compared to that of the vehicle and riluzole only dosed mice,  $p = 0.0020$  and  $p = 0.0041$  respectively (Figure 5.11c). Interestingly, there was no significant difference in GFAP staining area or GFAP staining index between the vehicle dosed mice and the riluzole only dosed mice,  $p = > 0.0500$  (Figure 5.11b-c). This suggests that riluzole does not reduce astrocyte activation, as shown by immunostaining with GFAP.

The ventral horns of lumbar SC sections were also stained with the microglial marker, Iba1 (Figure 5.12a). Similarly, there was an overall significant difference in Iba1 staining area and staining index between the different dose groups ( $p = < 0.0009$  and

$p = 0.0122$ , respectively). The Iba1 staining area in the ventral horns of riluzole plus HTL0014242 dosed mice was significantly reduced compared to that of both the vehicle dosed mice and riluzole only dosed mice,  $p = <0.0008$  and  $p = 0.0177$  respectively (Figure 5.12b-c). The Iba1 staining area in the ventral horns of riluzole only dosed mice was not significantly different from that of vehicle dosed mice (Figure 5.12b). Whilst the Iba1 staining index for the riluzole plus HTL0014242 dosed mice was significantly reduced compared with that of the vehicle dosed mice ( $p = 0.0173$ ), there was no significant difference between the riluzole plus HTL0014242 dose group and the riluzole only dose group,  $p = >0.0500$  (Figure 5.12c). Interestingly, the Iba1 staining index in the ventral horns of riluzole only dosed mice was significantly reduced compared with that of the vehicle dosed mice,  $p = 0.0207$  (Figure 5.12c). These data suggest that riluzole may be involved in reducing microglial activation, as shown by a reduction in Iba1 staining index (Figure 5.12c). However, for measurement of microglial activation the area of staining is the key parameter used. It is not clear what a change in intensity and consequently staining index of Iba1 correlates with, in regard to microglial activation.

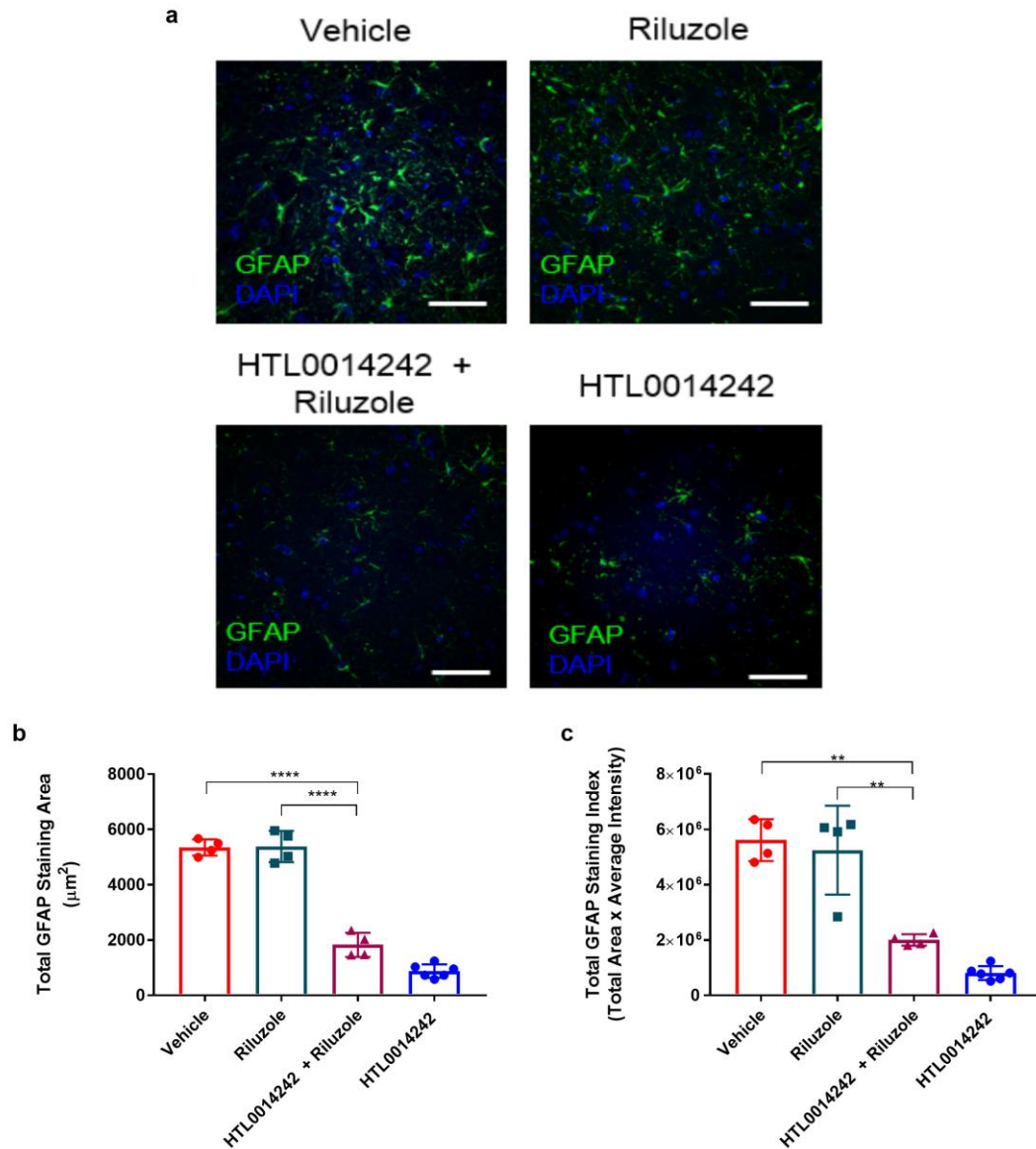


**Figure 5.11. Riluzole does not reduce astrocyte activation in 90-day old *SOD1<sup>G93A</sup>* mice.** *SOD1<sup>G93A</sup>* mice were orally dosed with vehicle (0.1% (v/v) DMSO in drinking water), riluzole (~70mg/kg), or riluzole (70mg/kg) plus HTL0014242 (30mg/kg) from 25 days of age through to 90 days of age. At 90 days of age lumbar spinal cord sections were fixed, paraffin-embedded and the ventral horns were immuno-stained with an anti-GFAP antibody and DAPI (a). Scale bars, 50μm. Quantification of the GFAP staining area and GFAP staining index showed that there was an overall significant difference between the dose groups, as shown by one-way ANOVA and Tukey's post-test,  $p = <0.0001$  and  $p = 0.0014$ , respectively (b-c). Multiple comparisons analysis showed that the mean GFAP staining area for the

riluzole plus HTL0014242 dosed mice was significantly reduced compared to both that of the vehicle dosed mice and that of the riluzole only dosed mice,  $p = <0.0001$  (b). Multiple comparisons analysis showed that the mean GFAP staining index for the riluzole plus HTL0014242 dosed mice was significantly reduced compared to both that of the vehicle dosed mice and that of the riluzole only dosed mice,  $p = 0.0020$  and  $p = 0.0041$ , respectively (c). The GFAP staining in ventral horns of lumbar spinal cord tissue collected at 90 days from mice dosed with HTL0014242 at 30mg/kg is included as a reference. Statistical analysis was not carried out for the GFAP staining in the HTL0014242 tissue as the data was generated from a separate *in vivo* study and the tissue was not stained at the same time as the tissue shown in this figure. Data presented as mean ( $\pm$  SD), data points represent individual animals (4 mice per group).

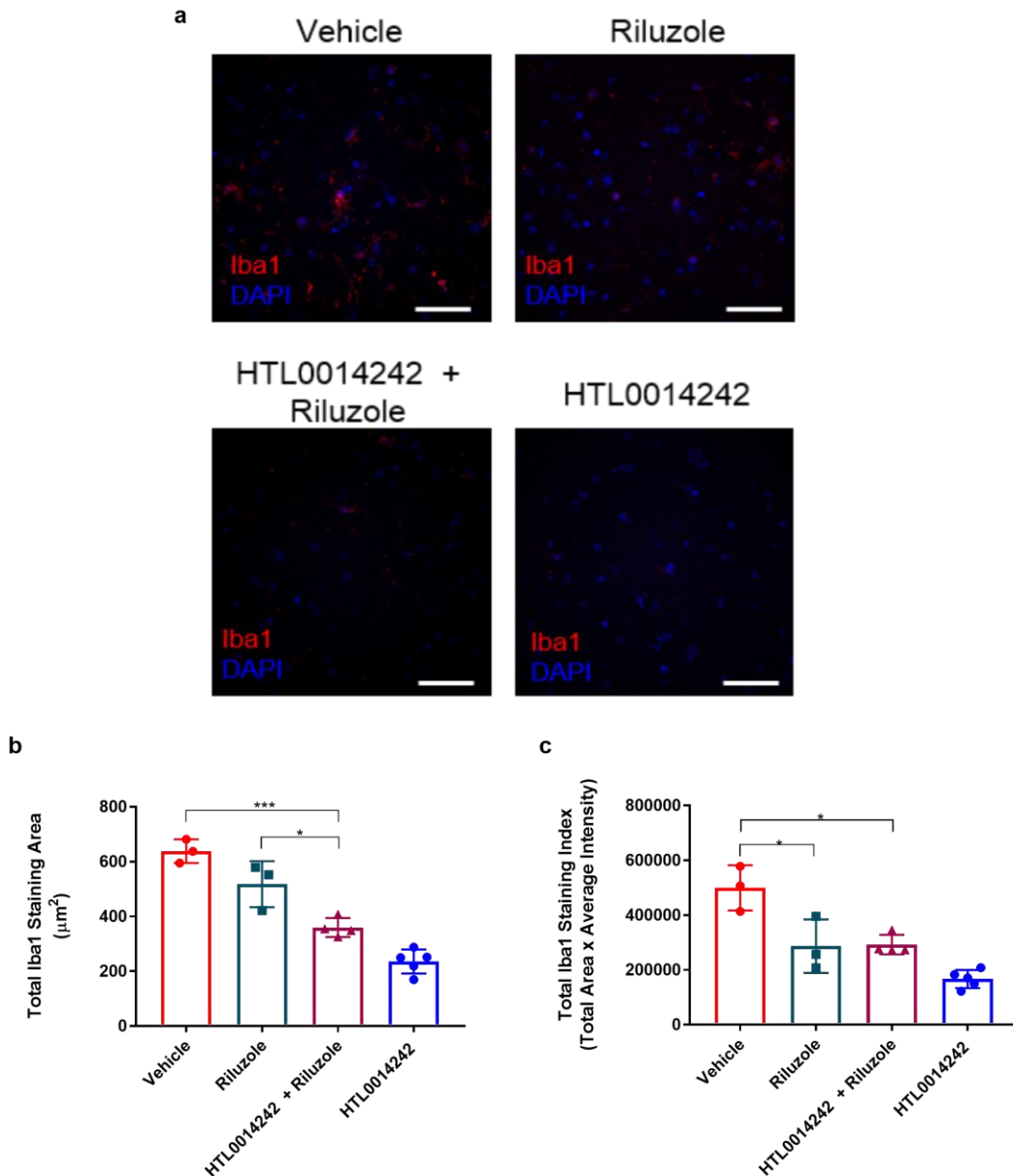


**Figure 5.12. Riluzole reduces microglial staining index but not staining area in 90 day old *SOD1*<sup>G93A</sup> mice.** *SOD1*<sup>G93A</sup> mice were orally dosed with vehicle (0.1% (v/v) DMSO in tap water), riluzole (~70mg/kg), or riluzole (70mg/kg) plus HTL0014242 (30mg/kg) from 25 days of age through to 90 days of age. At 90 days of age lumbar spinal cord sections were fixed, paraffin-embedded and the ventral horns were immuno-stained with an anti-Iba1 antibody and DAPI (a). Scale bars, 50μm. Quantification of the Iba1 staining area and Iba1 staining index showed that there was an overall significant difference between the dose groups, as shown by one-way ANOVA and Tukey's post-test,  $p = <0.0009$  and  $p = 0.0122$ , respectively (b-c). Multiple comparisons analysis showed that the mean Iba1 staining area for the riluzole plus HTL0014242 dosed mice was significantly reduced compared to both

that of the vehicle dosed mice and that of the riluzole only dosed mice,  $p = 0.0008$  and  $p = 0.0177$ , respectively) (b). Multiple comparisons analysis showed that the mean Iba1 staining index for both the riluzole only dosed mice and riluzole plus HTL0014242 dosed mice were significantly reduced compared to the vehicle dosed mice,  $p = 0.0207$  and  $p = 0.0173$ , respectively (c). The Iba1 staining in ventral horns of lumbar spinal cord tissue collected at 90 days from mice dosed with HTL0014242 at 30mg/kg is included as a reference. Statistical analysis was not carried out for the Iba1 staining in the HTL0014242 tissue as the data was generated from a separate *in vivo* study and the tissue was not stained at the same time as the tissue shown in this figure. Data presented as mean ( $\pm$  SD), data points represent individual animals (3-4 mice per group).

### 5.3 Discussion

Previously it was shown that the mGlu<sub>5</sub> NAM, MPEP, delays onset and extends survival in the *SOD1<sup>G93A</sup>* mouse model of MND. The main purpose of this chapter was to investigate the efficacy of the optimised mGlu<sub>5</sub> NAM, HTL0014242, in the *SOD1<sup>G93A</sup>* mouse model of MND. The focus of this study was to establish the effects of blocking mGlu<sub>5</sub> activity on early and intermediate stages of the disease. Consequently, *SOD1<sup>G93A</sup>* mice were dosed with vehicle or 3,10, 30mg/kg of HTL0014242, from 25 days of age up to 90 days of age. Both voluntary and forced motor activity of the mice were monitored using in-cage fastrac running wheels and rotarod tests. These motor readouts are particularly sensitive for detecting subtle changes in motor function at earlier time points in the *SOD1<sup>G93A</sup>* disease course (Mead et al. 2011). Neurological scoring took place twice a week from 60 days of age to establish whether dosing with HTL0014242 had any effect on *SOD1<sup>G93A</sup>* onset of visible signs of disease. Catwalk gait analysis was performed at 84 days of age (post-onset), to pick up any subtle differences in features of gait and locomotion between the HTL0014242 and vehicle dosed mice. At 90 days of age, tissue was collected to determine mGlu<sub>5</sub> RO in brain at different doses of HTL0014242. Furthermore, lumbar SC sections collected at 90 days of age were immuno-stained with anti-GFAP and anti-Iba1 to compare markers of disease pathology between the different dose groups. Assessing motor function, onset of disease and pathology at different mGlu<sub>5</sub> receptor occupancies, enabled the efficacy of therapeutically blocking mGlu<sub>5</sub> up to 90 days of age, in the *SOD1<sup>G93A</sup>* mouse model of MND to be rigorously investigated. Finally, a 90D *in vivo* study whereby riluzole was dosed both with and without HTL0014242, was carried out to establish whether these two compounds have a similar mechanism of action on astrocyte activation.

#### 5.3.1 90D dose-response study of HTL0014242 in the *SOD1<sup>G93A</sup>* mouse model of MND

In contrast to previous findings by Rossi et al. (2008), this study found that blocking mGlu<sub>5</sub> activity did not significantly delay onset of visible signs of disease in the *SOD1<sup>G93A</sup>* mouse model of MND. Average age of onset was similar across all dose-groups, ranging from ~75 days for the vehicle and 10mg/kg HTL0014242 dose groups, to ~77 days for the 3mg/kg and 30mg/kg HTL0014242 dose groups.

This study defined onset of visible signs of disease as a combination of hind-limb tremor with a hind-limb splay defect as determined by twice-weekly neurological scoring from 60 days of age. However, Rossi et al. (2008), defined disease onset as

peak body weight from measurements taken weekly. The different methods applied for determining disease onset may account, in part, for the discrepancy between the findings of these two studies. Whilst the weight of the mice in this study was monitored daily, it was not used as an indicator of disease onset, mainly because we do not see significant weight decline in this model up to 90 days of age. In addition, the peak weight of individual mice would be extremely hard to narrow down to a single day or even a week due to normal fluctuations in weight. For example, the weight of a mouse would often drop for a week or so before returning to its original weight a week later. For this reason, peak weight was deemed too variable a parameter to define disease onset. Especially when considering that factors like the oestrus cycle and the consistency of the time that the measurement is taken each day could all impact the weight of the mouse without having any relation to its disease state.

It has previously been shown that monitoring the neurological score of *SOD1<sup>G93A</sup>* mice to determine onset of visible signs of disease results in low intra-study variability as shown by low coefficient of variations, ranging from 3.8% - 6.9% (Mead et al. 2011). In this study the coefficient of variation for the onset data ranged from 2% - 3.8%, which is well within the range observed within previous *SOD1<sup>G93A</sup>* mouse studies (Mead et al. 2011). Keeping the same individual responsible for scoring the mice throughout this study was the main way of ensuring minimal variability was observed for the onset data.

In cage fastrac running wheels monitored the voluntary running behaviour of each mouse every day. Whilst an overall significant difference was observed between dose groups for total time and total distance ran per night, the variability of the data resulted in there being no detectable difference between dose-groups at any individual time-point. Despite the average speed of the mice dosed with 3mg/kg HTL0014242 being significantly faster than the mice dosed with 10mg/kg HTL0014242 at various time points throughout the disease course, the relevance of this finding is somewhat dubious. Considering this was an isolated finding observed for only one of the running wheel parameters it is unlikely to correspond to an improved motor function as a direct consequence of dosing with 3mg/kg HTL0014242. This is especially the case when considering that there was only an effect observed for the 3mg/kg HTL0014242 dose group in the absence of a dose-response effect.

The advantage of using fastrac running wheels to monitor motor function is that they measure the voluntary motor activity of mice, giving an indication of their habitual activity (Bennett et al. 2014). Whilst it could be argued that this is more realistic of

their normal motor behaviour, a limitation with using this method as a readout of their motor function was that some mice were inconsistent with their use of the running wheels throughout the study. It is thought that daily oral dosing was a contributing factor to the highly variable data observed across the running wheel parameters from this study. For example, the previous studies using fastrac running wheels were either non-dosed observational studies or the mice were dosed in drinking water (Bennett et al. 2014).

In contrast, rotarod testing measures forced activity of the mice to monitor changes in their motor function. Rotarod performed once a week from 5 weeks of age demonstrated an overall treatment effect for HTL0014242 dosed mice. Whilst there was no dose-response effect observed, the mice dosed with HTL0014242 performed better on rotarod than the vehicle dosed mice (Figure 5.4a). However, multiple comparisons analysis demonstrated that there was no significant difference in rotarod performance between the dose groups at any of the time points. Interestingly, at 12 weeks there is a reduction in rotarod performance of the vehicle dosed mice compared to the HTL0014242 dosed mice (Figure 5.4a). This could indicate that HTL0014242 has a greater effect on motor function at later stages of the disease. It would be interesting to follow this up to see if HTL0014242 has more of an effect on rotarod performance from 12 weeks onwards.

It has previously been shown that time taken to reach a 20% decline in rotarod performance is associated with less variability than measuring latency to fall (Mead et al. 2011). Despite a trend for the vehicle dosed mice to reach a 20% decline in rotarod performance before the HTL0014242 dosed mice, there was no overall significant difference between the dose groups (Figure 5.4b). This could imply that dosing with HTL0014242 does not influence early stages of the disease.

A shortfall of this study was that it was statistically powered to use parameters measured by fastrac running wheels as the main readout of motor function, which requires fewer mice per group than if the study was powered for rotarod. To detect a 1 week extension in time taken to reach a 20% decline in rotarod performance, 14 mice per group are required (Mead et al. 2011). Consequently, this study which was powered for fastrac running wheel readouts was underpowered for rotarod as a readout of motor function. Unfortunately, the mice did not perform as well as expected on fastrac running wheels and the data generated from rotarod is inconclusive and therefore it must be interpreted with caution.

Notably, the study by Rossi et al. (2008), did not measure motor function of the mice directly. Instead they used reduction in weight from peak body weight as an indirect measure of decline in motor performance. Whilst this may give some indication of the preserved motor units following muscle atrophy, it does not account for subtle differences in motor unit function that are observed using fastrac running wheels and rotarod. For example, rotarod is particularly sensitive for detecting early behavioural changes that take place prior to the classical signs of disease onset (Mead et al. 2011). Notably, an initial decline in rotarod performance early on in this disease model is observed before classical disease onset and correlates extremely well with the early denervation and reinnervation, described previously in this model (S Pun et al. 2006).

Interestingly, the weight data collected for this study seem to suggest that dosing with HTL0014242 is associated with some weight loss. Whilst, the weights of the mice in the HTL0014242 and vehicle dose groups were comparable at 25 days of age, subsequent dosing with HTL0014242 resulted in a small but significant reduction in weight compared with the vehicle dosed mice. This was observed across all HTL0014242 dose groups at various time points throughout the disease. Despite this finding, the weights of the HTL0014242 dosed mice were only significantly different from the vehicle dosed mice, up to 75 days of age. From 75 days onwards, there was no significant difference between the weights of the mice in any of the dose groups. This suggests that dosing with HTL0014242 throughout the initial pre-onset stage of the disease negatively affects the weight of the mice.

Catwalk gait analysis at 84 days of age demonstrated that both forelimb and hindlimb stride lengths of the mice in the 10mg/kg HTL0014242 dose group were significantly shorter than the 3mg/kg and 30mg/kg HTL0014242 dose groups. However, no other differences were observed between the groups for percentage time spent on three paws or diagonal paws. If there was anything substantially different going on between the different HTL0014242 dose groups, the same trend would be expected across multiple catwalk parameters. However, this was not the case and the findings from the catwalk parameters would suggest that there were no obvious differences between the gait of HTL0014242 and vehicle dosed mice, at 84 days of age. This is perhaps not very surprising considering that the 84-day time point is relatively soon after onset of disease and dosing with HTL0014242 did not demonstrate a delay in the onset of visible signs of disease.

### 5.3.2 Glial staining in ventral horns of lumbar spinal cord sections collected from dose-response study at 90 days

Despite mild effects on motor function, there was a significant dose-related reduction in GFAP staining in ventral horns of 90D lumbar SC from HTL0014242 dosed mice. Given that only a mild effect was observed on rotarod performance following dosing with HTL0014242 and no dose response, it was a surprise to see such a profound reduction in astrocyte activation (as shown by GFAP staining area). This may suggest that astrocyte activation does not significantly contribute in a negative way to motor system degeneration, up to 90 days in the *SOD1<sup>G93A</sup>* mouse model of MND. This is consistent with the idea that mutant *SOD1* mediated glial toxicity drives later stages of disease progression, for which there is substantial evidence in the literature. For example, whilst mutant *SOD1* expression in motor neurons has been shown to trigger disease onset, mutant *SOD1* expression in astrocytes and microglial cells has been shown to drive disease progression after disease onset (Boillee et al. 2006a; Yamanaka et al. 2008). Therefore, it is conceivable that dosing with HTL0014242 from 75 days of age onwards, following the average age of onset of visible signs of disease, may confer a more beneficial effect in terms of reducing motor neuron degeneration in the *SOD1<sup>G93A</sup>* mouse model of MND.

A reduction in Iba1 staining in the ventral horns of 90D lumbar SC sections was also observed in the HTL0014242 dosed mice. It was not quite as profound an effect as seen for astrocyte activation, but there was significantly less Iba1 staining in the 30mg/kg HTL0014242 dose group versus the vehicle dose group. This indicates that only the higher dose of HTL0014242 was sufficient to significantly reduce microglial activation (as shown by Iba1 staining area). It has been reported that activated astrocytes can trigger and amplify microglial activation and vice versa demonstrating that these glial cells communicate in a bidirectional manner (Yamanaka et al. 2008; Liddelow et al. 2017a). If astrocyte activation is implicated in driving microglial activation it is perhaps not that surprising that only when astrocyte activation is most reduced as a result of dosing with 30mg/kg HTL0014242 that this translates into a reduction in microglial activation. Furthermore, whilst astrogliosis is mediated by pre-existing resident astrocytes and changes in their expression of proteins (for example an up-regulation of GFAP), microgliosis is mediated by the proliferation of resident microglia (Bruijn et al. 1997; Philips & Rothstein 2014). Consequently, it is possible that GFAP is a more sensitive marker of astrogliosis than Iba1 is of microgliosis.

Previously it has been suggested that inhibiting astrocytic mGlu<sub>5</sub> activity has a beneficial effect on slowing disease progression and extending survival in the *SOD1<sup>G93A</sup>* mouse model of MND. Whilst reducing mGlu<sub>5</sub> activity did indeed seem to have a modest beneficial effect, it is not convincing that this effect was mediated by astrocytic mGlu<sub>5</sub> (Rossi et al. 2008). Rossi et al. (2008) ascribed the beneficial effects of dosing with MPEP *in vitro* to inhibiting mGlu<sub>5</sub> receptors on primary astrocytes cultured from spinal cords of *SOD1<sup>G93A</sup>* mice. However, these primary astrocyte cultures were prepared from new born *SOD1<sup>G93A</sup>* mice. It has been previously shown that mGlu<sub>5</sub> is developmentally regulated and whilst it is expressed on murine astrocytes up to post-natal week 3, evidence suggests it is not expressed on adult astrocytes (W. Sun et al. 2013). In support of this, mGlu<sub>5</sub> expression was not colocalised on spinal cord astrocytes at 90 days of age in our *SOD1<sup>G93A</sup>* mouse model of MND (see Chapter 3). If mGlu<sub>5</sub> is not expressed on astrocytes, then an obvious question is why does inhibiting mGlu<sub>5</sub> activity reduce astrocyte activation? In our *SOD1<sup>G93A</sup>* mouse model, mGlu<sub>5</sub> was found to be expressed on some spinal cord motor neurons at 90 days of age. Evidence suggests that there is a bidirectional cross-talk between motor neurons and glial cells and therefore it is conceivable that blocking neuronal mGlu<sub>5</sub> activity could in turn reduce glial activation (Araque et al. 1999; Verkhratsky et al. 1998). One possible mechanism might be through inhibiting downstream signalling cascades mediated by excessive levels of synaptic glutamate interacting with and activating neuronal mGlu<sub>5</sub> receptors.

It is worth noting that the comparison of GFAP and Iba1 staining was carried out on a relatively low number of mice per dose group. For example, the vehicle dose group comprised of two mice, the 3mg/kg and 30mg/kg HTL0014242 dose groups comprised of three mice and the 10mg/kg HTL0014242 dose group comprised of 5 mice. Unfortunately, there were limited SC sections that were of a good enough quality for use in comparing GFAP and Iba1 staining. Indeed, whilst the result was very interesting, further experiments are needed to validate this finding. Of note, a recent study by Bonifacino et al. (2017) found that heterozygous knockdown of mGlu<sub>5</sub> reduced both astrocyte and microglia activation in *SOD1<sup>G93A</sup>* mice. This finding provides additional support for mGlu<sub>5</sub> activity playing a role in mediating glial activation.

### **5.3.3 [<sup>3</sup>H] M-MPEP binding assay to measure RO of mGlu<sub>5</sub> receptors by HTL0014242 in mouse brain collected from dose-response study at 90 days**

Radioligand binding experiments were used to measure RO in brain tissue collected at peak and trough HTL0014242 exposures for the 3, 10 and 30mg/kg HTL0014242 dose groups. The mean proportion of mGlu<sub>5</sub> receptors occupied in brain at peak HTL0014242 exposure varied from ~63% for the 3mg/kg dose to ~93% for both the 10mg/kg and 30mg/kg doses. This confirms target engagement at all doses of HTL0014242 and validates the use of HTL0014242 at 3, 10 and 30mg/kg to probe the efficacy of blocking mGlu<sub>5</sub> in the *SOD1<sup>G93A</sup>* mouse model of MND.

The mean proportion of mGlu<sub>5</sub> receptors occupied in brain at trough HTL0014242 exposure was 0% for the 3mg/kg dose group, ~43% for the 10mg/kg dose group and ~92% for the 30mg/kg dose group. This demonstrates that when the dose of HTL0014242 is increased, the change in the peak to trough ratio is lost. It is possible that this is a result of HTL0014242 having poor solubility which is perhaps exacerbated at higher exposure to the compound. Whilst there was a lot of variability observed for the 10mg/kg HTL0014242 mean RO value at trough, the 30mg/kg HTL0014242 mean RO value was much less variable at trough.

HTL0014242 dosed at 30mg/kg resulted in over 90% RO in brain, at both peak and trough exposures. Considering over 90% of mGlu<sub>5</sub> receptors were occupied in brain at a dose of 30mg/kg HTL0014242, it is clear that whilst blocking mGlu<sub>5</sub> activity from 25 days of age through to 90 days of age perhaps has a small effect on motor function (as shown by rotarod performance), this does not delay onset of visible signs of disease in the *SOD1<sup>G93A</sup>* mouse model of MND. In contrast, blocking mGlu<sub>5</sub> activity had a profoundly significant effect on astrocyte activation, in 90 day SC. In addition, the RO data at 3, 10 and 30mg/kg of HTL0014242 correlates well with the trend for a dose-dependent reduction in astrocyte activation. However, only at the highest dose of HTL0014242 (30mg/kg), whereby over 90% of the mGlu<sub>5</sub> receptors were occupied, was there a significant reduction in microglial activation. Unfortunately, the MPEP study carried out by Rossi et al. (2008), did not include any data on RO and therefore it is not possible to compare the data on target engagement generated for the 90D dose-response study.

#### **5.3.4 90D study in the *SOD1<sup>G93A</sup>* mice to compare the difference in ventral horn glial staining of mice dosed with HTL0014242 and riluzole versus riluzole alone**

*SOD1<sup>G93A</sup>* mice were dosed with riluzole in combination, with and without, HTL0014242 to investigate the effect of riluzole on astrocyte and microglial activation in the ventral horns of 90D lumbar SC sections. HTL0014242 was dosed at 30mg/kg as this was the only dose that a significant reduction in microglial activation was observed in the previous 90D dose-response study.

When riluzole was dosed with HTL0014242, a significant reduction in GFAP staining area and GFAP staining index was observed in mouse SC ventral horns. This finding supports previous observations from the 90D dose-response study whereby dosing with HTL0014242 significantly reduced astrocyte activation. Interestingly, riluzole alone did not have any effect on astrocyte activation. The GFAP staining area and staining index in the ventral horns of riluzole dosed mice were comparable to that of vehicle dosed mice. This suggests that riluzole does not exert its therapeutic effect by reducing astrocyte activation in SC ventral horns of *SOD1<sup>G93A</sup>* mice up to 90 days of age.

The Iba1 staining area in ventral horns of mice dosed with riluzole and HTL0014242 was significantly reduced. However, Iba1 staining area was not reduced in the ventral horns of riluzole only dosed mice and instead was comparable to that of vehicle dosed mice. Interestingly, the Iba1 staining index (which considers the staining intensity of the antibody as well as the area of staining), was significantly reduced in the ventral horns of mice dosed with both riluzole in combination with HTL0014242 and mice dosed with riluzole only. These results consolidate previous findings from the 90D dose-response study that HTL0014242 dosed at 30mg/kg, significantly reduces microglial activation in mouse SC ventral horns. Furthermore, whilst Iba1 staining index was reduced in riluzole dosed mice, this was not consolidated by the results for Iba1 staining area which is the typical measurement for microglial activation. Consequently, riluzole is not thought to reduce microglial activation in SC ventral horns of *SOD1<sup>G93A</sup>* mice at 90 days of age.

To summarise, HTL0014242 dosed at 3,10 and 30mg/kg demonstrated a small improvement on motor function (as seen on rotarod), up to 90 days in the *SOD1<sup>G93A</sup>* mouse model of MND. However, as there was no dose response effect and no overall significant difference between the groups for time taken to reach a 20% decline in rotarod performance, the data obtained for this parameter is deemed inconclusive.

Interestingly the motor performance of the vehicle dosed mice declined rapidly compared to that of the HTL0014242 dosed mice at 12 weeks of age. Therefore, it is conceivable that dosing with HTL0014242 may demonstrate greater efficacy on motor function at a later stage of the disease. All doses of HTL0014242 demonstrated a significant reduction in astrocyte activation in the ventral horns of mouse SC (as seen by GFAP staining). This suggests that mGlu<sub>5</sub> plays a role in astrocyte activation up to 90 days of age in the *SOD1<sup>G93A</sup>* mouse model of MND. In addition, the highest dose of HTL0014242 (30mg/kg) significantly reduced Iba1 staining in mouse ventral SC section at 90 days of age, suggesting that mGlu<sub>5</sub> may also be involved in microglial activation (see Table 5.2 for summary). Radioligand binding experiments demonstrated a good range of mGlu<sub>5</sub> RO in brain across all doses of HTL0014242. Interestingly, the RO for the 3,10 and 30mg/kg doses at peak exposure of HTL0014242 correlated well with the dose-dependent reduction in astrocyte activation suggesting this is a key marker of HTL0014242 effect in the CNS. Investigations into the effect of riluzole on glial activation found that riluzole dosed at ~70mg/kg in drinking water did not reduce glial activation in the ventral horns of *SOD1<sup>G93A</sup>* mouse SC up to 90 days of age. Despite this, it was clear that dosing riluzole in combination with HTL0014242 demonstrated a profound reduction of glial activation. These findings would suggest that riluzole and HTL0014242 have different mechanisms of action and co-dosing in a clinical context may lead to a synergistic benefit.

Finally, whilst dosing with HTL0014242 demonstrated a profound reduction in glial activation, this did not translate into a substantial effect on motor function up to 90 days of age in the *SOD1<sup>G93A</sup>* mouse model of MND. However, this finding is consistent with reports that mutant *SOD1* glial toxicity drives later stages of disease progression (Boillee et al. 2006a; Yamanaka et al. 2008). Therefore, it would be interesting to see if dosing HTL0014242 at a later stage of the *SOD1<sup>G93A</sup>* disease trajectory, demonstrates a greater improvement of motor function.

**Table 5.2. Summary of the key 90D dose-response study readouts**

90D Dose-Response Readouts	Vehicle Control	3mg/kg HTL0014242 (62.9 - 0% RO)	10mg/kg HTL0014242 (93.5 - 42.9% RO)	30mg/kg HTL0014242 (93.7- 91.9% RO)
Delayed onset of visible signs of disease	×	×	×	×
Improvement in motor function as seen on rotarod	×	INC	INC	INC
Reduction in GFAP staining at 90 days in SC	×	✓	✓	✓
Reduction in Iba1 staining at 90 days in SC	×	×	×	✓

INC: Inconclusive

## 6 Early vs late dosing of HTL0014242 through to end-stage disease in the *SOD1*<sup>G93A</sup> mouse model of MND

### 6.1 Introduction

The 90D dose-response study demonstrated that oral dosing with 3, 10 and 30mg/kg of HTL0014242 had a profound effect on reducing astrocyte activation in the ventral horns of lumbar SC sections, collected at 90 days of age. In addition, the highest dose of HTL0014242 (30mg/kg) resulted in a significant microglial reduction in ventral SC sections. However, these reductions in glial activation culminated in a somewhat modest improvement in motor function (as shown on rotarod), up to 90 days in the *SOD1*<sup>G93A</sup> mouse model of MND. With a wide body of evidence in the literature supporting a role for mutant *SOD1* expressing astrocytes and microglial cells driving later stages of disease progression and duration (Boillee et al. 2006a; Yamanaka et al. 2008; Wang et al. 2009; Wang et al. 2011b), an *in vivo* study was designed to investigate the therapeutic potential of dosing with HTL0014242 through to end-stage disease in the *SOD1*<sup>G93A</sup> mouse model of MND. A dose of 30mg/kg HTL0014242 was selected for the survival study as this dose demonstrated the highest mGlu<sub>5</sub> RO in brain over a 24h period (> 90% RO at both peak and trough HTL0014242 exposures). In addition, this was the only dose that demonstrated both reduced astrocyte and microglial activation in SC at 90 days of age. To identify the optimal time to commence dosing throughout the *SOD1*<sup>G93A</sup> disease trajectory, a cohort of mice were dosed with 30mg/kg HTL0014242 from 25 days of age, 25D cohort, (to replicate the previous study starting point) and an additional cohort of mice were dosed with 30mg/kg HTL0014242 from 75 days of age, 75D cohort. By having one cohort of mice dosed before onset of visible signs of disease (25D cohort) and a second cohort of mice dosed from around the time of visible signs of disease onset (75D cohort), it would be possible to determine if the efficacy of HTL0014242 is time-dependent. It is somewhat unfeasible to treat MND patients with a therapeutic drug before they are diagnosed with the disease (especially considering that most cases are sporadic). By dosing a cohort of mice from 75 days onwards, any efficacy observed for this group may be a more realistic predictor of the efficacy observed if patients were dosed with HTL0014242 following diagnosis and therefore post onset of disease.

Furthermore, it has been shown previously that whilst mutant *SOD1* expression in motor neurons is key for initiating disease onset, its expression in astrocytes and microglial cells drive later stages of disease progression (Boillee et al. 2006a; Yamanaka et al. 2008). In light of this evidence, it is conceivable that the effects of dosing HTL0014242 may be more profound in terms of reducing glial activation and delaying disease progression of MND when dosing is commenced at a later stage of disease (post-onset of visible signs of disease). The average age at onset of visible signs of disease in the *SOD1*<sup>G93A</sup> mouse model is ~75 days of age. Therefore, whilst the mice in the 25D cohort will demonstrate the effect of reducing glial activation early in the disease trajectory (before the classical signs of disease onset), the 75D cohort will demonstrate the effect of reducing glial activation at a later stage of the disease (from around the time of visible signs of disease onset onwards). By having a 25D cohort and a 75D cohort it will be possible to identify the differential efficacy from reducing glial activation pre-onset versus post-onset of disease in the *SOD1*<sup>G93A</sup> mouse model of MND.

The effect of dosing HTL0014242 at 30mg/kg from 25 days of age versus 75 days of age on *SOD1*<sup>G93A</sup> motor function was monitored by rotarod tests conducted twice per week from 5 weeks of age. Of note, rotarod testing was chosen as the main readout of motor function as the previous 90D dose-response study demonstrated that in-cage fastrac running wheel data was highly variable when mice were dosed daily. Neurological scoring took place three times a week from 60 days of age to determine the age at onset of visible signs of disease. Also, catwalk gait analysis was carried out at 70, 84, 98 and 112 days of age to monitor changes in several gait parameters of the mice throughout the disease trajectory.

At 90 days of age spinal cord (SC) tissue was collected from 6 mice per dose group to determine the effect of HTL0014242 on pathologic markers of disease progression, such as glial activation in the ventral horns of lumbar SC. From this, it was possible to determine whether the previous findings from the 90D dose response study, whereby dosing with 30mg/kg HTL0014242 reduced glial activation, could be consolidated by the 25D cohort mice in this study. It was also interesting to compare glial staining in ventral horns of the 25D cohort versus that of the 75D cohort to see whether dosing from 75 days of age also resulted in a similar reduction of glial activation in SC. In addition, the ventral horns were ChAT stained throughout the lumbar region of the SC to quantify the number of remaining motor neurons at 90 days of age for each of the dose groups. This gave an indication of preserved motor function at an intermediate stage of the disease. Additional staining for mGlu<sub>5</sub> and the

motor neuronal marker, ChAT, took place in the ventral horns of 90-day lumbar SC. It was previously shown in Chapter 3 that mGlu<sub>5</sub> is co-expressed on motor neurons found in the ventral horns of *SOD1<sup>G93A</sup>* lumbar SC sections at 90 days of age. It was interesting to note whether reducing mGlu<sub>5</sub> activity with HTL0014242 from both 25 days of age and 75 days of age had any effect on mGlu<sub>5</sub> or ChAT expression in the ventral horns of lumbar SC.

During the end-stage of the disease (125 days of age onwards), mice were distress scored daily and tested for righting reflex to determine their humane end-point. The time taken to reach the humane end-point (inability to right from prone position within 10 seconds or  $\geq 30\%$  weight loss for 72h) was recorded for mice in each of the dose groups to determine if there was any difference in mean survival. At the end of the study (end-stage), tissue was collected from 8 mice in each of the dose groups at peak and trough exposures of HTL0014242 for bioanalysis of total and unbound concentrations of HTL0014242 in brain and spinal cord.

Brain tissue was also collected at end-stage from 8 mice per dose group, 4 mice at peak and 4 mice at trough HTL0014242 exposure. From this, mGlu<sub>5</sub> RO for both the 25D cohort and the 75D cohort was determined to give an indication of mGlu<sub>5</sub> target engagement in brain at the end-stage of disease. Comparing the proportion of mGlu<sub>5</sub> receptors that were occupied by HTL0014242 in 90-day old brain collected from the 90D dose response study with that in end-stage brain from the survival study demonstrated whether mGlu<sub>5</sub> target engagement was altered by chronic dosing.

Finally, SC tissue was collected from 6 mice per dose group at end-stage for histology. The ventral horns of lumbar spinal cord were stained with markers of glial activation such as GFAP and Iba1. From this, the effect of HTL0014242 on glial activation could be compared at end-stage versus 90 days of age. End-stage ventral horns were also ChAT stained throughout the lumbar region of the SC to quantify the number of remaining motor neurons. This served as an indication of preserved motor function at the end of the disease and was compared to the number of preserved motor neurons at 90 days of age. It was interesting to compare how markers of MND disease pathology changed throughout the *SOD1<sup>G93A</sup>* disease trajectory in the 25D cohort versus the 75D cohort.

## 6.2 Results

### 6.2.1 Pre-onset vs post-onset dosing of HTL0014242 up to end-stage in the *SOD1<sup>G93A</sup>* mouse model of MND

An *in vivo* survival study was designed to investigate the therapeutic potential of dosing HTL0014242 at 30mg/kg from both 25 days of age (25D cohort) and 75 days of age (75D cohort) through to end-stage of the disease in the *SOD1<sup>G93A</sup>* mouse model of MND (~140 days of age). In addition, a vehicle control group of mice were orally dosed with 0.5% methylcellulose at 10ml/kg per day, from 25 days of age onwards. Statistical power analysis demonstrated that a group size of 20 mice per dose group was needed for this survival study (see 2.2.5.3 HTL0014242 Survival Study Design). Of the 20 mice per group, 14 mice per group were necessary to detect a 10-day extension in time taken to reach a 20% decline in rotarod performance and the remaining 6 mice per group were sacrificed at 90 days of age to compare markers of disease pathology (GFAP and Iba1), in the ventral horns of lumbar spinal cord sections. Not only would this serve to consolidate that dosing with HTL0014242 at an early stage of the disease (25D cohort) reduces glial activation in ventral horns of 90D lumbar SC sections, but also to investigate whether dosing with HTL0014242 at a later stage of the disease (75D cohort), has the same effect on glial activation in 90D SC.

Neurological scoring (see section 2.2.6.1 Neurological Scoring and Distress Scoring for details on scoring system) took place three times a week from 60 days of age to determine classical signs of disease onset (hind-limb tremor in combination with hind-limb splay defect). The first of two consecutive onset scores was used to determine the age of onset of visible signs of disease for each mouse. Figure 6.1 shows that the 75D cohort had a significantly delayed onset of visible signs of disease compared to the vehicle and 25D cohorts, as shown by one-way ANOVA ( $p = < 0.0001$ ). Whilst average age of onset for the vehicle and 25D cohort were 76.5 days and 76.9 days respectively, average onset of the 75D cohort was 80.6 days.

Onset of visible signs of disease was determined from the neurological scoring data which commenced at 60 days of age for both the vehicle and 25D cohort groups. However neurological scoring commenced from 75 days of age for the 75D cohort and consequently the onset of visible signs of disease of some of the mice in this group could potentially have been missed. To take account of this, onset of visible signs of disease was analysed using only the neurological scores obtained from 75 days of age onwards for all the dose groups. This was to ensure that the onset data

for the vehicle and 25D cohort were normalised to that of the 75D cohort. Looking at the distribution of the onset data for each dose group, there is much less variability in both the vehicle and 25D cohort dose groups compared with the 75D cohort. Notably, the spread of the data for the 75D cohort is skewed more towards a later age of disease onset than for the other two dose-groups. Furthermore, the onset data for the vehicle group shows that up to 5 mice may have had onset prior to 75 days of age, compared with only 2 mice in both the 25D cohort and in the 75D cohort. This suggests that the age at onset of visible signs of disease for most of the mice in each of the dose groups was at 75 days of age onwards.

Forced motor function was monitored twice a week from 5 weeks of age by measuring rotarod performance. Figure 6.2 demonstrates that there was an overall significant difference in latency to fall in seconds, between dose groups (as shown by two-way ANOVA,  $p = <0.0001$ ). Multiple comparisons analysis showed that the 75D cohort performed significantly better on rotarod than both the vehicle dose-group and 25D cohort at various stages throughout the disease trajectory. For example, between 10.5 – 12 weeks and at 17-18.5 weeks the 75D cohort performed significantly better than both the vehicle and 25D cohort groups ( $p = <0.05 - <0.0001$ ). There was also a significant difference between the performance of the 75D cohort and the vehicle group at 16-16.5 weeks and at 19 weeks ( $p = <0.05 - <0.01$ ). The data from this rotarod parameter shows that dosing with HTL0014242 from 75 days of age seems to have a biphasic effect on motor function, with the mice performing significantly better at both intermediate and late stages of the disease.

As rotarod testing commenced at 75 days of age for the 75D cohort mice it was not possible to compare the time taken to reach a 20% decline in rotarod performance for the 75D cohort versus the vehicle group and 25D cohort. However, Figure 6.3 demonstrates that there was no significant difference between the vehicle and 25D cohort mice for this parameter (as shown by Student's t-test,  $p = 0.981$ ). Notably, the data obtained for this rotarod measure were comparable to those observed for the vehicle and 30mg/kg HTL0014242 dose groups from the 90D dose-response study (Figure 5.4c). In keeping with previous findings, the coefficient of variations were within the range observed for historical data (Mead et al. 2011). In addition, the coefficient of variations were comparable between the 90D dose response study and survival study (Figure 5.4c and Figure 6.3b).

An observation from this survival study was that mice from the 75D cohort seemed to retain their motor function for longer compared to the mice from the other dose-

groups. To probe this observation with a quantifiable measure, the proportion of mice that reached a score of 0 on rotarod was plotted for each of the mice in all dose groups (Figure 6.4a). Kaplan-Meier curves demonstrated that the median time taken to reach a score of 0 on rotarod was significantly different between dose groups, as shown by the Mantel-Cox logrank test (18 weeks for the vehicle and 25D cohort and 21 weeks for the 75D cohort,  $p = <0.0001$ ). This was investigated further by pairwise comparisons of the individual curves which demonstrated that the 75D cohort curve was significantly different from both the vehicle and 25D cohort curves ( $p = 0.0001$ , Bonferroni correction was applied giving an adjusted threshold  $p$  value of  $\leq 0.017$ ).

In addition, the time to reach a rotarod score of 0 was plotted for each of the mice in all three dose groups (Figure 6.4b). The data show that the 75D cohort mice took significantly longer to reach a score of 0 on rotarod compared to the vehicle and 25D cohort mice, as shown by one-way ANOVA ( $p = < 0.0001$ ). Whilst the mean time to reach a score of 0 on rotarod for the vehicle and 25 cohort groups were  $17.8 \pm 0.9$  weeks and  $18.5 \pm 0.9$  weeks respectively, for the 75D cohort group it was  $20.9 \pm 1.6$  weeks. This finding shows that the vehicle and 25D cohort mice lose their ability to perform on rotarod much sooner than the 75D cohort mice.

The weights of the mice were recorded daily and mean weight for each dose group throughout the disease trajectory is shown in Figure 6.5. The average weight of the mice was significantly different between dose groups, as shown by two-way ANOVA ( $p = <0.0001$ ). Figure 6.5 demonstrated that the mean weight of the mice in the 25D cohort was significantly less than that of both the vehicle group and 75D cohort at various time points throughout the disease trajectory. For example, multiple comparisons analysis demonstrated that the 25D cohort mice weighed significantly less than the vehicle dosed mice between 81- 84 and 91- 101 days of age and significantly less than the 75D cohort mice between 120-126 days of age ( $p = 0.05 - <0.01$ ). However, there was no significant difference between the vehicle dosed mice and the 75D cohort mice at any of the time points ( $p = >0.05$ ). Findings from the previous 90D dose-response study seemed to suggest that dosing with HTL0014242 caused weight loss. Interestingly, the weight data from this survival study suggest that whilst dosing with HTL0014242 from 25 days of age is associated with weight loss, dosing from 75 days of age is not.

Catwalk gait analysis was carried out at 70, 84, 98 and 112 days of age to measure several gait parameters of the mice throughout the *SOD1<sup>G93A</sup>* disease trajectory. As described before, the mice were placed at the end of a glass platform in darkness

and left to voluntarily traverse to the opposite side of the platform. The footprints of the mice were video captured for analysis using the catwalk software which calculated statistics related to features of their gait and locomotion. The catwalk parameters shown in Figure 6.6 are amongst the most informative for detecting differences between non-transgenic and *SOD1<sup>G93A</sup>* mice (Mead et al. 2011). Normally with disease progression, *SOD1<sup>G93A</sup>* mice spend more time on three paws and less time on diagonal paws to account for their progressive unsteadiness, giving them more stability (Mead et al. 2011). However, surprisingly this was not the case in the present study. For example, the vehicle mice did not show an increase in the use of the three-paw stepping pattern or a reduction in the use of the diagonal paw stepping pattern over time. In contrast to what was expected, the vehicle control mice demonstrated a mild improvement for both parameters, spending less time on three paws and more time on diagonal paws. Given that the observations for the vehicle control mice were not consistent with historical findings, caution must be applied when making conclusions for both the 25D cohort and 75D cohort mice based on these parameters. The only time point at which there was a significant difference between dose groups was at 84 days of age. Figure 6.6 (a-b) shows that the 25D cohort mice display a significant increase in the use of the three-paw stepping pattern and a significant reduction in the use of the diagonal stepping pattern, compared to the vehicle and 75D cohort mice at the 84D time point ( $p = 0.0093$  and  $p = 0.0041$ , respectively). This finding suggests that dosing HTL0014242 from 25 days onwards adversely affects motor coordination between 70 and 84 days of age. However, considering the observations for the vehicle control mice were unprecedented compared with historical data, caution should be exercised in interpreting these data.

Two additional catwalk parameters measured were forelimb and hindlimb stride lengths. Throughout the disease course, *SOD1<sup>G93A</sup>* mice typically demonstrate a decrease in both their forelimb and hindlimb stride lengths. Figure 6.6 (c-d) shows that overall there was a significant difference between dose groups for both forelimb and hindlimb average stride-lengths (as shown by two-way ANOVA,  $p = 0.0147$  and  $p = 0.0194$ , respectively). Further, multiple comparisons analysis demonstrated that the forelimb and hindlimb mean stride lengths were significantly longer for the 75D cohort compared to the vehicle group at the 70D time point and compared to the 25D cohort at the 84D time point ( $p = <0.05$ ). However, unexpectedly forelimb and hindlimb mean stride lengths of the vehicle control mice were shown to increase over time (Figure 6.6c-d). Similarly, this finding is not in line with historical observations for vehicle control mice (Mead et al. 2011). Consequently, it would be difficult to conclude

that any of the findings based on these catwalk parameters are robust. To conclude, the data obtained from catwalk gait analysis is inconclusive and will not be used to compare the motor coordination of mice from the different dose groups.

From 125 days onwards, mice were classed as having reached the end-stage of disease and were distress scored daily to determine whether they had reached the humane end-point. In addition, several other changes were made within the cages of the mice to help with their deteriorating mobility. Cages were lined with blue roll paper instead of saw-dust to aid locomotion, bedding was changed to consist of short strands to prevent mice from getting stuck and hard food pellets were substituted with pre-wetted powdered food. The humane-end-point was defined as a loss of righting reflex for >10 seconds or  $\geq 30\%$  weight loss for 72 hours. Figure 6.7a shows the age of the mice at humane end-point for each of the dose groups. There was no significant difference between the mean age at humane-end point for each dose group, as shown by one-way ANOVA ( $p = 0.2044$ ). The mean age at humane-end point was  $153 \pm 7.3$  days for the vehicle group,  $151 \pm 7.5$  days for the 25D cohort and  $157 \pm 11.5$  days for the 75D cohort. In addition, Kaplan-Meier survival curves were plotted for each of the dose groups (Figure 6.7b). Statistical analysis using the Mantel-Cox logrank test demonstrated that there was no significant difference between survival curves for each of the dose groups ( $p = < 0.0560$ ). Interestingly, there was a significant trend across the data for increased survival for the 75D cohort compared to the vehicle dose group and increased survival for the vehicle dose group compared to the 25D cohort, as shown by the logrank test for trend ( $p = < 0.0210$ ).

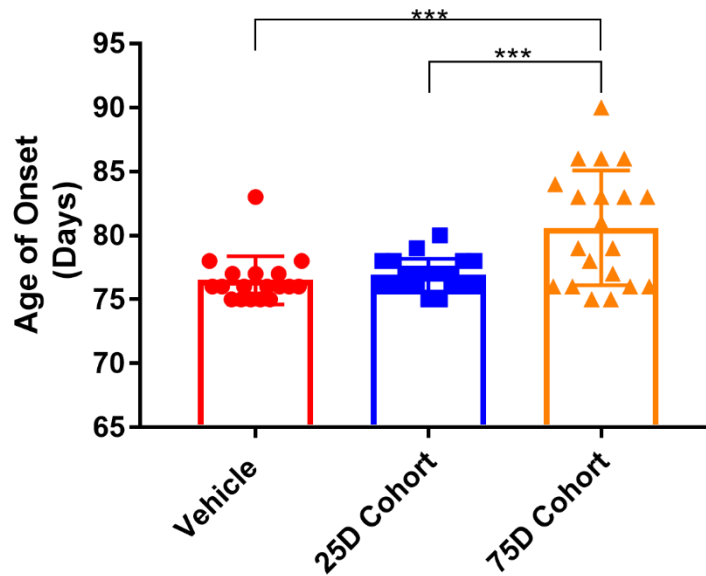


**Figure 6.1. Onset was significantly delayed for 75D cohort.** *SOD1<sup>G93A</sup>* mice were orally dosed with vehicle (0.5% methylcellulose in water), 30mg/kg HTL0014242 from 25 days of age (25D cohort) and 30mg/kg HTL0014242 from 75 days of age (75D cohort). Neurological scoring took place three times a week from 60 days of age to determine classical signs of disease onset. Onset was defined by hind-limb tremor in combination with a hind-limb splay defect. Mice were considered to have disease onset at the time of the first score of two consecutive onset recordings. The mean age of onset ( $\pm$ SD) was plotted for each dose group. The mean age of onset for the vehicle, 25D cohort and 75D cohort was 76.5, 76.9 and 80.6 days of age, respectively. Statistical analysis by one-way ANOVA and Tukey's post test showed that overall there was a significant difference between dose groups ( $p = <0.0001$ ). Further, multiple comparisons analysis demonstrated that disease onset for the 75D cohort was significantly later than that of both the vehicle and 25D cohort ( $p = 0.0002$  and  $p = 0.006$ , respectively). Data points represent individual animals (19-20 mice per group).

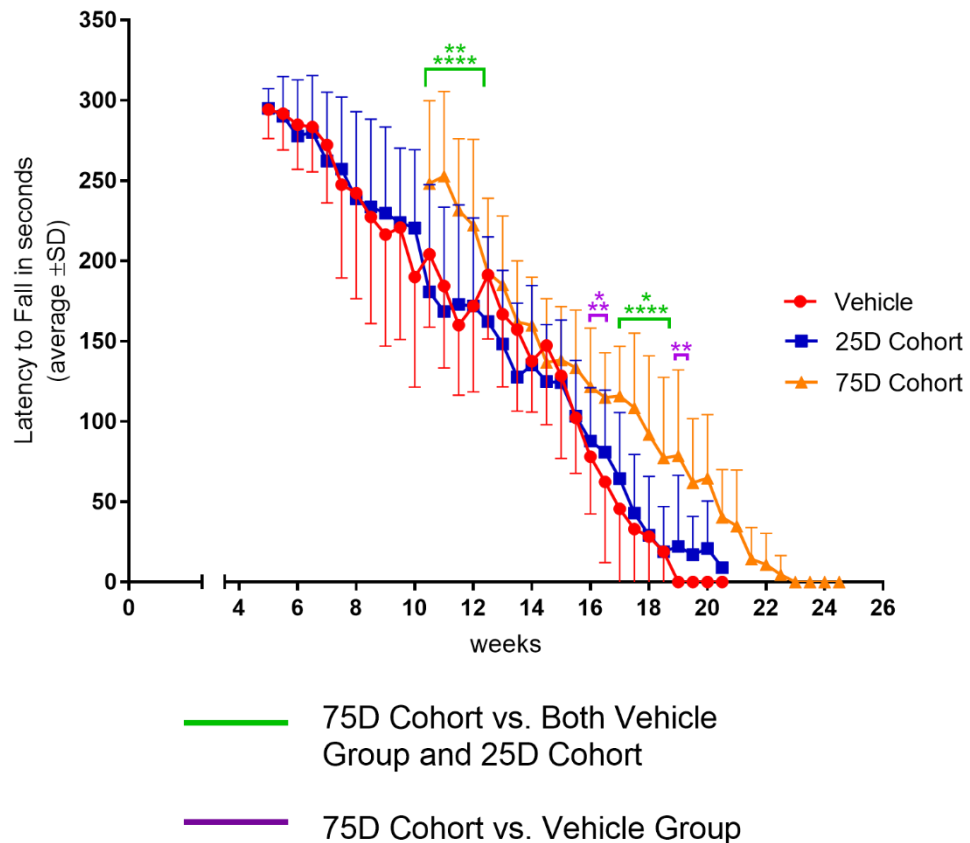
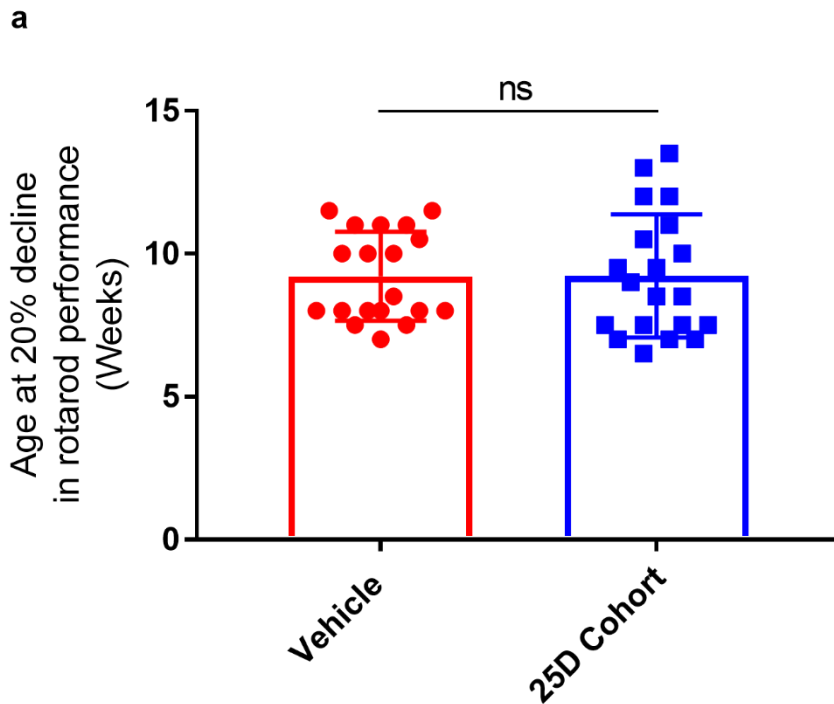


**Figure 6.2. The 75D cohort perform significantly better on rotarod than the vehicle group and 25D cohort at early and late stages of the disease.** *SOD1<sup>G93A</sup>* mice were orally dosed with vehicle (0.5% methylcellulose in water), 30mg/kg HTL0014242 from 25 days of age (25D cohort) and 30mg/kg HTL0014242 from 75 days of age (75D cohort). Rotarod tests were conducted twice a week from 5 weeks of age (statistical analysis performed on data collected between 10.5 – 20.5 weeks for all groups). The rotarod test consists of a rotating rod that accelerates from 4-40 rpm over the course of 300 seconds. All rotarod testing consisted of two attempts with the best score recorded for analysis. Mean latency to fall ( $\pm$  SD) was plotted for each mouse. Statistical analysis by two-way ANOVA and Tukey's post-test demonstrated an overall significant difference between dose groups ( $p = <0.0001$ ). Multiple comparisons analysis showed that the 75D cohort performed better on rotarod than both the vehicle group and the 25D cohort at 10.5 -12 weeks and at 17-18.5 weeks ( $p = <0.05 - <0.0001$ ). The 75D cohort performed better on rotarod than the vehicle group at 16 -16.5 weeks and again at 19 weeks ( $p = <0.05 - <0.01$ ). Data points represent individual animals (14 mice per group).



**b**

Group	Mean Age (Weeks)	Standard Deviation	Coefficient of variation
Vehicle	9.2	1.6	16.9
25D Cohort	9.2	2.2	23.9

**Figure 6.3. No difference in time taken to reach 20% decline in rotarod performance.** The mean age ( $\pm$ SD) for each mouse to reach a 20% decline in rotarod performance was also plotted (a). The mean age at which a 20% decline in rotarod performance was recorded for each dose group and is presented in the table (b). Statistical analysis demonstrated no significant difference between groups, as shown by student's t-test ( $p= 0.9811$ ). Data points represent individual animals (19-20 mice per group).

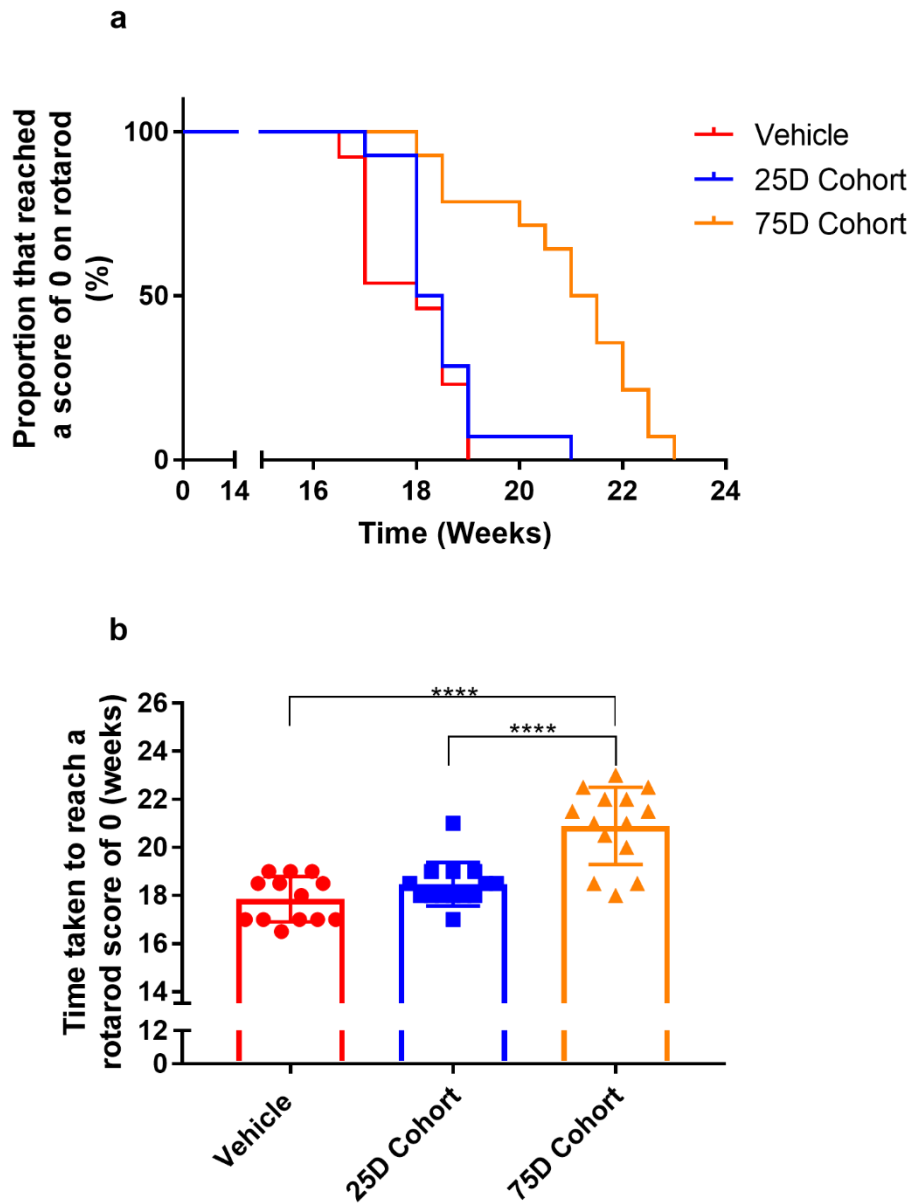


**Figure 6.4. 75D cohort retain motor function for longer.** *SOD1<sup>G93A</sup>* mice were orally dosed with vehicle (0.5% methylcellulose in water), 30mg/kg HTL0014242 from 25 days of age (25D cohort) and 30mg/kg HTL0014242 from 75 days of age (75D cohort). Time taken to reach a score of 0 on the rotarod test was plotted for the mice in each dose group (a-b). a) Statistical analysis demonstrated that the median time taken to reach a score of 0 on rotarod was significantly different between dose groups, as shown by the Mantel-Cox logrank test (18 weeks for the vehicle group and 25D cohort and 21 weeks for the 75D cohort,  $p = <0.0001$ ). There is also a significant trend across the data set, as shown by the logrank test for trend ( $p = < 0.0002$ ). In order to determine which curves are significantly different from each other a pairwise comparison of the three possible combinations was performed; 75D cohort vs vehicle

group ( $p = <0.0001$ ), 75D cohort vs 25D cohort ( $p = 0.0001$ ) and 25D cohort vs vehicle group ( $p = 0.305$ ). A Bonferroni correction was applied to these values giving an adjusted threshold  $p$  value of  $\leq 0.017$ . b) In addition, the time taken to reach a score of 0 on rotarod ( $\pm$ SD) was plotted for each dose group. The mean time taken to reach a score of 0 on rotarod for the vehicle, 25D cohort and 75D cohort were  $17.8\pm 0.9$ ,  $18.5\pm 0.9$  and  $20.9\pm 1.6$  weeks, respectively. Statistical analysis by one-way ANOVA and Tukey's post test showed that overall there was a significant difference between dose groups ( $p = <0.0001$ ). Further, multiple comparisons analysis demonstrated that the average time taken to reach a rotarod score of 0 for the 75D cohort was significantly later than that of both the vehicle and 25D cohort groups ( $p = <0.0001$ ). Data points represent individual animals (13-14 mice per group).

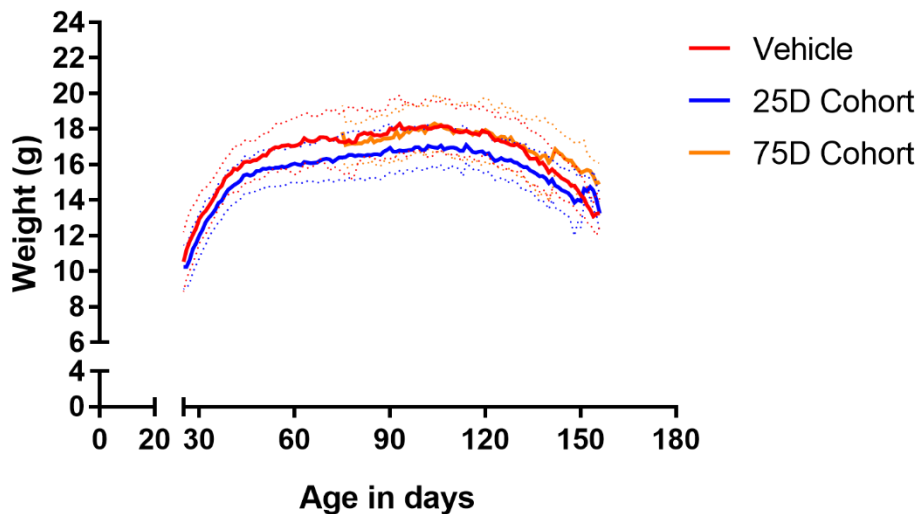


**Figure 6.5. HTL0014242 dosed from 25D is associated with weight loss.** *SOD1<sup>G93A</sup>* mice were orally dosed with vehicle (0.5% methylcellulose in water), 30mg/kg HTL0014242 from 25 days of age (25D cohort) and 30mg/kg HTL0014242 from 75 days of age (75D cohort). Mice were weighed daily prior to oral dosing. The weight for each mouse was plotted from 25 days onwards. Data presented as mean ( $\pm$  SD), 20 mice per group. Statistical analysis by two-way ANOVA and Tukey's post-test demonstrated a significant difference between dose groups ( $p = <0.0001$ ). Multiple comparisons analysis showed that the mean weight of the 25D cohort was significantly lower than the vehicle group between 81- 84 and 91-101 days of age and significantly reduced compared to the 75D cohort between 120- 126 days of age ( $p = < 0.05 - <0.01$ ). The mean weight of the vehicle group was not significantly different from that of the 75D cohort at any of the time points ( $p = > 0.05$ ).

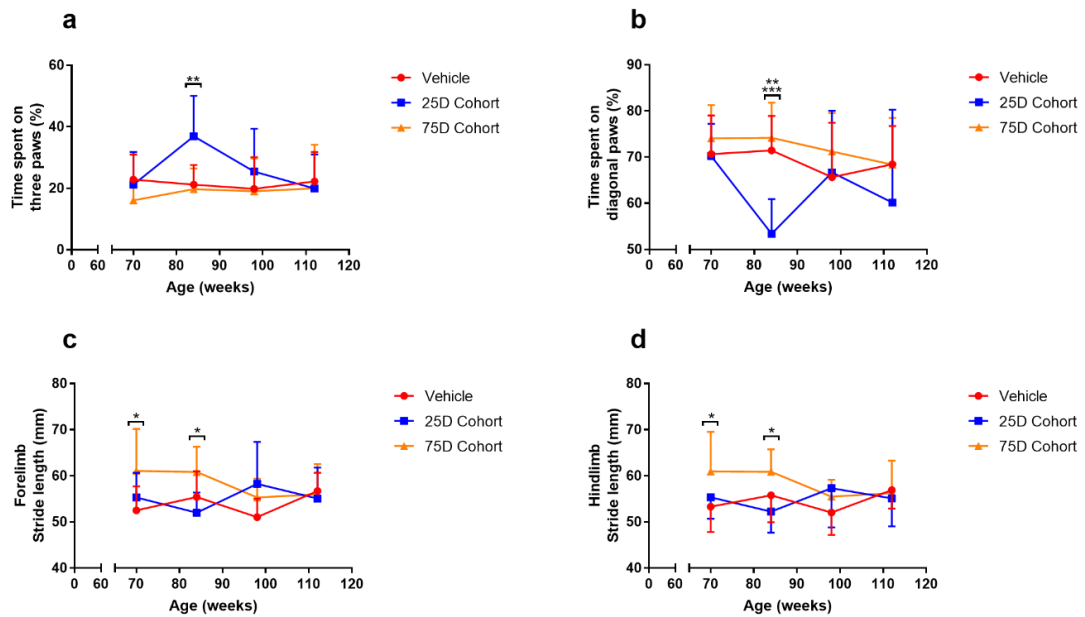


**Figure 6.6. Catwalk gait analysis across several parameters was inconclusive.**

*SOD1<sup>G93A</sup>* mice were orally dosed with vehicle (0.5% methylcellulose in water), 30mg/kg HTL0014242 from 25 days of age (25D cohort) and 30mg/kg HTL0014242 from 75 days of age (75D cohort). Catwalk gait analysis was performed at 70, 84, 98 and 112 days of age to monitor several aspects of their gait following video capture and manual segmentation of their step pattern. Percentage time spent on three paws and diagonal paws was plotted for each dose group (a and b, respectively). Statistical analysis by two-way ANOVA and Tukey's post-test demonstrated an overall significant difference between dose groups for both parameters,  $p = 0.0257$  (a) and  $p = 0.0019$  (b). Multiple comparisons analysis showed that the mean time spent on three paws was significantly longer for the 25D cohort compared to both the vehicle group and the 75D cohort, at 84 days of age, ( $p = 0.0093$  and  $p = 0.0041$ , respectively). Also, at 84 days of age, the mean time spent on diagonal paws was significantly shorter for the 25D cohort vs both the vehicle group and the 75D cohort ( $p = 0.0024$  and  $p = 0.0004$ , respectively).

Forelimb and hindlimb stride length were plotted for each dose group (c and d, respectively). Statistical analysis by two-way ANOVA and Tukey's post-test demonstrated an overall significant difference between groups for both forelimb and hindlimb stride length,  $p = 0.0147$  (c) and  $p = 0.0194$  (d). Multiple comparisons analysis showed that the mean forelimb and mean hindlimb stride lengths were significantly longer for the 75D cohort, compared to the vehicle group at 70 days of age and compared to the 25D cohort at 84 days of age ( $p < 0.05$ ). Data presented as mean ( $\pm$  SD), data points represent individual animals (8 mice per group).

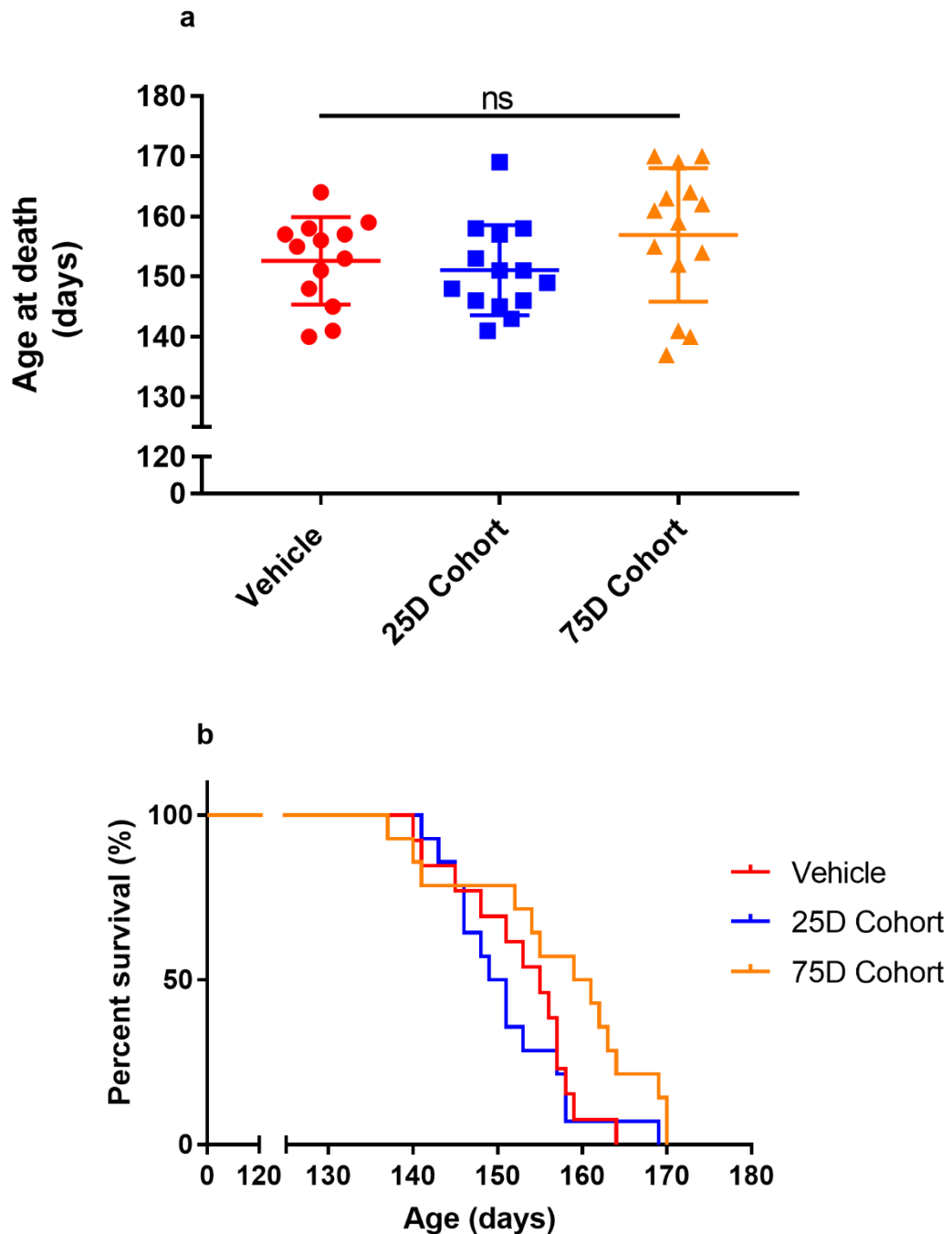


**Figure 6.7. Dosing with HTL0014242 has no effect on survival.** *SOD1<sup>G93A</sup>* mice were orally dosed with vehicle (0.5% methylcellulose in water), 30mg/kg HTL0014242 from 25 days of age (25D cohort) and 30mg/kg HTL0014242 from 75 days of age (75D cohort). Age at humane end point was plotted for the mice in each dose group (a). Statistical analysis by one-way ANOVA and Tukey's post-test demonstrated no overall significant difference between groups ( $p = 0.2044$ ). The mean survival was  $153 \pm 7.3$  days for the vehicle group,  $151 \pm 7.5$  days for the 25D cohort and  $157 \pm 11.5$

days for the 75D cohort. The percent survival was plotted for the mice in each dose group (b). The median survival was 155 days for the vehicle group, 150 days for the 25D cohort and 160 days for the 75D cohort. Statistical analysis using the Mantel-Cox logrank test demonstrated that the survival curves for the different dose groups are not significantly different ( $p = <0.0560$ ). There is a significant trend across the data set, as shown by the logrank test for trend ( $p = < 0.0210$ ). As these statistical tests do not give pairwise comparisons, the data were also compared in a pairwise fashion for all three possible combinations; 75D cohort vs vehicle group ( $p = 0.056$ ), 75D cohort vs 25D cohort ( $p = 0.034$ ) and 25D cohort vs vehicle group ( $p = 0.701$ ). A Bonferroni correction was applied to these values giving an adjusted threshold  $p$  value of  $\leq 0.017$ . Data points represent individual animals (13-14 mice per group).

### **6.2.2 Glial staining in ventral horns of lumbar spinal cord sections collected at 90D and end-stage from the survival study**

At 90 days of age tissue was collected from 6 mice per dose group and the ventral horns of lumbar SC sections were immuno-stained with the glial markers, anti-GFAP (Figure 6.8) and anti-Iba1 (Figure 6.9). SC tissue was also collected from 4 drug naive non-transgenic mice at 90 days of age for comparison of glial staining in the ventral horns. Interestingly, the 25D cohort and 75D cohort mice demonstrated a 71% and 68% reduction respectively, in GFAP staining area and a 76% and 80% reduction respectively, in GFAP staining index in their ventral horns versus the vehicle dosed mice (Figure 6.8a-b), as shown by one-way ANOVA ( $p = <0.0001$ ). Furthermore, there was a significant reduction in GFAP staining area (81%) and GFAP staining index (91%) in the ventral horns of the non-transgenic mice compared to that of vehicle control mice ( $p = <0.0001$ ). Whilst GFAP staining in the ventral horns of the non-transgenic mice was not significantly different from that of the 25D cohort and 75D cohort mice, there was less GFAP staining in the ventral horns of the non-transgenic mice compared to that of any other dose group.

Comparison of Iba1 staining in the ventral horns of lumbar SC sections revealed that there was a significant difference in Iba1 staining area and Iba1 staining index between the different dose groups, as shown by one-way ANOVA,  $p = <0.0001$  and  $p = 0.0003$ , respectively (Figure 6.9a-b). Whilst the reductions in Iba1 staining were not as profound as seen for GFAP staining, multiple comparisons demonstrated that Iba1 staining area (Figure 6.9a) and Iba1 staining index (Figure 6.9b) were significantly reduced in the ventral horns of the 25D cohort (38% and 40%, respectively) and 75D cohort mice (31% and 42%, respectively) compared to that of the vehicle dosed mice ( $p = <0.01$ ). In addition, the non-transgenic mice displayed the biggest reduction in Iba1 staining within ventral horns compared to the vehicle dosed mice (55% reduction in Iba1 staining area and 58% reduction in Iba1 staining index,  $p = <0.001$ ). Whilst there was less Iba1 staining in the ventral horns of non-transgenic mice compared to that of the 25D cohort and 75D cohort mice, there was only a significant reduction in Iba1 staining area (Figure 6.9a) for the non-transgenic mice compared to the 75D cohort mice ( $p = 0.0287$ ). Notably, the Iba1 staining data was more variable than the GFAP staining data.

Tissue was also collected from 6 mice per dose group at end-stage and the ventral horns of lumbar SC sections were immuno-stained with the same glial markers, anti-GFAP (Figure 6.10) and anti-Iba1 (Figure 6.11). Whilst it had been shown previously

in the 90D dose-response study that dosing with HTL0014242 at 30mg/kg reduced glial activation at 90 days of age, it was not clear whether HTL0014242 would have the same effect on glial activation at a later stage of the disease. The findings at end-stage were rather unexpected, Figure 6.10 shows that there was only a significant difference in GFAP staining area between dose groups overall, (one-way ANOVA,  $p = <0.0037$ ) with multiple comparisons showing that the mean GFAP staining area in ventral horns of the 75D cohort mice was significantly increased compared to that of the 25D cohort mice ( $p = <0.0027$ ). Interestingly, one of the vehicle dosed mice had an uncharacteristically high ventral horn GFAP staining area, which was more comparable with the staining observed for the 75D cohort mice (Figure 6.10a). The same trend was apparent for GFAP staining index, with most staining observed in the ventral horns of the 75D cohort mice and the 25D cohort mice displayed the least staining out of all the dose groups. The variability observed for the vehicle and 75D cohort data was considerably greater than that observed for the 25D cohort and for earlier time points. This increased variability has confounded statistical analysis to some extent as well as reduced numbers ('n') due to the poor-quality tissue in some dose groups. For example, whilst GFAP staining index was elevated for two of the 75D cohort mice, the other two 75D cohort mice had comparable staining levels to the 25D cohort mice (Figure 6.10b).

In addition, Iba1 staining was characterised in the ventral horns of lumbar SC sections collected at end-stage. Figure 6.11 (a-b) demonstrate that there was a significant difference in Iba1 staining area (Figure 6.11a) and Iba1 staining index (Figure 6.11b) between the different dose groups overall, as shown by one-way ANOVA ( $p = <0.0010$  and  $p = 0.0028$ , respectively). Similar to the observations for GFAP staining in SC ventral horns at end-stage, Iba1 staining was most elevated in the ventral horns of the 75D cohort mice. Multiple comparisons showed that both Iba1 staining area (Figure 6.11a) and Iba1 staining index (Figure 6.11b) was significantly increased in the ventral horns of 75D cohort mice compared to 25D cohort mice and vehicle dosed mice ( $p = \leq 0.0101$  Tukey's post-test). The biggest difference in Iba1 staining was observed between the 75D cohort mice and the 25D cohort mice, demonstrating a similar trend to GFAP staining in end-stage ventral horns. Also, in keeping with previous findings for GFAP staining, the variability of the Iba1 staining was considerably higher for the vehicle group and 75D cohort compared to the 25D cohort. For example, whilst two of the 75D cohort mice demonstrated increased Iba1 staining index in their ventral horns, one of the 75D cohort mice had comparable levels to the 25D cohort and vehicle group mice.

Whilst both GFAP staining index and Iba1 staining index in end-stage SC ventral horns were analysed from relatively few 75D cohort mice (4 mice for GFAP staining and 3 mice for Iba1 staining), the data are consistent in showing that glial activation is elevated in ventral horn lumbar SC sections of 75D cohort mice at end-stage.

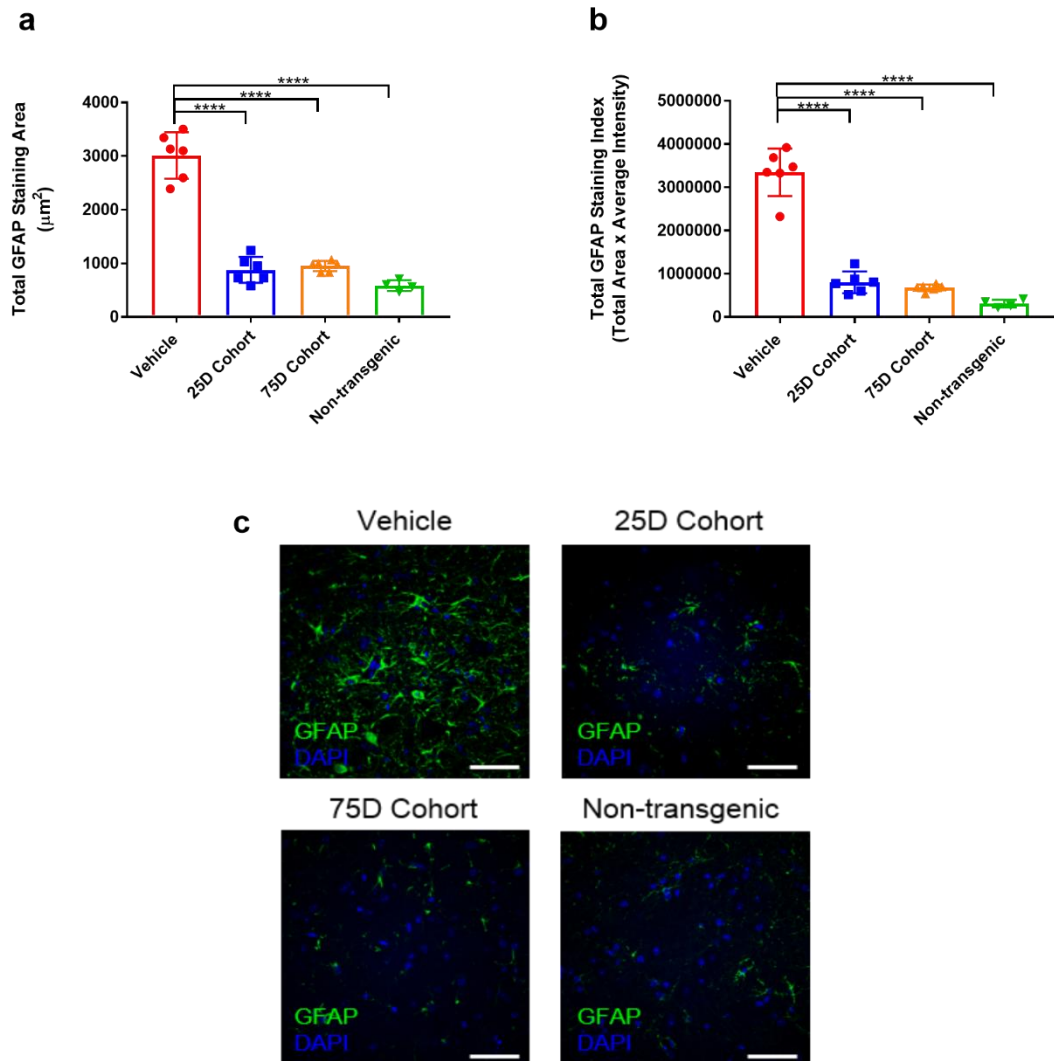


**Figure 6.8. Reduced astrocyte staining in ventral horns of HTL0014242 dosed mice at 90 days of age.** *SOD1<sup>G93A</sup>* mice were orally dosed with vehicle (0.5% methylcellulose in water), 30mg/kg HTL0014242 from 25 days of age (25D cohort) and 30mg/kg HTL0014242 from 75 days of age (75D cohort). At 90 days of age lumbar spinal cord sections were fixed, paraffin-embedded and the ventral horns were immuno-stained with an anti-GFAP antibody and DAPI. In addition, lumbar spinal cord sections from drug naïve non-transgenic mice were also fixed, paraffin-embedded and ventral horns immuno-stained with an anti-GFAP antibody and DAPI (c). Scale bars, 50µm. Quantification of the GFAP staining area (a) and GFAP staining index (b) both demonstrated that there was an overall significant difference between dose-groups, shown by one-way ANOVA and Tukey's post-test ( $p = <0.0001$ ). Multiple comparisons analysis showed that the mean GFAP staining area (a) and mean GFAP

staining index (b) for both the 25D cohort, 75D cohort and the drug naïve non-transgenic mice were significantly reduced compared to that of the vehicle dose group ( $p = <0.0001$ ). Data presented as mean ( $\pm$  SD), data points represent individual animals (4-6 mice per group).

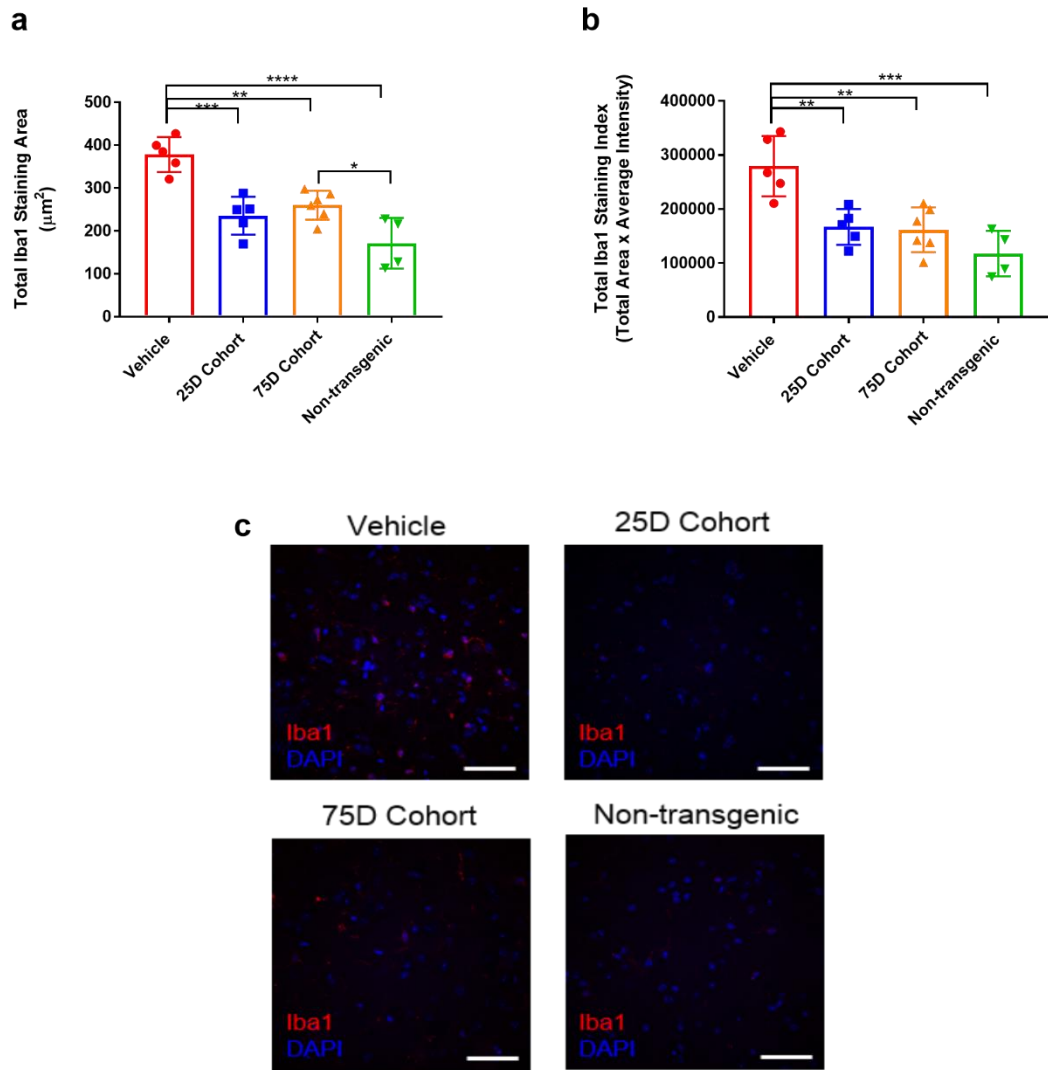


**Figure 6.9. Reduced microglial staining in ventral horns of HTL0014242 dosed mice at 90 days of age.** *SOD1<sup>G93A</sup>* mice were orally dosed with vehicle (0.5% methylcellulose in water), 30mg/kg HTL0014242 from 25 days of age (25D cohort) and 30mg/kg HTL0014242 from 75 days of age (75D cohort). At 90 days of age lumbar spinal cord sections were fixed, paraffin-embedded and the ventral horns were immuno-stained with an anti-Iba1 antibody and DAPI. In addition, lumbar spinal cord sections from drug naïve non-transgenic mice were also fixed, paraffin-embedded and ventral horns immuno-stained with an anti-Iba1 antibody and DAPI (c). Scale bars, 50µm. Quantification of the Iba1 staining area (a) and Iba1 staining index (b) both demonstrated that there was an overall significant difference between dose-groups, shown by one-way ANOVA and Tukey's post-test,  $p = <0.0001$  (a) and  $p = 0.0003$  (b). Multiple comparisons analysis showed that the mean Iba1 staining area (a) in SC ventral horns was significantly elevated in the vehicle group compared to the 25D cohort ( $p = 0.0005$ ), 75D cohort ( $p = 0.0020$ ) and the drug naïve non-

transgenic mice ( $p = <0.0001$ ). Also, the Iba1 staining area in ventral horns of 75D cohort mice was significantly elevated compared to that of drug naïve non-transgenic mice ( $p = 0.0287$ ). In addition, multiple comparisons analysis showed that the mean Iba1 staining index (b) in SC ventral horns was significantly elevated in the vehicle group compared to the 25D cohort ( $p = 0.0045$ ), 75D cohort ( $p = 0.0021$ ) and the drug naïve non-transgenic mice ( $p = 0.0002$ ). Data presented as mean ( $\pm$  SD), data points represent individual animals (4-6 mice per group).

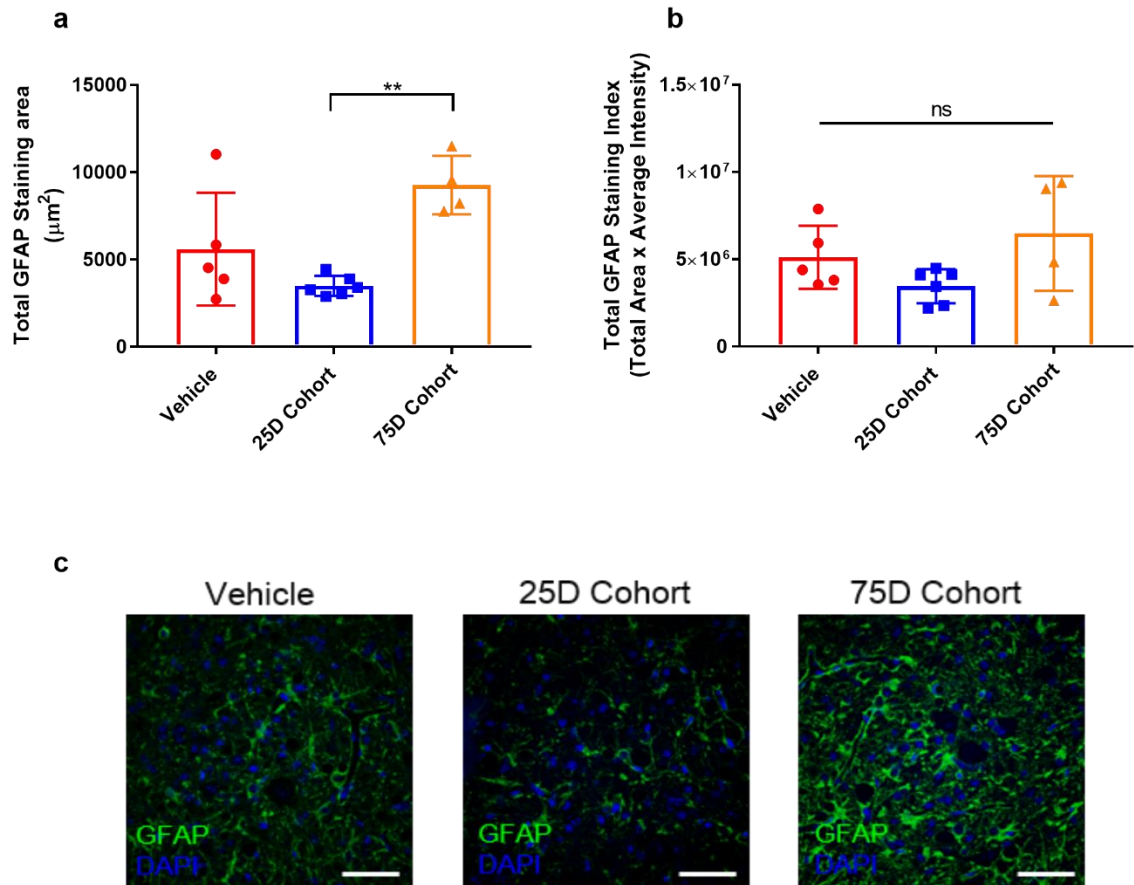


**Figure 6.10. Increased area of astrocyte staining in ventral horns of 75D cohort at end-stage of disease.** *SOD1<sup>G93A</sup>* mice were orally dosed with vehicle (0.5% methylcellulose in water), 30mg/kg HTL0014242 from 25 days of age (25D cohort) and 30mg/kg HTL0014242 from 75 days of age (75D cohort). At end-stage of the disease lumbar spinal cord sections were fixed, paraffin-embedded and the ventral horns were immuno-stained with an anti-GFAP antibody and DAPI (c). Scale bars, 50μm. Quantification of the GFAP staining area (a) but not GFAP staining index (b) demonstrated that there was an overall significant difference between dose-groups, shown by one-way ANOVA and Tukey's post-test,  $p = <0.0037$  (a). Multiple comparisons analysis showed that the mean GFAP staining area (a) for the 75D cohort was significantly increased compared to that of the 25D cohort ( $p = <0.0027$ ). Data presented as mean ( $\pm$  SD), data points represent individual animals (4-6 mice per group).

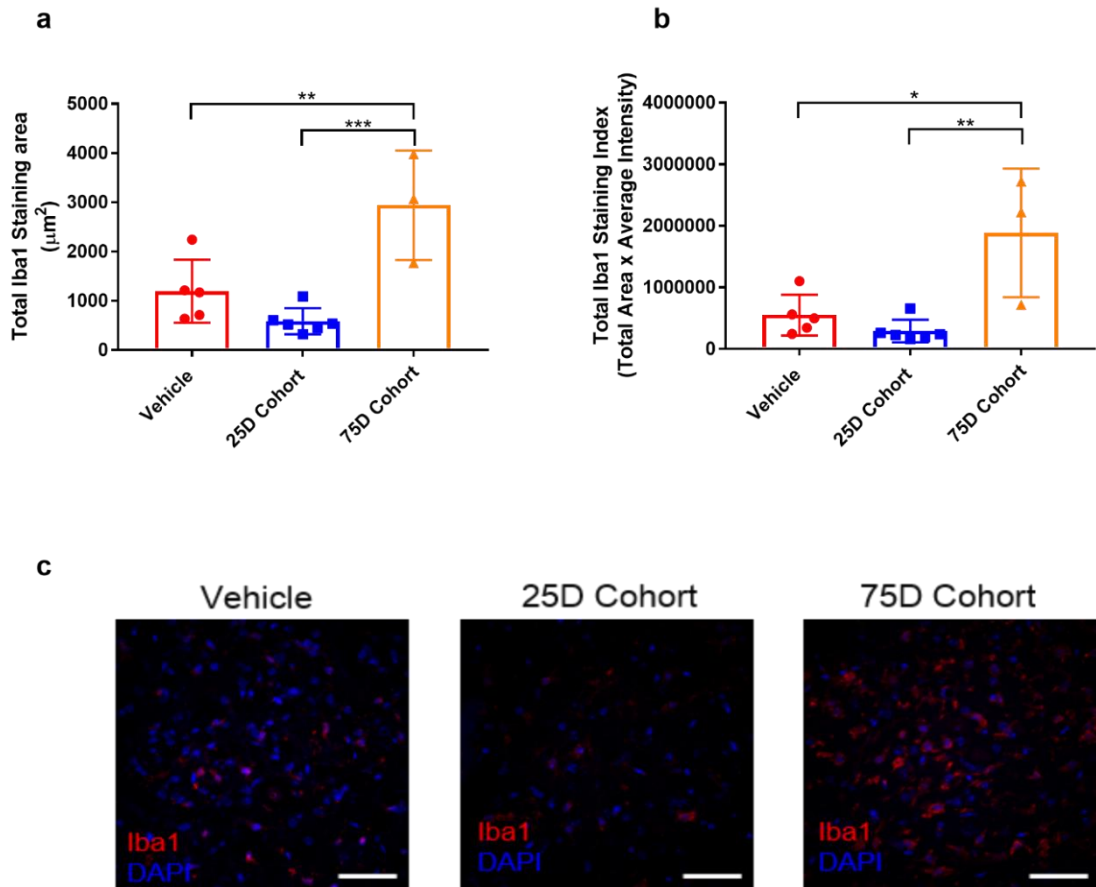


**Figure 6.11. Increased microglial staining in ventral horns of 75D cohort at end-stage of disease.** *SOD1<sup>G93A</sup>* mice were orally dosed with vehicle (0.5% methylcellulose in water), 30mg/kg HTL0014242 from 25 days of age (25D cohort) and 30mg/kg HTL0014242 from 75 days of age (75D cohort). At end-stage of disease lumbar spinal cord sections were fixed, paraffin-embedded and the ventral horns were immuno-stained with an anti-Iba1 antibody and DAPI (c). Scale bars, 50µm. Quantification of the Iba1 staining area (a) and Iba1 staining index (b) both demonstrated that there was an overall significant difference between dose-groups, shown by one-way ANOVA and Tukey's post-test,  $p = 0.0010$  (a) and  $p = 0.0028$  (b). Multiple comparisons analysis showed that the mean Iba1 staining area (a) and mean Iba1 staining index (b) for the 75D cohort were significantly increased compared to that of the vehicle group,  $p = 0.0082$  (a) and  $p = 0.0101$  (b). The mean Iba1 staining area (a) and mean Iba1 staining index (b) for the 75D cohort were also significantly increased compared to that of the 25D cohort,  $p = 0.0007$  (a) and  $p = 0.0024$  (b). Data presented as mean ( $\pm$  SD), data points represent individual animals (3-6 mice per group).

### **6.2.3 Motor neuron counts in ventral horns of lumbar spinal cord sections collected at 90D and end-stage from survival study**

SC tissue was collected at 90 days of age from 6 mice per dose group and ventral horns of lumbar SC sections were ChAT stained to determine the number of motor neurons per dose group. Eight lumbar spinal cord sections, with each section separated by 100µm were ChAT stained to determine the average number of motor neuron counts per ventral horn. Only large polygonal neurons with a distinguishable nucleus were included in the counts. Tissue was also collected at end-stage of disease (6 mice per dose group) to compare ChAT stained motor neuron counts in the ventral horns of 90D and end-stage lumbar SC sections.

Figure 6.12b demonstrates that overall there was a significant difference in the average number of motor neurons in the ventral horns of lumbar SC sections at 90 days of age, as shown by one-way ANOVA ( $p = 0.0390$ ). The average number of motor neurons per section at 90 days of age for the 75D cohort was  $3.1 \pm 1.2$  (data presented as mean  $\pm$  SD), whilst for the 25D cohort it was  $2.2 \pm 0.6$  and only  $1.6 \pm 0.8$  for the vehicle control group. Multiple comparisons demonstrated that the average motor neuron count in lumbar SC was significantly higher in the 75D cohort compared to the vehicle control group ( $p = <0.0328$ ). These data suggest that at 90 days of age, more motor neurons are preserved in ventral horns of lumbar SC sections of the 75D cohort versus the vehicle control group.

Motor neuron counts were also quantified in ventral horns of lumbar SC sections collected at end-stage. Figure 6.12c demonstrates that there was no significant difference in the average number of motor neurons in ventral horns of lumbar SC per section for any of the dose groups at end-stage, as shown by one-way ANOVA ( $p = 0.8347$ ). The average number of motor neurons per section at end-stage of disease for the 75D cohort was  $0.7 \pm 0.2$  (data presented as mean  $\pm$  SD), whilst for the 25D cohort it was  $0.6 \pm 0.3$  and  $0.8 \pm 0.5$  for the vehicle control group. There was a reduction in the average number of motor neurons in the ventral horns of the 75D cohort, 25D cohort and vehicle control group between 90 days of age and end-stage. Finally, it is worth noting that whilst ChAT staining gives an indication of the remaining motor neurons, it does not directly inform on the function of these remaining motor neurons. For example, it is conceivable that these motor neurons detected by ChAT staining are the remaining cell bodies of motor neurons which have already lost their connection with muscle.

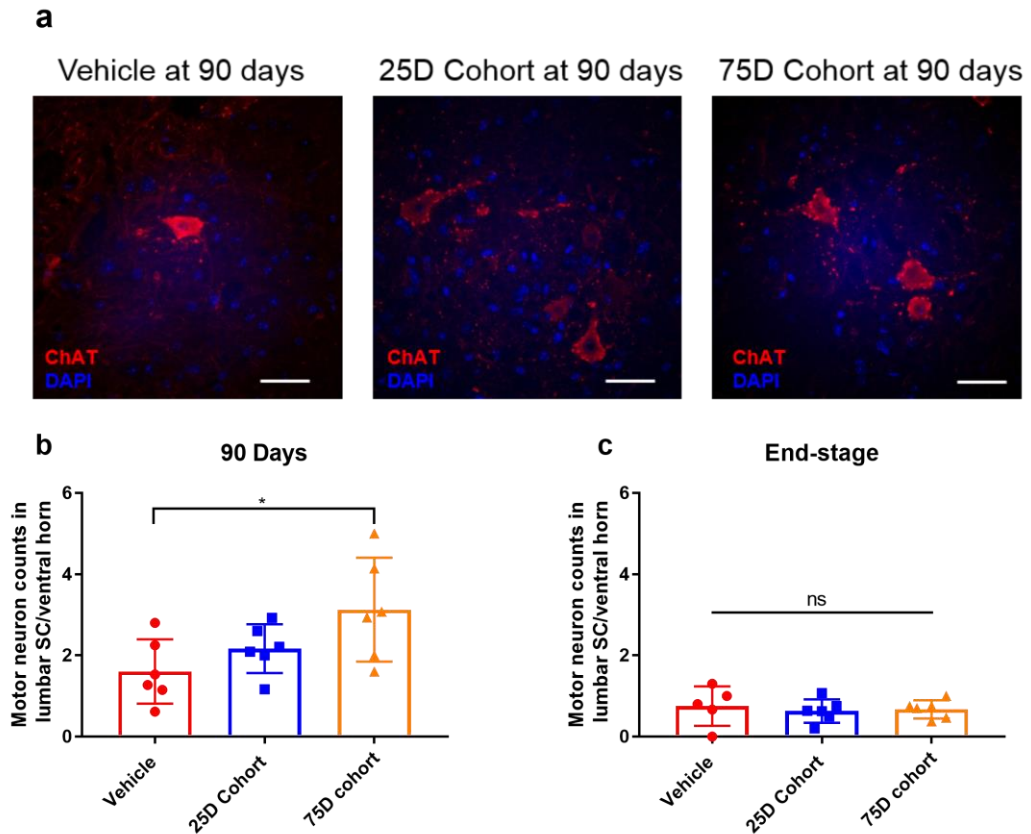


**Figure 6.12. Increased number of motor neuron counts in ventral horns of 75D cohort at 90 days of age.** *SOD1<sup>G93A</sup>* mice were orally dosed with vehicle (0.5% methylcellulose in water), 30mg/kg HTL0014242 from 25 days of age (25D cohort) and 30mg/kg HTL0014242 from 75 days of age (75D cohort). At 90 days of age and at end-stage of disease lumbar spinal cord sections were fixed, paraffin-embedded and the ventral horns were ChAT stained. a) Representative images of ChAT staining in ventral horns of lumbar spinal cord at 90 days of age. Scale bar = 50  $\mu$ m. b) Quantification of ChAT stained motor neurons at 90 days of age demonstrated that there was an overall significant difference between dose-groups, shown by one-way ANOVA and Tukey's post-test,  $p = <0.0390$ . Multiple comparisons analysis showed that the mean number of motor neuron counts per section for the 75D cohort was significantly increased compared to that of the vehicle group ( $p = 0.0328$ ). c) Quantification of the number of motor neuron counts at end-stage of disease showed that there was no overall significant difference between dose-groups, shown by one-way ANOVA and Tukey's post-test,  $p = 0.8347$ . Data presented as mean ( $\pm$  SD), data points represent individual animals (5-6 mice per group).

#### **6.2.4 Immunofluorescent staining with mGlu<sub>5</sub> and ChAT in ventral horns of lumbar spinal cord sections collected at 90D from survival study**

At 90 days of age tissue was collected from 6 mice per dose group and the ventral horns of lumbar SC sections were immuno-stained with anti-mGlu<sub>5</sub> (Figure 6.13) and anti-ChAT (Figure 6.14). Figure 6.13 (a-b) shows that both mGlu<sub>5</sub> staining area and mGlu<sub>5</sub> staining index were significantly elevated in the ventral horns of 75D cohort mice compared to that of 25D cohort mice (323% increase and 432% increase, respectively) and versus the vehicle dosed mice (260% increase and 345% increase, respectively), as shown by one-way ANOVA ( $p = <0.0001$ ). These data suggest that dosing with HTL0014242 from 75 days onwards results in increased levels of mGlu<sub>5</sub> in ventral horns of lumbar SC at 90 days of age. Furthermore, whilst there was a small reduction in both mGlu<sub>5</sub> staining area (15% reduction) and mGlu<sub>5</sub> staining index (16% reduction) in the ventral horns of the 25D cohort versus the vehicle control group, this was not significantly different ( $p = >0.05$ ).

Figure 6.14 shows that overall there was a significant difference in ChAT staining area in the ventral horns of lumbar SC sections of the different dose groups, as shown by one-way ANOVA ( $p = <0.0197$ ). Multiple comparisons demonstrated that ChAT staining area in the ventral horns of the 75D cohort was significantly increased compared to that in the vehicle control group (64% increase,  $p = <0.0152$ ). Whilst there was a trend for elevated ChAT staining area (22% increase) in the ventral horns of the 75D cohort compared with the 25D cohort and also a trend for elevated ChAT staining area (34% increase) in the ventral horns of the 25D cohort compared with the vehicle control group, these changes in staining were not significantly different ( $p = >0.05$ ). Interestingly, the differences observed for ChAT staining area in the ventral horns of the different dose groups were similar to the changes observed for ChAT stained motor neurons in ventral horns of lumbar SC sections at 90 days of age. For example, Figure 6.12b shows that the average number of ChAT stained motor neurons was highest in the ventral horns of the 75D cohort, followed by the 25D cohort, with the lowest number observed in the vehicle control group. The ChAT staining data in Figure 6.14a appear to consolidate the ChAT stained motor neuron data (Figure 6.12c), suggesting that dosing with HTL0014242 from 75 days of age results in an increased number of motor neurons in the ventral horns of lumbar SC sections at 90 days of age.

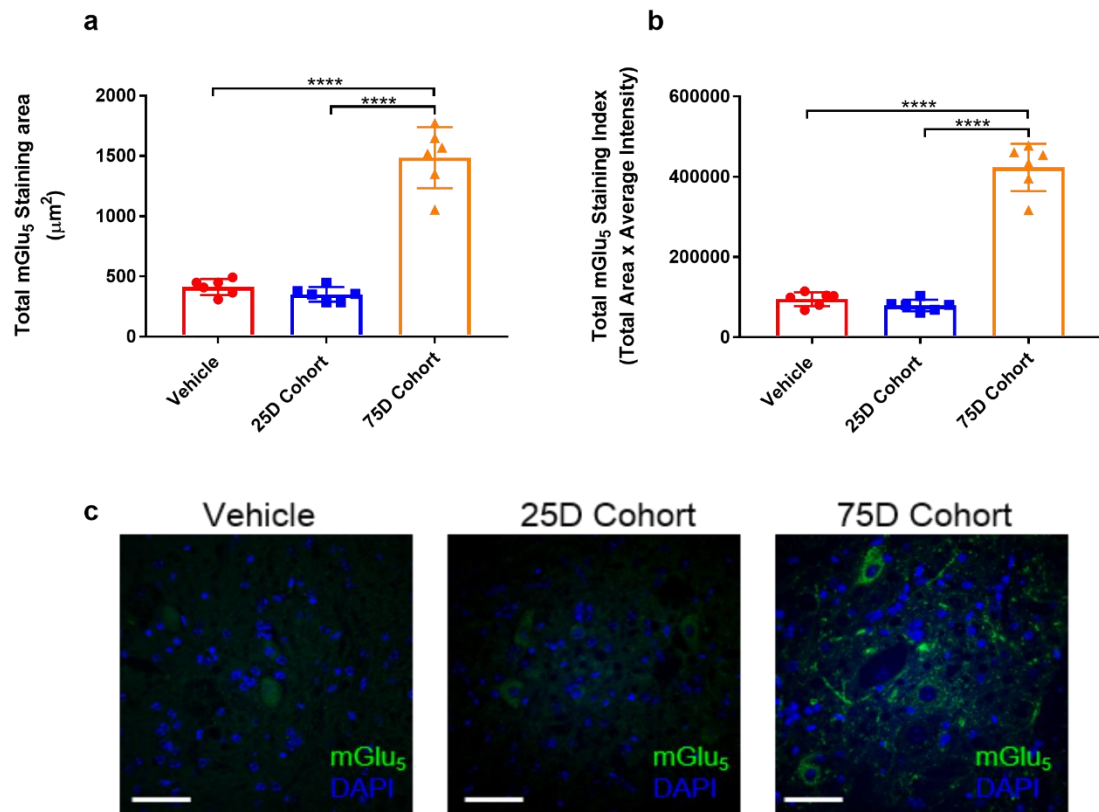


**Figure 6.13. Increased mGlu<sub>5</sub> staining in ventral horns of 75D cohort at 90 days of age.** *SOD1<sup>G93A</sup>* mice were orally dosed with vehicle (0.5% methylcellulose in water), 30mg/kg HTL0014242 from 25 days of age (25D cohort) and 30mg/kg HTL0014242 from 75 days of age (75D cohort). At 90 days of age lumbar spinal cord sections were fixed, paraffin-embedded and the ventral horns were immuno-stained with an anti-mGlu<sub>5</sub> antibody and DAPI (c). Scale bars, 50µm. Quantification of the mGlu<sub>5</sub> staining area (a) and mGlu<sub>5</sub> staining index (b) demonstrated that there was an overall significant difference between dose-groups, shown by one-way ANOVA and Tukey's post-test,  $p = <0.0001$ . Multiple comparisons analysis showed that the mean mGlu<sub>5</sub> staining area (a) and the mean mGlu<sub>5</sub> staining index (b) for the 75D cohort were significantly increased compared to that of the vehicle group,  $p = <0.0001$ . Further, the mean mGlu<sub>5</sub> staining area (a) and the mean mGlu<sub>5</sub> staining index (b) for the 75D cohort were significantly increased compared to that of the 25D cohort  $p = <0.0001$ . There was no significant difference between the mean mGlu<sub>5</sub> staining area (a) and the mean mGlu<sub>5</sub> staining index (b) for vehicle group and the 25D cohort ( $p = > 0.05$ ). Data presented as mean ( $\pm$  SD), data points represent individual animals (6 mice per group).

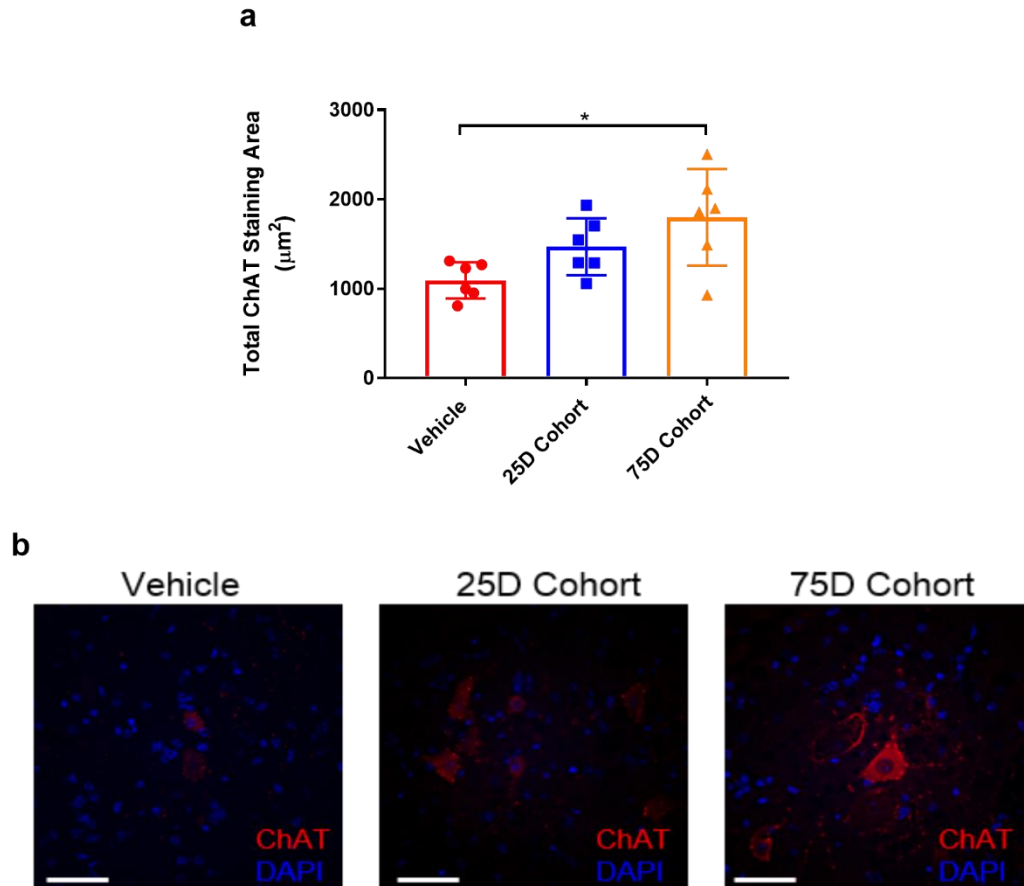


**Figure 6.14. Increased ChAT staining area in ventral horns of 75D cohort at 90 days of age.** *SOD1<sup>G93A</sup>* mice were orally dosed with vehicle (0.5% methylcellulose in water), 30mg/kg HTL0014242 from 25 days of age (25D cohort) and 30mg/kg HTL0014242 from 75 days of age (75D cohort). At 90 days of age lumbar spinal cord sections were fixed, paraffin-embedded and the ventral horns were immuno-stained with an anti-ChAT antibody and DAPI (b). Scale bars, 50µm. Quantification of the ChAT staining area (a) demonstrated that there was an overall significant difference between dose-groups, shown by one-way ANOVA and Tukey's post-test,  $p = 0.0197$ . Multiple comparisons analysis showed that the mean ChAT staining area (a) for the 75D cohort was significantly increased compared to that of the vehicle group,  $p = <0.0152$ . Data presented as mean ( $\pm$  SD), data points represent individual animals (6 mice per group).

### **6.2.5 [<sup>3</sup>H] M-MPEP binding assay to measure RO of mGlu<sub>5</sub> receptors by HTL0014242 in mouse brain collected from survival study at end-stage**

At end-stage of the disease, brain tissue was collected from 3 mice per dose group at both peak and trough HTL0014242 exposures for receptor occupancy (RO) analysis. Whilst half of the brain tissue was sent to Pharmidex for bioanalysis of compound exposure levels (Table 6.1), the other half of the brain was used to prepare brain membranes to determine the proportion of mGlu<sub>5</sub> receptors occupied by HTL0014242 in the 25D cohort and 75D cohort at peak and trough. This was established using the [<sup>3</sup>H] M-MPEP binding assay as described in Chapter 4. Mean RO was established from the average specific binding at peak and trough HTL0014242 exposures for both the 25D cohort mice and the 75D cohort mice, with the values from the brain membranes of the vehicle dosed mice taken as 100% RO. Figure 6.15 demonstrates that HTL0014242 dosed from both 25 days of age and 75 days of age demonstrate 100% RO in end-stage brain at peak exposure. These data confirm that mGlu<sub>5</sub> target engagement in end-stage brain is not altered by dosing HTL0014242 at 30mg/kg from 25 days onwards or 75 days onwards. Furthermore, considering that previously it was shown from the 90D dose-response study that RO in brain measured at 90 days of age was ~ 93% at peak exposure following a dose of 30mg/kg HTL0014242, this would suggest that chronic dosing of HTL0014242 between 90 days of age and end-stage of disease does not alter mGlu<sub>5</sub> target engagement.

Predicted mGlu<sub>5</sub> RO in both SC and brain were calculated at peak and trough HTL0014242 exposures for the 25D cohort and the 75D cohort (Table 6.1). Measured mGlu<sub>5</sub> RO in brain (Figure 6.15) was plotted versus both predicted mGlu<sub>5</sub> RO in SC and versus predicted mGlu<sub>5</sub> RO in brain, at both peak and trough HTL0014242 exposures for the 25D cohort and the 75D cohort (Figure 6.16). From this it was possible to establish whether predicted RO in spinal cord or brain was a better surrogate for measured RO in brain.

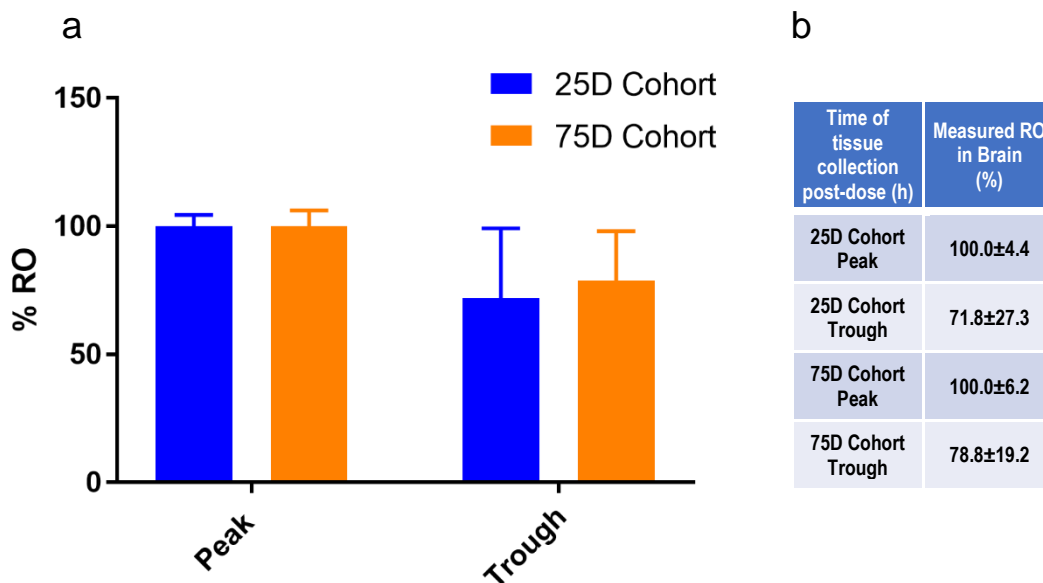


**Figure 6.15. Dosing with 30mg/kg HTL0014242 from 75 days compared with 25 days does not change mGlu<sub>5</sub> receptor occupancy at peak and trough exposure.** Membranes were crudely prepared from 90-day old whole brains of *SOD1<sup>G93A</sup>* mice. The mice had either been dosed with 30mg/kg of HTL0014242 from 25 days of age (25D cohort) or from 75 days of age (75D cohort) or with vehicle (0.5% methylcellulose in water), from 25 days of age. Brain tissue was either collected at peak (2 h post dose) or trough (24 h post dose) HTL0014242 exposures. The % receptor occupancy of mGlu<sub>5</sub> by HTL0014242 at peak and trough were calculated using a <sup>3</sup>[H] M-MPEP radioligand binding assay. a) Data presented as mean ± SD (3 mice per group). b) Average RO measured in brain at peak and trough HTL0014242 exposures for the 25D cohort and 75D cohort.

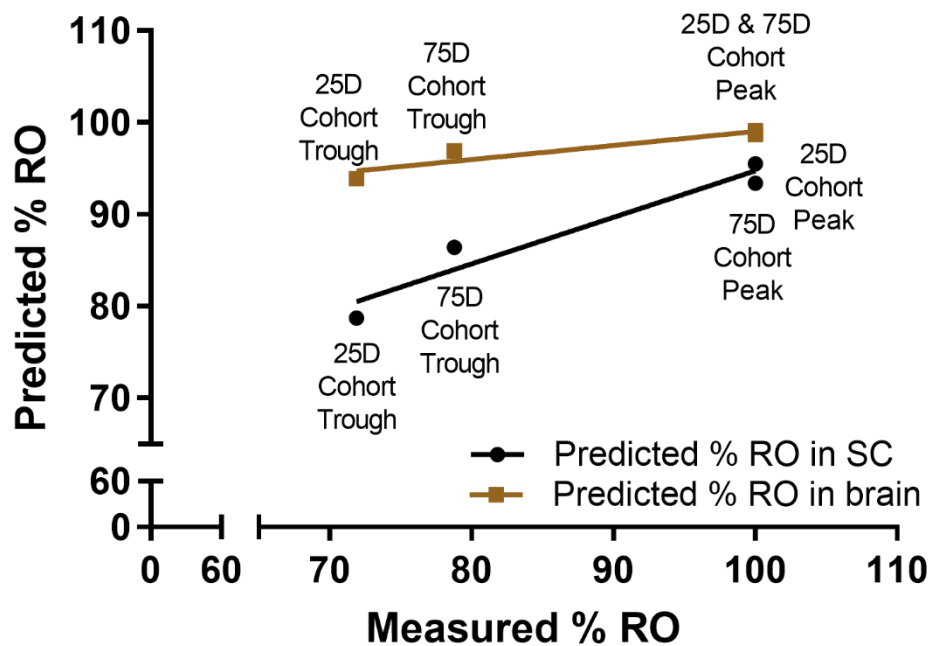


**Figure 6.16. Predicted RO in brain does not align with measured RO in brain.**

The predicted mGlu<sub>5</sub> receptor occupancy in both SC and brain was calculated using the equation  $(\text{Predicted \% RO} = (\text{HTL0014242 concentration} / \text{HTL0014242 concentration} + K_i \text{ of HTL0014242 for mGlu}_5))$  and plotted versus the measured mGlu<sub>5</sub> RO in brain, presented in Figure 6.15. Mean RO at peak and trough HTL0014242 exposure was plotted for the 25D cohort and the 75D cohort (3 animals at peak and trough per group).

**Table 6.1. Exposure data for HTL0014242 dosed at 30mg/kg from 25 days of age (25D cohort) and from 75 days of age (75D cohort).** Total HTL0014242 concentration, unbound HTL0014242 concentration and predicted receptor occupancy for both SC tissue and brain tissue collected at peak (2h) and trough (24h) HTL0014242 exposures.

<b>Time of tissue collection post-dose (h)</b>	<b>Total HTL0014242 in SC (nM)</b>	<b>Unbound HTL0014242 in SC (nM)</b>	<b>Predicted RO in SC (%)</b>	<b>Total HTL0014242 in Brain (nM)</b>	<b>Unbound HTL0014242 in Brain (nM)</b>	<b>Predicted RO in Brain (%)</b>
<b>25D Cohort Peak</b>	33395	13.36	<b>95.5</b>	24837	69.54	<b>99.1</b>
<b>25D Cohort Trough</b>	5817	2.33	<b>78.7</b>	3462	9.69	<b>93.9</b>
<b>75D Cohort Peak</b>	22247	8.90	<b>93.4</b>	17615	49.32	<b>98.7</b>
<b>75D Cohort Trough</b>	9993	4.00	<b>86.4</b>	7050	19.74	<b>96.9</b>

## 6.3 Discussion

The previous 90D dose-response study demonstrated that dosing with 30mg/kg of HTL0014242 from 25 days of age through to 90 days of age significantly reduced glial activation in the ventral horns of lumbar SC at 90 days of age. However, this only translated into a somewhat modest improvement in motor function, as measured using the rotarod readout. The main purpose of this study was to investigate the efficacy of HTL0014242 on survival (humane end-point). In addition, the study was designed to include both a 25D cohort and a 75D cohort, the reasons for which were twofold. Firstly, it enabled the efficacy of dosing with HTL0014242 to be investigated from a time point which may be more clinically relevant. Also, with evidence that glial cells expressing mutant *SOD1* drive later stages of disease progression after onset of visible signs of disease, having two distinct dosing cohorts enabled the efficacy of reducing glial activation at early and late stages of the disease course to be explored.

### 6.3.1 Early vs late dosing of HTL0014242 up to end-stage in the *SOD1*<sup>G93A</sup> mouse model of MND

Whilst dosing HTL0014242 at 30mg/kg from 25 days of age had no effect on time to reach visible signs of disease onset, dosing from 75 days of age was found to significantly delay onset of visible signs of disease in the *SOD1*<sup>G93A</sup> mouse model of MND. Average onset of visible signs of disease for the vehicle and 25D cohorts were both ~76-77 days of age, whereas the average age of onset for the 75D cohort was later at 80.6 days of age. It was somewhat surprising to see such a profound effect on disease onset for the 75D cohort as it suggests that dosing from 75 days of age had an immediate effect on visible signs of disease onset.

One drawback of this study was that neurological scoring only commenced from 75 days of age, whereas data for the vehicle group and the 25D cohort were available from 60 days of age and we know from previous studies that onset of visible signs can occur before 75 days of age. To account for this limitation, neurological scores obtained before 75 days of age for the vehicle group and the 25D cohort were removed in the final analysis and all mice scored for onset from 75 days onwards. This may have led to a slightly later onset being recorded for each group.

Comparison of the onset data for the vehicle group and 25D cohort from this study with the vehicle and 30mg/kg HTL0014242 dose groups from the 90D dose-response study shows remarkable consistency. The average age of onset for the vehicle group from the survival study was 76.5 days of age compared to 74.6 days of age for the

vehicle group from the 90D dose-response study. In contrast, the average age of onset for the 25D cohort from the survival study was 76.9 days of age compared with 76.8 days of age for the 30mg/kg HTL0014242 dose group from the 90D dose-response study. The consistency of the onset data between the 90D dose response study and the survival study would suggest that the onset data observed for 75D cohort was indeed robust, despite the 75D cohort mice only having been dosed for a relatively short period of time.

Of note, Bonifacino et al. (2017), found that heterozygous knockdown of mGlu<sub>5</sub> in the *SOD1<sup>G93A</sup>* mouse model of MND delayed average disease onset to 132 days of age for both male and female *SOD1<sup>G93A</sup>GRM5<sup>-/+</sup>* mice compared to 114 days of age for male and 120 days of age for female *SOD1<sup>G93A</sup>* mice. The *SOD1<sup>G93A</sup>GRM5<sup>-/+</sup>* mice were bred on the mixed C57BL6/SJL genetic background whereas the *SOD1<sup>G93A</sup>* mice in our survival study were bred on the inbred C57BL/6 genetic background. It is well known that genetic background can markedly influence disease course and duration. Therefore, it is not surprising that the average age of onset for the control mice in the survival study versus the control mice in the Bonifacino et al. (2017) study were quite different (76.5 days and 120 days of age, respectively). Considering the delayed disease onset observed for the *SOD1<sup>G93A</sup>GRM5<sup>-/+</sup>* mice, it was somewhat surprising that the mice dosed from 25 days of age with HTL0014242 at 30mg/kg in both the 90D dose-response study and the survival study did not demonstrate a delayed disease onset. However, unlike in our studies where mGlu<sub>5</sub> activity was inhibited from 25 days of age onwards, the mGlu<sub>5</sub> heterozygous knockdown mice expressed less mGlu<sub>5</sub> from birth. This may explain, in part, why the 25D cohort mice in our study did not exhibit a delayed disease onset. Furthermore, Rossi et al. (2008) showed that *SOD1<sup>G93A</sup>* mice dosed with 30mg/kg MPEP from 40 days of age demonstrated a delayed disease onset compared to control mice (111.4±2.1 days versus 102.4±2.7 days, respectively). Whilst the survival study showed that dosing with HTL0014242 from 75 days of age delayed onset of visible signs of disease, dosing HTL0014242 from 25 days of age did not. Our study clearly demonstrates that the timing of when HTL0014242 dosing is commenced influences its effect on delaying onset of visible signs of disease. Therefore, it is conceivable that whilst inhibiting mGlu<sub>5</sub> activity from both 40 days of age (MPEP) and 75 days of age (HTL0014242) confer beneficial effects in terms of delaying disease onset, blocking mGlu<sub>5</sub> activity from 25 days of age as shown by both the 90D dose-response study and the survival study does not. Of note, whilst neurological scoring was used to determine onset of visible signs of disease for the mice in the 90D dose-response

study and the survival study, both Bonifacino et al. (2017) and Rossi et al. (2008) measured disease onset retrospectively using time taken to reach peak body weight. Whilst this may be a useful measure of disease onset in the *SOD1<sup>G93A</sup>* mouse model on the mixed genetic background, it is not a good/reliable measure of onset in our *SOD1<sup>G93A</sup>* mouse model on the inbred genetic background. It is possible that the use of these two different measures to define 'disease onset' (neurological scores and peak body weight) may actually be a measure of two separate 'events' during the *SOD1<sup>G93A</sup>* disease course. Finally, in the absence of any target occupancy data in the Rossi et al. (2008) study, it is difficult to know whether the delay in disease onset observed by dosing MPEP at 30mg/kg was mediated directly through inhibiting mGlu<sub>5</sub> activity. This is especially the case when considering that MPEP dosed at 30mg/kg has been shown previously to have robust analgesic effects in mGlu<sub>5</sub> knockout mice (Montana et al. 2009).

Rotarod testing measured twice a week from 5 weeks of age monitored forced motor function of the mice from each of the dose groups. A significant improvement on rotarod was observed for the 75D cohort both at intermediate and late stages of the disease (Figure 6.2). Interestingly, at 10.5 weeks of age (~75 days of age), which was the earliest time point that the 75D cohort were tested on rotarod, the 75D cohort mice performed significantly better than the mice in the vehicle group and 25D cohort. The 75D mice performed better than the other two dose groups on rotarod until around 12 weeks of age (~85 days of age). Notably, this early improvement in motor function seen on rotarod is consistent with the finding that dosing with 30mg/kg HTL0014242 from 75 days of age significantly delayed onset of visible signs of disease to ~80 days of age and increased the number of motor neuron counts. As rotarod tests at 75 days of age were conducted following dosing this may suggest that HTL0014242 dosed at 30mg/kg had an immediate effect on motor excitability. It is conceivable that reducing excitability alleviated fatigued motor units of the 75D cohort mice which enabled them to perform better on rotarod. Why the same effect was not observed for the 25D cohort is not exactly clear. However, it may suggest that there is a critical window/time point throughout the disease trajectory in which blocking mGlu<sub>5</sub> activity is beneficial.

Interestingly, the 75D cohort also performed significantly better than the vehicle group and the 25D cohort at later stages of the disease (between ~17-18.5 weeks). This suggests that dosing with HTL0014242 from 75 days of age has an immediate beneficial effect at the time of visible signs of disease onset and also appears to mediate a beneficial effect when nearing the end-stage of the disease. One explanation for this could be that mGlu<sub>5</sub> activity plays a role in the selective

vulnerability of certain muscle fibres to denervation. For example, it has been shown that fast-twitch fatigable motor units demonstrate the earliest vulnerability to axonal denervation in both *SOD1<sup>G93A</sup>* mice and MND patients (San Pun et al. 2006; Fischer, Culver, Tennant, A. A. Davis, et al. 2004). This is then followed by denervation of the fast-twitch fatigue-resistant motor units and then finally at a later stage of the disease process denervation of slow-twitch fatigue-resistant motor units (Frey et al. 2000).

In-house data consistently show that rotarod performance of vehicle control *SOD1<sup>G93A</sup>* mice significantly declines between 40 and 60 days of age which then stabilises before a further decline at ~80 days of age (Mead et al. 2011). The initial decline is thought to correlate with the loss of innervation of hind-limb muscles, particularly fast-twitch fatigable motor units (Kanning et al. 2010). There is some reinnervation which is thought to account for the plateau in rotarod performance between 60 days of age and 80 days of age. From ~80 days onwards there is a second wave of denervation, this is thought to be mainly of fast-twitch fatigue-resistant motor units (Kanning et al. 2010). The significant improvement in rotarod performance for the 75D cohort mice was observed between 10.5 weeks and 12 weeks of age. For this reason, it seems unlikely that mGlu<sub>5</sub> activity plays a role in the denervation of fast-twitch fatigable motor units as this process starts early on before 75 days of age and especially considering that the 25D cohort mice did not demonstrate any significant improvement in rotarod performance versus the vehicle mice at any time point throughout the disease trajectory. Whilst it is unlikely that mGlu<sub>5</sub> activity is involved in axonal denervation of fast-twitch fatigable motor units, it is conceivable that mGlu<sub>5</sub> activity plays a role in axonal denervation of fast-twitch fatigue-resistant motor units. For example, this process is thought to take place at around 80 days of age onwards and the 75D cohort mice demonstrated a significant improvement in rotarod performance at similar time points compared to when this process would have commenced (between  $74 \pm 3$  –  $84 \pm 3$  days of age) (Kanning et al. 2010). Whilst it is possible that inhibiting mGlu<sub>5</sub> activity from 75 days of age onwards may have helped to delay the initial denervation of the fast-twitch fatigue-resistant motor units, this process still ensued suggesting that if mGlu<sub>5</sub> activity is involved there must be several other important drivers of this process that are independent of mGlu<sub>5</sub> activity. The 75D cohort mice also demonstrate a significant improvement in rotarod performance between 17-18.5 weeks (which corresponds to  $119 \pm 3$  –  $130 \pm 3$  days of age). Interestingly this could coincide with the denervation of slow-twitch fatigue-resistant motor units which usually takes place at a later stage of the disease (~130 days of age) (Kanning et al. 2010). Once more this could indicate that mGlu<sub>5</sub> activity plays a role in initiating denervation but this time

of slow-twitch fatigue-resistant motor units. Whilst it is plausible that mGlu<sub>5</sub> activity may play a role in mediating the selective vulnerability of certain motor units to denervation, it is not clear why the timing of when HTL0014242 dosing is initiated (75 days of age versus 25 days of age) influences the beneficial effects of inhibiting mGlu<sub>5</sub> activity.

It was obvious that the mice in the 75D cohort were able to perform the rotarod test (time >0) for much longer than the vehicle group or 25D cohort. This is highlighted in Figure 6.4 whereby the average time taken to reach a score of 0 was plotted for each of the dose groups. Whilst the average time taken to reach a score of 0 on rotarod was ~125 days of age for the vehicle dose group, it was ~130 days of age for the 25D cohort and ~146 days of age for the 75D cohort. The three-week extension in this measure clearly demonstrates that the 75D cohort mice retain their motor function for much longer than the mice in any of the other dose groups. Indeed, this observation is very important when considering that a desirable therapeutic compound for treating MND patients would not only extend survival but also preserve motor function, improving quality of life.

The rotarod data from the previous 90D dose-response study demonstrated that, whilst there was a modest treatment effect for dosing with HTL0014242 from 25 days of age, there was no dose-response effect (Figure 5.4). Further, at 12 weeks of age the rotarod performance of the vehicle group appeared to sharply decline giving the impression that dosing with HTL0014242 may have more of an effect on motor function at a later stage of the disease. However, somewhat surprising was that the rotarod data from the survival study showed that there was no significant difference between the vehicle group and the 25D cohort in terms of their motor performance at any time point throughout the disease trajectory. Considering that the survival study was powered appropriately for rotarod as a readout of motor function, the rotarod findings from this study are much more robust compared with that of the 90D dose-response study.

Bonifacino et al. (2017) also used rotarod tests to monitor the motor function of *SOD1<sup>G93A</sup>GRM5<sup>-/+</sup>* mice compared with *SOD1<sup>G93A</sup>* mice from 80 days of age onwards. Interestingly, it was found that whilst there was no difference between *SOD1<sup>G93A</sup>* mice and *SOD1<sup>G93A</sup>GRM5<sup>-/+</sup>* mice when comparing the rotarod performance of both male and female *SOD1<sup>G93A</sup>GRM5<sup>-/+</sup>* mice, comparison of the rotarod performance of just the male *SOD1<sup>G93A</sup>GRM5<sup>-/+</sup>* mice demonstrated a significant improvement in rotarod performance compared with the *SOD1<sup>G93A</sup>* mice. Therefore, reducing the expression

of mGlu<sub>5</sub> in *SOD1<sup>G93A</sup>* mice only reduced motor decline of the male *SOD1<sup>G93A</sup> GRM<sup>+/+</sup>* mice. In contrast to the study by Bonifacino et al. (2017), only female mice were used in our 90D dose-response study and survival study. The rotarod data generated by Bonifacino et al. (2017) suggest that more profound effects on rotarod may have been demonstrated had male mice been used in our studies. However, it has been previously shown that there are no significant differences between male and female *SOD1<sup>G93A</sup>* mice bred on the inbred C57BL/6 genetic background for any of the parameters measured in the survival study, including rotarod (Mead et al. 2011). Whilst this is true, it has been noted that female mice demonstrate a trend for less variability than male mice for time taken to reach a 20% decline in rotarod performance (Mead et al. 2011). Even though it has been shown previously that there are no gender differences for the *SOD1<sup>G93A</sup>* mice on the inbred background, considering the recent finding by Bonifacino et al. (2017) it would be advisable to also investigate the effect of HTL0014242 dosed at 30mg/kg within male *SOD1<sup>G93A</sup>* mice. Of note, Bonifacino et al. (2017) reported that the female *SOD1<sup>G93A</sup>* mice performed significantly better than the male *SOD1<sup>G93A</sup>* mice for both survival and readouts of motor function. They suggest that this gender difference which is a feature of the mixed C57BL6/SJL genetic background may account for the reduced beneficial effect of halving mGlu<sub>5</sub> expression in the *SOD1<sup>G93A</sup> GRM<sup>5/+</sup>* mice.

One limitations of this survival study was the lack of a vehicle control group which commenced from 75 days of age. The rationale behind the study design of the survival study was twofold. It was felt that having one vehicle control group whereby 20 mice were dosed from 25 days of age through to end-stage of disease would involve using less mice than if an additional vehicle cohort of mice had been recruited to commence from 75 days of age, in keeping with the 'Three Rs' policy. Furthermore, it had been shown previously in our *SOD1<sup>G93A</sup>* mouse model of MND that the rotarod data is remarkably consistent between vehicle control dosed mice (Mead et al. 2011). For example, it has previously been shown that the vehicle control data from six historical survival studies in our *SOD1<sup>G93A</sup>* mouse model of MND follow a similar profile for rotarod performance regardless of the vehicle used to dose the mice and the timepoint throughout the disease trajectory at which the vehicle was commenced (Mead et al. 2011). This suggests that dosing the mice with vehicle does not alter the disease course of our mice and further that the rotarod performance of mice dosed with vehicle from 25 days of age versus mice dosed with vehicle from 75 days of age should not differ. However, to conclusively determine whether the timing of dosing with vehicle had an impact on rotarod performance throughout this study it would

have been better to have included a vehicle dose group commencing from 75 days of age for comparison. That way all of the mice in this study would have been exposed to exactly the same environmental stressors.

Furthermore, it has previously been shown that dosing methyl cellulose (the vehicle used to orally dose the control group in all of our *in vivo* studies) is potentially associated with toxic liability when dosed intraperitoneally (Gibbs et al. 2018). However, when dosing this inert compound orally, it is the vehicle of choice and we observed no signs of toxicity in our mice.

Interestingly, the weight data collected from both the 90D dose-response study and the survival study seem to suggest that dosing with HTL0014242 from 25 days of age is associated with a small but significant amount of weight loss compared to the vehicle group. Rather unexpectedly, the survival study weight data demonstrated that the weight of the 75D cohort mice did not significantly differ from that of the vehicle dosed mice at any time point throughout the disease trajectory (Figure 6.5). This suggests that whilst dosing with 30mg/kg HTL0014242 from 25 days of age culminates in some weight loss, dosing from 75 days of age does not. The precise reason for this is not known. However, it has been shown previously using both pharmacological and genetic approaches that mGlu<sub>5</sub> modulates central reward pathways in rodents and that reducing mGlu<sub>5</sub> activity suppresses appetite (Bradbury et al. 2004). Perhaps the HTL0014242 mediated weight loss observed in the 25D cohort is caused by a sustained reduction in mGlu<sub>5</sub> activity that is related to the mice being juvenile.

Catwalk gait analysis was measured at several time points before onset of visible signs of disease and throughout the disease course (Figure 6.6). However, the catwalk data obtained from this study for the vehicle group were inconsistent with historical vehicle control data across all the parameters investigated. For example, the survival study catwalk data suggested that vehicle control group motor coordination improved with disease progression. Considering the lack of reproducibility between the past and current vehicle data and the observation that motor function improved with time for the vehicle control group, the data obtained by catwalk gait analysis for the survival study were deemed inconclusive.

Finally, the mean time taken to reach the humane-end point was recorded for each dose group to determine whether dosing with 30mg/kg HTL0014242 from 25 days of age versus 75 days of age improved survival (Figure 6.7). Survival curves plotted for the vehicle, 25D cohort and 75D cohort mice showed no overall significant difference

between dose groups (Figure 6.7b). Interestingly, logrank test for trend demonstrated that there was a significant survival trend across the data set, that is that the survival of the 75D cohort was greater than that of the vehicle group which was greater than that of the 25D cohort.

Of note, the differences between the dose groups for the parameters measured throughout the survival study seem to collapse at the end-stage of disease. For example, the 75D cohort mice demonstrate a delay in onset of visible signs of disease, significant improvements in motor performance on rotarod both at intermediate and late stages of disease and most impressively of all, a 3-week extension in the time taken to reach a score of 0 on rotarod. However, in terms of survival the 75D cohort only demonstrate a 4-6 day difference compared to the vehicle group and 25D cohort, respectively. One explanation for this phenomenon could be that the severity of the disease accelerates exponentially. It has previously been shown that SOD1 aggregation proceeds exponentially in *SOD1<sup>G93A</sup>* mice and in this case the driver of cell death also proceeds exponentially (Lang et al. 2015). Consequently, any therapeutic strategy other than reducing SOD1 levels will eventually be overcome. In our *SOD1<sup>G93A</sup>* mouse model the burden of exponential SOD1 aggregation will be more pronounced as *SOD1* is massively overexpressed.

### **6.3.2 Glial staining in ventral horns of lumbar spinal cord sections collected from dose-response study at 90 days**

Consistent with the findings from the 90D dose response study, dosing with 30mg/kg HTL0014242 from 25 days of age resulted in both reduced GFAP and Iba1 staining in 90-day old ventral horns of lumbar SC (Figure 6.8 and Figure 6.9). As shown previously in the 90D dose-response study, dosing with 30mg/kg HTL0014242 from 25 days of age had a more profound effect on astrocyte activation than microglial activation at 90 days of age. Interestingly, dosing with 30mg/kg HTL0014242 from 75 days of age also resulted in a reduction of both GFAP and Iba1 staining in 90-day old lumbar SC. This suggests that dosing HTL0014242 at 30mg/kg for 15 days (from 75 days of age through to 90 days of age), is sufficient to reduce glial activation in lumbar SC ventral horns. Glial staining was also quantified in the ventral horns of non-transgenic lumbar SC sections at 90 days of age. As expected, both GFAP and Iba1 staining were reduced in non-transgenic ventral horns compared to that of vehicle control mice. Furthermore, whilst dosing with HTL0014242 from both 25 days of age and 75 days of age reduced glial staining to levels comparable with that observed in non-transgenic ventral horns, there was a trend for the ventral horns of non-

transgenic mice to display even less glial staining than that of the 25D cohort and 75D cohort.

Somewhat surprising was that dosing with HTL0014242 from both 25 days of age and 75 days of age reduced glial activation in ventral horns of lumbar SC sections at 90 days of age, yet only the 75D cohort mice demonstrated beneficial effects in terms of a delayed onset of visible signs of disease and significant improvements in motor performance as seen on rotarod. This either suggests that the beneficial effects observed for the 75D cohort are not related to the reduction in SC glial activation at 90 days of age or alternatively that there is a critical time point during the disease trajectory at which reducing mGlu<sub>5</sub> activity and in turn reducing glial activation is beneficial.

Interestingly, it has been shown previously that both microglia and astrocytes can exist in a classically activated state, termed M1 or A1 respectively, or an alternatively activated state, termed M2 or A2 respectively (Henkel et al. 2009; Liddelow et al. 2017a). Whilst M1 and A1 glial cells are associated with a neurotoxic phenotype, M2 and A2 glial cells have a neuroprotective phenotype. For example, classically activated microglia (M1) and astrocytes (A1) highly upregulate several classical complement cascade genes and secrete pro-inflammatory molecules inducing neuronal cell death. In contrast, the alternatively activated microglia (M2) and astrocytes (A2) upregulate several neurotrophic factors and secrete anti-inflammatory molecules which promote neuronal survival and repair (Henkel et al. 2009; Chhor et al. 2013; Liddelow et al. 2017a).

Of note, it has been shown that mutant *SOD1* expressing microglia isolated from mice at disease onset have a phenotypic profile consistent with the M2 protective activation state, whereas microglia isolated at end-stage display a M1 neurotoxic phenotype (Liao et al. 2012). There is a body of evidence in support of a phenotypic transformation of microglia from a neuroprotective to a neurotoxic state during the MND disease trajectory. However rather than microglial cells switching from one activation state to the other at a specific time point during the disease course, the phenotypic transformation has been characterised as a continuum between the two polar activation states (Liao et al. 2012). With similar reports of astrocytes existing in two distinct activation states (Liddelow et al. 2017a), it is conceivable that astrocytes may too undergo a shift in their phenotype with disease progression. However, more research is needed to confirm this hypothesis.

Considering that microglial activation in MND is a dynamic process between two polar phenotypes, the time point at which HTL0014242 dosing is commenced throughout the disease trajectory could be a fundamental component that determines efficacy. Consequently, this may serve in part to explain the differential efficacy observed for HTL0014242 when dosed from 25 days of age versus 75 days of age. For example, if glial activation has beneficial effects early in the disease course then dosing with HTL0014242 from 25 days of age was perhaps unfavourable as it would have served to reduce the protective effects mediated by glial activation. This may account for why the 25D cohort mice did not demonstrate any beneficial effects in terms of a delayed disease onset or improvements in motor function. In contrast, dosing with HTL0014242 from 75 days of age onwards may have had a more beneficial effect as this may have correlated with a stage in the disease course whereby the glial activation state had switched to a more neurotoxic phenotype. Consequently, reducing glial activation at this stage of the disease trajectory would have been protective. Further work to determine the different activation states of the glial cells at various stages throughout the *SOD1<sup>G93A</sup>* disease trajectory would help delineate when the best time point to commence dosing with HTL0014242 would be. For example, whilst the 75D cohort mice demonstrated a beneficial effect, it is conceivable that dosing with HTL0014242 at a later stage of the disease may demonstrate an even better effect.

Glial staining was also investigated in the ventral horns of lumbar SC collected at end-stage of disease (Figure 6.10 and Figure 6.11). Of note, GFAP staining area was increased in the ventral horns of all three dose groups at end-stage compared to 90 days of age. In some respects, it is not surprising that glial activation was elevated at end-stage as this could just be a reflection of the exponential progression of disease. Interestingly, there was a difference in glial staining between the different dose groups at end-stage. For example, GFAP staining area in the ventral horns of the 75D cohort was significantly increased at end-stage compared with that of the 25D cohort. In addition, Iba1 staining at end stage was significantly elevated in the ventral horns of the 75D cohort versus both the 25D cohort and the vehicle group. Overall, it seemed that glial activation was increased within ventral horns of the 75D cohort at end-stage. Whether this increase in glial staining observed within the ventral horns of the 75D cohort was beneficial or detrimental to cell survival is unclear. Of note the trend for glial activation at end-stage was comparable to the trend in survival. For example, whilst the 75D cohort mice demonstrated the most glial activation at end-stage followed by the vehicle group and then the 25D cohort, the same trend was observed

for survival (75D >vehicle >25D). Also, it was somewhat surprising that there was more glial activation in the ventral horns of the 75D cohort compared with the 25D cohort at end-stage of disease yet not at 90 days of age. Further investigation is needed to characterise the activation state of the glial cells at both 90 days of age and at end-stage of disease for each of the dose groups. This may help to delineate the changes in glial activation states during the *SOD1<sup>G93A</sup>* disease trajectory and how dosing with HTL0014242 at different time points may affect the glial activation states. From these data, it may be possible to determine the most appropriate time point for commencing HTL0014242 dosing.

Whilst GFAP and Iba1 are standard antibodies used for detecting glial activation in mouse SC tissue, it would be good practice to consolidate these findings with additional markers of astrocytic and microglial activation. For example, filament proteins other than GFAP are known to be upregulated in activated astrocytes such as vimentin, nestin and synemin (Garwood et al. 2017; Pekny & Nilsson 2005). Considering the larger body of evidence, beyond that of the 90D dose response study and survival study, that have demonstrated that inhibiting or knocking down mGlu<sub>5</sub> reduces glial activation in the *SOD1<sup>G93A</sup>* mouse model of MND (Rossi et al. 2008; D'Antoni et al. 2011; Bonifacino et al. 2017), it is highly likely that the observed findings for glial activation are valid.

### **6.3.3 Motor neuron counts in ventral horns of lumbar spinal cord sections collected at 90D and end-stage from the survival study**

Motor neuron counts at 90 days of age demonstrated that the 75D cohort had significantly more motor neurons present in lumbar SC ventral horns than the vehicle control group,  $p = <0.0328$  (Figure 6.12b). In light of this finding, it might be expected that the motor performance of the 75D cohort mice was better than the vehicle mice at ~90 days of age. Interestingly, the rotarod data (Figure 6.2) show that the 75D cohort mice performed significantly better than both the 25D cohort mice and vehicle dosed mice at ~10.5-12 weeks of age. Whilst 12 weeks is slightly before 90 days of age, the actual ages of the mice at this rotarod time point was plus or minus 3 days due to the study's staggered recruiting process. Therefore, some of the mice measured at 12 weeks would have been 87 days of age which is very close to the 90-day motor neuron time point.

The finding that the 75D cohort mice retained the most motor neurons (as seen by ChAT staining for motor neuron counts) at 90 days of age in lumbar SC sections was also confirmed by ChAT staining area. The 75D cohort mice had significantly more

ChAT staining in lumbar SC sections collected at 90 days of age compared to the vehicle group. Whilst the difference between the 75D cohort and the 25D cohort was not significant, there was a trend for increased ChAT staining area in the 75D cohort. This trend was also observed with the ChAT staining used to determine motor neuron counts per ventral horn.

It was interesting that there was a trend for increased number of motor neurons in 90D lumbar SC sections of the 75D cohort mice compared with the 25D cohort mice. As discussed previously, this may suggest that there is a specific window within the disease trajectory when inhibiting mGlu<sub>5</sub> activity is beneficial. For example, whilst blocking mGlu<sub>5</sub> activity from 75 days of age confers some protection to lumbar SC motor neurons, blocking mGlu<sub>5</sub> activity from 25 days of age does not. One explanation for the differential protection observed when dosing HTL0014242 at 25 days of age versus 75 days of age might relate to differences in the levels of glutamate at these two different time points. For example, at 75 days of age inhibiting mGlu<sub>5</sub> activity may protect motor neurons from excessive levels of glutamate, whereas at 25 days of age glutamate levels may not be as abundant and consequently blocking mGlu<sub>5</sub> activity at 25 days of age may not offer motor neurons the same benefit. In contrast, mGlu<sub>5</sub> blockade at 25 days of age may even be detrimental as it may inhibit physiological mGlu<sub>5</sub> mediated processes from taking place.

Motor neuron counts from lumbar SC ventral horns collected at end-stage of disease demonstrated that there was no significant difference between dose groups (Figure 6.12c). As expected, there were fewer motor neurons present in all dose groups at end-stage versus 90 days of age. Whilst there was no significant difference between the different dose groups in terms of the average number of motor neurons at end-stage in the ventral horns of lumbar SC sections, it is possible that significant differences would have been observed in other regions of the SC at end-stage. For example, the *SOD1*<sup>G93A</sup> mouse model follows a pattern of disease whereby hind limb paralysis precedes forelimb paralysis (Kanning et al. 2010). Consequently, whilst counting the average number of motor neurons in ventral horns of lumbar SC sections at 90 days of age seems rational, perhaps at end-stage of disease it would be more relevant to count the average number of motor neurons in the ventral horns of cervical SC sections.

Additional characterisation is needed to determine whether the motor neurons remaining in the ventral horns of lumbar SC sections at 90 days of age and at end-stage of the disease were functionally intact. Whilst motor neuron counts are useful

in evaluating preserved motor function at different stages of the disease course, ideally the entire neuromuscular unit would be investigated. For example, axon counts in nerve roots and neuromuscular junction staining in combination with quantifying the number of motor neuron cell bodies would be more indicative of preserved motor unit function. Furthermore, an electrophysiological study to compare compound muscle action potential (CMAP) amplitudes for the mice in the different dose groups, at various time points throughout the disease course, would be beneficial as a functional readout of motor innervation.

#### **6.3.4 Immunofluorescent staining with mGlu<sub>5</sub> and ChAT in ventral horns of lumbar spinal cord sections collected at 90D from survival study**

The ventral horns of the lumbar SC sections collected at 90 days of age were also stained with anti-mGlu<sub>5</sub> and anti-ChAT (Figure 6.13 and Figure 6.14, respectively). Interestingly, mGlu<sub>5</sub> staining was shown to be significantly elevated for the 75D cohort compared with both the vehicle group and 25D cohort at 90 days of age. This finding perhaps was not that surprising considering that there were significantly more motor neurons in 75D cohort ventral horns of lumbar SC sections at 90 days of age compared to that of both the 25D cohort and vehicle group and it was previously shown that mGlu<sub>5</sub> is co-expressed on motor neurons in ventral horns of 90D *SOD1<sup>G93A</sup>* mouse SC. However, looking at the mGlu<sub>5</sub> staining for the 75D cohort it appears to be expressed on fine axonal processes too, which was also noted in the initial characterisation of mGlu<sub>5</sub> expression (Chapter 3).

Presumably, the levels of mGlu<sub>5</sub> were similar between the 75D cohort and the vehicle group prior to 75 days of age. Therefore, dosing with HTL0014242 from 75 days of age onwards appears to have triggered a significant increase in mGlu<sub>5</sub> expression. One explanation for this increase in mGlu<sub>5</sub> expression could be related to the initial response to dosing with HTL0014242. For example, evidence shows that when opioid receptors are antagonised this can result in a temporary compensatory up-regulation of opioid receptor number (Yoburn et al. 1994). It is conceivable that therapeutic blockade of mGlu<sub>5</sub> with HTL0014242 causes an initial up-regulation of mGlu<sub>5</sub> receptors. However, following sustained HTL0014242 dosing the lack of mGlu<sub>5</sub> activity may cause mGlu<sub>5</sub> receptor expression to become down-regulated. Whether mGlu<sub>5</sub> levels remained increased in the 75D cohort compared to the other dose groups throughout the remainder of the disease course is unclear. For example, it is possible that dosing with HTL0014242 from 25 days of age also caused an initial up-regulation of mGlu<sub>5</sub> receptors which subsequently returned to baseline levels. To fully

comprehend this phenomenon, further investigation comparing mGlu<sub>5</sub> receptor levels at various stages of the *SOD1*<sup>G93A</sup> disease trajectory is needed.

In terms of HTL0014242 receptor pharmacology, if mGlu<sub>5</sub> expression increases at 90 days of age when HTL0014242 is dosed from 75 days of age, it is worth considering that mGlu<sub>5</sub> receptor occupancy (RO) at 90 days of age for the 75D cohort may be different from what was originally determined based on dosing from 25 days of age. For example, mGlu<sub>5</sub> RO measured at 90 days of age in the previous 90D dose-response study was determined by dosing with HTL0014242 from 25 days of age. Consequently, with an increase in mGlu<sub>5</sub> expression observed for the 75D cohort (Figure 6.13), the proportion of mGlu<sub>5</sub> receptors occupied by HTL0014242 at 90 days of age could be less for the 75D cohort than was measured previously. However, it is worth considering that the increase in mGlu<sub>5</sub> expression for the 75D cohort was observed within ventral horns of lumbar SC whereas mGlu<sub>5</sub> RO was measured in brain. For instance, whilst the 75D cohort demonstrated an increase in mGlu<sub>5</sub> expression within ventral horns of lumbar SC collected at 90 days of age, this does not necessarily translate into a global increase in mGlu<sub>5</sub> expression or even an overall increase in mGlu<sub>5</sub> expression in SC. This is especially the case when considering that in SC most of the mGlu<sub>5</sub> expression was observed in the dorsal horn (see Chapter 3).

ChAT staining area in 90-day old ventral horns of lumbar SC demonstrated a comparable trend to ChAT staining of motor neurons at 90 days of age. For example, most ChAT staining was observed within the ventral horns of the 75D cohort, followed by the 25D cohort and then the vehicle group (Figure 6.14). However, whilst the mean ChAT staining area was significantly increased in the 75D cohort versus the vehicle group, there was no significant difference in ChAT staining area between the 75D cohort and the 25D cohort or between the 25D cohort and the vehicle group. Considering the consistency in the findings demonstrated by ChAT staining area and ChAT staining for motor neuron counts, it is certainly convincing that dosing with HTL0014242 from 75 days of age seems to result in an increase in the number of preserved motor neurons in ventral horns of lumbar SC at 90 days of age.

### **6.3.5 [<sup>3</sup>H] M-MPEP binding assay to measure RO of mGlu<sub>5</sub> receptors by HTL0014242 in mouse brain collected from survival study at end-stage**

Radioligand binding experiments were used to measure RO in brain tissue collected at peak and trough HTL0014242 exposures for the 25D cohort and the 75D cohort at end-stage. The mean proportion of mGlu<sub>5</sub> receptors occupied in end-stage brain at peak HTL0014242 exposure for both the 25D cohort and the 75D cohort was 100%.

This confirms target engagement at end-stage is comparable whether 30mg/kg HTL0014242 is dosed from 25 days of age or 75 days of age. Furthermore, the 90D dose-response study demonstrated that the mean proportion of mGlu<sub>5</sub> receptors occupied in 90-day old brain at peak HTL0014242 exposure when HTL0014242 was dosed at 30mg/kg from 25 days of age was ~93%. Therefore, it would seem like target engagement is not altered between 90 days of age and end-stage when HTL0014242 at 30mg/kg is dosed from 25 days of age. The RO in 90-day old brain at peak HTL0014242 exposure when HTL0014242 is dosed at 30mg/kg from 75 days of age is unknown. However, based on the available evidence there is no reason to expect that it would not be similar to that for the 25D cohort.

The proportion of mGlu<sub>5</sub> receptors occupied by HTL0014242 in mouse brain membranes collected at peak HTL0014242 exposure were similar for the 25D cohort and the 75D cohort. However, there was much more variability amongst the individual mouse brain membranes when collected at trough HTL0014242 exposure (Figure 6.15). The variability for measured RO in brain at trough exposure was comparable with the measured concentrations of HTL0014242 at trough exposure in SC and brain (Table 6.1). This is comparable to findings from previous *in vivo* studies whereby variability of the data is increased at trough exposure versus peak exposure. This variability observed at trough exposure is thought to relate to differences in compound absorption between individual mice.

Both predicted RO in brain and SC at peak and trough HTL0014242 exposures broadly positively correlated with measured RO in brain at peak and trough exposures. However, whilst estimated RO in brain was more predictive of measured RO in brain at peak exposure, estimated RO in SC was more predictive of measured RO in brain at trough exposure. It has consistently been shown that the predictive capabilities of estimated RO in SC are not very representative of measured RO in brain. However, predicted RO in brain and SC is determined using an equation that relies on knowing the free fraction of HTL0014242 in brain and SC, respectively. Considering that HTL0014242 is a highly protein bound compound (e.g. the % free compound in SC was calculated as 0.04%), this could explain, in part, the disparity observed between predicted and measured RO. For example, it is possible that the equilibrium dialysis assay used by Pharmidex to calculate HTL0014242 free fraction was at the upper limit of detection and consequently with such a low value being measured it may not be very precise.

In summary, HTL0014242 dosed at 30mg/kg from 75 days of age delayed onset of visible signs of disease and improved motor performance at both early and late stages of the disease (as seen on rotarod). In addition, 75D cohort mice retained motor function for longer compared to both the vehicle and 25D cohort mice. However, the average time taken to reach the humane end-point demonstrated that overall there was no significant difference in survival between the different dose groups. Whilst the time taken to reach the humane end-point is the standard measure of survival, the fact that HTL0014242 preserved motor function of the 75D cohort mice well into end-stage of the disease, is an important consideration when considering the prospect of improving MND patients' quality of life. For example, the preserved motor function shown for the 75D cohort, as demonstrated by the extension in the time taken to reach a score of 0 on rotarod, is the most impressive therapeutic effect seen to date, within our *SOD1<sup>G93A</sup>* mouse model at such a late stage of the disease.

To conclude, dosing with HTL0014242 at 30mg/kg from 75 days of age delays onset of visible signs of disease, enhances motor performance at both early and late stages of the disease and improves motor function at end-stage of the disease in the *SOD1<sup>G93A</sup>* mouse model of MND. It seems that HTL0014242 exerts its therapeutic effect by inhibiting mGlu<sub>5</sub> activity and in turn reducing glial activation within the ventral horns of 90-day old lumbar SC, the timing of which seems to be crucial to observe efficacy.

**Table 6.2 Summary of the key survival study readouts**

Survival Study Readouts	Vehicle Control	25D Cohort (100 – 71.8% RO)	75D Cohort (100 - 78.8% RO)
Delayed onset of visible signs of disease	-	-	+
Increased number of motor neurons at 90D in SC	-	-	++
Increased mGlu <sub>5</sub> staining at 90D in SC	-	-	++
Reduction in GFAP staining at 90D in SC	-	++	++
Reduction in Iba1 staining at 90D in SC	-	+	+
Improvement in motor function as seen on rotarod	-	-	++
Effect on survival	-	-	-

- no effect; + moderate effect; ++ large effect

## 7 Discussion

### 7.1 mGlu<sub>5</sub> as a novel therapeutic target in the *SOD1*<sup>G93A</sup> mouse model of MND

Glutamate-mediated excitotoxicity and glial activation are recognised mechanisms of disease involved in both familial and sporadic cases of MND (Van Den Bosch et al. 2006; Heath & Shaw 2002; Gonzalez-Scarano & Baltuch 1999; Barbeito et al. 2004). It has previously been demonstrated that modulating mGlu<sub>5</sub> activity can attenuate both glutamate toxicity and glial activation in MND. Whilst the majority of this evidence stems from *in vitro* and *in vivo* mouse models of *SOD1* MND (Rossi et al. 2008; Giribaldi et al. 2013; D'Antoni et al. 2011; Milanese et al. 2014; Bonifacino et al. 2017), mGlu<sub>5</sub> activity has also been implicated in mediating astrocyte activation in human cases of MND (Anneser 2004).

Characterisation of mGlu<sub>5</sub> expression in our *SOD1*<sup>G93A</sup> mouse model of MND demonstrated that mGlu<sub>5</sub> was expressed on some of the motor neurons located in the ventral horns of lumbar spinal cord at 90 days of age, both in transgenic and control mouse tissue. In contrast to the literature, mGlu<sub>5</sub> was not found on astrocytes and microglial cells (Biber et al. 1999; Martorana et al. 2012; Aronica et al. 2001; Anneser et al. 2004). However, the work by Sun et al, (2013), which indicates that astrocytic mGlu<sub>5</sub> is developmentally regulated seems to be widely accepted in the field and despite Rossi et al. (2008), reporting that the beneficial effects of inhibiting mGlu<sub>5</sub> activity *in vivo* was a result of inhibiting astrocytic mGlu<sub>5</sub> activity, there is a lack of robust data to back this up. Interestingly, it has been demonstrated previously in adult human spinal cord post-mortem tissue that astrocytes weakly express mGlu<sub>5</sub> and that this expression is upregulated in patients with both sporadic and familial cases of MND (Aronica et al. 2001; Anneser et al. 2004). This points to increased expression of astrocytic mGlu<sub>5</sub> being a disease related feature of MND. However, this finding was not recapitulated in our *SOD1*<sup>G93A</sup> mouse model of MND. It is possible that this discrepancy was a result of the human astrocyte staining taking place in post-mortem SC tissue, whereas the astrocyte staining in the *SOD1*<sup>G93A</sup> mouse spinal cord took place in 90-day old tissue.

The expression of mGlu<sub>5</sub> was also characterised in human fibroblast derived iAstrocytes from MND patients with *SOD1* mutations and age matched healthy controls. Both the *SOD1* and control iAstrocytes showed weak expression of mGlu<sub>5</sub>, supporting the findings of Anneser et al. (2004), which demonstrated that control

human adult astrocytes express low levels of mGlu<sub>5</sub>. Whilst it was previously shown that mGlu<sub>5</sub> levels were upregulated on activated astrocytes in MND patients (Anneser et al. 2004; Aronica et al. 2001), there was no difference in mGlu<sub>5</sub> expression levels between the *SOD1* and control derived iAstrocytes. However, this may be ascribed to *SOD1* derived iAstrocytes not recapitulating an activated astrocyte profile that is perhaps reliant on the native architecture found *in vivo*.

Whilst there was conflicting evidence regarding mGlu<sub>5</sub> receptor level changes throughout the *SOD1*<sup>G93A</sup> disease trajectory (Martorana et al. 2012; Brownell et al. 2015), [<sup>3</sup>H] M-MPEP saturation binding experiments in whole brain demonstrated that there was no significant difference in mGlu<sub>5</sub> receptor levels between 30 days of age and 120 days of age in our *SOD1*<sup>G93A</sup> mouse model of MND. This does not rule out significant changes in mGlu<sub>5</sub> receptor levels within spinal cord tissue or brain regions known to be implicated in MND. Finally, the lack of a significant change in mGlu<sub>5</sub> receptor density, does not exclude the possibility that mGlu<sub>5</sub> receptor function is altered at various stages throughout the disease course.

In light of the finding that MPEP delayed onset and prolonged survival in the *SOD1*<sup>G93A</sup> mouse model of MND (Rossi et al. 2008), characterisation of the mGlu<sub>5</sub> NAM, HTL0014242, with its improved pharmacological properties for *in vivo* testing ensued. A pharmacokinetic (PK) study in the *SOD1*<sup>G93A</sup> mouse model of MND on the C57BL/6 inbred genetic background demonstrated that HTL0014242 has an excellent PK profile - good CNS exposure, long half-life and moderate clearance. HTL0014242 target engagement in *SOD1*<sup>G93A</sup> mouse brain following oral dosing with 10mg/kg of HTL0014242 was confirmed by *ex vivo* RO using a [<sup>3</sup>H] M-MPEP radioligand binding assay. The PK study was also instrumental in guiding a dosing strategy and design of an *in vivo* 90D dose-response study to investigate the efficacy of HTL0014242, at an intermediate stage of the disease in the *SOD1*<sup>G93A</sup> mouse model of MND.

HTL0014242 dosed at 3, 10 and 30mg/kg from 25 days of age onwards demonstrated a marginal improvement on motor function (as seen on rotarod), up to 90 days of age in the *SOD1*<sup>G93A</sup> mouse model of MND. However, unlike dosing with MPEP from 40 days of age or heterozygous knockdown of mGlu<sub>5</sub> from birth (Rossi et al. 2008; Bonifacino et al. 2017), HTL0014242 did not significantly delay onset of visible signs of disease. Considering that HTL0014242 dosed at 30mg/kg resulted in >90% receptor occupancy (RO) in brain at both peak and trough exposures of HTL0014242, clearly reducing mGlu<sub>5</sub> activity from 25 days of age does not affect onset of visible signs of disease in our *SOD1*<sup>G93A</sup> mouse model of MND. As Rossi et al. (2008) did

not demonstrate MPEP target engagement one cannot conclusively know whether the observed delay in disease onset in this study was a direct consequence of reducing mGlu<sub>5</sub> activity. This is especially the case, considering that MPEP dosed at 30mg/kg (the same dose used in the Rossi et al. (2008) study) has previously been shown to have significant analgesic effects in mGlu<sub>5</sub> knockout mice (Montana et al. 2009). Furthermore, differences in how the onset of disease was determined in addition to the different genetic backgrounds that the *SOD1*<sup>G93A</sup> mice were bred on, could be contributing factors for why heterozygous knockdown of mGlu<sub>5</sub> resulted in a delayed disease onset (Bonifacino et al. 2017), yet therapeutic blockade of >90% of mGlu<sub>5</sub> receptors from 25 days of age did not.

Interestingly, HTL0014242 dosed at 3,10 and 30mg/kg demonstrated a dose-dependent reduction in astrocyte activation in the ventral horns of mouse SC at 90 days of age and HTL0014242 dosed at 30mg/kg significantly reduced Iba1 staining in 90D SC. These findings suggest that mGlu<sub>5</sub> is implicated in astrocyte activation up to 90 days of age in the *SOD1*<sup>G93A</sup> mouse model of MND and perhaps to a lesser extent mGlu<sub>5</sub> may also be involved in microglial activation. This is particularly interesting as mGlu<sub>5</sub> was not detected on these cells, so the mechanism of activation is not occurring directly through activating mGlu<sub>5</sub>, but some other process linked to mGlu<sub>5</sub> inhibition. Bonifacino et al. (2017) also found that heterozygous knockdown of mGlu<sub>5</sub> expression reduced both astrocyte and microglial activation in the *SOD1*<sup>G93A</sup> mouse model of MND. Considering that the 90D dose response study demonstrated reduced glial activation yet no significant delay in disease onset, this would suggest that glial activation does not play a role in initiating disease onset. Consequently, the delayed disease onset observed by heterozygous knockdown of mGlu<sub>5</sub> expression must be the result of a different mechanism, independent of glial activation. The hypothesis that glial activation does not play a role in initiating disease onset is supported by several *in vivo* studies using mice carrying a Cre-lox deletable mutant *SOD1* gene (Boillee et al. 2006a; Yamanaka et al. 2008). For example, evidence shows that whilst deletion of mutant *SOD1* from microglial cells delays disease progression following the onset of disease, it had no effect on disease onset (Boillee et al. 2006a). Similarly, deletion of mutant *SOD1* from astrocytes was shown to delay disease progression and extend disease duration following disease onset (Yamanaka, Chun, et al. 2008). Of note, the evidence relating to whether mutant *SOD1* expressing astrocytes contribute to disease onset is conflicting and seems to be dependent on the *SOD1* mutant variant (Yamanaka, Chun, et al. 2008; Wang et al. 2011a). It has been shown that reduction of mutant *SOD1* in astrocytes can delay

microglial activation (Yamanaka, Chun, et al. 2008). This finding may offer some explanation as to why a reduction in microglial activation was only observed for the highest dose of HTL0014242 in the 90D dose-response study. For example, if astrocyte activation drives microglial activation then it seems logical that only at the highest dose of HTL0014242 where there is the biggest reduction in astrocyte activation would this translate as a significant reduction in microglial activation.

RO in brain for the 3,10 and 30mg/kg doses of HTL0014242 correlated well with the dose-dependent reduction in astrocyte activation demonstrating that this parameter was a good marker of HTL0014242 effect in the CNS. Furthermore, whilst HTL0014242 dosed at 30mg/kg reduced both astrocyte and microglial activation in 90D lumbar SC, it was found that riluzole dosed at ~70mg/kg did not affect glial activation in lumbar SC at 90 days. Riluzole and HTL0014242 therefore appear to have different mechanisms of action suggesting that co-dosing in a clinical context may lead to a synergistic benefit.

As the highest dose of HTL0014242 (30mg/kg) demonstrated >90% RO over a 24h period and significantly reduced both astrocyte and microglial activation in 90D lumbar SC, this dose was chosen to probe the role of mGlu<sub>5</sub> in later stages of the *SOD1*<sup>G93A</sup> disease course. Based on the evidence that mutant *SOD1* expression in glial cells drives disease progression following onset of disease, a survival study was designed to compare the effects of reducing glial activation from 25 days of age (25D cohort) versus 75 days of age (75D cohort). It was interesting to note that whilst both the 25D cohort and 75D cohort showed a significant reduction in glial activation in lumbar SC at 90 days of age, the 75D cohort mice demonstrated a delayed onset of visible signs of disease, the greatest increase in number of SC motor neurons at 90 days of age and an improvement in motor performance (as seen on rotarod) at both an intermediate and late stage of the disease. Furthermore, the 75D cohort mice displayed a 3-week extension in the retention of motor function compared to both the vehicle control group and the 25D cohort. The findings from the survival study suggest that the time point at which mGlu<sub>5</sub> activity is reduced is crucial to drive efficacy in the *SOD1*<sup>G93A</sup> mouse model of MND. Of note, the delayed onset of disease observed by Rossi et al. (2008) was achieved by dosing MPEP from 40 days of age in the *SOD1*<sup>G93A</sup> mouse model. It is likely that the beneficial effects of therapeutically blocking mGlu<sub>5</sub> activity can be observed when dosing is commenced between 40-75 days of age. It would be interesting to delineate the 'window of efficacy' within the *SOD1*<sup>G93A</sup> mouse model. For example, it is clear that the beneficial effect of reducing mGlu<sub>5</sub> activity is absent when this pathway is targeted from 25 days of age. Therefore,

at what point during the disease trajectory does targeting this pathway become efficacious?

One theory for why HTL0014242 has a differential effect depending on the point of intervention, stems from the phenomenon that glial cells can exist in different activation states throughout the *SOD1<sup>G93A</sup>* disease course (Henkel et al. 2009; Liddel et al. 2017a). For example, whilst it was shown that the phenotypic profile of mutant *SOD1* expressing microglia isolated from mice at disease onset were consistent with a protective M2 activation state, microglia isolated at end-stage displayed a neurotoxic M1 phenotype (Liao et al. 2012). If glial cells are protective early on in the disease course, it would make sense that reducing mGlu<sub>5</sub> activity and in turn reducing glial activation from 25 days of age may confer a negative effect on cell survival. In contrast, if most glial cells have undergone a phenotypic transformation to a neurotoxic activation state by 75 days of age, this could account for why reducing glial activation from 75 days of age promotes cell survival. Rather than there being a specific time-point at which the activation states of glial cells switch from one polar activation state to another, the phenotypic transformation has been characterised as a continuum between the two polar activation states (Liao et al. 2012). It would be worthwhile characterising the activation states of glial cells throughout the *SOD1<sup>G93A</sup>* disease course in order to determine the time point at which reducing glial activation is likely to result in the greatest benefit. Commencing HTL0014242 dosing at an even later time point may be even more beneficial if more glial cells have undergone a phenotypic transformation to a toxic activation state.

Intriguingly, the beneficial effects observed for the 75D cohort across several of the parameters measured throughout the survival study such as increased number of motor neurons at 90 days of age, improved motor performance on rotarod and a 3-week extension of motor function, all seem to collapse by the end-stage of the disease. There was no significant difference in survival between the different dose groups, with the 75D cohort only demonstrating a 4-6 day difference compared to the vehicle group and 25D cohort, respectively. It is possible that the collapsing efficacy observed for the 75D cohort may be due to the exponential acceleration of disease severity towards the end-stage of disease. It has been shown previously that *SOD1* aggregation advances exponentially in *SOD1<sup>G93A</sup>* mice and in doing so cell death also advances exponentially (Lang et al. 2015). As *SOD1* is considerably overexpressed in our *SOD1<sup>G93A</sup>* mouse model, the burden of exponential *SOD1* aggregation will be much more evident. Therefore, any therapeutic strategy other than reducing *SOD1* levels will eventually be overcome.

Rossi et al. (2008) and Bonifacino et al. (2017) demonstrated that 30mg/kg MPEP and genetic ablation of ~45% of mGlu<sub>5</sub> receptors respectively, prolonged survival of *SOD1<sup>G93A</sup>* mice on the mixed genetic background. As mentioned previously, MPEP dosed at 30mg/kg has been shown to have off-target effects and consequently it is possible that the extension in survival demonstrated by Rossi et al. (2008) was not a direct consequence of blocking mGlu<sub>5</sub> activity. MPEP has also been shown to interact with other glutamate receptors such as the NMDA receptor and mGlu<sub>4</sub>. The extension in survival demonstrated by Bonifacino et al. (2017) by heterozygous knockdown of mGlu<sub>5</sub> expression may be a consequence of having used a different genetic background of *SOD1<sup>G93A</sup>* mice to our *SOD1<sup>G93A</sup>* mouse model of MND. Alternatively, it is possible that reducing mGlu<sub>5</sub> expression from birth resulted in developmental changes that may have influenced the *SOD1<sup>G93A</sup>* disease course.

The findings from our survival study suggest that whilst dosing 30mg/kg HTL0014242 from 75 days of age delays onset of visible signs of disease, improves motor performance, reduces SC glial activation, increases SC motor neuron numbers and preserves motor function well into end-stage of disease, this therapeutic strategy does not extend survival in our *SOD1<sup>G93A</sup>* mouse model of MND. However, considering the preserved motor function shown for the 75D cohort, as demonstrated by the 3-week extension in the time taken to reach a score of 0 on the rotarod, the prospect of HTL0014242 dosed from 75 days of age in terms of improving MND patients' quality of life is an important consideration. This is especially the case when considering that this is the most impressive therapeutic effect seen to date, within our *SOD1<sup>G93A</sup>* mouse model at such a late stage of the disease.

## 7.2 Updated Hypothesis

It was initially hypothesised that astrocytic mGlu<sub>5</sub> plays a role in disease progression in the *SOD1<sup>G93A</sup>* mouse model of MND and that blocking astrocytic mGlu<sub>5</sub> activity with HTL0014242 would slow disease progression and extend survival of *SOD1<sup>G93A</sup>* transgenic mice. This hypothesis was based on the findings in the literature at the time which implicated elevated astrocytic expression of mGlu<sub>5</sub> on activated astrocytes as a disease specific feature of MND (Aronica et al. 2001; Anneser et al. 2004). Since then it has been demonstrated that mGlu<sub>5</sub> is not expressed on astrocytes and is only expressed on some SC motor neurons in our *SOD1<sup>G93A</sup>* mouse model of MND at 90 days of age. In consideration of this, it is now hypothesised that, whilst mGlu<sub>5</sub> plays a role in *SOD1<sup>G93A</sup>* disease progression it is likely mediated via motor neuronal mGlu<sub>5</sub> activity. Furthermore, it was demonstrated that HTL0014242 dosed from 75 days of

age slows disease progression but has no significant effect on survival in our *SOD1<sup>G93A</sup>* mouse model of MND. Most interesting of all, was the differential effect of HTL0014242 depending on when dosing was commenced. Clearly there is a critical time point during the *SOD1<sup>G93A</sup>* disease trajectory at which modulating mGlu<sub>5</sub> activity provides a beneficial effect. Further work is necessary to determine the mechanism by which HTL0014242 exerts its therapeutic effect. The next section will discuss some of the potential mechanisms considering the evidence in the literature.

### **7.3 Potential mechanisms by which HTL0014242 exerts its therapeutic effect**

It was interesting to note that dosing HTL0014242 from 75 days of age resulted in a delayed onset of visible signs of disease as well as an improvement in rotarod performance. Considering that the beneficial effect from dosing with HTL0014242 at 75 days of age was almost immediate, this may suggest that the effect was related to glutamate neurotransmission.

It is well documented that glutamate levels are elevated in the CNS of MND patients (Rothstein et al. 1991; Shaw et al. 1994; Shaw et al. 1995; Spreux-Varoquaux et al. 2002) and glutamate-mediated excitotoxicity is a recognised pathogenic mechanism in MND (Van Den Bosch et al. 2006; Heath & Shaw 2002). The excessive levels of glutamate are attributed to a combination of overstimulation of glutamate receptors and a failure to rapidly remove glutamate from the synapse. The astroglial excitatory amino acid transporter 2 (EAAT2/GLT-1) protein is the major glutamate reuptake transporter in the mammalian brain and its expression and function is impaired both in human MND cases and in rodent models of MND (Rothstein et al. 1995; Fray et al. 1998; Bendotti et al. 2001).

Ionotropic receptors such as AMPA receptors are responsible for mediating a large proportion of the initial response to glutamate-mediated excitotoxicity (Van Den Bosch et al. 2006), as unlike NMDA receptors they are not ligand-gated ion channels. The permeability of AMPA receptors to calcium and in turn their vulnerability to glutamate-mediated excitotoxicity is governed by the presence of a GluR2 subunit (Hollmann et al. 1991). Astrocytes are responsible for positively regulating AMPA expression of GluR2 subunits on motor neurons to protect them from glutamate-mediated excitotoxicity. However, mutant *SOD1* expressing astrocytes lose their ability to positively regulate calcium homeostasis within neighbouring motor neurons and consequently these motor neurons become more vulnerable to glutamate toxicity (Van Damme et al. 2007).

It is conceivable that reducing mGlu<sub>5</sub> activity by dosing with HTL0014242 may alleviate some of the burden ascribed to glutamate toxicity. For example, the beneficial effect observed by dosing HTL0014242 from 75 days of age onwards may be the result of reducing the response to excessive glutamate levels and/or reducing synaptic glutamate levels. Whilst group I mGlu receptors (mGlu<sub>1</sub> and mGlu<sub>5</sub>) are predominantly expressed post-synaptically, mGlu<sub>5</sub> autoreceptors are pre-synaptically expressed and facilitate glutamate release (Musante et al. 2008). It has also been shown by confocal microscopy that group I mGlu receptors are expressed pre-synaptically on synaptosomes from lumbar spinal cord of *SOD1<sup>G93A</sup>* and control mice (Giribaldi et al. 2013). Surprisingly, pre-synaptic group I mGlu receptors in the *SOD1<sup>G93A</sup>* mouse synaptosomes were found to be much more sensitive to the glutamate agonist 3,5-DHPG, in contrast to that of control mice (as shown in a dose-dependent manner by increasing the concentration of 3,5-DHPG). Activation of group I mGlu receptors produced an abnormal release of glutamate in the *SOD1<sup>G93A</sup>* mice compared to the group I mGlu receptors in control mice. Of note, the excessive release of glutamate was shown to be predominantly mediated by the mGlu<sub>5</sub> receptor (Giribaldi et al. 2013). The increased efficacy of group I mGlu receptor signalling appears to be a *SOD1<sup>G93A</sup>* disease-specific feature and an additional origin of excessive glutamate (see Figure 7.1).

It is possible that HTL0014242 prevents the abnormal release of glutamate mediated by the improved efficacy of pre-synaptic mGlu<sub>5</sub> signalling in SC motor neurons of *SOD1<sup>G93A</sup>* mice (summarised in Figure 7.1). Whilst there are other sources of abnormal glutamate release other than via mGlu<sub>5</sub> (for example mGlu<sub>1</sub>), blocking mGlu<sub>5</sub> activity may contribute to an overall reduction in glutamate neurotransmission to motor neurons. In turn this may result in decreased muscle fatigue and could account for the immediate delay in onset of visible signs of disease and the initial improvement in rotarod performance observed for the 75D cohort mice.

Prolonged blockade of mGlu<sub>5</sub> activity could promote motor neuron survival through reducing glutamate-mediated excitotoxicity. As mentioned previously, motor neurons in *SOD1<sup>G93A</sup>* mice express a high proportion of AMPA receptors that lack the GluR2 subunit, increasing the motor neuron's permeability to calcium ions (Van Den Bosch et al. 2006). Consequently motor neurons are much more vulnerable to glutamate toxicity mediated by Ca<sup>2+</sup>-permeable AMPA receptors (Van Den Bosch et al. 2000). Glutamate signalling results in an increased influx of calcium ions which, in combination with a reduced number of calcium buffering proteins, results in the transportation of cytoplasmic calcium ions into mitochondria (Lewinski & Keller 2005).

It has been shown previously that mitochondrial calcium overload drives pathological processes causing cell death (Duchen 2000). The increased efficacy of pre-synaptic mGlu<sub>5</sub> signalling in *SOD1<sup>G93A</sup>* mice (Giribaldi et al. 2013) may exacerbate glutamate-mediated excitotoxicity via the aforementioned Ca<sup>2+</sup>-permeable AMPA receptors expressed on motor neurons. HTL0014242 inhibition of pre-synaptic mGlu<sub>5</sub> signalling may attenuate the abnormal release of glutamate and in doing so reduce motor neuron cell death mediated by Ca<sup>2+</sup>-permeable AMPA receptors (summarised in Figure 7.2). This may explain why the 75D cohort mice demonstrated an increased number of SC motor neurons at 90 days of age and consequently a 3-week extension in motor function (as shown by the time taken to reach a score of 0 on rotarod).

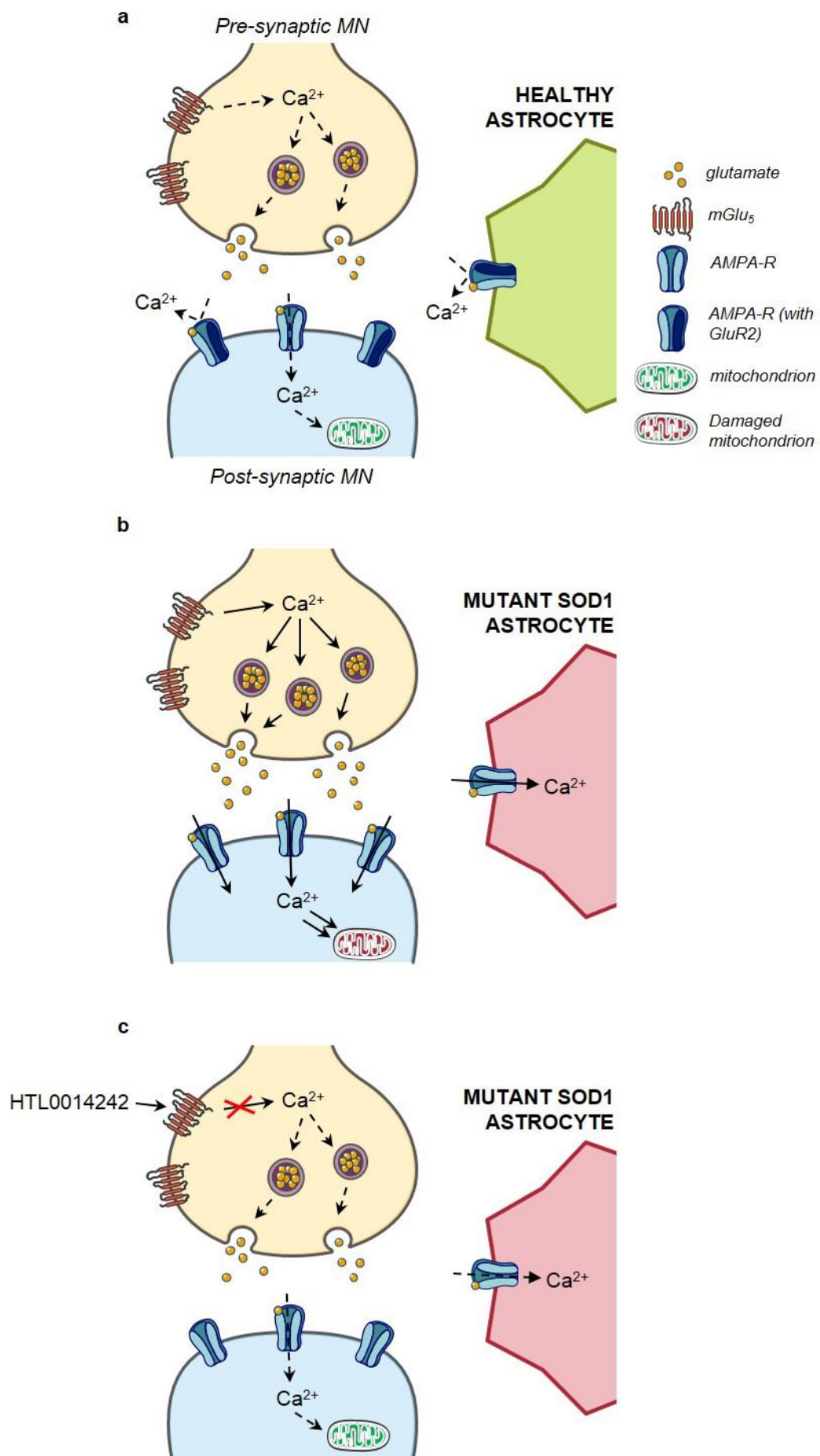


**Figure 7.1. Potential mechanism by which HTL0014242 exerts its therapeutic effect.** a) Under physiological conditions pre-synaptic mGlu<sub>5</sub> signalling results in downstream calcium signalling, which potentiates the release of intracellular glutamate stores from pre-synaptic membranes into the synaptic cleft. Healthy astrocytes are responsible for positively regulating AMPA expression of GluR2 subunits on motor neurons and this governs the cell's permeability to calcium ions. As the majority of AMPA receptors express the GluR2 subunit, the influx of calcium ions is limited, maintaining calcium homeostasis within the cell. b) *SOD1<sup>G93A</sup>* mice demonstrate improved efficacy of pre-synaptic group I mGlu receptor signalling which is predominantly mediated by the mGlu<sub>5</sub> receptor. The increased mGlu<sub>5</sub> signalling results in increased intracellular calcium signalling and consequently more glutamate is released into the synapse. Mutant SOD1 expressing astrocytes no longer positively express GluR2 subunit expression on AMPA receptors of neighbouring motor neurons and consequently these motor neurons become more vulnerable to glutamate toxicity mediated by Ca<sup>2+</sup>-permeable AMPA receptors. The increased influx of calcium ions results in the transportation of cytoplasmic calcium ions into mitochondria causing calcium overload and this triggers pathological processes culminating in cell death. c) HTL0014242 inhibition of pre-synaptic mGlu<sub>5</sub> signalling may reduce intracellular calcium signalling and attenuate the abnormal release of glutamate. In turn, this may reduce motor neuron cell death mediated by excessive calcium influx through Ca<sup>2+</sup>-permeable AMPA receptors. This figure illustrates one potential mechanism through which HTL0014242 could exert its therapeutic effect, which for simplicity only involves AMPA receptors. There are additional glutamate receptors other than AMPA receptors which contribute to calcium influx.

Why HTL0014242 dosing only led to a beneficial effect when dosed from 75 days of age versus 25 days of age is not fully understood. One explanation may relate to the fact that the 25D cohort mice are still juvenile and are able to compensate for a lack of mGlu<sub>5</sub> activity. mGlu<sub>5</sub> is known to modulate the activity and expression of other ionotropic glutamate receptors such as NMDA and AMPA receptors (reviewed by Sengmany & Gregory 2016). Whilst HTL0014242 may initially reduce glutamate-mediated neurotransmission through inhibiting mGlu<sub>5</sub> activity and modulating the activity of ionotropic glutamate receptors, sustained HTL0014242 dosing may trigger mGlu<sub>5</sub> independent mechanisms to compensate for the lack of activity at multiple glutamate receptors. Consequently, the 25D cohort mice may become desensitised to the effects of HTL0014242 at later stages of the disease course.

It is also possible that at 25 days of age glutamate levels are not in excess and there would be less of a burden ascribed to glutamate toxicity. Considering that glutamate is the major excitatory neurotransmitter in the CNS and is involved in a variety of different physiological processes (Alexander 2009), reducing glutamate activity from 25 days of age may prevent the beneficial functions of glutamate mediated neurotransmission. This could account for why inhibiting glutamate activity from 25 days of age was not found to offer any beneficial effect overall.

Finally, inhibiting mGlu<sub>5</sub> activity with HTL0014242 clearly reduces glial activation. Evidence suggests that glial activation is a complex and dynamic process. Whilst the initial response of glial cells to CNS injury may be one of neuroprotection, prolonged activation can cause the cells to take on a neurotoxic activation state (Sofroniew 2009; Henkel et al. 2009; Liddelow & Barres 2017b). If glial activation is protective at early stages in the *SOD1<sup>G93A</sup>* mouse model of MND, then reducing glial activation from 25 days of age may have been detrimental to motor neuron cell survival. In contrast, if glial activation is more toxic at later stages of the disease then reducing glial activation from 75 days of age may have beneficial effects in terms of motor neuron survival. Therefore, it is conceivable that the phenomenon whereby glial activation states undergo a phenotypic transformation throughout the disease trajectory may account (Liao et al. 2012), in part, for the differential effect of HTL0014242 observed between the 25D cohort and the 75D cohort.

HTL0014242 inhibition of mGlu<sub>5</sub> activity resulted in a reduction of SC glial activation at 90 days of age when dosed from both 25 and 75 days of age. This finding implicates a role for mGlu<sub>5</sub> activity in triggering glial activation. This is especially true of astrocyte activation considering that HTL0014242 demonstrated a dose dependent reduction

in GFAP staining in the 90D dose-response study. As mGlu<sub>5</sub> was expressed on motor neurons in our *SOD1<sup>G93A</sup>* mouse model of MND and not on glial cells, this would suggest that the mechanism by which HTL0014242 reduces glial activation involves mGlu<sub>5</sub> signalling via motor neurons (see Figure 7.2). It has previously been shown that glial cells actively participate in synaptic neurotransmission (Araque et al. 1999). For example, not only do glial cells express many of the receptors for the neurotransmitters in their surrounding area but they also express gliotransmitters which can activate neuronal receptors (Rossi & Volterra 2009b). Consequently, neuronal cells and glial cells can communicate with each other in a bidirectional manner. Of note glutamate is one of the molecular triggers of astrocyte activation (Sofroniew 2009). In this context, it is conceivable that abnormal glutamate release through increased efficacy of mGlu<sub>5</sub> signalling on pre-synaptic neurons is one of the drivers of astrocyte activation in the *SOD1<sup>G93A</sup>* mouse model of MND. Whilst astrocytes are normally resistant to glutamate-mediated toxicity, expression of mutant *SOD1* increases astrocyte vulnerability to extracellular glutamate (Van Den Bosch et al. 2006). Interestingly, microglial cells are said to be the least susceptible to glutamate-mediated toxicity as they only express glutamate receptors once activated (Matute et al. 2002). In the 90D dose-response study therapeutic blockade of mGlu<sub>5</sub> only reduced microglial activation at the highest dose of HTL0014242 (30mg/kg). It is well recognised that astrocyte activation can trigger microglial activation and vice-versa (Yamanaka et al. 2008; Liddel et al. 2017a). If astrocyte activation drives microglial activation in the *SOD1<sup>G93A</sup>* mouse model of MND this may account for why microglial activation was only reduced at the highest dose of HTL0014242. For example, when HTL0014242 was dosed at 30mg/kg astrocyte activation was reduced by 88% and consequently there would have been less activated astrocytes to drive activation of microglial cells.

Interestingly, the data from the survival study demonstrated that both GFAP and Iba1 staining area were increased in the ventral horns of all three dose groups at end-stage of the disease versus 90 days of age. Whilst increased efficacy of pre-synaptic mGlu<sub>5</sub> signalling may contribute to glutamate mediated activation of glial cells up to 90 days of age, considering that there are multiple sources that contribute to increased synaptic glutamate, it is possible that HTL0014242 inhibition of mGlu<sub>5</sub> signalling loses its effect on reducing glutamate mediated glial activation towards the end-stages of disease. When motor neurons undergo cell death they release their cellular contents of glutamate which may serve to exacerbate glutamate mediated activation of glial cells (summarised in Figure 7.2).

In addition to glutamate, there are other molecular triggers of glial activation. For example, ATP can also trigger astrocyte activation. It has been shown that dying motor neurons release ATP (Buffo et al. 2010). With increased motor neuron degeneration towards the end-stages of disease, levels of ATP may become elevated which could also serve to accelerate astrocyte activation (summarised in Figure 7.2). Finally, it is worth keeping in mind that mutant SOD1 contributes to other MND disease mechanisms other than glutamate-mediated excitotoxicity. This could explain, in part, why inhibiting mGlu<sub>5</sub> activity had a somewhat less profound effect on glial activation at the end-stage of the disease compared to at 90 days of age.

#### **7.4 Potential mechanism to explain the improved efficacy of pre-synaptic mGlu<sub>5</sub> signalling in *SOD1*<sup>G93A</sup> mice**

Prion diseases are caused by the spread of misfolded prion proteins and are characterised by progressive neurological dysfunction and neurodegeneration (Prusiner 1991). Cellular prion proteins interact with and form complexes with both mGlu<sub>1</sub> and mGlu<sub>5</sub> receptors (Um et al. 2013; Beraldo et al. 2011). Inhibition of both group I mGlu receptors in organotypic brain slice cultures dose-dependently reduced neurotoxicity mediated by aggregated prion proteins (Goniotaki et al. 2017). Furthermore, in a mouse model of prion disease the mGlu<sub>5</sub> negative allosteric modulator, MPEP, delayed onset of disease symptoms, slowed disease progression, reduced astrocyte activation and modestly extended survival (Goniotaki et al. 2017). It is thought that when cellular prion proteins interact with group I mGlu receptors they modulate the signalling activity of mGlu<sub>5</sub>, sensitising mGlu<sub>5</sub> receptors to synaptic glutamate and amplifying their response (Goniotaki et al. 2017). Of note, the mGlu<sub>5</sub> negative allosteric modulator, HTL0014242, dosed from 75 days of age similarly delayed onset of visible signs of disease onset, slowed motor decline and reduced astrocyte activation in the *SOD1*<sup>G93A</sup> mouse model of MND. Misfolded mutant SOD1 has been compared to the mutant cellular prion protein in that cell-to-cell protein propagation of misfolded SOD1 in MND has been described as a prion-like mechanism (Lee & Kim 2015). Perhaps in the *SOD1*<sup>G93A</sup> mouse model of MND, the mutant SOD1 protein interacts with group I mGlu receptors in a similar way to misfolded prion proteins. It is conceivable that mutant SOD1 forms complexes with mGlu<sub>5</sub> receptors and amplifies the receptors' signalling response (see Figure 7.2). As discussed previously, Giribaldi et al. (2013) found that synaptosomes from the lumbar spinal cord of *SOD1*<sup>G93A</sup> mice demonstrated improved efficacy of pre-synaptic group I mGlu receptor signalling, producing abnormal glutamate release. Of note, this

abnormal release of glutamate was found to be predominantly mediated by the mGlu<sub>5</sub> receptor. Whilst an interaction between the mutant SOD1 protein and the mGlu<sub>5</sub> receptor could potentially explain the improved efficacy of pre-synaptic mGlu<sub>5</sub> signalling in the *SOD1*<sup>G93A</sup> mouse model of MND, further work is necessary to validate this mechanism.

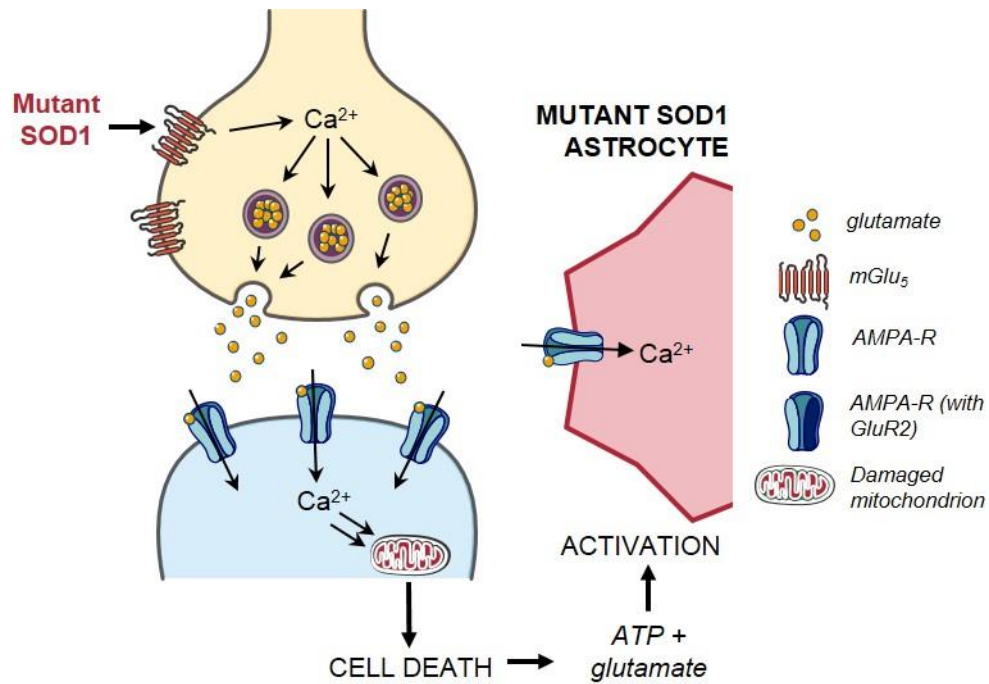


**Figure 7.2. Potential mechanism to explain how improved efficacy of pre-synaptic mGlu<sub>5</sub> signalling in *SOD1<sup>G93A</sup>* mice causes astrocyte activation.** It is possible that the mutant SOD1 protein interacts with mGlu<sub>5</sub> to increase the efficacy of mGlu<sub>5</sub> signalling on pre-synaptic neurons of *SOD1<sup>G93A</sup>* mice. Enhanced mGlu<sub>5</sub> signalling causes increased intracellular calcium signalling which results in more glutamate being released into the synapse. Not only are mutant SOD1 expressing astrocytes more vulnerable to extracellular glutamate levels (*glutamate is one of the molecular triggers of astrocyte activation*) but also, they are no longer able to positively regulate the expression of GluR2 subunits on AMPA receptors of neighbouring motor neurons. Consequently, these motor neurons become more vulnerable to glutamate toxicity mediated by Ca<sup>2+</sup>-permeable AMPA receptors. The increased influx of calcium ions results in the transportation of cytoplasmic calcium ions into mitochondria causing calcium overload and this results in cell death. When motor neurons undergo cell death they release their cellular contents of glutamate and ATP, both of which are molecular triggers of glial activation.

## 7.5 Future Directions

The efficacy of HTL0014242 in the *SOD1*<sup>G93A</sup> mouse model of MND has been investigated proving that dosing from 75 days of age delays onset of visible signs of disease and slows disease progression. Our data suggest that whilst HTL0014242 is unlikely to cure MND it does have the potential to improve patients' quality of life by preserving their motor function and slowing disease progression. Furthermore, HTL0014242 may even be capable of extending survival in human cases of MND. After all, to date HTL0014242 has only been tested in an aggressive model of MND (the *SOD1*<sup>G93A</sup> transgenic mouse model). Whilst these findings indicate that HTL0014242 has the potential to be applied as a novel disease-modifying therapy in the treatment of MND, further work is necessary to validate this mechanism within human models of MND.

The *SOD1*<sup>G93A</sup> mouse model of MND is one of the most widely used *in vivo* models for testing the efficacy of therapeutic compounds for use in MND patients. However, one of the long-standing questions remains and that is how well do the *SOD1*<sup>G93A</sup> transgenic mice model MND? One of the limitations with the *SOD1*<sup>G93A</sup> mouse model of MND is that the mutant *SOD1* transgene is massively overexpressed in the *SOD1*<sup>G93A</sup> mice. Whilst there are many shared similarities between the *SOD1*<sup>G93A</sup> disease in mice and human cases of *SOD1* MND, patients with MND only have one mutant *SOD1* allele. This difference may affect the interpretation of results from the *SOD1*<sup>G93A</sup> mouse model in terms of drawing parallels for the translation of the findings in mouse to human cases of the disease. Consequently, it would be useful to test the efficacy of HTL0014242 in a human derived model of MND.

Previously mGlu<sub>5</sub> expression was characterised in iAstrocytes derived from fibroblasts collected from patients with *SOD1* mutations and age matched healthy control patients. Of note, these cells are used in-house in a co-culture model with non-transgenic mouse motor neurons to investigate the toxicity towards motor neurons of iAstrocytes derived from MND patients versus healthy control iAstrocytes. However, to test our potential mechanism of disease which is proposed to be mediated via increased efficacy of mGlu<sub>5</sub> signalling on pre-synaptic neurons of *SOD1*<sup>G93A</sup> mice, it would be better to use both fibroblast derived astrocytes and fibroblast derived motor neurons from MND patients with *SOD1* mutations rather than motor neurons from *SOD1*<sup>G93A</sup> mice. This way, the co-culture system would recapitulate aspects associated with human *SOD1* MND and allow the efficacy of HTL0014242 in a human model of MND to be tested. If HTL0014242 is shown to

extend *SOD1* motor neuron survival it would also make sense to test the efficacy of HTL0014242 within the co-culture system using cells derived from MND patients with different causative genes (e.g. *C9ORF72* and *TDP43*) and also from sporadic MND patients. These findings would not only elucidate whether the mechanism by which HTL0014242 exerts its therapeutic effect in the *SOD1*<sup>G93A</sup> mouse model is applicable to human *SOD1* MND, but also whether it is relevant to the wider MND population. Furthermore, the co-culture system may also help to probe the functional mechanism by which HTL0014242 mediates its effect. It is worth noting that whilst mGlu<sub>5</sub> was not expressed on astrocytes within our *SOD1*<sup>G93A</sup> mouse model of MND, characterisation of mGlu<sub>5</sub> on iAstrocytes derived from MND patients with *SOD1* mutations demonstrated low level expression. Consequently, the mechanism by which HTL0014242 exerts its therapeutic effect may differ between the *SOD1*<sup>G93A</sup> mouse model of MND and human *SOD1* MND. In human *SOD1* MND, mGlu<sub>5</sub> signalling on both motor neurons and astrocytes may be involved in the disease mechanism targeted by HTL0014242.

As mentioned previously it is possible that the mutant *SOD1* protein interacts with mGlu<sub>5</sub> to improve the efficacy of mGlu<sub>5</sub> signalling on pre-synaptic neurons of *SOD1*<sup>G93A</sup> mice. Albeit somewhat controversial, there is evidence to suggest that *SOD1* misfolding is also a feature of sporadic MND (Haidet-Phillips et al. 2011; Bosco et al. 2010). If increased pre-synaptic mGlu<sub>5</sub> signalling is a mutant *SOD1* driven effect, HTL0014242 mediated inhibition of mGlu<sub>5</sub> signalling could be applicable to more than just the *SOD1* MND population. To investigate this potential interaction a co-immunoprecipitation assay could be performed using, for example, human embryonic kidney cells 293 (HEK-293) transiently transfected with human mGlu<sub>5</sub> and either human *SOD1* wild-type or mutant G93A. This would determine whether there are differences between the wild-type and mutant *SOD1* protein binding to mGlu<sub>5</sub>.

In order to establish whether the activation state of astrocytes changes throughout the *SOD1*<sup>G93A</sup> disease trajectory, the astrocyte transcriptome could be investigated at different stages of the disease. Liddel et al, (2017a) have previously demonstrated that A1 and A2 astrocyte activation states can be defined by their differential gene expression profiles. RNA- sequencing could be used to determine the transcriptome of spinal cord astrocytes at different time points throughout the *SOD1*<sup>G93A</sup> disease trajectory. Initially, *SOD1*<sup>G93A</sup> mice would need to be crossed with transgenic bacterial artificial chromosome (BAC) mice that express enhanced green fluorescent protein (EGFP) under the control of the S100 $\beta$  astrocytic marker promoter (methods described in Zhang et al. 2014b). Following this, spinal cords would be extracted from

the *SOD1*<sup>G93A</sup> transgenic mice at various time points throughout the disease course and a single cell suspension prepared. Astrocytes would then be isolated by fluorescent-activated cell sorting (FACS). Once the purified astrocytes are harvested the cell pellet could then be used for RNA extraction and sequencing to determine the astrocyte enriched genes.

Considering that HTL0014242 only demonstrated a beneficial effect when dosed from 75 days of age onwards, it would be useful to carry out a HTL0014242 dose-response study in the *SOD1*<sup>G93A</sup> mouse model of MND commencing at 75 days of age and dosing through to end-stage disease. Target occupancy in brain at end-stage of disease demonstrated that HTL0014242 dosed at 30mg/kg resulted in 100% mGlu<sub>5</sub> receptor occupancy (RO) at peak exposure. However, it would be useful to determine the lowest dose of HTL0014242 and in turn the lowest mGlu<sub>5</sub> RO required for HTL0014242 to demonstrate efficacy in the *SOD1*<sup>G93A</sup> mouse model of MND. For example, it may be possible to demonstrate HTL0014242 efficacy at a lower dose of HTL0014242 and therefore at a reduced mGlu<sub>5</sub> RO. This would be more desirable in terms of taking this compound into the clinic as it would limit the on-target side effects of HTL0014242.

Furthermore, it would also be worthwhile investigating whether dosing HTL0014242 concomitantly with riluzole from 75 days of age through to end-stage in the *SOD1*<sup>G93A</sup> mouse model of MND results in an improved benefit. For example, whilst HTL0014242 and riluzole are both thought to exert their therapeutic effect by reducing glutamate-mediated excitotoxicity, the previous co-dosing study suggests that these two compounds exert their effect through different mechanisms of action. Consequently, the two compounds dosed together may have a synergistic effect in reducing glutamate-mediated excitotoxicity. It could also be argued that dosing HTL0014242 concomitantly with riluzole is more clinically relevant as any compound used to treat patients with MND, from an ethical standpoint, would need to be dosed in combination with riluzole.

Before moving HTL0014242 from the *SOD1*<sup>G93A</sup> mouse model of MND into clinical trials, a pre-clinical toxicology assessment of HTL0014242 would need to be conducted. Assuming the toxicology assessment was promising, a phase I clinical trial could be designed to determine the receptor occupancy of HTL0014242 at the lowest efficacious dose in brains of healthy volunteers. For example, RO in brains of healthy volunteers following a dose of HTL0014242 could be determined using a positron emission tomography (PET) ligand for mGlu<sub>5</sub>, such as ([<sup>18</sup>F]F-PEB)

(characterised by Hamill et al. 2005). This would confirm mGlu<sub>5</sub> occupancy and validate the use of HTL0014242 at the chosen dose to probe the efficacy of blocking mGlu<sub>5</sub> activity in an MND patient population. The healthy volunteers would also be monitored closely for any side effects associated with HTL0014242.

Following on from this, a phase II clinical trial could be conducted to determine whether HTL0014242 has any therapeutic effect in an MND patient population. Zurcher et al. (2015), have previously used PET imaging to measure levels of activated microglia using the PET ligand, [<sup>11</sup>C] PBR28. They found that patients with MND demonstrate increased *in vivo* microglial activation versus healthy volunteers. Interestingly, they also found that microglial activation in the motor cortex of MND patients correlated with MND disease severity. Considering that HTL0014242 dosed at 30mg/kg in our *SOD1<sup>G93A</sup>* mouse model of MND consistently reduced microglial activation, the microglial PET ligand, [<sup>11</sup>C] PBR28, could potentially be used as a marker of HTL0014242 target engagement in the MND patient population. For example, any effect that is directly related to HTL0014242 should also demonstrate a reduction in the microglial PET ligand, [<sup>11</sup>C] PBR28, linking HTL0014242 to the observed beneficial effect.

## **7.6 Concluding remarks**

This project has broadened our understanding of the role mGlu<sub>5</sub> plays in MND and the therapeutic potential of HTL0014242. Clearly, mGlu<sub>5</sub> is involved in driving glial activation and HTL0014242 treatment can reduce this activation, particularly astrocyte activation. The therapeutic benefit from dosing at an intermediate stage of disease (75 days) versus an early stage (25 days of age) is in agreement with substantial evidence in the literature that glial activation is a driver of late stage disease and also suggests that the point of intervention is crucial, with an early intervention leading to no therapeutic benefit. Mice dosed with HTL0014242 from 75 days of age onwards showed a three-week extension in the time taken to fail on the rotarod test, demonstrating that HTL0014242 slows late stage disease progression in the *SOD1<sup>G93A</sup>* mouse model of MND. Whilst it seems unlikely that HTL0014242 will cure MND, our data demonstrate that HTL0014242 has a profound effect on SC glial activation at an intermediate stage of the disease and has the potential to preserve late stage motor function and in turn slow MND disease progression, improving MND patients' quality of life.

## 8 References

- Abe, T. et al., 1992. Molecular characterization of a novel metabotropic glutamate receptor mGluR5 coupled to inositol phosphate/Ca<sup>2+</sup> signal transduction. *The Journal of biological chemistry*, 267(19), pp.13361–8.
- Alexander, S.P.H., 2009. Glutamate. In *Encyclopedia of Neuroscience*. Elsevier, pp. 885–894.
- Alexianu, M.E., Kozovska, M. & Appel, S.H., 2001a. Immune reactivity in a mouse model of familial ALS correlates with disease progression. *Neurology*, 57(7), pp.1282–9.
- Alshikho, M.J. et al., 2018. Integrated magnetic resonance imaging and [ <sup>11</sup> C]-PBR28 positron emission tomographic imaging in amyotrophic lateral sclerosis. *Annals of Neurology*, 83(6), pp.1186–1197.
- Andrews, S.P., Brown, G.A. & Christopher, J.A., 2014. Structure-based and fragment-based GPCR drug discovery. *ChemMedChem*, 9(2), pp.256–75.
- Anneser, J.M. et al., 2004. Glial proliferation and metabotropic glutamate receptor expression in amyotrophic lateral sclerosis. *J Neuropathol Exp Neurol*, 63(8), pp.831–840.
- Anneser, J.M.H., Chahli, C. & Borasio, G.D., 2006. Protective effect of metabotropic glutamate receptor inhibition on amyotrophic lateral sclerosis-cerebrospinal fluid toxicity in vitro. *Neuroscience*, 141(4), pp.1879–86.
- Araque, A. et al., 1999. Tripartite synapses: glia, the unacknowledged partner. *Trends in Neurosciences*, 22(5), pp.208–215.
- Aronica, E. et al., 2001. Immunohistochemical localization of group I and II metabotropic glutamate receptors in control and amyotrophic lateral sclerosis human spinal cord: upregulation in reactive astrocytes. *Neuroscience*, 105(2), pp.509–520.
- Aronica, E. et al., 2000. Upregulation of metabotropic glutamate receptor subtype mGluR3 and mGluR5 in reactive astrocytes in a rat model of mesial temporal lobe epilepsy. *The European journal of neuroscience*, 12(7), pp.2333–44.

- Arundine, M. & Tymianski, M., 2003. Molecular mechanisms of calcium-dependent neurodegeneration in excitotoxicity. *Cell Calcium*, 34(4–5), pp.325–337.
- Balázs, R. et al., 1997. Metabotropic glutamate receptor mGluR5 in astrocytes: pharmacological properties and agonist regulation. *Journal of neurochemistry*, 69(1), pp.151–63.
- Barbeito, L.H. et al., 2004. A role for astrocytes in motor neuron loss in amyotrophic lateral sclerosis. *Brain Res Rev*, 47(1–3), pp.263–274.
- Barber, R.P. et al., 1984. The morphology and distribution of neurons containing choline acetyltransferase in the adult rat spinal cord: An immunocytochemical study. *The Journal of Comparative Neurology*, 229(3), pp.329–346.
- Barber, S.C. & Shaw, P.J., 2010. Oxidative stress in ALS: key role in motor neuron injury and therapeutic target. *Free radical biology & medicine*, 48(5), pp.629–41.
- Battaglia, G. & Bruno, V., 2018. Metabotropic glutamate receptor involvement in the pathophysiology of amyotrophic lateral sclerosis: new potential drug targets for therapeutic applications. *Current Opinion in Pharmacology*, 38, pp.65–71.
- Bear, M.F., Huber, K.M. & Warren, S.T., 2004. The mGluR theory of fragile X mental retardation. *Trends in Neurosciences*, 27(7), pp.370–377.
- Bellingham, M.C., 2011. A Review of the Neural Mechanisms of Action and Clinical Efficiency of Riluzole in Treating Amyotrophic Lateral Sclerosis: What have we Learned in the Last Decade? *CNS Neuroscience & Therapeutics*, 17(1), pp.4–31.
- Benatar, M., 2007. Lost in translation: treatment trials in the SOD1 mouse and in human ALS. *Neurobiology of disease*, 26(1), pp.1–13.
- Bendotti, C. et al., 2001. Transgenic SOD1 G93A mice develop reduced GLT-1 in spinal cord without alterations in cerebrospinal fluid glutamate levels. *J Neurochem*, 79(4), pp.737–746.
- Bennett, E.J. et al., 2014. Early Detection of Motor Dysfunction in the SOD1G93A Mouse Model of Amyotrophic Lateral Sclerosis (ALS) Using Home Cage Running Wheels T. H. Gillingwater, ed. *PLoS ONE*, 9(9), p.e107918.

- Bennett, K.A. et al., 2015. Structures of mGluRs shed light on the challenges of drug development of allosteric modulators. *Current Opinion in Pharmacology*, 20, pp.1–7.
- Bensimon, G., Lacomblez, L. & Meininger, V., 1994. A Controlled Trial of Riluzole in Amyotrophic Lateral Sclerosis. *New England Journal of Medicine*, 330(9), pp.585–591.
- Beraldo, F.H. et al., 2011. Metabotropic glutamate receptors transduce signals for neurite outgrowth after binding of the prion protein to laminin  $\gamma$ 1 chain. *The FASEB Journal*, 25(1), pp.265–279.
- Berg, D. et al., 2011. AFQ056 treatment of levodopa-induced dyskinesias: Results of 2 randomized controlled trials. *Movement Disorders*, 26(7), pp.1243–1250.
- Biber, K. et al., 1999. Expression and signaling of group I metabotropic glutamate receptors in astrocytes and microglia. *Journal of neurochemistry*, 72(4), pp.1671–80.
- Boillee, S. et al., 2006a. Onset and Progression in Inherited ALS Determined by Motor Neurons and Microglia. *Science*, 312(5778), pp.1389–1392.
- Boill e, S., Vande Velde, C. & Cleveland, D.W., 2006b. ALS: A Disease of Motor Neurons and Their Nonneuronal Neighbors. *Neuron*, 52(1), pp.39–59.
- Bonifacino, T. et al., 2017. In-vivo effects of knocking-down metabotropic glutamate receptor 5 in the SOD1G93A mouse model of amyotrophic lateral sclerosis. *Neuropharmacology*, 123, pp.433–445.
- De Bono, J.P. et al., 2006. Novel quantitative phenotypes of exercise training in mouse models. *American journal of physiology. Regulatory, integrative and comparative physiology*, 290(4), pp.R926-34.
- Van Den Bosch, L. et al., 2000. Ca<sup>2+</sup>-permeable AMPA receptors and selective vulnerability of motor neurons. *J Neurol Sci*, 180(1–2), pp.29–34.
- Van Den Bosch, L. et al., 2006a. The role of excitotoxicity in the pathogenesis of amyotrophic lateral sclerosis. *Biochimica et biophysica acta*, 1762(11–12), pp.1068–82.
- Bosco, D. a et al., 2010. Wild-type and mutant SOD1 share an aberrant conformation and a common pathogenic pathway in ALS. *Nature neuroscience*, 13(11), pp.1396–403.

- Boxall, S.J. et al., 1996. Metabotropic glutamate receptor activation contributes to nociceptive reflex activity in the rat spinal cord in vitro. *Neuroscience*, 74(1), pp.13–20.
- Bradbury, M.J. et al., 2004. Metabotropic Glutamate Receptor mGlu5 Is a Mediator of Appetite and Energy Balance in Rats and Mice. *Journal of Pharmacology and Experimental Therapeutics*, 313(1), pp.395–402.
- Brownell, A.-L. et al., 2015. PET imaging studies show enhanced expression of mGluR5 and inflammatory response during progressive degeneration in ALS mouse model expressing SOD1-G93A gene. *Journal of neuroinflammation*, 12, p.217.
- Bruijn, L.I. et al., 1997. ALS-Linked SOD1 Mutant G85R Mediates Damage to Astrocytes and Promotes Rapidly Progressive Disease with SOD1-Containing Inclusions. *Neuron*, 18(2), pp.327–338.
- Bruno, V. et al., 2001. Metabotropic glutamate receptor subtypes as targets for neuroprotective drugs. *Journal of cerebral blood flow and metabolism : official journal of the International Society of Cerebral Blood Flow and Metabolism*, 21(9), pp.1013–33.
- Bruno, V. et al., 2017. The impact of metabotropic glutamate receptors into active neurodegenerative processes: A “dark side” in the development of new symptomatic treatments for neurologic and psychiatric disorders. *Neuropharmacology*, 115, pp.180–192.
- Bryson, H.M., Fulton, B. & Benfield, P., 1996. Riluzole. A review of its pharmacodynamic and pharmacokinetic properties and therapeutic potential in amyotrophic lateral sclerosis. *Drugs*, 52(4), pp.549–63.
- Buffo, A., Rolando, C. & Ceruti, S., 2010. Astrocytes in the damaged brain: Molecular and cellular insights into their reactive response and healing potential. *Biochemical Pharmacology*, 79(2), pp.77–89.
- Chhor, V. et al., 2013. Characterization of phenotype markers and neuronotoxic potential of polarised primary microglia in vitro. *Brain, behavior, and immunity*, 32, pp.70–85.
- Chiò, A. et al., 2008. Prevalence of SOD1 mutations in the Italian ALS population. *Neurology*, 70(7), pp.533–7.

- Chiu, A.Y. et al., 1995. Age-Dependent Penetrance of Disease in a Transgenic Mouse Model of Familial Amyotrophic Lateral Sclerosis. *Molecular and Cellular Neuroscience*, 6(4), pp.349–362.
- Choi, D.W., 1988a. Calcium-mediated neurotoxicity: relationship to specific channel types and role in ischemic damage. *Trends in Neurosciences*, 11(10), pp.465–469.
- Choi, D.W., 1995. Calcium: still center-stage in hypoxic-ischemic neuronal death. *Trends in Neurosciences*, 18(2), pp.58–60.
- Choi, D.W., 1988b. Glutamate neurotoxicity and diseases of the nervous system. *Neuron*, 1(8), pp.623–34.
- Choi, D.W., 1985. Glutamate neurotoxicity in cortical cell culture is calcium dependent. *Neuroscience Letters*, 58(3), pp.293–297.
- Choi, D.W., 1987. Ionic dependence of glutamate neurotoxicity. *The Journal of neuroscience : the official journal of the Society for Neuroscience*, 7(2), pp.369–79.
- Christopher, J.A. et al., 2015. Fragment and Structure-Based Drug Discovery for a Class C GPCR: Discovery of the mGlu<sub>5</sub> Negative Allosteric Modulator HTL14242 (3-Chloro-5-[6-(5-fluoropyridin-2-yl)pyrimidin-4-yl]benzotrile). *Journal of Medicinal Chemistry*, 58(16), pp.6653–6664.
- Clement, a M. et al., 2003. Wild-type nonneuronal cells extend survival of SOD1 mutant motor neurons in ALS mice. *Science (New York, N.Y.)*, 302(5642), pp.113–117.
- Cole, P., 2012. Mavoglurant. *Drugs of the Future*, 37(1), p.7.
- Conn, P.J. & Pin, J.-P., 1997. PHARMACOLOGY AND FUNCTIONS OF METABOTROPIC GLUTAMATE RECEPTORS. *Annual Review of Pharmacology and Toxicology*, 37(1), pp.205–237.
- Cooper-Knock, J., Jenkins, T. & Shaw, P.J., 2013. Clinical and Molecular Aspects of Motor Neuron Disease. *Colloquium Series on Genomic and Molecular Medicine*, 2(2), pp.1-60.
- D'Antoni, S. et al., 2011. A prolonged pharmacological blockade of type-5 metabotropic glutamate receptors protects cultured spinal cord motor neurons against excitotoxic death. *Neurobiology of disease*, 42(3), pp.252–64.

- Van Damme, P. et al., 2005. Excitotoxicity and Amyotrophic Lateral Sclerosis. *Neurodegenerative Diseases*, 2(3–4), pp.147–159.
- Van Damme, P. et al., 2007. Astrocytes regulate GluR2 expression in motor neurons and their vulnerability to excitotoxicity. *Proceedings of the National Academy of Sciences of the United States of America*, 104(37), pp.14825–30.
- Debono, M.-W. et al., 1993. Inhibition by riluzole of electrophysiological responses mediated by rat kainate and NMDA receptors expressed in *Xenopus* oocytes. *European Journal of Pharmacology*, 235(2–3), pp.283–289.
- Doré, A.S. et al., 2014. Structure of class C GPCR metabotropic glutamate receptor 5 transmembrane domain. *Nature*, 511(7511), pp.557–62.
- Duchen, M.R., 2000. Mitochondria and calcium: from cell signalling to cell death. *The Journal of physiology*, 529 Pt 1(Pt 1), pp.57–68.
- Duffy, L.M. et al., 2011. Review: The role of mitochondria in the pathogenesis of amyotrophic lateral sclerosis. *Neuropathology and Applied Neurobiology*, 37(4), pp.336–352.
- Durham, T.B. & Blanco, M.-J., 2015. Target Engagement in Lead Generation. *Bioorganic & Medicinal Chemistry Letters*, 25(5), pp.998–1008.
- Egawa, N. et al., 2012. Drug screening for ALS using patient-specific induced pluripotent stem cells. *Science translational medicine*, 4(145), p.145ra104.
- Emmitte, K.A., 2013. mGlu<sub>5</sub> negative allosteric modulators: a patent review (2010 – 2012). *Expert Opinion on Therapeutic Patents*, 23(4), pp.393–408.
- Emmitte, K.A., 2011. Recent Advances in the Design and Development of Novel Negative Allosteric Modulators of mGlu<sub>5</sub>. *ACS Chemical Neuroscience*, 2(8), pp.411–432.
- Faul, F. et al., 2007. G\*Power 3: a flexible statistical power analysis program for the social, behavioral, and biomedical sciences. *Behavior research methods*, 39(2), pp.175–91.
- Ferraiuolo, L., Higginbottom, A., et al., 2011a. Dysregulation of astrocyte–motoneuron cross-talk in mutant superoxide dismutase 1-related amyotrophic lateral sclerosis. *Brain*, 134(9), pp.2627–2641.
- Ferraiuolo, L., Kirby, J., et al., 2011b. Molecular pathways of motor neuron injury in amyotrophic lateral sclerosis. *Nature reviews. Neurology*, 7(11), pp.616–30.

- Fischer, L.R., Culver, D.G., Tennant, P., Davis, A. a., et al., 2004. Amyotrophic lateral sclerosis is a distal axonopathy: evidence in mice and man. *Experimental Neurology*, 185(2), pp.232–240.
- Fray, A.E. et al., 1998. The expression of the glial glutamate transporter protein EAAT2 in motor neuron disease : an immunohistochemical study. , 10(February), pp.2481–2489.
- Frey, D. et al., 2000. Early and selective loss of neuromuscular synapse subtypes with low sprouting competence in motoneuron diseases. *The Journal of neuroscience : the official journal of the Society for Neuroscience*, 20(7), pp.2534–42.
- Garber, K.B., Visootsak, J. & Warren, S.T., 2008. Fragile X syndrome. *European journal of human genetics : EJHG*, 16(6), pp.666–72.
- Garwood, C.J. et al., 2017. Review: Astrocytes in Alzheimer's disease and other age-associated dementias: a supporting player with a central role. *Neuropathology and Applied Neurobiology*, 43(4), pp.281–298.
- Gasparini, F. et al., 1999. 2-Methyl-6-(phenylethynyl)-pyridine (MPEP), a potent, selective and systemically active mGlu5 receptor antagonist. *Neuropharmacology*, 38(10), pp.1493–1503.
- Geurts, J.J.G. et al., 2003. Altered expression patterns of group I and II metabotropic glutamate receptors in multiple sclerosis. *Brain*, 126(8), pp.1755–1766.
- Gibbs, K.L. et al., 2018. Inhibiting p38 MAPK alpha rescues axonal retrograde transport defects in a mouse model of ALS. *Cell death & disease*, 9(6), p.596.
- Di Giorgio, F.P. et al., 2008. Human embryonic stem cell-derived motor neurons are sensitive to the toxic effect of glial cells carrying an ALS-causing mutation. *Cell stem cell*, 3(6), pp.637–48.
- Giribaldi, F. et al., 2013. Group I metabotropic glutamate autoreceptors induce abnormal glutamate exocytosis in a mouse model of amyotrophic lateral sclerosis. *Neuropharmacology*, 66, pp.253–63.
- Goniotaki, D. et al., 2017. Inhibition of group-I metabotropic glutamate receptors protects against prion toxicity M. A. M. Prado, ed. *PLoS Pathogens*, 13(11), p.e1006733.

- Gonzalez-Scarano, F. & Baltuch, G., 1999. Microglia as mediators of inflammatory and degenerative diseases. *Annu Rev Neurosci*, 22, pp.219–240.
- Goodall, EF. Bury, JJ. Cooper-Knock, J., 2012. Genetics of Familial Amyotrophic Lateral Sclerosis. In M. Maurer, ed. *Amyotrophic Lateral Sclerosis*. Rijeka: Intech, pp. 517–36.
- Gordon, P.H., 2011. Amyotrophic lateral sclerosis: pathophysiology, diagnosis and management. *CNS drugs*, 25(1), pp.1–15.
- Gurney, M., Pu, H. & Chiu, A., 1994. Motor neuron degeneration in mice that express a human Cu, Zn superoxide dismutase mutation. *Science*, 264(5166), pp.1772–1775.
- Gurney, M.E. et al., 1996. Benefit of Vitamin E, N-methyl-D-aspartate receptor antagonist, and babapenun in a Transgenic Model of Familial Amyotrophic Lateral Sclerosis. *J Neurosci*, 16(1), pp.147–157.
- Haidet-Phillips, A.M. et al., 2011. Astrocytes from familial and sporadic ALS patients are toxic to motor neurons. *Nature Biotechnology*, 29(9), pp.824–828.
- Hall, E.D., Oostveen, J.A. & Gurney, M.E., 1998. Relationship of microglial and astrocytic activation to disease onset and progression in a transgenic model of familial ALS. *Glia*, 23(3), pp.249–56.
- Hamill, T.G. et al., 2005. Synthesis, characterization, and first successful monkey imaging studies of metabotropic glutamate receptor subtype 5 (mGluR5) PET radiotracers. *Synapse*, 56(4), pp.205–216.
- Hardiman, O. et al., 2017a. Amyotrophic lateral sclerosis. *Nature Reviews Disease Primers*, 3, p.17085.
- Hardiman, O. & van den Berg, L.H., 2017b. Edaravone: a new treatment for ALS on the horizon? *The Lancet. Neurology*, 16(7), pp.490–491.
- Harras, M.M. et al., 2008. SOD1 mutations disrupt redox-sensitive Rac regulation of NADPH oxidase in a familial ALS model. *Journal of Clinical Investigation*, 118(2).
- Heath, P.R. & Shaw, P.J., 2002. Update on the glutamatergic neurotransmitter system and the role of excitotoxicity in amyotrophic lateral sclerosis. *Muscle & nerve*, 26(4), pp.438–58.

- Heiman-Patterson, T.D. et al., 2011. Effect of genetic background on phenotype variability in transgenic mouse models of amyotrophic lateral sclerosis: A window of opportunity in the search for genetic modifiers. *Amyotrophic Lateral Sclerosis*, 12(2), pp.79–86.
- Heneka, M.T., Rodríguez, J.J. & Verkhratsky, A., 2010. Neuroglia in neurodegeneration. *Brain Research Reviews*, 63(1–2), pp.189–211.
- Henkel, J.S. et al., 2009. Microglia in ALS: The Good, The Bad, and The Resting. *Journal of Neuroimmune Pharmacology*, 4(4), pp.389–398.
- Hollmann, M., Hartley, M. & Heinemann, S., 1991. Ca<sup>2+</sup> permeability of KA-AMPA-gated glutamate receptor channels depends on subunit composition. *Science*, 252(5007), pp.851–853.
- Howland, D.S. et al., 2002. Focal loss of the glutamate transporter EAAT2 in a transgenic rat model of SOD1 mutant-mediated amyotrophic lateral sclerosis (ALS). *Proceedings of the National Academy of Sciences*, 99(580), pp.1604–1609.
- Hughes, Z.A. et al., 2013. Negative allosteric modulation of metabotropic glutamate receptor 5 results in broad spectrum activity relevant to treatment resistant depression. *Neuropharmacology*, 66, pp.202–214.
- Ilieva, H., Polymenidou, M. & Cleveland, D.W., 2009. Non-cell autonomous toxicity in neurodegenerative disorders: ALS and beyond. *The Journal of cell biology*, 187(6), pp.761–72.
- Ince, P. et al., 1993. Parvalbumin and calbindin D-28k in the human motor system and in motor neuron disease. *Neuropathology and Applied Neurobiology*, 19(4), pp.291–299.
- Ito, H. et al., 2008. Treatment with edaravone, initiated at symptom onset, slows motor decline and decreases SOD1 deposition in ALS mice. *Experimental Neurology*, 213(2), pp.448–455.
- Joly, C. et al., 1995. Molecular, functional, and pharmacological characterization of the metabotropic glutamate receptor type 5 splice variants: comparison with mGluR1. *The Journal of neuroscience : the official journal of the Society for Neuroscience*, 15(5 Pt 2), pp.3970–81.

- Kalgutkar, A. et al., 2005. A Comprehensive Listing of Bioactivation Pathways of Organic Functional Groups. *Current Drug Metabolism*, 6(3), pp.161–225.
- Kanning, K.C., Kaplan, A. & Henderson, C.E., 2010. Motor neuron diversity in development and disease. *Annual review of neuroscience*, 33(March), pp.409–440.
- Kawamata, T. et al., 1992. Immunologic reactions in amyotrophic lateral sclerosis brain and spinal cord tissue. *The American journal of pathology*, 140(3), pp.691–707.
- Kilkenny, C. et al., 2010. Improving Bioscience Research Reporting: The ARRIVE Guidelines for Reporting Animal Research. *PLoS Biology*, 8(6), p.e1000412.
- Kirby, A. et al., 2018. Caudal-rostral progression of alpha motoneurone degeneration in the SOD1G93A mouse model of amyotrophic lateral sclerosis. *European Journal of Neuroscience*.
- Klivenyi, P. et al., 1999. Neuroprotective effects of creatine in a transgenic animal model of amyotrophic lateral sclerosis. *Nat Med*, 5(3), pp.347–350.
- Kretschmer, B.D., Kratzer, U. & Schmidt, W.J., 1998. Riluzole, a glutamate release inhibitor, and motor behavior. *Naunyn-Schmiedeberg's archives of pharmacology*, 358(2), pp.181–90.
- Lacomblez, L. et al., 1996. Dose-ranging study of riluzole in amyotrophic lateral sclerosis. Amyotrophic Lateral Sclerosis/Riluzole Study Group II. *Lancet (London, England)*, 347(9013), pp.1425–31.
- Lagerström, M.C. & Schiöth, H.B., 2008. Structural diversity of G protein-coupled receptors and significance for drug discovery. *Nature reviews. Drug discovery*, 7(4), pp.339–57.
- Lang, L. et al., 2015. SOD1 aggregation in ALS mice shows simplistic test tube behavior. *Proceedings of the National Academy of Sciences of the United States of America*, 112(32), pp.9878–83.
- Lasiene, J. & Yamanaka, K., 2011. Glial cells in amyotrophic lateral sclerosis. *Neurology research international*, 2011, p.718987.
- Lea, P.M. & Faden, A.I., 2006. Metabotropic Glutamate Receptor Subtype 5 Antagonists MPEP and MTEP. *CNS Drug Reviews*, 12(2), pp.149–166.
- Lea, P.M., Movsesyan, V.A. & Faden, A.I., 2009. Neuroprotective activity of the

- mGluR5 antagonists MPEP and MTEP against acute excitotoxicity differs and does not reflect actions at mGluR5 receptors. *British Journal of Pharmacology*, 145(4), pp.527–534.
- Lee, S. & Kim, H.-J., 2015. Prion-like Mechanism in Amyotrophic Lateral Sclerosis: are Protein Aggregates the Key? *Experimental neurobiology*, 24(1), pp.1–7.
- Lewerenz, J. & Maher, P., 2015. Chronic Glutamate Toxicity in Neurodegenerative Diseases-What is the Evidence? *Frontiers in neuroscience*, 9, p.469.
- Lewinski, F. von & Keller, B.U., 2005. Ca<sup>2+</sup>, mitochondria and selective motoneuron vulnerability: implications for ALS. *Trends in Neurosciences*, 28(9), pp.494–500.
- Liao, B. et al., 2012. Transformation from a neuroprotective to a neurotoxic microglial phenotype in a mouse model of ALS. *Experimental neurology*, 237(1), pp.147–52.
- Liddel, S.A. et al., 2017a. Neurotoxic reactive astrocytes are induced by activated microglia. *Nature*, 541(7638), pp.481–487.
- Liddel, S.A. & Barres, B.A., 2017b. Reactive Astrocytes: Production, Function, and Therapeutic Potential. *Immunity*, 46(6), pp.957–967.
- Lill, C.M. et al., 2011. Keeping up with genetic discoveries in amyotrophic lateral sclerosis: the ALSod and ALSGene databases. *Amyotrophic lateral sclerosis : official publication of the World Federation of Neurology Research Group on Motor Neuron Diseases*, 12(4), pp.238–49.
- Lin, H.-H., 2013. G-protein-coupled receptors and their (Bio) chemical significance win 2012 Nobel Prize in Chemistry. *Biomedical journal*, 36(3), pp.118–24.
- Lino, M.M., Schneider, C. & Caroni, P., 2002. Accumulation of SOD1 Mutants in Postnatal Motoneurons Does Not Cause Motoneuron Pathology or Motoneuron Disease. , 22(12), pp.4825–4832.
- Lobsiger, C.S. & Cleveland, D.W., 2007. Glial cells as intrinsic components of non-cell-autonomous neurodegenerative disease. *Nature neuroscience*, 10(11), pp.1355–60.
- Ludolph, A.C. et al., 2010. Guidelines for preclinical animal research in ALS/MND: A consensus meeting. *Amyotrophic lateral sclerosis : official publication of the World Federation of Neurology Research Group on Motor Neuron Diseases*,

11(1–2), pp.38–45.

Mackenzie, I.R., Rademakers, R. & Neumann, M., 2010. TDP-43 and FUS in amyotrophic lateral sclerosis and frontotemporal dementia. *The Lancet. Neurology*, 9(10), pp.995–1007.

Maguire, J.J., Kuc, R.E. & Davenport, A.P., 2012. Radioligand Binding Assays and Their Analysis. In Humana Press, Totowa, NJ, pp. 31–77.

Mancuso, R. et al., 2012. Effect of genetic background on onset and disease progression in the SOD1-G93A model of amyotrophic lateral sclerosis. *Amyotrophic Lateral Sclerosis*, 13(3), pp.302–310.

Marden, J.J. et al., 2007. Redox modifier genes in amyotrophic lateral sclerosis in mice. , 117(10), pp.2913–2919.

Martorana, F. et al., 2012. The BH4 domain of Bcl-X(L) rescues astrocyte degeneration in amyotrophic lateral sclerosis by modulating intracellular calcium signals. *Human molecular genetics*, 21(4), pp.826–40.

Mathiesen, J.M. et al., 2003. Positive allosteric modulation of the human metabotropic glutamate receptor 4 (hmGluR4) by SIB-1893 and MPEP. *British journal of pharmacology*, 138(6), pp.1026–30.

Mattiazzi, M. et al., 2002. Mutated human SOD1 causes dysfunction of oxidative phosphorylation in mitochondria of transgenic mice. *The Journal of biological chemistry*, 277(33), pp.29626–33.

Matus, S. et al., 2013. ER Dysfunction and Protein Folding Stress in ALS. *International journal of cell biology*, 2013, p.674751.

Matute, C. et al., 2002. Excitotoxicity in glial cells. *European Journal of Pharmacology*, 447(2–3), pp.239–246.

McDermott, C.J. & Shaw, P.J., 2008. Diagnosis and management of motor neurone disease. *BMJ (Clinical research ed.)*, 336(7645), pp.658–62.

Mead, R.J. et al., 2011. Optimised and rapid pre-clinical screening in the SOD1(G93A) transgenic mouse model of amyotrophic lateral sclerosis (ALS). *PloS one*, 6(8), p.e23244.

- Meehan, C.F. et al., 2010. Intrinsic properties of lumbar motor neurones in the adult G127insTGGG superoxide dismutase-1 mutant mouse in vivo: evidence for increased persistent inward currents. *Acta Physiologica*, 200(4), pp.361–376.
- Meldrum, B. & Garthwaite, J., 1990. Excitatory amino acid neurotoxicity and neurodegenerative disease. *Trends in pharmacological sciences*, 11(9), pp.379–87.
- Menzies, F.M., Ince, P.G. & Shaw, P.J., 2002. Mitochondrial involvement in amyotrophic lateral sclerosis. *Neurochem Int*, 40(6), pp.543–551.
- Meyer, K. et al., 2014. Direct conversion of patient fibroblasts demonstrates non-cell autonomous toxicity of astrocytes to motor neurons in familial and sporadic ALS. *Proceedings of the National Academy of Sciences*, 111(2), pp.829–832.
- Micheli, F., 2000. Methylphenylethynylpyridine (MPEP) Novartis. *Current opinion in investigational drugs (London, England : 2000)*, 1(3), pp.355–9.
- Milanese, M. et al., 2014. Knocking down metabotropic glutamate receptor 1 improves survival and disease progression in the SOD1(G93A) mouse model of amyotrophic lateral sclerosis. *Neurobiology of disease*, 64, pp.48–59.
- Miller, R. et al., 2003. Riluzole for amyotrophic lateral sclerosis (ALS)/motor neuron disease (MND). In R. Miller, ed. *Cochrane Database of Systematic Reviews*. Chichester, UK: John Wiley & Sons, Ltd, p. CD001447.
- Miller, S. et al., 1996. Exposure of astrocytes to thrombin reduces levels of the metabotropic glutamate receptor mGluR5. *Journal of neurochemistry*, 67(4), pp.1435–47.
- Miller, S., Romano, C. & Cotman, C.W., 1995. Growth factor upregulation of a phosphoinositide-coupled metabotropic glutamate receptor in cortical astrocytes. *The Journal of neuroscience : the official journal of the Society for Neuroscience*, 15(9), pp.6103–9.
- Montana, M.C. et al., 2009. The metabotropic glutamate receptor subtype 5 antagonist fenobam is analgesic and has improved in vivo selectivity compared with the prototypical antagonist 2-methyl-6-(phenylethynyl)-pyridine. *The Journal of pharmacology and experimental therapeutics*, 330(3), pp.834–43.
- Morikawa, K. et al., 2000. Structural basis of glutamate recognition by a dimeric

metabotropic glutamate receptor. *Nature*, 407(6807), pp.971–977.

Morrison, B.M. et al., 1996. Quantitative immunocytochemical analysis of the spinal cord in G86R superoxide dismutase transgenic mice: Neurochemical correlates of selective vulnerability. *The Journal of Comparative Neurology*, 373(4), pp.619–631.

Mullard, A., 2015. Fragile X disappointments upset autism ambitions. *Nature Reviews Drug Discovery*, 14(3), pp.151–153.

Münch, C. & Bertolotti, A., 2011. Self-propagation and transmission of misfolded mutant SOD1: Prion or prion-like phenomenon? *Cell Cycle*, 10(11), pp.1711–1711.

Musante, V. et al., 2008. Presynaptic mGlu1 and mGlu5 autoreceptors facilitate glutamate exocytosis from mouse cortical nerve endings. *Neuropharmacology*, 55(4), pp.474–82.

Nagai, M. et al., 2007. Astrocytes expressing ALS-linked mutated SOD1 release factors selectively toxic to motor neurons. *Nature neuroscience*, 10(5), pp.615–22.

Nakanishi, S., 1992. Molecular diversity of glutamate receptors and implications for brain function. *Science (New York, N. Y.)*, 258(5082), pp.597–603.

Neumann, M. et al., 2006. Ubiquitinated TDP-43 in frontotemporal lobar degeneration and amyotrophic lateral sclerosis. *Science (New York, N. Y.)*, 314(5796), pp.130–3.

Nicoletti, F. et al., 2011. Metabotropic glutamate receptors: from the workbench to the bedside. *Neuropharmacology*, 60(7–8), pp.1017–41.

Olney, J.W., 1969. Brain Lesions, Obesity, and Other Disturbances in Mice Treated with Monosodium Glutamate. *Science*, 164(3880), pp.719–721.

Orlando, L.R. et al., 2001. The Role of Group I and Group II Metabotropic Glutamate Receptors in Modulation of Striatal NMDA and Quinolinic Acid Toxicity. *Experimental Neurology*, 167(1), pp.196–204.

- Ozyurt, E. et al., 1988. Protective Effect of the Glutamate Antagonist, MK-801 in Focal Cerebral Ischemia in the Cat. *Journal of Cerebral Blood Flow & Metabolism*, 8(1), pp.138–143.
- Pekny, M. & Nilsson, M., 2005. Astrocyte activation and reactive gliosis. *Glia*, 50(4), pp.427–434.
- Perea, G., Navarrete, M. & Araque, A., 2009. Tripartite synapses: astrocytes process and control synaptic information. *Trends in Neurosciences*, 32(8), pp.421–431.
- Perrin, S., 2014. Preclinical research: Make mouse studies work. *Nature*, 507(7493), pp.423–425.
- Perry, T.L. et al., 1990. Amyotrophic lateral sclerosis: amino acid levels in plasma and cerebrospinal fluid. *Annals of neurology*, 28(1), pp.12–7.
- Pfohl, S.R., Halicek, M.T. & Mitchell, C.S., 2015. Characterization of the Contribution of Genetic Background and Gender to Disease Progression in the SOD1 G93A Mouse Model of Amyotrophic Lateral Sclerosis: A Meta-Analysis. *Journal of Neuromuscular Diseases*, 2(2), pp.137–150.
- Philips, T. & Rothstein, J.D., 2014. Glial cells in amyotrophic lateral sclerosis. *Experimental neurology*, 262 Pt B, pp.111–20.
- Pin, J.-P., Galvez, T. & Prézeau, L., 2003. Evolution, structure, and activation mechanism of family 3/C G-protein-coupled receptors. *Pharmacology & therapeutics*, 98(3), pp.325–54.
- Pin, J.P. et al., 1992. Alternative splicing generates metabotropic glutamate receptors inducing different patterns of calcium release in *Xenopus* oocytes. *Proceedings of the National Academy of Sciences of the United States of America*, 89(21), pp.10331–5.
- Pramatarova, A. et al., 2001. Neuron-specific expression of mutant superoxide dismutase 1 in transgenic mice does not lead to motor impairment. *J Neurosci*, 21(10), pp.3369–3374.
- Prusiner, S.B., 1991. Molecular biology of prion diseases. *Science (New York, N.Y.)*, 252(5012), pp.1515–22.
- Pun, S. et al., 2006. Selective vulnerability and pruning of phasic motoneuron axons in motoneuron disease alleviated by CNTF. *Nature Neuroscience*, 9(3),

pp.408–419.

Pun, S. et al., 2006. Selective vulnerability and pruning of phasic motoneuron axons in motoneuron disease alleviated by CNTF. *Nat Neurosci*, 9(3), pp.408–419.

Rao, S.D. & Weiss, J.H., 2004. Excitotoxic and oxidative cross-talk between motor neurons and glia in ALS pathogenesis. *Trends in neurosciences*, 27(1), pp.17–23.

Reaume, A.G. et al., 1996. Motor neurons in Cu/Zn superoxide dismutase-deficient mice develop normally but exhibit enhanced cell death after axonal injury. *Nature genetics*, 13(1), pp.43–7.

Renton, A.E., Chiò, A. & Traynor, B.J., 2014. State of play in amyotrophic lateral sclerosis genetics. *Nature neuroscience*, 17(1), pp.17–23.

Romano, C., van den Pol, A.N. & O'Malley, K.L., 1996. Enhanced early developmental expression of the metabotropic glutamate receptor mGluR5 in rat brain: protein, mRNA splice variants, and regional distribution. *The Journal of comparative neurology*, 367(3), pp.403–12.

Rosen, D.R. et al., 1993. Mutations in Cu/Zn superoxide dismutase gene are associated with familial amyotrophic lateral sclerosis. *Nature*, 362(6415), pp.59–62.

Rossi, D. et al., 2008. Focal degeneration of astrocytes in amyotrophic lateral sclerosis. *Cell death and differentiation*, 15(11), pp.1691–700.

Rossi, D. & Volterra, A., 2009a. Astrocytic dysfunction: Insights on the role in neurodegeneration. *Brain Research Bulletin*, 80(4–5), pp.224–232.

Rossi, D. & Volterra, A., 2009b. Astrocytic dysfunction: Insights on the role in neurodegeneration. *Brain Research Bulletin*, 80(4–5), pp.224–232.

Rothstein, J.D. et al., 1990. Abnormal excitatory amino acid metabolism in amyotrophic lateral sclerosis. *Annals of Neurology*, 28(1), pp.18–25.

Rothstein, J.D. et al., 1991. Excitatory amino acids in amyotrophic lateral sclerosis: An update. *Annals of Neurology*, 30(2), pp.224–225.

Rothstein, J.D. et al., 1995. Selective loss of glial glutamate transporter GLT-1 in

- amyotrophic lateral sclerosis. *Annals of neurology*, 38(1), pp.73–84.
- Sattler, R. & Tymianski, M., 2000. Molecular mechanisms of calcium-dependent excitotoxicity. *Journal of molecular medicine (Berlin, Germany)*, 78(1), pp.3–13.
- Schwarcz, R. et al., 1983. Quinolinic acid: an endogenous metabolite that produces axon-sparing lesions in rat brain. *Science*, 219(4582), pp.316–318.
- Scott, S. et al., 2008. Design, power, and interpretation of studies in the standard murine model of ALS. *Amyotrophic Lateral Sclerosis*, 9(1), pp.4–15.
- Sengman, K. & Gregory, K.J., 2016. Metabotropic glutamate receptor subtype 5: molecular pharmacology, allosteric modulation and stimulus bias. *British journal of pharmacology*, 173(20), pp.3001–17.
- Shaw, C.E., Al-Chalabi, A. & Leigh, N., 2001. Progress in the pathogenesis of amyotrophic lateral sclerosis. *Current Neurology and Neuroscience Reports*, 1(1), pp.69–76.
- Shaw, P.J. et al., 1995. CSF and plasma amino acid levels in motor neuron disease: elevation of CSF glutamate in a subset of patients. *Neurodegeneration : a journal for neurodegenerative disorders, neuroprotection, and neuroregeneration*, 4(2), pp.209–16.
- Shaw, P.J., 2005. Molecular and cellular pathways of neurodegeneration in motor neurone disease. *Journal of neurology, neurosurgery, and psychiatry*, 76(8), pp.1046–57.
- Shaw, P.J., Chinnery, R.M. & Ince, P.G., 1994. [3H]d-aspartate binding sites in the normal human spinal cord and changes in motor neuron disease: a quantitative autoradiographic study. *Brain Research*, 655(1–2), pp.195–201.
- Shimada, T. et al., 2007. Different mechanisms for inhibition of human cytochromes P450 1A1, 1A2, and 1B1 by polycyclic aromatic inhibitors. *Chemical research in toxicology*, 20(3), pp.489–96.
- Siklós, L. et al., 1996. Ultrastructural evidence for altered calcium in motor nerve terminals in amyotrophic lateral sclerosis. *Annals of Neurology*, 39(2), pp.203–216.
- Smith, D.A. et al., 2017. Relevance of Half-Life in Drug Design. *Journal of Medicinal Chemistry*, p.acs.jmedchem.7b00969.
- Sofroniew, M. V., 2009. Molecular dissection of reactive astrogliosis and glial scar

- formation. *Trends in Neurosciences*, 32(12), pp.638–647.
- Sperry, J.B. et al., 2012. A Robust Process for an mGluR5 Negative Allosteric Modulator: Difluoromethylation and Sonogashira Coupling on Large Scale. *Organic Process Research & Development*, 16(11), pp.1854–1860.
- Spreux-varoquaux, O. et al., 2002. Glutamate levels in cerebrospinal fluid in amyotrophic lateral sclerosis : a reappraisal using a new HPLC method with coulometric detection in a large cohort of patients. , 193, pp.73–78.
- Spreux-Varoquaux, O. et al., 2002. Glutamate levels in cerebrospinal fluid in amyotrophic lateral sclerosis: a reappraisal using a new HPLC method with coulometric detection in a large cohort of patients. *J Neurol Sci*, 193(2), pp.73–78.
- Sreedharan, J. et al., 2008. TDP-43 mutations in familial and sporadic amyotrophic lateral sclerosis. *Science (New York, N. Y.)*, 319(5870), pp.1668–72.
- Sun, W. et al., 2013. Glutamate-dependent neuroglial calcium signaling differs between young and adult brain. *Science (New York, N. Y.)*, 339(6116), pp.197–200.
- Tison, F. et al., 2016. A Phase 2A Trial of the Novel mGluR5-Negative Allosteric Modulator Dipraglurant for Levodopa-Induced Dyskinesia in Parkinson's Disease. *Movement Disorders*, 31(9), pp.1373–1380.
- Turner, M. et al., 2004. Evidence of widespread cerebral microglial activation in amyotrophic lateral sclerosis: an [11C](R)-PK11195 positron emission tomography study. *Neurobiology of Disease*, 15(3), pp.601–609.
- Tymianski, M. & Tator, C.H., 1996. Normal and abnormal calcium homeostasis in neurons: a basis for the pathophysiology of traumatic and ischemic central nervous system injury. *Neurosurgery*, 38(6), pp.1176–95.
- Um, J.W. et al., 2013. Metabotropic Glutamate Receptor 5 Is a Coreceptor for Alzheimer A $\beta$  Oligomer Bound to Cellular Prion Protein. *Neuron*, 79(5), pp.887–902.
- Venkatakrishnan, A.J. et al., 2013. Molecular signatures of G-protein-coupled receptors. *Nature*, 494(7436), pp.185–94.
- Verkerk, A.J. et al., 1991. Identification of a gene (FMR-1) containing a CGG repeat coincident with a breakpoint cluster region exhibiting length variation in fragile

- X syndrome. *Cell*, 65(5), pp.905–14.
- Verkhratsky, A., ORKAND, R.K. & KETTENMANN, H., 1998. Glial Calcium: Homeostasis and Signaling Function. *Physiological Reviews*, 78(1), pp.99–141.
- Vermeiren, C. et al., 2006. Loss of metabotropic glutamate receptor-mediated regulation of glutamate transport in chemically activated astrocytes in a rat model of amyotrophic lateral sclerosis. *Journal of Neurochemistry*, 96(3), pp.719–731.
- Wang, L. et al., 2009. The effect of mutant SOD1 dismutase activity on non-cell autonomous degeneration in familial amyotrophic lateral sclerosis. *Neurobiology of disease*, 35(2), pp.234–40.
- Wang, L., Gutmann, D.H. & Roos, R.P., 2011. Astrocyte loss of mutant SOD1 delays ALS disease onset and progression in G85R transgenic mice. *Human Molecular Genetics*, 20(2), pp.286–293.
- Watabe, A.M., Carlisle, H.J. & O'Dell, T.J., 2002. Postsynaptic Induction and Presynaptic Expression of Group 1 mGluR-Dependent LTD in the Hippocampal CA1 Region. *Journal of Neurophysiology*, 87(3), pp.1395–1403.
- Wood, J.D., Beaujeux, T.P. & Shaw, P.J., 2003. Protein aggregation in motor neurone disorders. *Neuropathology and Applied Neurobiology*, pp.529–545.
- Wu, D.C. et al., 2006. The inflammatory NADPH oxidase enzyme modulates motor neuron degeneration in amyotrophic lateral sclerosis mice. *Proc Natl Acad Sci U S A*.
- Xiao, Q. et al., 2007. Mutant SOD1<sup>G93A</sup> microglia are more neurotoxic relative to wild-type microglia. *Journal of Neurochemistry*, 102(6), pp.2008–2019.
- Yamanaka, K., Chun, S.J., et al., 2008a. Astrocytes as determinants of disease progression in inherited amyotrophic lateral sclerosis. *Nature neuroscience*, 11(3), pp.251–3.
- Yamanaka, K., Boillee, S., et al., 2008b. Mutant SOD1 in cell types other than motor neurons and oligodendrocytes accelerates onset of disease in ALS mice. *Proceedings of the National Academy of Sciences of the United States of America*, 105(21), pp.7594–9.

- Yoburn, B.C. et al., 1994. Opioid antagonist-induced receptor upregulation: effects of concurrent agonist administration. *Brain research bulletin*, 33(2), pp.237–40.
- Yoshino, H. & Kimura, A., 2006. Investigation of the therapeutic effects of edaravone, a free radical scavenger, on amyotrophic lateral sclerosis (Phase II study). *Amyotrophic Lateral Sclerosis*, 7(4), pp.247–251.
- Zalewska, M., Siara, M. & Sajewicz, W., G protein-coupled receptors: abnormalities in signal transmission, disease states and pharmacotherapy. *Acta poloniae pharmaceutica*, 71(2), pp.229–43.
- Zang, D.W. & Cheema, S.S., 2002. Degeneration of corticospinal and bulbospinal systems in the superoxide dismutase 1(G93A G1H) transgenic mouse model of familial amyotrophic lateral sclerosis. *Neuroscience letters*, 332(2), pp.99–102.
- Zerangue, N. & Kavanaugh, M.P., 1996. Flux coupling in a neuronal glutamate transporter. *Nature*, 383(6601), pp.634–637.
- Zhang, L. et al., 2014a. Discovery and Preclinical Characterization of 1-Methyl-3-(4-methylpyridin-3-yl)-6-(pyridin-2-ylmethoxy)-1 H -pyrazolo-[3,4- b ]pyrazine (PF470): A Highly Potent, Selective, and Efficacious Metabotropic Glutamate Receptor 5 (mGluR5) Negative Allosteric Modulator. *Journal of Medicinal Chemistry*, 57(3), pp.861–877.
- Zhang, Y. et al., 2014b. An RNA-sequencing transcriptome and splicing database of glia, neurons, and vascular cells of the cerebral cortex. *The Journal of neuroscience : the official journal of the Society for Neuroscience*, 34(36), pp.11929–47.
- Zhou, Y. & Danbolt, N.C., 2013. GABA and Glutamate Transporters in Brain. *Frontiers in endocrinology*, 4, p.165.